

This study aims to model the changes in the behaviour of motor neurons of the vastus lateralis in response to unilateral isometric knee extension exercise (UIKEE). For this, the phenomenological motor control model by Fuglevand et al. (1993) has been used. Input parameters for this model have been calibrated against data from experimental studies available in literature by using Bayesian updating. The pre-exercise state of the motor neuron pool of the muscle describing the recruitment behaviour as well as the contractile properties of the motor neurons have been constructed. Data collected from a systematic review on the change in isometric strength due to UIKEE has been modelled using Bayesian longitudinal model-based meta-analysis. Using the model of the change in isometric strength, increase in the average motor neuron discharge rate following UIKEE has been quantified.

N. E. Altan

Data-driven modelling of neuromechanical adaptation

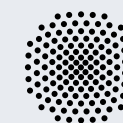
# Data-driven modelling of neuromechanical adaptation in skeletal muscles in response to isometric exercise

Neriman Ekin Altan

Neriman Ekin Altan

ISBN 978-3-946412-07-6

CBM-09 (2022)



vorgelegt an der  
**Universität Stuttgart**





**Data-driven modelling of neuromechanical  
adaptation in skeletal muscles  
in response to isometric exercise**

Von der Fakultät Bau- und Umweltingenieurwissenschaften und  
dem Stuttgart Center for Simulation Science  
der Universität Stuttgart zur Erlangung der Würde  
eines Doktor-Ingenieurs (Dr.-Ing.)  
genehmigte Abhandlung

von

Neriman Ekin Altan

aus

Ankara

Hauptberichter: Prof. Oliver Röhrle, PhD

Mitberichter: Prof. Dr. Heiko Wagner

Tag der mündlichen Prüfung: 26. November 2021

Institut für Modellierung und Simulation Biomechanischer Systeme  
der Universität Stuttgart

2022

Report No.: CBM-09 (2022)  
Institute for Modelling and Simulation of Biomechanical Systems  
Chair of Continuum Biomechanics and Mechanobiology  
University of Stuttgart, Germany, 2022

**Editor:**

Prof. O. Röhrle, PhD

© Neriman Ekin Altan  
Institute for Modelling and Simulation of Biomechanical Systems  
Chair of Continuum Biomechanics and Mechanobiology  
University of Stuttgart  
Pfaffenwaldring 5a  
70569 Stuttgart, Germany

All rights reserved. No part of this publication may be reproduced, stored in a retrieval system, or transmitted, in any form or by any means, electronic, mechanical, photocopying, recording, scanning or otherwise, without the permission in writing of the author.

ISBN 978-3-946412-07-6  
(D-93 Dissertation, Universitt Stuttgart)

# Declaration of originality

I hereby declare that this thesis and the work reported herein was composed by and originated entirely from me. Information derived from the published and unpublished work of others has been acknowledged in the text and references are given in the list of sources.

Stuttgart, March 2022



---

Neriman Ekin Altan



*Anneme...*





# Acknowledgements

First and foremost, I would like to thank and express my gratitude for Prof. Oliver Röhrle for providing me with the means to conduct my research at the University of Stuttgart. His guidance, insight, expertise and patience have been very helpful for me. I enjoyed our many discussions on muscle modelling.

Insight and expertise of Dr. Leonardo Gizzi have been very significant as I was trying to understand the highly complex skeletal muscle anatomy and physiology and trying to shape the structure of my work. Thank you very much for taking your time for the many discussions I-lost-count-of.

My aim from the beginning was to combine the best of the two worlds of computational modelling and experimental research. In doing so, I received significant guidance and support from Prof. Dr. Sergey Oladyshkin. You were kind enough to share your research, knowledge, time and patience with me. I really enjoyed our discussions and I have learnt a great deal from you on Bayesian statistics.

Assoc. Prof. Dr. Serdar Göktepe from my home university, the Middle East Technical University in Ankara, was kind enough to support me on setting up my study. Serdar Hocam, you are one of the key people, who helped me finish what I have started and not give up. I appreciate your approach towards research and succinct approach to advising. Thank you very much for your insight, patience and guidance.

One part of my work was done in close collaboration with Svenja Seide from the Uni Klinikum Heidelberg. She took the time to perform the statistical analysis of the data we collected from a systematic review. You were kind and patient enough to help me out on a very important part of my work with your expertise on meta-analysis. Prof. Hayri Ertan and Dr. Ismail Bayram were also kind enough to help me on data elicitation and finalizing our manuscript. I would also like to thank Dr. Utku Yavuz for introducing me to Prof. Ertan and Dr. Bayram as well as for his input on neuromechanics. Thank you all very much.

Prof. Heiko Wagner agreed to review my dissertation. Thank you very much for taking the time to give me feedback and the interesting discussion during my exam.

I would also like to thank the German Research Foundation (DFG) for the financial support for my project within the Cluster of Excellence in Simulation Technology (EXC310/1) at the University of Stuttgart.

PhD studies are challenging in many ways, not only because of the complexity of the research topic, but because it is a highly personal, at many times a turbulent, but also a fun journey. If you are a PhD student reading this, please know and remind yourself that there is an end to it. I learnt as much on skeletal muscles and computational modelling as I learned about my own capabilities, strengths and weaknesses. My friends, former colleagues at our research group and family have been a huge support throughout this journey, maybe without them even noticing.

I would like to give my sincere thanks to Dr. Mehmet Tümer for his kind support and

help during my entire time living abroad and my PhD studies. He has played a key role for me to keep on going and also remember to take care of myself. I would also like to thank Frau Sorg for her guidance and help. The lessons I learned during our sessions will stay with me for my whole life. Vielen herzlichen Dank.

My friends have helped me remember that there are things in life other than my PhD. All of them have had their fair share of my nagging and struggles, but they were patient and kind enough to stick around. Their support has been eminent for me to keep on going and remember to enjoy life outside of the university. I refer to my dear friends, whom I met in Stuttgart and in Ankara, as my extended family as we went through various stages of our lives together. Thank you all very much for the fun times and the support.

The last but not at all the least, I was able to complete my research and dissertation thanks to the presence, support and endless patience of my dearest mother. She dedicated her own PhD thesis to me and I'm flattered to be able to do the same for her. Not only is she the reason why I'm on this earth, her mere presence, understanding, tolerance and eternal patience was of vital importance for me. I am at a loss of words to express my gratitude for your support. I'm honored to have you as my mother.

# Contents

<b>1</b>	<b>Introduction</b>	<b>1</b>
1.1	Motivation . . . . .	1
1.2	State of the art in muscle modelling . . . . .	2
1.2.1	Computational models of skeletal muscle mechanics . . . . .	3
1.2.2	Computational models of motor control . . . . .	5
1.2.3	Data-driven modelling in biomechanics . . . . .	7
1.3	State of the art in experimental studies on isometric exercise . . . . .	8
1.4	Thesis outline and research questions . . . . .	8
1.5	List of publications . . . . .	11
<b>2</b>	<b>Anatomical and physiological background</b>	<b>13</b>
2.1	Skeletal muscle structure and function . . . . .	13
2.1.1	From the cell to organ - the hierarchical structure . . . . .	13
2.1.2	Types of contractions . . . . .	14
2.1.3	Knee extensors . . . . .	14
2.2	Voluntary muscle contraction . . . . .	15
2.2.1	Motor neuron . . . . .	15
2.2.2	The motor unit . . . . .	17
2.2.3	Fibres of motor units . . . . .	18
2.2.4	Twitch properties of motor units . . . . .	19
2.2.5	Motor unit recruitment . . . . .	20
2.2.6	Force output . . . . .	22
2.2.7	Measuring motor unit activity . . . . .	23
2.3	Adaptation mechanisms in skeletal muscles . . . . .	26
2.3.1	Overview . . . . .	26
2.3.2	Principles of training . . . . .	26
2.3.3	Isometric resistance training . . . . .	27
2.3.4	Changes caused by isometric resistance training . . . . .	28
2.3.4.1	Morphological changes . . . . .	28
2.3.4.2	Changes related to the neuromechanical system . . . . .	29
2.4	Summary of the ‘end of a new beginning’ . . . . .	30
<b>3</b>	<b>Incorporating experimental data into the modelling framework</b>	<b>33</b>
3.1	Bayesian inference . . . . .	34
3.2	Bayes’ theorem . . . . .	35
3.2.1	Conditional probability . . . . .	36
3.2.2	The coin tossing example . . . . .	37
3.2.3	Prior . . . . .	38
3.2.4	Posterior . . . . .	38
3.2.5	Likelihood . . . . .	39

3.2.6	The denominator . . . . .	40
3.3	Implementation of Bayesian inference . . . . .	40
3.3.1	The likelihood model . . . . .	40
3.3.2	Setting up the prior set . . . . .	41
3.3.3	Rejection Sampling . . . . .	42
3.4	How the framework is used in this thesis . . . . .	42
3.4.1	Scheme I: Estimation of the input parameters for the recruitment model for vastus lateralis . . . . .	43
3.4.2	Scheme II: Estimation of the contractile properties of vastus lateralis . . . . .	44
3.4.3	Scheme III: Estimation of the change in discharge rate of vastus lateralis due to UIKEE . . . . .	44
<b>4</b>	<b>Modelling total force output</b>	<b>45</b>
4.1	The motor neuron pool model . . . . .	45
4.1.1	Fixed-point iteration . . . . .	49
4.2	Computing force output . . . . .	51
4.2.1	Motor unit force . . . . .	52
4.2.1.1	Twitch response . . . . .	52
4.2.1.2	Discharge instances . . . . .	53
4.2.1.3	Obtaining the muscle force output . . . . .	53
4.3	Notes on the use of the modelling scheme in this work . . . . .	54
4.3.1	Inclusion of the variation in firing instances . . . . .	54
4.3.2	Distribution of the contractile properties . . . . .	56
<b>5</b>	<b>Modelling isometric contraction</b>	<b>59</b>
5.1	Introduction . . . . .	59
5.2	Methods . . . . .	59
5.2.1	Selection of the set of input parameters . . . . .	61
5.2.2	Selection of the calibration data . . . . .	61
5.2.3	Computing the mean discharge rate as model output . . . . .	62
5.2.4	Estimation of the total motor neuron number in vastus lateralis . . . . .	63
5.2.5	Bayesian updating . . . . .	64
5.3	Results . . . . .	65
5.3.1	Characteristics of the prior set of admissible input parameters . . . . .	65
5.3.2	Characteristics of the posterior set of admissible input parameters . . . . .	67
5.3.3	Recruitment behaviour of vastus lateralis . . . . .	68
5.4	Discussion . . . . .	71
5.5	Conclusions . . . . .	74
<b>6</b>	<b>Modelling contractile properties</b>	<b>75</b>
6.1	Methods . . . . .	76
6.1.1	Estimating the isometric strength of vastus lateralis . . . . .	77
6.1.2	Experimental data on contractile properties . . . . .	78
6.1.3	Constructing admissible sets of contractile properties . . . . .	79
6.1.4	Prior sets for time-to-peak-force . . . . .	83
6.1.5	Prior sets for the peak twitch force . . . . .	84
6.2	Results . . . . .	87

---

6.3	Discussion . . . . .	91
<b>7</b>	<b>Strength gain due to isometric knee extension exercise</b>	<b>95</b>
7.1	Introduction . . . . .	95
7.2	Methods . . . . .	96
7.2.1	Study selection . . . . .	96
7.2.2	Inclusion criteria . . . . .	96
7.2.3	Exclusion criteria . . . . .	96
7.2.4	Data collection and extraction . . . . .	97
7.2.5	Synthesis of results . . . . .	98
7.2.6	Risk of bias in individual studies . . . . .	100
7.2.7	Summary of evidence . . . . .	100
7.2.8	Assessment of the risk of bias across studies . . . . .	102
7.2.9	Longitudinal model-based meta-analysis . . . . .	103
7.3	Discussion . . . . .	104
7.4	Conclusions . . . . .	108
<b>8</b>	<b>Changes in discharge behaviour due to isometric exercise</b>	<b>111</b>
8.1	Introduction . . . . .	111
8.2	Methods . . . . .	111
8.2.1	Admissible set of model input parameters . . . . .	112
8.2.2	Prior set of model input parameters . . . . .	113
8.2.3	Calibration points . . . . .	114
8.3	Results . . . . .	115
8.3.1	Size of parameter sets . . . . .	115
8.3.2	Posterior sets over trained weeks . . . . .	115
8.3.3	Change in mean discharge rate over trained weeks . . . . .	116
8.4	Summart and discussion . . . . .	116
<b>9</b>	<b>Discussion and Outlook</b>	<b>121</b>
9.1	Discussion . . . . .	121
9.2	Outlook . . . . .	123
<b>A</b>	<b>Admissible sets for the contractile properties</b>	<b>127</b>
<b>B</b>	<b>Systematic review and meta-analysis</b>	<b>129</b>
B.1	Background information and significance . . . . .	129
B.2	Search strategy . . . . .	131
B.3	Risk of bias assessment . . . . .	132
B.4	Additional data . . . . .	134
B.5	Descriptive visualization of collected data . . . . .	138
B.5.1	Spaghetti Plots . . . . .	138
B.5.2	Forest plots . . . . .	144
	<b>Bibliography</b>	<b>147</b>



# Abstract

Movement is crucial for organisms to survive as it enables mobility. The movement actuators of humans and animals are skeletal muscles. These muscles are controlled voluntarily. Voluntary movement is possible when muscles are able to generate a sufficient amount of force in a coordinated manner. In order to improve the movement capabilities, there exist a variety of training/exercise schemes, which target different muscles or muscle groups. The improvement in the capabilities of muscles have multiple advantages, such as decreased risk of several diseases, e.g. cardiovascular diseases or type II diabetes, and improved mental health.

A vast amount past and on-going studies exist, which investigate the mechanisms related to exercise-induced adaptation in muscles. However, exact mechanisms responsible for the changes occurring in the central nervous system and skeletal muscles are not fully understood. This is mainly due to the complexity of the physiology of voluntary control, muscles and exercise, as well as, limitations in experimental methods.

Isometric exercise is the simplest known type of exercise as it is composed of contractions, during which the muscle length stays constant and the trained limb does not move. This exercise type is commonly used in experimental studies to investigate the neuromechanical adaptation mechanisms that occur as a result of training. Practically, this exercise regime is used in post-operative training programs after knee operations or for individuals suffering from neuromuscular disorders to improve muscle function. Besides its ease to execute and control in an experimental setting, this exercise is known to trigger muscle volume increase, as well as an increase in muscle strength.

In order to observe the changes due to exercise, the current (pre-and post-exercise) state of the muscle system needs to be investigated. To do that, the anatomy of the central nervous system and muscles need to be understood, which was done using dissection studies of cadavers. However, fast-progressing technological advancements related to experimental measurement apparatus and methods, enable to investigate various aspects of active muscle movement also in-vivo.

Motor neurons are an important part of the neuromechanical system. They transmit the voluntary input from the spinal chord to the muscle organ, which triggers the muscle contraction. Due to their significance in executing voluntary muscle movement, investigation of their behaviour has been the focus of research since early 1900s. Despite the advances in the technology used in experimental measurements of skeletal muscles, experimental methods are limited in their ability to capture the complete behaviour of the motor neurons. These limitations becomes significant, for example, when data on the recruitment behaviour of the entire motor neuron pool of especially large muscles at high force levels are needed.

In order to enhance the insight obtained by experiments and make up for the limitations of the experimental methods, computational models of voluntary control are frequently used. These models might investigate multiple aspects or concentrate on one aspect of



voluntary control. This work aims to make use of the pioneering computational motor control model suggested in Fuglevand et al. (1993) together with experimental data from literature to fill the gaps with regards to the understanding of the recruitment behaviour of motor neurons at high force levels and investigate changes triggered by isometric exercise.

To make a model more realistic, experimental data may be incorporated into computational models. There exists a variety of approaches to integrate experimental data into computational models. For example, data may be fed into model, making it a data-integrated modelling scheme. Another way is to compare the model outcome with experimental data. This way, the model may be modified to increase the accuracy of the model output. One other way is to calibrate the model parameters against the experimental data, which is known as data-driven modelling approach. This approach allows to select the set of input parameters that describe the phenomenon being modelled, by ensuring accurate results.

To develop a better insight into changes triggered by isometric exercise, first, the pre-exercise state of the motor neuron pool needs to be constructed. The aim of the thesis is to complement the computational model with experimental data in literature. Relatively many experimental studies on the recruitment behaviour of the vastus lateralis muscle of the knee extensors exist. Therefore, the modelling framework is constructed specifically for the vastus lateralis muscle. Experimental data on unilateral (one-sided) isometric knee extension training is used to investigate the changes in the motor neuron recruitment behaviour of this muscle. In this work, experimental data is also used to select admissible ranges for the input parameters of a phenomenological motor control by Fuglevand et al. (1993). The model output is calibrated against experimental data to determine the set of input parameters, which describe the recruitment behaviour during an isometric contraction and the contractile properties of the motor neuron pool of vastus lateralis muscle. For this purpose, the Bayesian updating framework is employed, which is a data-based decision making scheme. Even though only a few studies on the changes in the recruitment behaviour of the motor neurons of the vastus lateralis exist, numerous studies report data on the increase in muscle strength due to unilateral isometric knee extension exercise. Literature data on the increase in muscle strength due to this exercise type is collected by means of a systematic literature review. The collected data is then analysed by means of Bayesian longitudinal model-based meta-analysis, which allows to model the evolution of muscle strength over trained weeks. Changes in the recruitment behaviour of the motor neurons are then quantified, which would yield the increase in the muscle strength provided by the experimental evidence.

# Deutsche Zusammenfassung

Bewegung ist entscheidend für das Überleben von Organismen, da sie Mobilität ermöglicht. Die Bewegungsaktoren von Mensch und Tier sind Skelettmuskeln. Diese Muskeln werden freiwillig kontrolliert, wohingegen Herz- und Glattmuskulatur unbewusst kontrolliert werden. Freiwillige Bewegung ist möglich, wenn die Muskeln auf koordinierte Weise eine ausreichende Kraft erzeugen können. Um die Bewegungsfähigkeiten zu verbessern, gibt es eine Vielzahl von Trainings- / Übungsschemata, die auf verschiedene Muskeln oder Muskelgruppen abzielen. Die Verbesserung der Fähigkeiten der Muskeln, d.h. die Erhöhung der Kraft, der Ausdauer oder der Beweglichkeit, hat mehrere Vorteile, wie beispielsweise ein verringertes Risiko für verschiedene Krankheiten, wie Herz-Kreislauf-Erkrankungen oder Typ-II-Diabetes und eine verbesserte psychische Gesundheit.

Es gibt eine Vielzahl von früheren und laufenden Studien, die die Mechanismen untersuchen und erforschen, die mit der durch körperliche Betätigung verursachten Anpassung der Muskeln zusammenhängen. Die genauen Mechanismen, die für die Veränderungen des Zentralnervensystems und der Skelettmuskulatur verantwortlich sind, sind jedoch bis heute nicht vollständig bekannt. Dies ist hauptsächlich auf die Komplexität der Muskeln und des Trainings an sich, sowie der Komplexität der Physiologie der freiwilligen Kontrolle zurückzuführen. Auch die Möglichkeiten experimenteller Methoden sind ethisch, wie technologisch begrenzt.

Isometrisches Training ist die einfachste bekannte Art von Training, da es aus Kontraktionen besteht, bei denen die Muskellänge konstant bleibt und sich das trainierte Glied nicht bewegt. Dieser Übungstyp wird häufig in experimentellen Studien verwendet, um die neuromechanischen Anpassungsmechanismen zu untersuchen, die als Ergebnis des Trainings auftreten. In der Praxis wird dieses Trainingsprogramm in postoperativen Trainingsprogrammen nach Knieoperationen oder bei Personen mit neuromuskulären Störungen zur Verbesserung der Muskelfunktion angewendet. Neben der einfachen Ausführung und Kontrolle in einer experimentellen Umgebung löst diese Übung bekanntermaßen eine Erhöhung des Muskelvolumens sowie eine Erhöhung der Muskelkraft aus.

Um die Veränderungen aufgrund des Trainings zu beobachten, muss der aktuelle Zustand (vor und nach dem Training) des Muskelsystems untersucht werden. Dazu muss die Anatomie des Zentralnervensystems und der Muskeln verstanden werden, was in früheren Untersuchungen anhand von Dissektionsstudien an Leichen geschehen ist. Die schnell fortschreitenden technologischen Fortschritte in Bezug auf experimentelle Messgeräte und -methoden ermöglichen es heute jedoch, verschiedene Aspekte der aktiven Muskelbewegung auch *in vivo* zu untersuchen.

Motoneuronen sind ein wichtiger Bestandteil des neuromechanischen Systems. Sie übertragen den freiwilligen Input vom Rückenmark zum Muskelorgan, was die Muskelkontraktion auslöst. Aufgrund ihrer Bedeutung für die Ausführung freiwilliger Muskelbewegungen steht die Untersuchung ihres Verhaltens seit Anfang des 20. Jahrhunderts im Mittelpunkt

der Forschung. Trotz der technologischen Fortschritte in der experimentellen Messung der Skelettmuskulatur, sind experimentelle Methoden in ihrer Fähigkeit auch heute noch begrenzt um das vollständige Verhalten der Motoneuronen zu erfassen. Diese Einschränkungen werden beispielsweise dann erheblich, wenn Daten zum Rekrutierungsverhalten des gesamten Motoneuronenpools besonders großer Muskeln bei hohen Kraftniveaus benötigt werden.

Um die durch Experimente gewonnenen Erkenntnisse zu verbessern und die Grenzen der experimentellen Methoden auszugleichen, werden häufig Rechenmodelle der freiwilligen Kontrolle verwendet. Diese Modelle können mehrere Aspekte untersuchen oder sich auf einen Aspekt der freiwilligen Kontrolle konzentrieren. Diese Arbeit zielt darauf ab, das wegweisende Modell der rechnergestützten Motorsteuerung von Fuglevand et al. (1993) zusammen mit experimentellen Daten aus der Literatur zu nutzen, um die Lücken im Hinblick auf das Verständnis des Rekrutierungsverhaltens von Motoneuronen bei hohen Kräften zu schließen und Veränderungen simulativ zu untersuchen, die durch isometrisches Training ausgelöst werden.

Um ein Modell realistischer zu machen, können experimentelle Daten in Rechenmodelle aufgenommen werden. Es gibt verschiedene Ansätze, um experimentelle Daten in Rechenmodelle zu integrieren. Beispielsweise können Daten in das Modell eingespeist werden, wodurch es zu einem datenintegrierten Modellierungsschema wird. Eine andere Möglichkeit besteht darin, das Modellergebnis mit experimentellen Daten zu vergleichen. Auf diese Weise kann das Modell modifiziert werden, um die Genauigkeit der Modellausgabe zu erhöhen. Eine andere Möglichkeit besteht darin, die Modellparameter gegen die experimentellen Daten zu kalibrieren, was als datengesteuerter Modellierungsansatz bekannt ist. Dieser Ansatz ermöglicht die Auswahl eines passenden Satzes von Eingabeparametern, welche das zu modellierende Phänomen am besten beschreiben.

Um einen besseren Einblick in Veränderungen zu erhalten, die durch isometrisches Training ausgelöst werden, muss zunächst der Zustand vor dem Training des Motoneuronenpools konstruiert werden. Ziel der Arbeit ist es, das Rechenmodell durch experimentelle Daten aus der Literatur zu ergänzen. Es gibt relativ viele experimentelle Studien zum Rekrutierungsverhalten des *Musculus vastus lateralis*, einer der Knieextensoren. Daher ist der Fokus dieser Arbeit speziell für den *Musculus vastus lateralis* (äußerer Oberschenkelmuskel) konstruiert. Experimentelle Daten zum einseitigen isometrischen Knieextensionstraining werden verwendet, um die Veränderungen im Rekrutierungsverhalten von Motoneuronen dieses Muskels zu untersuchen.

In dieser Arbeit werden experimentelle Daten auch verwendet, um zulässige Bereiche für die Eingabeparameter einer phänomenologischen Motorsteuerung von Fuglevand et al. (1993) zu wählen. Die Ergebnisse aus der Simulation werden gegen experimentelle Daten kalibriert, um den Satz von Eingabeparametern zu bestimmen, die das Rekrutierungsverhalten während einer isometrischen Kontraktion und die kontraktile Eigenschaften des Motoneuronenpools des *Musculus vastus lateralis* beschreiben. Zu diesem Zweck wird das Bayes'sche Aktualisierungsframework verwendet, bei dem es sich um ein datenbasiertes Entscheidungsschema handelt.

Obwohl nur wenige Studien zu Veränderungen des Rekrutierungsverhaltens der Motoneuronen des *Vastus lateralis* vorliegen, berichten zahlreiche Studien über Daten zur Zunahme der Muskelkraft aufgrund einseitiger isometrischer Knieextensionsübungen. Literaturdaten zur Steigerung der Muskelkraft aufgrund dieser Übungsart werden mittels einer

systematischen Literaturrecherche erhoben. Die gesammelten Daten werden dann mittels einer auf dem Bayes'schen Längsschnittmodell basierenden Metaanalyse analysiert, die es ermöglicht, die Entwicklung der Muskelkraft im Laufe der Trainingswochen zu modellieren. Änderungen im Rekrutierungsverhalten der Motoneuronen werden dann quantifiziert, was zu einer Erhöhung der Muskelkraft führen würde, die durch die experimentellen Beweise bereitgestellt wird.



# Nomenclature

## Abbreviations

Symbol	Description
CP	contractile properties
EMG	electromyography
sEMG	surface electromyography
MAP	maximum a-posteriori
MU	motor unit
MUAPT	motor unit action potential trains
MVC	maximum voluntary contraction
RF	rectus femoris
RM	recruitment model
UIKEE	unilateral isometric knee extension
VM	vastus medialis
VL	vastus lateralis

## Conventions

Symbol	Description
$(\cdot)$	placeholder for arbitrary quantities
$\overline{(\cdot)}$	normalized quantity
$\widetilde{(\cdot)}$	prior set
$\underline{\underline{(\cdot)}}$	posterior set

## Operators

Symbol	Description
$\text{conv}(\cdot)$	the convolution operator
$\text{cov}(\cdot)$	covariance
$\text{var}(\cdot)$	variance

## List of symbols in Greek letters

Symbol	Unit	Description
$\alpha_k^{PTF}$	[mN]	scaling factor for $PTF$
$\alpha_r^{TTP}$	[ms]	scaling factor for $\overline{TTP}$
$\Theta$		set of model input parameters
$\Theta^{\overline{CP}}$		initial set of normalized contractile properties
$\tilde{\Theta}^{CP}$		prior set of contractile properties
$\approx^{CP}$		
$\Theta$		posterior set of contractile properties
$\approx^{\text{MAP}}$		
$\Theta$		maximum a-posteriori in the set of model inputs
$\Theta^{\overline{PTF}}$		initial selection of sets for $\overline{PTF}$
$\tilde{\Theta}^{PTF}$	[mN]	prior set for $PTF$
$\approx^{PTF}$		
$\Theta$	[mN]	posterior set for $PTF$
$\Theta^{\overline{TTP}}$		initial set of normalized $\overline{TTP}$
$\tilde{\Theta}^{TTP}$	[ms]	prior set of $TTP$
$\approx^{TTP}$		
$\Theta$	[ms]	posterior set for $TTP$
$\tau$	[ms]	time in milliseconds
$\Omega^{\text{exp}}$		calibration data obtained from experimental data
$\Omega(\Theta)$		set of model outputs
$\Omega^{\text{sim}}$		model output obtained from simulations

## List of symbols in Latin letters

Symbol	Unit	Description
$a$		shape parameter one in probability distribution functions following alpha and beta distributions
$b$		shape parameter two in probability distribution functions following alpha and beta distributions
$i$		element in set of time-to-peak
$j$		element in set of peak twitch force
$k$		element in the set of normalized contractile properties
$m$		time step
$n$		motor neuron number
$iter_{\max}$		maximum number of iterations
$g_e$	[au]	excitatory gain
$p$	[%MVC]	force level
$p^s$	[%MVC]	force level at which an experimental data is available
$p(\Theta)$		probability distribution function of the model input
$p(D)$		probability distribution function of the calibration data
$p(\Theta   D)$		probability distribution function of the model input given calibration data, i.e., posterior set
$p(D   \Theta)$		probability distribution function of the calibration data given model input
$t$	[s]	time
$t_{end}$	[s]	end of the entire contraction
$t^*, \Delta t^*$	[s, s]	fixed discharge instance and the change thereof
$t_n^m, \Delta t_n^m$	[s, s]	discharge instance of motor neuron $n$ at the current time step $m$ and the change thereof
$t_n^{m-1}$	[s]	discharge instance of motor neuron $n$ at the previous time step
$t_{ramp}$	[s]	end of ramped contraction
$w$	[au]	weight
$D$		set of calibration data



---

$E_1$		event 1
$E_2$		event 2
$E$		expected value
$E$	[Hz]	excitatory drive
$E_{\max}$	[Hz]	maximum excitatory drive
$E^N$	[Hz]	excitatory drive to recruit motor neuron $N$
$E_{\max}^{\text{II}}$	[Hz]	second part of $E_{\max}$
$E_{\text{target}}$	[Hz]	target excitatory drive
$\hat{F}$	[N]	hypothetical total muscle force output
$F^{\text{exp}}$	[N]	isometric strength of knee extensors obtained from experimental data
$F_{\text{Full Recr}}$	[%MVC]	force level when all motor neurons are recruited
$\mathcal{F}$		set of discharge instances obtained from simulations
$I$		size of the prior set of time-to-peak
$J$		size of set of normalized peak twitch force
$K$		size of the set of normalized contractile properties
$\mathcal{L}$		the likelihood function
$MFR$	[Hz]	minimum discharge rate
$N$		total number of motor neurons in the pool, i.e., size of the pool
$P(E_1)$		probability of event 1
$P(E_1   E_2)$		probability of event 1 given event 2
$P(E_1 \cap E_2)$		probability of event 1 and 2 occurring at the same time
$P(E_2)$		probability of event 2
$P(E_2   E_1)$		probability of event 2 given event 1
$P(E_2 \cap E_1)$		same as $P(E_1 \cap E_2)$ if $E_1$ and $E_2$ are independent
$PFR_1$	[Hz]	peak discharge rate of motor neuron 1
$PFRD$		slope of the peak discharge rate
$PFR_n$	[Hz]	peak discharge rate of motor neuron $i$
$PFR_N$	[Hz]	peak discharge rate of motor neuron $N$

---

$\overline{PTF}, PTF$	[-,mN]	(normalized) peak twitch force
$\mathbf{R}$		covariance matrix
$RR$		range of recruitment
$RTE_n$	[Hz]	recruitment threshold of motor neuron $i$
$TF$	[mN]	twitch force
$\overline{TTP}, TTP$	[-,s]	(normalized) time required to reach peak twitch force, i.e., time-to-peak



# 1 Introduction

## 1.1 Motivation

Movement is crucial for all organisms as it allows them to perform basic functions required for survival such as running away when there is a threat, eating and so on. The movement actuators of humans are skeletal muscles.

Physical exercise schemes have been used extensively up to date to improve movement capabilities. Besides the improvement in movement capabilities, exercise has numerous positive effects on the overall health. Such positive effects include, but not limited to, anti-depressive effects in depressive disorders [209], improved blood circulation and a reduced risk of cardiovascular diseases [232].

Exercise simultaneously improves bone health and joint mobility, thus decreases injury risk [232]. At the muscle level, one of the most prominent effects of exercise on the muscle function is improved muscle force output. It is therefore important to understand first the mechanisms behind how muscle force output is generated and how it improves with exercise.

To generate voluntary force output, signals from the brain are transmitted to the spinal chord via upper motor neurons. Lower motor neurons transmit the signal from the upper motor neurons on to muscles.

Since motor neurons act as the enabler to generate muscle force, we need to understand how they behave. When their behaviour is understood, we can then investigate the corresponding changes in their behaviour, which would yield increased force output.

Experimental studies have been used to investigate the mechanisms behind how muscles generate force and the motor neuron behaviour. It is straightforward to measure muscle force output and muscle strength experimentally, however, motor neuron behaviour is not as straightforward to observe in an experimental setting.

Muscle force output is a mechanical property whereas in motor neuron behaviour, neural aspects play a significant role. To investigate motor neuron activity, electrical signals produced by motor neurons that initiate muscle contraction are measured. This measurement can be performed by electromyogram (EMG).

EMG measurements can be made by placing electrodes on the surface of the muscle over the skin. Another method is placing needle electrodes inside the muscle. Despite the fact that both methods have their own strengths and can provide valuable insight into neural behaviour, they both provide data for only a portion of the motor neurons controlling a given muscle.

When experimental methods are tedious to perform or cannot provide enough insight on the phenomenon of interest, it is common to use computational models to fill the gaps left by experimental data [308]. The advantage of computational models is that individual parameters of any phenomenon can be isolated and investigated individually, which is not possible for experiments. However, experimental methods are based on real-

life measurements in a specific setup whereas models are only an abstraction of reality.

This study makes use of a computational approach to investigate the motor neuron behaviour and the corresponding changes as a result of exercise. In doing so, a data-driven modelling framework is established, by using experimental data for calibration of modelling parameters. This way, advantages of experimental and modelling approaches are combined together to establish an evidence-based framework to investigate neuromechanical adaptation in muscles.

We first try to quantify the rate of discharge of electrical signals from the motor neurons by means of a phenomenological motor control model during voluntary muscle contraction. Force output of individual motor neurons are then quantified to obtain the total muscle force output. The ultimate aim is to determine the change in the motor neuron discharge rate, which would yield the expected increase in force output due to exercise.

The focus is on one type of exercise, namely isometric exercise, which is performed by contracting the muscle at a fixed length. This form of exercise is known for being simple, as joints remain at a fixed angle. Using data from literature on the changes in muscle force output due to isometric exercise, specifically unilateral (performed by one limb) isometric knee extension exercise, model parameters are calibrated. As a result, change in the discharge rate of motor neurons yielding the expected change in force output due to the selected exercise form are determined.

## 1.2 State of the art in muscle modelling

In order to analyse the complex musculoskeletal system, one needs to develop a clear understanding of the physical nature of the system and of the mathematical representation of its dynamics [327]. Computational models are developed to enhance the understanding of the musculoskeletal system. The selection of the modelling scheme depends on the feature of the muscle that is of interest to the modeller. To illustrate, if the aim is to model the response of the muscle to a given displacement of the muscle under a given load, a well-established material model is required. When the focus is on the response of the muscle to a given activation pattern, the modelling scheme needs to include a model of motor unit recruitment. It is also possible to couple different models together to observe multiple aspects of muscle function.

Modelling approaches can broadly be divided into two groups. The first one is known as “phenomenological models”, also called as “black box models” [71]. The reason why they are considered as black box models is that such models are based on a theory that expresses the outcomes of the phenomena being investigated mathematically [303]. The correspondence to any real entities within the system may be completely lacking or be present only partially. The second modelling approach appeals to biophysical models, which include subsystems that describe the chemical, electrical, and structural entities of the muscle [71]. These subsystems may be described using ordinary/-partial differential equations.

The scale at which the phenomenon is modelled also plays an important role in muscle modelling. This is due to the hierarchical structure of skeletal muscles (see Section 2.1). Models investigating the muscle at the cellular level may contain descriptions of the cross-bridge dynamics or the ion exchange at the cell membrane of the muscle cell or the motor neuron. If macroscopic deformations are of interest, a continuum-mechanical setting can

be used.

The following sections provide an overview of the literature on phenomenological models with respect to the mechanics of isometric skeletal muscle contractions. This is followed by an overview on models of voluntary muscle control. Note that the emphasis of the literature review provided in this section lies on phenomenological skeletal muscle models. Next, computational models in exercise science are presented. These models, however, investigate the performance expectations of athletes and not non-athletes. In this study, neuromuscular adaptation in response to one type of isometric exercise performed by sedentary subjects, i.e., non-athletes has been investigated. Therefore, a review of experimental studies on the isometric exercise performed by sedentary subjects has been provided. Finally, data-driven computational models in biomechanics are reviewed as this work makes use of a driven modelling scheme.

### 1.2.1 Computational models of skeletal muscle mechanics

Phenomenological models are developed in conjunction with experimental data, either conducted specifically for the study at hand or using data from other studies or a combination of both. One fundamental phenomenological model is the Hill's model, which describes muscle force output using a rheological model [139]. The model is composed of three rheological elements: two springs and one contractile element. One spring is serially connected to the contractile element and the second spring is connected to the other two elements in parallel. This way, the total force output is composed of two additive parts, one describing the active force output and the other the passive force output. The active force output is modelled as a combination of the force-length, force-velocity and a viscoelastic response of the element to a given traction, e.g.[79, 113, 255, 286]. Due to its phenomenological nature, this model can only describe the mechanical properties of muscles, but not how the contraction is generated [285]. However, it is a fundamental model, since it provides insight into the mechanical aspects of the active force output in a simple setting.

Hill's model is being developed further up to this date, e.g., [119, 127, 328] and is commonly integrated within a continuum-mechanical setting. Sharifimajd & Stålhand [286] suggest a thermodynamically consistent model of the skeletal muscle. They replace the contractile element of Hill's model by a friction clutch to mimic the slipping of the actin filament against myosin under a given load. The reason for this is to formulate the element based on mechanical properties and not as a "black box". Authors of this study use an additive decomposition of the stress, despite modelling large deformations. They claim that this does not introduce the problem regarding the principle of objectivity as the model is described for a 1D setting and not a 3D setting. Although the authors provide a solution to this problem, they also hint that verification of muscle models in a 3D setting is not possible. This is a strong statement, because numerous experimental studies on the macroscopic behaviour of skeletal muscles do exist and they investigate the passive as well as the active states.

Various authors have modified the rheological muscle models, e.g. by more detailed continuum-mechanical models. Such a model is suggested by Ehret et al. [79]. In this study, authors make use of a constitutive material model of muscle tissue based on a transversely isotropic hyperelastic material model. The active state is motivated by the

change of fibre length, which is prescribed by a weight parameter in the generalized invariant. This weight is additively decomposed into an active and passive part. An active contraction occurs when the active part of the weight parameter is larger than zero. However, the active force output, at the end, is reduced to a simplified form of the model of the force output as already suggested by previously Fuglevand et al. [104]. The active part of the weight was later coupled to an electrical source term that describes the action potential in Böl et al. [29].

One other example of the integration of Hill's model in a continuum-mechanical setting is described in the study by Göktepe et al. [113]. On top of a phenomenological description of the active force motivated by Hill's model, Göktepe et al. [113] make use of a micromechanically motivated active strain. The active strain evolves with the intracellular calcium ion concentration. Therefore, the suggested modelling framework couples phenomenological and biophysical descriptions of muscle contraction.

Based on experiments performed on isolated tibialis anterior muscles of rats, Ramírez et al. [255] used the generic form of the force output of the contractile element based on Hill's model. They additionally introduce a force-voltage relationship, which describes the influence of electrical stimulation on the force output. They also include the effect of the concentration of various ions in the muscle cell as the contraction proceeds without focusing on any specific ion. This allows to take the effect of fatigue-related force decrease at the force plateau into account. Combining these components multiplicatively provides the total force output. Results of the simulations fit well with the experimental data. Being relatively simple to implement, the model, however, does not take into account the differences related to motor neuron types and it assumes a single motor neuron type for all contractions.

To model the active force output realistically, passive force output of the skeletal muscle should also be included in models, since the passive force output is significant when the muscle operates at a long length. In a continuum-mechanical setting, passive force output is included using representations of the experimentally measured force-length curve of the muscle. This curve can be modelled using piecewise functions, which describe the J-like curve of biological tissue response. Blemker et al. [25] utilized this framework to investigate the causes of non-uniform strains in biceps brachii muscle. Various activation levels are modelled by a scaling parameter ranging from 0 to 1. Röhrle & Pullan [268] used a similar framework to investigate human mastication, using a detailed geometry of the masseter muscles including the fibre directions. These models allow to inquire insight into the influence of fibre direction and the distribution of stress, strain, and hence muscle force, during muscle contraction.

In order to understand the mechanism of muscle contraction at the molecular level and to interpret the results of mechanical, thermodynamic, and biochemical experiments on skeletal muscle, Huxley-type models are used [327]. These models are based on the work by Hodgkin & Huxley [140], for which the authors won a Nobel prize in Physiology or Medicine in 1963. Using non-linear equations, the model describes the mechanism of the generation and propagation of action potentials in the giant squid axon. The model describes the cell membrane as an electrical circuit. Potassium, sodium current as well as a "leakage current" caused by other ions are expressed in terms of the cell's resting and equilibrium potential of each ion. The authors were able to capture the experimentally measured action potential curve using the model. The development of a multi-scale,

chemo-electro-mechanical model of muscle contraction using components of the Hodgkin-Huxley model will be illustrated in this section. Further examples of biophysical modelling frameworks are not elaborated on as such models are out of scope of the current work.

Shorten et al. [289] employ a mechanistic description of the force response of skeletal muscle to applied electric fields based on the biological mechanisms that link cell excitation to contraction. They combine and modify multiple models of cellular dynamics, initially developed for cardiac muscle. Utilizing the model suggested in Shorten et al. [289], Heidlauf & Röhrle [132] propose a detailed model of the excitation-contraction coupling mechanism based on the work by [274]. To do that, a half-sarcomere model is used, which is composed of five sub-models of membrane electrophysiology, calcium release from the sarcoplasmic reticulum, calcium dynamics, cross-bridge and fatigue. The wholesome model of the excitation-contraction coupling is constructed in a continuum-mechanical setting, which allowed for the 3D analysis of the tissue during contraction. Motor neuron recruitment behaviour is modelled following Fuglevand et al. [104]. Constitutive models for the tissue behavior were used as suggested in Röhrle & Pullan [268]. This framework was later enhanced in [133] as a chemo-electro-mechanical model by including the force-length and force-velocity response of the sarcomere. The differences between fibres spanning the entire fascicle and the ones terminated inside the fascicle were compared to fusiform or unipennate muscles.

### 1.2.2 Computational models of motor control

With regards to the investigation of skeletal muscle contraction, one other way is to include principles of motor control within a modelling framework. Computational motor control models allow, among other options, to describe the rate coding behaviour of motor neurons at various levels of contraction and to model the electromyographical (EMG) signals. This can be done by incorporating the complete feedback loop of the central nervous system, by including reflex mechanisms. It is also possible to investigate the feedback loop only partially.

Based on Hatze [127], Hatze [128] suggests a model of motor control using ordinary differential equations describing the dynamics of excitation-contraction coupling. The rate of change of length is dependent, among other factors, on the fibre arrangement, i.e., pennation of the muscle. The model accounts for the orderly recruitment of motor neurons, which requires a variable number of active motor neurons according to level of activation. The history of the activation of motor neurons is also modelled, by introducing a semi-active state, which refers to motor neurons that were activated previously and were later deactivated [128]. EMG data from each muscle of the quadriceps during a ballistic maximum effort contraction is collected. The outcomes are used to define the input parameters. The modelling scheme correctly describes the lag time between the excitation and the contraction, but not entirely the force output of the muscle group.

In an early model by Christakos [51], the motor neuron population of a muscle and the corresponding muscle force output for contraction levels up to 70% MVC is modelled. The aim of this study is to investigate the tremor, i.e., fluctuations, in the force output. The model consists of individual motor neurons acting as parallel systems, which mimic how the neuromuscular system utilizes the contribution of the motor neurons to generate force or electrical signal and hence the power spectrum of tremor is investigated. A



closed feedback loop of the central nervous system is not included in the model. The first dorsal interosseus muscle of the hand has been used to demonstrate the capabilities of the model. The recruitment threshold is defined by means of a critical mean firing rate. The mean firing rate of a motor neuron is modelled to increase linearly according to the difference between the force at which the motor neuron is recruited and the target force output.

The range of the values for the contractile properties (here, peak twitch force and time to peak twitch force) of motor neurons are borrowed from the experimental study by Milner-Brown et al. [220]. The distribution of the contractile properties are defined in relation to the force level for the recruitment of a given motor neuron. The impulse response of the system is defined as a function of the contractile properties and implicitly of the mean firing rate of the motor neuron. The force output of a motor neuron is computed by superimposing the impulse response with the twitch response and summed up linearly to obtain the total muscle force.

When the histograms for the mean firing rate of the active motor neurons given in Milner-Brown et al. [220] are investigated, an exponential distribution is observed. This would point to a high proportion of type I motor neurons, since type I motor neurons fire faster than type II motor neurons, cf. the onion skin principle [62]. Milner-Brown et al. [220] found that the 80% of the first interosseus muscle is comprised of type II fibres. Although the experimental data on the contractile properties of this muscle is incorporated in the model, the output for the firing rate cannot capture the rate coding behaviour of the motor neurons of this muscle.

Shadmehr & Arbib [284] suggested a modelling framework of voluntary control and studied the force-stiffness curve of a single joint system, by improving Feldman's model from 1966. Feldman's model on motor control show that muscle force is a function of the muscle length and the neural command received by the muscle. This neural command may be composed of the spindle feedback, Golgi tendon pathways or the amount of efferent input. Feldman showed that stiffness of muscles during contraction does not follow Hooke's law, i.e., a muscle is not a linear spring. To maintain a given joint angle, stiffness of co-contracting muscles (as a function of joint angle) needs to display non-linear behaviour in order to reach equilibrium when the external load changes. Shadmehr & Arbib [284] improved this model to include the behaviour of the system for low force levels by including the stretch reflex.

The steady-state, isometric input-output relationship of the motor neuron pool is modelled by Heckman & Binder [130]. Reflex circuitry is not included in the model. The effective synaptic input at the motor neuron soma is used in conjunction with the firing rate-injected current function to determine mechanical output. The motor neuron contractile properties were assigned according to experimental data on cat gastrocnemius muscle. The model was tested using 100 motor neurons, less than the size of the motor neuron pool experimentally measured for the muscle, thus the force output was scaled to obtain a realistic total force output. The model was later used to investigate age-related neuromuscular changes, e.g., [318].

Contrary to the detailed description of the synaptic input-output relationship in Heckman & Binder [130], Fuglevand et al. [104] suggested a modelling framework to model the isometric force output by reducing the synaptic input to a common excitatory drive. They model the discharge instances, the twitch response of motor neurons and the res-

ulting EMG signal for an isometric contraction. The model captures the rate coding behaviour of motor neurons. The number of active motor neuron for a given level of force is variable. There is no limit for the size of the motor neuron pool that can be modelled using the framework in Fuglevand et al. [104] as the motor neuron pool size is an independent variable. The model is still being used extensively to generate discharge instances of the motor neuron pool, e.g., [93, 95, 124, 137, 144, 154, 165, 245, 324]. The model itself is capable of integrating and investigating various experimentally observed aspects of motor unit recruitment behavior, see e.g., [72, 156, 224, 301]. Further, individual parts of the model have been utilised within other modelling approaches, e.g., to drive biophysically based three-dimensional, multi-scale chemo-electro-mechanical skeletal muscle models as in Heidlauf & Röhrle [132, 133] or Röhrle et al. [267].

A more recent model by Cisi & Kohn [52] propose a closed loop model of the spinal chord circuitry. Three types of motor neurons (slow twitch, fast fatiguing and fatigue resistant) are modelled. The model generates a motor unit potential and a motor unit twitch following a conduction delay. Summation of the motor unit twitch yields the total force whereas the superposition of the motor unit action potential simulates EMG. The populations of interneurons and stochastic processes associated with the descending tracts provide the inputs for the motor neuron pool. The reflex mechanisms are also modelled by incorporating external nerve stimulation. The soma and the dendritic tree are modelled in detail using a system of ordinary differential equations describing the membrane potential and conductance. The motor neuron twitch is modelled in arbitrary units, therefore, the model's capability to predict force output is only possible by comparing the rate of force development and not the absolute force output.

Contessa et al. [56] propose a model of motor control in which they drive the gain function scaling the twitch response of motor neurons by means of the firing rate of motor neurons. A non-linear function for the firing rate is suggested, which composed of four constants and is a function of the recruitment rate of motor neurons. The constants are calibrated against experimental data on the first dorsal interosseus muscle of the hand and the vastus lateralis. Firing instances and the recruitment threshold of motor neurons are modelled following Fuglevand et al. [104].

### 1.2.3 Data-driven modelling in biomechanics

Developments in computational intelligence have expanded the capabilities of empirical modelling. Data-driven modelling is the field that encompasses these new approaches and is based on analysing the data about a system without explicit knowledge of the physical behaviour of the system [3].

One approach in data-driven modelling is Bayesian updating. Based on the Bayes' theorem, which briefly describes the probability of an event given some evidence, Bayesian updating provides a (model-invariant) framework that can be used to estimate the parameters of any model. The framework allows to include information from multiple data sources for model calibration, even if the data exhibits inter-subject variability and/or experimental uncertainty.

Bayesian updating has previously been applied modelling sensorimotor learning [173], carbon dioxide storage [234] and in fisheries science [73]. It has also been recently applied to model the mechanical behaviour of passive structures in muscles (e.g., fibres [28],

tendons [162]), aortal mechanics [283].

### 1.3 State of the art in experimental studies on isometric exercise

Training our muscular system in an effective and controlled way may lead to increased mobility [57], fosters faster recovery from injuries or surgical interventions through specialised and, thus, more efficient and subject-specific training/rehabilitation programs [251, 313]. An effective exercise plan potentially lead to performance enhancement in (professional) athletes [229]. Exercise induces changes in skeletal muscles. These changes have been investigated by means of experimental studies for a long period of time. Here, the focus is on isometric exercise, therefore, we narrow the state-of-the art on exercise studies to studies on (unilateral) isometric exercise. Readers interested in experimental studies on dynamic exercise can refer to systematic reviews by e.g., [179, 269, 280, 281].

Studies, in which the training is isometric and unilateral, provide a natural way to study the influence of training by comparing the trained limb with the contralateral limb. There exists a number of studies on unilateral training of the upper extremities e.g., [54, 55, 60, 75, 78, 136, 148, 161, 168, 170, 188, 202, 214, 218, 257, 302] and the lower extremities e.g., [6, 19, 37, 65, 325] as well as the hand e.g., [43, 47, 59, 60, 76, 206, 241, 326].

Most unilateral isometric knee extension exercise (UIKEE) studies focus on neuromechanical changes by analysing EMG data e.g., [12–14, 46, 81, 110, 193, 263, 319, 320], morphological changes through monitoring muscle mass/cross-sectional area/volume e.g., [12, 13, 110, 155, 182, 193], comparison of the training effect of UIKEE with non-isometric modes of training e.g., [30, 101, 102, 155, 190, 239, 273], changes in co-activation of the synergistic muscles, e.g., [46, 306], cross-education, e.g., [193, 320], comparison of externally stimulated and voluntary exercises on the training outcome, e.g., [16, 126, 180, 222], specificity of the joint angle and it's influence at the trained as well as non-trained angles, e.g., [14, 319, 320] and metabolic changes, e.g., [118, 172, 193].

Besides the complex nature of muscle adaptation and limitations of experimental methods, small sample size of experimental studies pose a difficulty in drawing definitive conclusions on the outcome of a given training intervention. To overcome the limitation of small sample sizes of individual studies, systematic review studies are used frequently. Carlson et al. [45], Inder et al. [149] and Owen et al. [238] have investigated the implications of isometric training on the management of blood pressure by means of systematic review and meta-analyses. Munn et al. [226] and Bohm et al. [27] include isometric exercise on various muscles/muscle groups in their systematic reviews together with dynamic modes of training. They concentrated on the strength gain in the contralateral limb and the impact of the exercise on tendon stiffness, respectively. By pooling studies on the training of large muscles, Oranchuk et al. [237] focused on the longitudinal adaptation due to isometric exercise, but did not distinguish between uni-/bilateral training.

### 1.4 Thesis outline and research questions

The aim of this study is to investigate one adaptation mechanism in skeletal muscles in response to resistance exercise, namely the change in the discharge rate of motor neurons,

using a data-driven modelling approach. A modelling framework composed of four sections has been established. The framework has been set up with a focus on unilateral isometric knee extension exercise (UIKEE). This choice has been made on the basis of the simplicity of this exercise. It is easy to perform, also for sedentary subjects, since the muscle length remains constant. Furthermore, its effect on the muscle strength is straightforward to measure within a laboratory setting. Therefore ample data on the change in strength due to UIKEE is available in literature.

A number of mechanisms are responsible for the adaptation in muscles to exercise. One of these mechanisms is the neuromechanical adaptation. Neuromechanical adaptation has multiple components. In order to reduce the complexity of the problem, only one aspect of neuromechanical adaptation has been selected. Specifically, the change in the discharge rate of the motor neurons of the exercised muscle has been investigated and quantified. Chapter 2 provides detailed information on the physiology of muscles, exercise as well as exercise related adaptation mechanisms.

The suggested framework is muscle-specific. Since the exercise type has been selected as UIKEE, the focus lies on the muscles of the knee extensors. Knee extensors are composed of four muscles (see Chapter 2, Section 2.1.3). Among those, the vastus lateralis has been selected for further investigation, since it is a monoarticular muscle and ample data on its neuromechanical behaviour exists.

The framework treats the configuration of the vastus lateralis before and during/after the exercise period, which have been referred to as pre-and post-exercise states, respectively. The force output of the motor neurons of the vastus lateralis has been modelled during these states. Note that only the isometric force output has been considered in this study, therefore force output refers to the isometric force output in the following. To model the force output, the motor neuron recruitment model introduced by Fuglevand et al. [104] has been chosen.

Calibration of model parameters for each section of the modelling framework has been performed using Bayesian updating, which relies on Bayesian statistics. Therefore, an overview of Bayesian statistics and specifically Bayesian updating has been provided in Chapter 3. The Bayesian updating scheme treats models as a black-box. It requires an estimate of the range of values the model input may take. Furthermore, it requires the model output to be dictated.

Chapter 4 introduces the capabilities as well as the limitations of the motor control model by Fuglevand et al. [104] in detail.

The modelling framework in this study is composed of four separate modelling schemes. Each of these schemes build up on each other, ultimately to quantify the change in the discharge rate of the motor neurons of vastus lateralis due to UIKEE. First two schemes of the framework (in Chapter 5 and Chapter 6) deal with model parameters that are required to compute the total force output of vastus lateralis in the pre-exercise state. To compute the total force output, the discharge instances and the twitch properties of the motor neurons are required. Why and how these components are used to compute the force output has been explained in Chapter 2, Section 2.2.6.

To determine the parameter set for the discharge instance of the motor neurons at the pre-exercise state, two components are required. These are the discharge instances and the twitch properties of the motor neurons. Why and how these components are used to compute the force output is provided in Chapter 2, Section 2.2.6.

To set up the pre-exercise state of the muscle, model parameters that describe the discharge instances of vastus lateralis are first required. The input parameters of the motor neuron recruitment model responsible for generating the discharge instances are determined in Chapter 5. As stated earlier, the input parameters are calibrated against experimental data using Bayesian updating. The calibration has been performed against available experimental data on the mean discharge rate of vastus lateralis. Data collected from healthy, young subjects are used for this purpose.

In Chapter 6, twitch properties of the motor neurons at the pre-exercise state are determined. Possible configurations of how the twitch properties are distributed for each motor neuron have been generated based on experimental data on human muscles. Using the set of input parameters determined in Chapter 5 and the motor neuron recruitment model, the force output is computed for each configuration of the twitch properties. The force output obtained as a result of the model runs provide us the necessary model outputs. To determine the configuration of twitch properties that are specific to vastus lateralis, the model output is calibrated against the force output of vastus lateralis that has been measured experimentally. The set, which yields the most accurate force output has been selected by Bayesian updating.

Upon the completion of Chapter 5 and Chapter 6, we have now obtained the pre-exercise state of the motor neurons. The next step is to determine their post-exercise state. As stated earlier, there exist ample data on the change in muscle strength in response to UIKEE. The change in strength due to UIKEE has been used as calibration data to determine the post-exercise state, which makes up the third scheme of the modelling framework. A systematic approach has been employed to gather data from literature on the change in strength due to UIKEE. This data has then been modelled longitudinally over trained weeks. How the data have been collected and the set-up the longitudinal model of the strength change are provided in Chapter 7. Note that the work presented in this chapter is a collaborative effort among the author of this dissertation, Ms. Svenja Seide from the University of Heidelberg, Mr. Ismail Bayram and Prof. Hayri Ertan from Technical University of Eskişehir, Dr. Leonardo Gizzi and Prof. Oliver Röhrle from the University of Stuttgart.

The last scheme of the modelling framework deals with the change in the discharge rate of the motor neurons of vastus lateralis during the post-exercise state. Using the longitudinal model of the change strength from Chapter 7 as calibration data, parameters of the motor neuron recruitment model have been determined. Using these parameters, we were able to quantify the change in the discharge rate of vastus lateralis, such that the muscle can generate force over trained weeks as predicted in the longitudinal model of the strength change.

Finally, the results obtained from all modelling schemes employed in this study have been discussed in Chapter 9. The novelties of the schemes as well as their limitations have been explored. Suggestions for the implications for future research have been also presented.

Below is a list of the research questions we tried to answer in each modelling scheme and their aims:

**Aim 1:** We aim to provide methods and schemes to model the force output of the motor units of vastus lateralis in the pre-exercise state. Particularly, we focus on the

following research objectives.

Research Question 1 (Chapter 5): What is the optimal parameter set to describe the discharge instances of the pre-exercise state for the motor unit pool of the vastus lateralis?

Research Question 2 (Chapter 6): What are the contractile properties of the motor units of vastus lateralis?

**Aim 2:** We aim to build a time-dependent model predicting the change in isometric strength of knee extensors due to unilateral isometric exercise exploiting experimental data from literature.

Research Question 3a (Chapter 7): Based on which criteria should the experimental studies be chosen to obtain a homogeneous data set that focuses only on unilateral isometric exercises?

Research Question 3b(Chapter 7): How can the data set be modelled longitudinally?

**Aim 3:** We aim to quantify the influence of unilateral isometric knee extension exercise on the discharge rate of the motor neurons of the vastus lateralis.

Research Question 4 (Chapter 8): How much should the discharge rate of motor neurons in vastus lateralis should increase to attain the gain in isometric strength, which has been modelled in Scheme 3, i.e., due to unilateral isometric knee extension exercise?

## 1.5 List of publications

Below is a list of journal papers and proceedings related to this doctoral project:

### Journal paper

Altan, E.; Seide, S.; Bayram, I.; Gizzi, L.; Ertan, H.; Rhrle, O.: A Systematic Review and Meta-Analysis on the Longitudinal Effects of Unilateral Knee Extension Exercise on Muscle Strength. *Frontiers in Sports and Active Living* **2** (2020), 169, ISSN 2624-9367

### Conference proceedings

1. Saini, H.; Altan, E.; Ramasamy, E.; Klotz, T.; Gizzi, L.; Röhrle, O.: Predicting skeletal muscle force from motor-unit activity using a 3D finite element model. *Proceedings in Applied Mathematics and Mechanics* (2018), e201800035
2. Altan, E.; Zöllner, A.; Avc, O. ; Röhrle, O.: Towards modelling skeletal muscle growth and adaptation. *Proceedings in Applied Mathematics and Mechanics*(2016), 921924

## Presentations at conferences

### Oral presentations

1. Predicting twitch properties of a motor unit pool. *9<sup>th</sup> International Congress on Biomechanics*. Eskişehir, Turkey, September 2018
2. Estimation of the individual motor unit properties in a motor unit pool using a motor unit recruitment model. *XXII Congress of the International Society of Electrophysiology and Kinesiology* Dublin, Ireland June 2018
3. Modelling voluntary contraction of knee extensors using a motor unit recruitment model (Presentation at a workshop). *XXII Congress of the International Society of Electrophysiology and Kinesiology*, Dublin, Ireland, July 2018
4. Modelling the growth of skeletal muscles *GAMM Annual Meeting* Munich, Germany March 2018
5. Modelling the adaptation of skeletal muscles in response to isometric exercise *VII. International Congress on Computational Bioengineering*, Compigne, France, September 2017

### Poster presentations

1. Modelling isometric-exercise-induced skeletal muscle adaptation *8<sup>th</sup> World Congress of Biomechanics* Dublin, Ireland, July 2018
2. Modelling of exercise-induced adaptation in skeletal muscles *2nd International Conference on Simulation Technology 2018* Stuttgart, Germany, March 2018
3. Modelling isometric exercise induced neural adaptation in skeletal muscles *SimTech Status Seminar*, Bad Boll, Germany, December 2018

## 2 Anatomical and physiological background

### 2.1 Skeletal muscle structure and function

#### 2.1.1 From the cell to organ - the hierarchical structure

Muscles have tendinous origins and insertions. These attach to bones at either end. Between the insertions is the muscle belly, which is composed of thousands of individual muscle fibers [44]. A three-level network of collagenous connective tissue surrounds the muscle. The outermost tissue covering the entire muscle is known as the epimysium. Fascicles, composed of multiple muscle fibres, are surrounded by the perimysium. Lastly, endomysium envelopes individual muscle fibres [87]. Each of connective tissue layer is interconnected to the next one [44] (see Fig. 2.1).

Muscle fibres are also known as myofibrils. Myofibrils are units responsible for the contraction and relaxation of the fibre. They are aligned in parallel to each other and run through the entire muscle length [316]. Myofibrils are separated from each other by mitochondria, sarcoplasmic reticulum (SR) and transverse tubular systems (T-tubules). The cell membrane sarcolemma encloses these units and is an excitable membrane [87, 204]. T-tubules are aligned transversely to the long axis of fibres whereas the SR is an axial system of tubules and vesicles, which acts as a signal-transducing apparatus that triggers contraction together with the T-tubular system [87].

Skeletal muscles have a striated structure. This striation is caused by the dark and light bands of the myofibrils, namely the A-band (A referring to anisotropic) and I-band (I referring to isotropic). A-bands contain thin and I-bands contain the thick filaments [204].

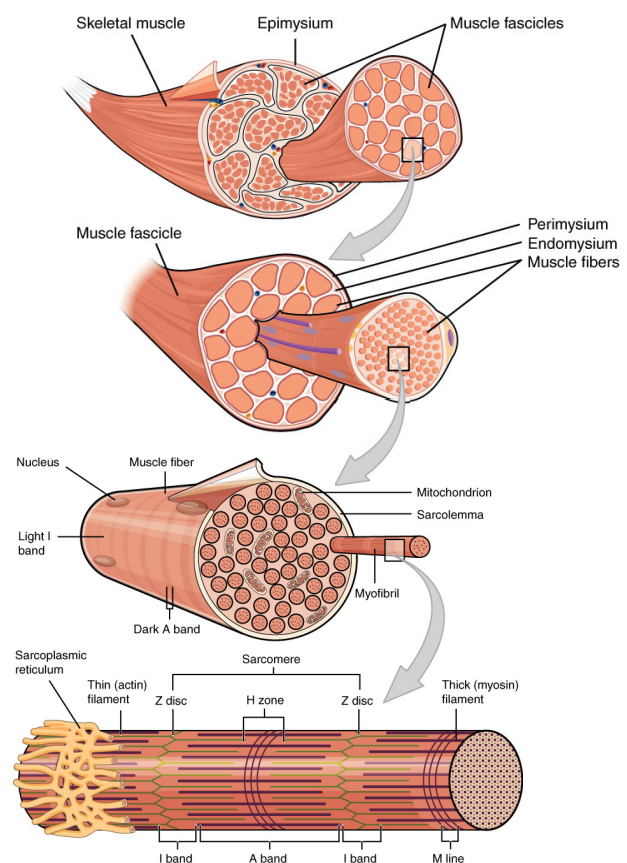


**Figure 2.1:** The hierarchical skeletal muscle structure, adapted from [236].



Thin filament has a high composition of actin, but also contains tropomyosin and troponin proteins. Each thin filament is composed of two helical strands of fibrous actin that have two-stranded and globular proteins, tropomyosin and troponin respectively, attached to them. Tropomyosin and troponin are also known as regulatory proteins as they facilitate the interaction of actin and myosin [87].

Thick filament is composed of myosin and other myosin-binding proteins. Myosin molecule is a long, helical structure and ends with two globular heads. Each globular head contains an adenosine triphosphate (ATP) binding site, an actin-binding site and another site for hydrolyzing ATP [87].

## 2.1.2 Types of contractions

There are two main modes of muscle contraction, which are dynamic and static modes (see Fig. 2.2). During dynamic contractions, the muscle lengthens (eccentric contraction) or shortens (concentric contraction), i.e., the distance between the distal and proximal ends of the muscle changes. Such contractions moves a given joint by changing the joint angle.

During a static contraction, the overall length of the muscle and its tendons do not change [87]. The static contraction mode is also described as isometric, where “iso” means constant and “metric” means length in Greek [87] At the sarcomere level, true isometric state is attained after the contractile structures have extended the elastic components of the sarcomere to an equilibrium state [129].

In isometric contraction against an external resistance, the external torque can easily be measured and is equal to the resisting force multiplied by the lever of this force in relation to the axis chosen. To illustrate, knee extension strength might thus be defined as the maximum external torque of the quadriceps muscles [121].

## 2.1.3 Knee extensors

Quadriceps femoris (Quadriceps extensor) includes four muscles on the front of the thigh (see Fig. 2.3). It is the great extensor muscle of the leg and forms a large fleshy mass that covers the front and sides of the femur. It is subdivided into separate portions. The portion occupying the middle of the thigh taking its name from its straight course, is the Rectus femoris. The other three are connected to the body of the femur. The portion on the lateral side of the femur is known as the Vastus lateralis, the one covering the medial side is the Vastus medialis and the one in the front is the Vastus intermedius [115]. The Quadriceps tendon inserts into the proximal aspect of patella (the kneecap). It continues distally past the patella as the patellar tendon [192].

The study by Handsfield et al. [125] shows that the vastus lateralis for 24 young, healthy subjects has the highest volume within the knee extensor muscles followed by vastus medialis, vastus intermedius and rectus femoris. This order has also been reported in the same way in the study by Ward et al. [314], but the measurements have been taken from cadavers.

All four muscles of the quadriceps contribute to the force output during knee extension. Due to the differences in their physiological cross-sectional area (PCSA) and line of action, contribution of each muscle to the overall force output is uneven. As it is not possible

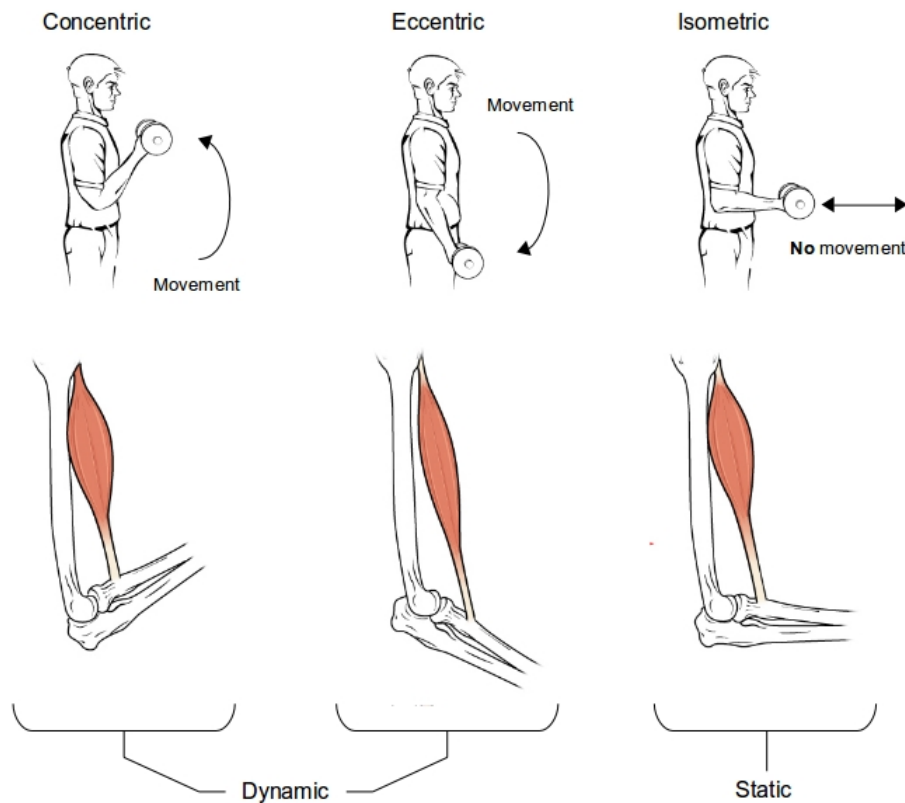


**Figure 2.2:** Dynamic and static modes of contraction. Concentric and eccentric contractions belong to the dynamic mode of contraction, whereas the isometric contraction is a static mode (adapted from [236]).

to measure the force output of a living subject, in-vivo, the contribution of each muscle cannot be measured directly. There exist some methods to estimate the contribution of each muscle, by using electromyography (EMG) data based on the activity level of each muscle and by using PCSA of each muscle. To illustrate, Elias et al. [80] reports that the force output of Vastus lateralis takes up 38% of the total knee extensor force output.

## 2.2 Voluntary muscle contraction

### 2.2.1 Motor neuron

Motor neurons are neuronal cells, which are located in the central nervous system. They can be divided into two types depending on the identity of the target they innervate. One type is the upper motor neurons that originate from the cerebral cortex in the brain and lower motor neurons. The second type describes the lower motor neurons, which are located in the brain stem and the spinal chord [296]. This study is concerned with alpha-motor neurons, therefore, only clusters and structures related to alpha-motor neurons are described in the following.

Spinal motor neurons are located in the ventral horn of the spinal cord (see Fig. 2.6 (b)). They control skeletal muscles. They form the ultimate component of the neuronal

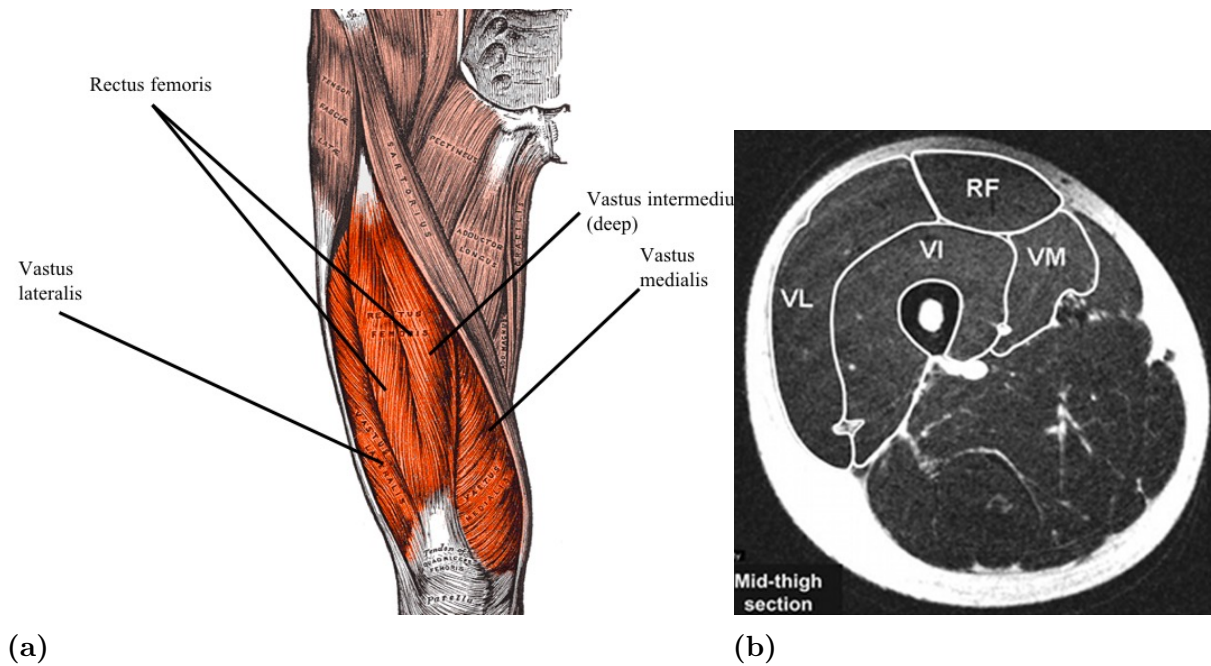


**Figure 2.3:** (a) Muscles of the frontal upper part of the lower limb, i.e., the quadriceps femoris (adapted from [115]). (b) Cross-section MRI scan of the upper limb. Knee extensors are marked with the abbreviation of the respective muscle, where RF: rectus femoris, VI: vastus intermedius, VL: vastus lateralis, VM: vastus medialis (from [15], with permission).

circuitry as there exists no alternative way to transfer commands from the processing centres in the CNS to the effector (skeletal) muscles in the periphery (within a distance from the centre). Axons of motor neurons can extend several meters in mammals, which makes them the longest known cell type.

Lower motor neurons are classified into three groups according to the type of target they innervate, namely branchial, visceral, and somatic motor neurons. Somatic motor neurons exclusively control skeletal muscles and are further categorized into three types according to muscle fibre type they innervate. These are alpha, beta and gamma motor neurons (see Fig. 2.4 for an overview) [296].

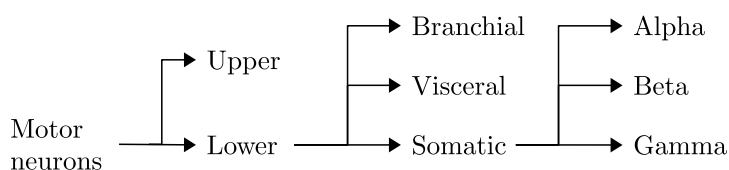


**Figure 2.4:** Types of motor neurons

Skeletal muscles contain extrafusal fibers, which are responsible for generating the force output, and muscle spindles and they provide proprioceptive information on the position and the state of extension of the muscle (see Fig. 2.5). Alpha-(alternatively,  $\alpha$ ) motor neurons innervate extrafusal fibres. These have large cell bodies and well-characterized neuromuscular endings (see Fig. 2.6 (a)). They receive direct monosynaptic input from sensory neurons, which minimizes the delay of the response of the spinal reflex circuitry [296].

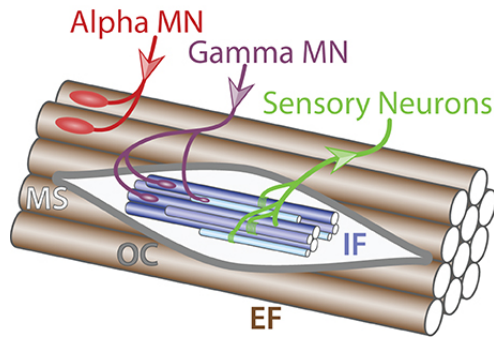


**Figure 2.5:** Types of somatic motor neurons and the fibres they control. Here abbreviations denote, MN: motor neuron, MS: muscle spindle, OC: outer capsule, EF: extrafusal muscle fibres, IF: intrafusal fibres [from [296], open access under the Creative Commons Attribution License.]

Somatic motor neurons form functional groups, which connect to a unique muscle target. These groups are known as motor neuron pools [296]. The size of the motor neuron pool of a muscle denotes the total number of motor neurons innervating the muscle. This number may go up to several hundreds and is muscle-specific. Although each motor neuron innervates one type of muscle fibre, the motor neurons in a pool innervates different fibre types.

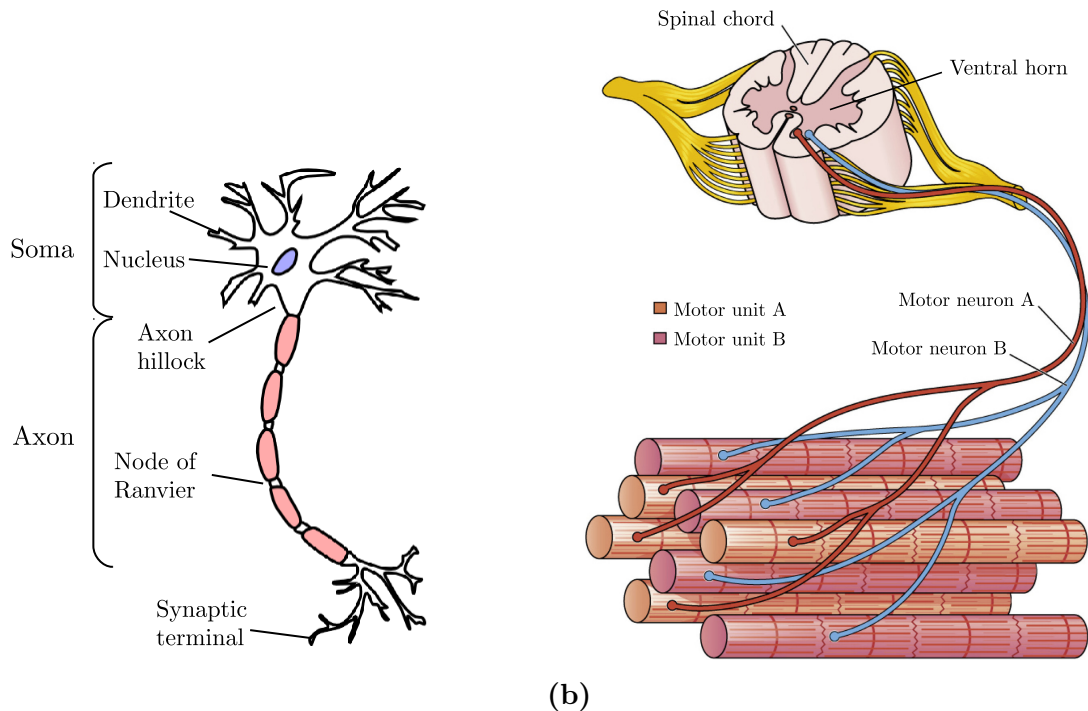


**Figure 2.6:** (a) The structure of a motor neuron (from tchol.org/, labels are added). (b) The motor unit [(minimally) adapted with permission from [44]].

### 2.2.2 The motor unit

As cited in Clark [53], the motor unit as a term has first been introduced in Sherrington [287]. It was defined as follows:

*The term ‘motor-unit’ includes, together with the muscle-fibres innervated by the unit, the whole axon of the motor neuron from its hillock in the perikaryon down to its terminals in the muscle.*

Alternatively, the motor unit is composed of an alpha-motor neuron together with the bunch of muscle fibres it innervates [53, 68, 187, 293]. An action potential travelling from the soma of the  $\alpha$ -motoneuron, along its axon reaches its terminal branches. These branches are connected to a muscle fibre at the neuromuscular junction [293] (see Fig. 2.6 (b)).

Motor units are categorized according to the size of their axons as well as its cross-sectional area and the number of fibres they innervate. Smaller motor units are composed of motor neurons with smaller axon diameter. They innervate less number of muscle fibres, which are smaller in size, in comparison to large motor units.

The number of fibres a motor unit innervates is known as the innervation ratio. Data from humans are quite difficult to obtain, as the measurement of the innervation ratio requires counting the motor neurons and the innervated muscle fibres [276]. It is estimated in human bodies the innervation ratio may go up to the order of thousands depending on the muscle.

### 2.2.3 Fibres of motor units

The first systematic description of the differences in fibre types is often attributed to the work of Louis-Antoin Ranvier, suggesting that mammalian muscles differ in speeds of contraction [276, 290]. Histological and biochemical analyses of biopsy samples of skeletal muscles help to identify differences in morphological, contractile, and metabolic properties of muscle fibres [330].

Myofibrillar proteins of sarcomeres of striated muscles are known to show wide molecular heterogeneity, so that they may exist in several <sup>1</sup>isoforms. They are also known to be interchangeable, which means that the isoforms may convert to each other.

One such myofibrillar protein is myosin, which is characterised according to its myosin heavy chain (MHC) isoform content. MHC is mainly responsible for power generation and velocity of muscle shortening [278, 297]. In adult human skeletal muscles mainly three isoforms of MHC exist. These are namely MHC-I, MHC-IIA and MHC-IIX (sometimes also referred to as MHC-2D)[278]. Fibres are categorized according to the MHC type they possess.

Different fibre types have a wide variation between their contractile properties [297]. Furthermore, their morphological characteristics are also different. To illustrate, type I fibres contract slower, are smaller in cross-sectional area, recruited earlier and are more fatigue-resistant than type II fibres. How the contractile properties, e.g., contraction speed, force output, and morphological characteristics compare according to fibre type are outlined in Table 2.1.

It is known that each motor neuron innervates multiple fibres, which are all of the same type. Using this information, motor neuron type can be determined based on the fibres they innervate. One common method is histochemical staining for glycogen of the muscle sample and stimulating individual, isolated motor neurons repetitively. Glycogen depleted fibres belong to the stimulated motor neurons. After identifying the active motor fibres, it is possible to identify their characteristics. Being of invasive nature, these methods, however, cannot be directly applied to investigate human skeletal muscles [276].

---

<sup>1</sup>Isoform is defined as “any of two or more functionally similar proteins that have a similar but not an identical amino acid sequence” [217]

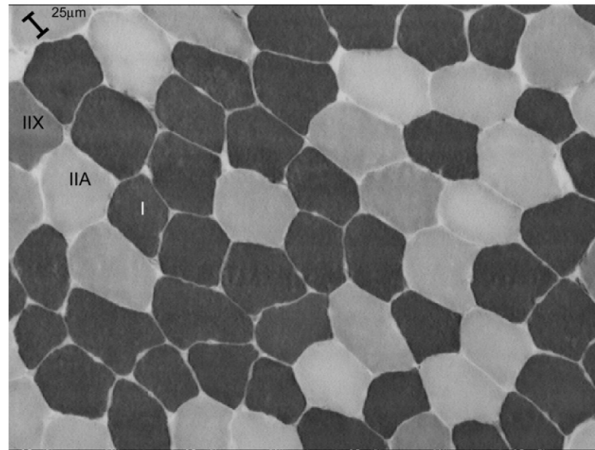


**Figure 2.7:** Photomicrograph image of a muscle biopsy cross section stained for myofibrillar ATPase. The sample is obtained from the middle portion of vastus lateralis. Type I fibres are marked with dark grey, type IIa with light grey and type IIx with an “intermediate” hue of grey [from Aagaard et al. [2], with permission].

**Table 2.1:** Comparison of the fatigue resistance, speed of contraction, force output and the time it takes the fibre to reach the maximum force output (time-to-peak force) of the pure fibre types (type I, IIa, IIx).

<b>Fatigue resistance</b>	type I	>	type IIa	>	type IIx
<b>Contraction speed</b>	type I	<	type IIa	<	type IIx
<b>Force output</b>	type I	<	type IIa	<	type IIx
<b>Time-to-peak force</b>	type I	>	type IIa	>	type IIx
<b>Size</b>	type IIx	>	type IIa	>	type I
<b>Recruitment order</b> (first to last)	type I	,	type IIa	,	type IIx

### 2.2.4 Twitch properties of motor units

Force generating capabilities of individual motor units are significant for the estimation of the force output of the entire muscle [41]. To estimate the motor unit force, information on the motor unit’s discharge instances as well as its twitch response is required.

When the potential difference across the plasma membrane is depolarized beyond a given threshold, fibres and motor neurons generate action potentials. This process follows the “all or none” rule, since increase in the stimulus does not change the shape of the action potential (see Fig. 2.12) [163].

The force-time response of a motor unit to a single presynaptic action potential is called a twitch (see Fig. 2.8) [87, 141, 187]. It is the simplest case of the measurement of mechanical and electrical recruitment of a motor unit.

The twitch response of a motor unit can be modelled as a “second-order damped system” [104]. For this, two components of the twitch response are required, which are the the peak twitch force time required to reach that peak twitch force, a.k.a. time-to-peak.

Depending on its type, the twitch response of motor units can have a relatively long time to peak force (a slow twitch, see Fig. 2.8 (a)) or a short time to peak tension (a fast twitch, see Fig. 2.8 (b)). The peak twitch force and the time-to-peak are inversely proportional, i.e., a slow twitch response generated less force than a fast twitch force [276].

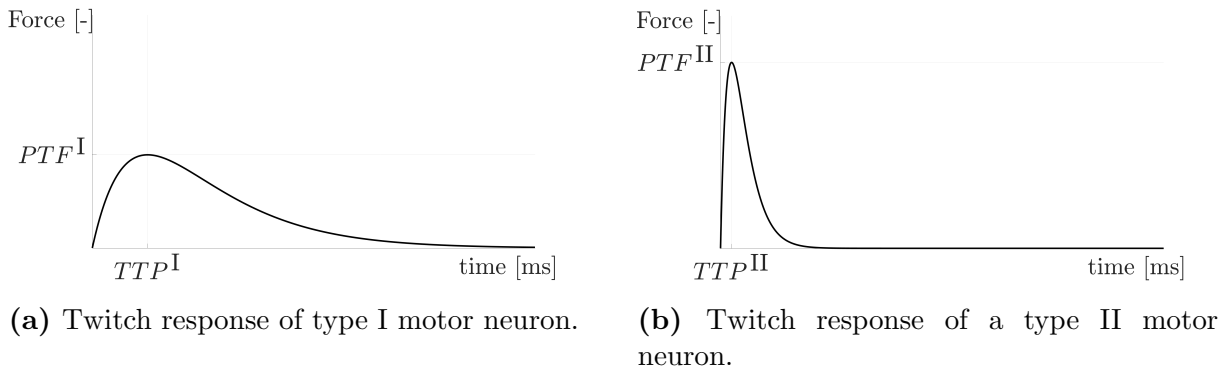


**Figure 2.8:** The twitch response of type I and type II motor neuron. Here,  $PTF$  denotes the peak twitch force and  $TTP$  time required to reach the peak twitch force. Note that  $PTF^I < PTF^{II}$  and  $TTP^I > TTP^{II}$ .

Different motor units vary greatly in force generating capacity. A given motor unit pool may contain motor units that can produce a wide range of peak twitch force. The difference/ratio between the highest and lowest peak twitch force of motor neurons of human muscles are thought to be 100-fold or more [83, 216]. However, data on the peak twitch force is sparser in comparison to the data available on the time-to-peak.

When the data on the time-to-peak is assessed, the range of values measured for a given muscle is of 4-5 fold [83]. Mean values measured from a number of human muscles range from 45 to 80 ms (see Fig. 2.9).

### 2.2.5 Motor unit recruitment

The orderly recruitment of motor units is regarded as one of the most robust principles of neurophysiology [82, 83]. The first observations regarding this principle was made by Denny-Brown & Pennybacker [69] when they observed that "... a particular voluntary movement appears to begin always with discharge of the same motor unit. More intense contraction is secured by the addition of more and more units added in a particular sequence. ... The early motor units in normal gradual voluntary contraction are always in our experience small ones. ... The larger and more powerful motor units, each controlling many more muscle fibres, enter contraction late."

This suggests that during a given contraction, the force output is increased as more motor units are recruited following a fixed sequence, namely from the smallest motor unit to the largest. Henneman [135] suggests that this order was dictated by the surface area of the soma and dendrites of the motor neurons. Knowing that type I motor units are smaller in size than type II motor units, motor units recruited at the beginning of any contraction are of type I. This principle is known as "(Henneman's) size principle" and is defined in Henneman [135] as:

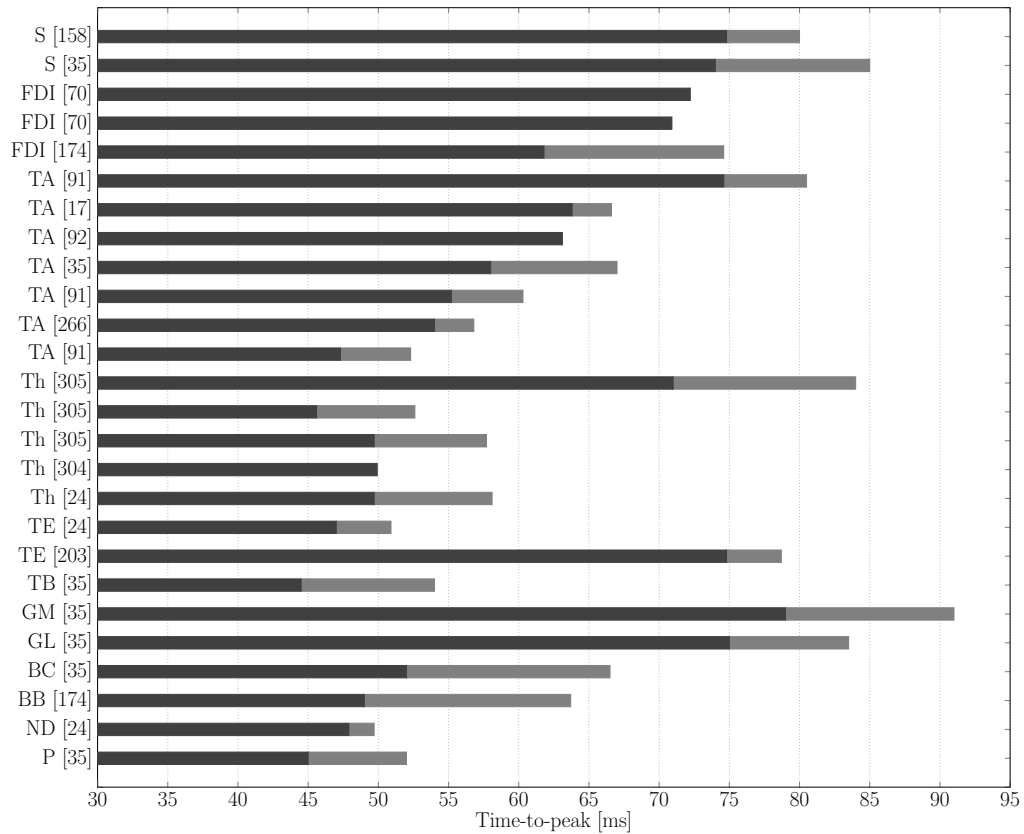


**Figure 2.9:** Mean (depicted in black) and standard deviation (depicted in grey) of the time-to-peak data reported in experimental studies. Here, VL: vastus lateralis, S: soleus, FDI: first distal intermedius, TA: tibialis anterior, Th: thenar, TE: toe extensors, TB: triceps brachii, GM: gastrocnemius caput mediale, GL: gastrocnemius caput laterale, ND: nasal distalators, P: platysma.

*The amount of excitatory input required to discharge a motoneuron, the energy it transmits as impulses, the number of fibres it supplies, the contractile properties of the motor unit it innervates, its mean rate of firing and even its rate of protein synthesis are all closely correlated with its size. This set of experimental facts and interrelations has been called the size principle.*

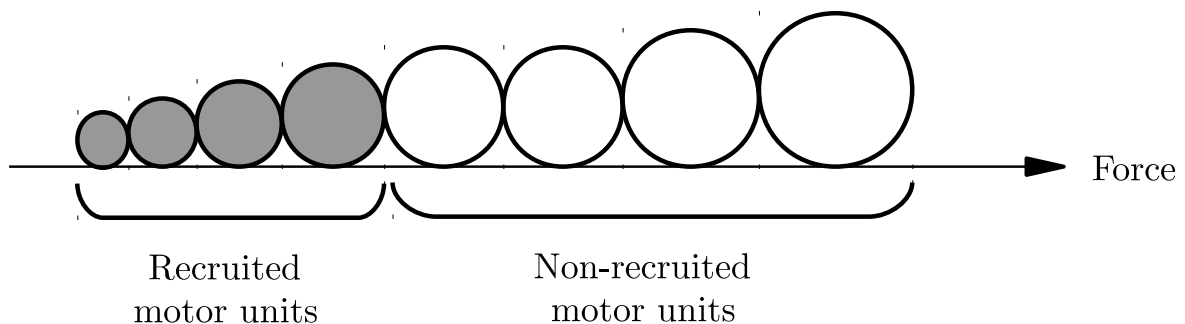


**Figure 2.10:** Representation of the size principle. Each bubble represents one motor unit and the size of the bubbles, the size of the motor unit. Recruited motor units are colored in gray [adapted from [100]].



## 2.2.6 Force output

An action potential travels from the soma of the  $\alpha$  motor neuron, along its axon to its terminal branches. Each of the terminal branches of motor neurons are connected to a fibre [293]. When the action potential reaches the neuromuscular junction, motor neurons release the neurotransmitter, acetylcholine. When acetylcholine binds to the acetylcholine receptors on the muscle fibre, an action potential propagates along the muscle fiber starting from the middle and progressing in both directions. This initiates the motor unit, and hence, muscle contraction [293].

Excitation-contraction coupling describes the process, when a neural activation signal triggers the release of calcium by the sarcoplasmic reticulum [196]. This initiates the muscle contraction as it causes sarcomeres to shorten [23, 196].

Excitation-contraction coupling follows these steps:

1. An action potential travels along the muscle fibre, T tubules, and then the sarcoplasmic reticulum (SR).
2. The voltage-gated calcium channels<sup>2</sup> open. This causes the release of calcium through the ryanodine calcium-release channel in the SR.
3. Calcium increases in the cytosol and then binds to troponin.
4. Calcium bound to troponin yields a conformational change of the troponin-tropomyosin complex. This change exposes the actin-binding site to myosin.
5. Myosin binds to actin. This binding is caused by the hydrolysis of ATP and provides the energy for the movement by releasing ADP and phosphate.
6. Myosin detaches itself from actin to bind to another molecule of ATP.
7. Calcium is taken back to the SR by the ATPase pump.
8. Decreased cytosolic calcium concentration causes the troponin-tropomyosin complex to glide back and cover the myosin-binding site. The muscle then relaxes [23].

A single action potential coming from the  $\alpha$ -motoneuron generates the motor unit potential. After a delay caused by the excitation-contraction coupling, the motor unit produces a single twitch. Twitch response of motor units are already discussed in Section 2.2.4 (see Fig. 2.8).

Successive trains of stimuli delivered to a motoneuron causes the twitches to summate. This summation, however, is not linear (see Fig. 2.11). The difference in the force output due to a train of stimuli versus the twitch force produced by a single pulse is a function of rate of stimulation and the history of the stimulation [137, 293]. Summation of the individual motor unit force output yields the total force output of the muscle.

Upon maximal voluntary contraction of a muscle under isometric conditions (see Section 2.1.2), its isometric strength can be determined. This quantity is called as a maximum voluntary contraction (MVC), which is defined in Gandevia et al. [106] as a voluntary contraction that a subject believes to be maximal while providing continuous feedback and encouragement.

---

<sup>2</sup>Voltage-gated ion channels are a class of transmembrane proteins. They are activated in response to changes in electrical potential difference across the cell membrane when it opens [256]

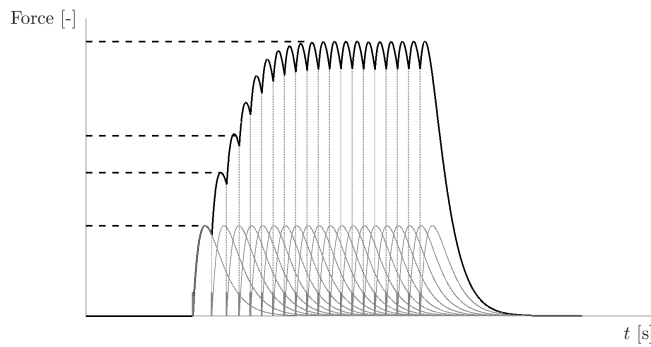


**Figure 2.11:** Summation of twitches depicting the force generated by a single motor unit. Black line depicts the motor unit force, grey upright lines denote the firing instances of the motor unit and the grey curves depict individual twitch response of the motor unit.

### 2.2.7 Measuring motor unit activity

When the potential difference across the plasma membrane is depolarized beyond a given threshold, fibres and motor neurons generate action potentials [163]. “*The currents associated with the muscle fibre action potential cause changes in the potential difference within the muscle that can be measured with electrodes*” [87]. The reading of this potential difference is known as an electromyogram (EMG). It represents the electrical activity in muscle fibres in response to the activation received from the motor neurons [87].

It is not possible to place electrodes inside the muscle fibre, on either ends of the fibre, to measure the potential difference of the fibre membrane. Instead, during a (surface) EMG recording, electrodes are placed outside the muscle, on the skin.<sup>3</sup> Therefore the measurements obtained from an EMG recording describe the extracellular field potentials associated with the currents that underlie muscle fibre action potentials [87].

The motor unit action potential is the summation of the extracellular potentials of the muscle fibre action potentials of a motor unit. The shape of the wave is dictated by the inherent properties of the motor unit as well as the spatial relationships between the electrode and individual muscle fibres [163]. Multiple motor unit action potentials recorded within a small time interval is known as a motor unit action potential train.

As more motor units are recruited during a contraction, the amplitude of the EMG signal increases [131]. This increase is attributed to an increase in the number of recruited motor units as well as their discharge rate, which determine the electrical activity in a muscle. These two factors also determine the muscle force. Therefore, a direct relationship between EMG and exerted force is expected [216].

On the other hand, a direct association with motor unit activity and the surface EMG signal would not be accurate as the EMG signal amplitude is further influenced by individual fibre potential, MU discharge synchronization<sup>4</sup> and fatigue. Therefore, the resulting EMG signal at a given force level only provides a global measure for the muscle activity [131].

The interpretation of the EMG signals is challenging, mainly due the shape of the surface-detected motor unit action potential trains. Their shapes are determined by the number and anatomical characteristics of the muscle fibres, contraction intensity, properties of the electrodes [131].

<sup>3</sup>Electrodes may also be placed inside the muscle, which is known as “intramuscular EMG”. However, here the focus is on surface EMG.

<sup>4</sup>Synchronization describes the simultaneous firing of different motor units

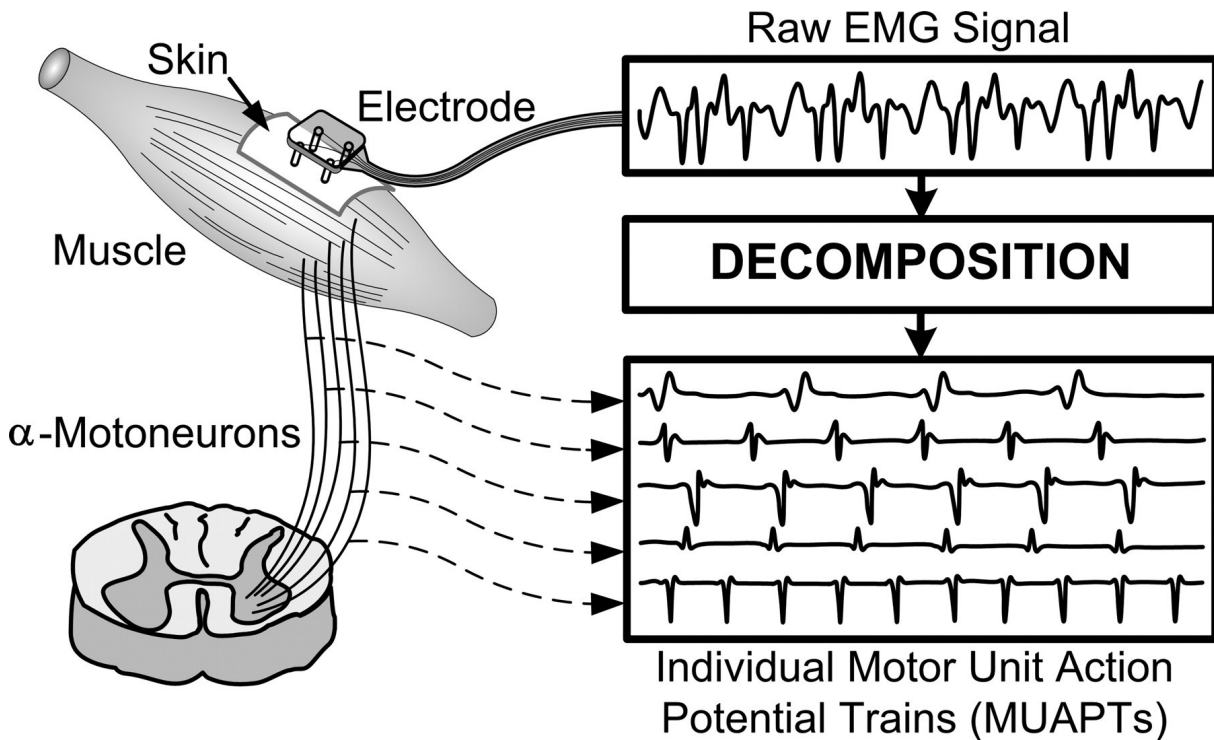


**Figure 2.12:** Representative scheme of EMG decomposition [from De Luca et al. [61] with permission].

### Surface electromyogram

Electrodes used for the surface EMG and the motor units are separated by biological tissue, which can be considered as a passive volume conductor. The properties of the volume conductor has a major influence on the features that are detected in the surface EMG signals. As the distance between the travelling wave of the motor unit potential and the electrode increases, the contribution of the wave rapidly decreases. As a result, motor units that are closer to the electrodes dominate the measured EMG signal [293].

Motor units are arranged in increasing size from deeper to the superficial portion of the muscle. Therefore, smaller/slower motor units lie deeper in the muscle and larger/faster motor units lie closer to the superficial portion of the muscle. Owing to the size principle, the majority of the motor units recruited early in the contraction would therefore be located deeper in the muscle. Therefore, EMG signal recorded from a given portion of the muscle would not necessarily be representative of the entire muscle, but is rather dominated by larger/faster motor units [293].

Changes in the neural activity of skeletal muscles are commonly quantified through surface EMG [117]. However, the amplitude of the EMG (surface or intramuscular depending on the method) measured after strength training is known to show contradictory results (see the data on the changes in EMG signal output after unilateral isometric knee extension exercise in Fig. 2.15) [65, 78]. This discrepancy in the EMG data is said to occur due to shifts in the location of electrodes, altered extracellular volume and/or os-

molarity<sup>5</sup>, changes in subcutaneous fat and skin temperature, as well as differences in phase cancellation following weeks of training [1, 117].

The raw EMG signal obtained during an experimental measurement, is composed of superposed motor unit action potentials detected from multiple motor units. To obtain individual motor unit action potential trains, the raw signal needs to be separated [97, 216].

### Measuring twitch properties of motor units

Contractile properties of individual motor units can be measured either by artificially activating motor axons or during voluntary contraction by means of spike-triggered averaging [91]. However, experimental measurements of the single twitch of individual motor units can still be most accurately measured through selective, invasive electrodes (e.g., intramuscular EMG). Therefore measuring the properties of the twitch response of the entire motor unit pool of skeletal muscles poses a challenge [89].

During an intramuscular EMG recording, needle or wire electrodes are inserted into the contracting muscle record. These are able to record individual motor unit action potentials. Depending on the type and location of the electrode used, the recorded action potentials can be the result of the activity of a small (1–3), moderate (15–20) or large (> 20) number of muscle fibres [215].

Spike-triggered averaging is a method to study the contractile properties of motor units. The method was first introduced by Buchthal and Schmalbruch in 1970 to measure the time course of the force response during a single twitch for seven different muscles [50].

The action potentials from a single motor unit firing at a low frequency is detected by an intramuscular needle electrode [50]. These action potentials are used as the spike triggers. When there is no synchronized firing of other motor units, the random background force fluctuation will be averaged to zero and the force signal associated with the triggering motor unit can thus be extracted. This commonly requires averaging of up to several hundred spikes Chan et al. [50].

The technique can be applied at low firing frequencies, thus at low levels of voluntary contractions. Furthermore, the contractions are non-physiological as the subjects are asked to maintain a constant firing rate of the measured motor unit using special feedback techniques [216].

The spike-triggered averaging technique is, however, significant, since it is the only method, which can be used to examine the twitch properties of single motor units activated during voluntary recruitment. This further allows to correlate the twitch properties of the motor units with their recruitment and derecruitment thresholds Chan et al. [50], Merletti et al. [216]. Later in this thesis (see Chapter 6), data on the contractile properties of motor units obtained as a result of spike-triggered averaging are used to determine the contractile properties of the entire motor unit pool of vastus lateralis.

---

<sup>5</sup>Osmolarity is “the number of ionic species in molarity that has a characteristic range depending on the species examined” [105].

## 2.3 Adaptation mechanisms in skeletal muscles

### 2.3.1 Overview

Properties of skeletal muscles are known to alter when there is a change in the level of muscle activity [196]. Muscle activity can be increased in a sustained/chronic manner by means of exercise with an aim to improve muscle function. There exist a variety of exercise types, each causing different properties of muscles to change, i.e., adapt.

Exercise can most generally be categorised into resistance and endurance type of exercise. Resistance exercise, also known as strength training, is composed of movements exerted against an obstacle. In resistance training, contractions are exerted against a high-resistance, but for a small number of repetitions, e.g., 8–12 times [228, 276]. Endurance exercise, as the name suggests, aims to improve the endurance of the trained muscle. Some common examples for endurance training are swimming, marathon running and cycling. Contrary to resistance exercise, contractions of the trained muscle are exerted against a low-resistance with a higher number of repetitions [277].

This thesis investigates the changes set forth due to resistance training, therefore, changes caused by endurance exercise will not be elaborated. The reader is referred to an early review by Holloszy & Booth [143] on the biochemical changes caused by endurance training and the comprehensive review by Joyner & Coyle [157], which explains the key factors in the performance output due to endurance exercise and the mechanisms responsible for the improvement in muscle function.

### 2.3.2 Principles of training

The following sections will outline basic principles of training, introduce isometric training and the corresponding changes in muscle properties when isometric training is . The modelling schemes suggested in this thesis in the following chapters aim to investigate the changes caused by a specific type of isometric resistance training. Therefore, although changes caused by resistance training due to both dynamic and static modes of resistance training will be introduced, the focus will lie on isometric resistance training,

#### **Overload and reversibility**

According to the principle of overload, the level of training must exceed what the system (e.g., cardiovascular system) or tissue (e.g., skeletal muscle) is accustomed to for the particular exercise to be effective. It is therefore important to increase the training load progressively to observe the desired improvement in muscle function. For this, the intensity, duration and the frequency of the training sessions should be systematically improved. When the overload is removed, i.e., training is stopped, the system/tissue returns to its initial state in time, which is described by the principle of reversibility [252].

#### **Training specificity/task specificity**

The form of training is known to be highly influential to induce changes observed in the muscle. This is due to a phenomenon known as training, or in some cases, task specificity. Adaptations in the trained muscle(s) is most evident when the training form

and the measurement overlaps as the training effect is specific to the muscle involved in the activity as well as, but not limited to, the contraction type [107, 225, 252]. This is thought to be caused by the neuromuscular system optimizing the primarily the practiced movement Bawa [18].

Among one of the many experimental studies, training specificity is shown in Bandy & Hanten [14]. In this study, three subject groups were trained with UIKEE at three different knee angles. Increase in isometric strength is measured from 15–105 degrees of the knee. Highest increase in isometric strength is observed at the knee angle the subject groups trained at.

Isometric exercise trains the isometric voluntary contraction. In isometric exercise, the training form and the training output are the same. This allows to further simplify the complex nature of exercise one step further.

### Cross-education

The term contralateral is used to describe the opposite side of a body part. When a muscle/muscle group is trained unilaterally, the muscle(s) contralateral to trained side is untrained. Even though the contralateral muscle(s) do(es) not take part in unilateral training, changes observed in the trained muscle(s) are also evident, though at a lesser extent, in the contralateral muscle(s). This phenomenon is known as "cross-education" [107, 252].

### 2.3.3 Isometric resistance training

The muscle being trained during a resistance exercise bout may contract eccentrically, concentrically or isometrically (see Section 2.1.2). Resistance training with eccentric or concentric contractions are referred to as dynamic training and bouts composed of isometric contractions are known as static training.

In comparison to dynamic exercises, static exercises are simpler to execute. The reason is that isometric contraction is known to be the simplest form of muscle activity in which the muscle is activated, but the length stays constant [82]. It is also easy to control in an experimental setting, since the complexity introduced by movement of the body part (e.g., range of motion, speed of movement) are not present [117].

Common reasons for training isometrically include maintaining muscle functionality during rehabilitation process (e.g., post-operation, recovering from an injury) [5]. Since the trained muscle(s) do not move or change length, the exercise intensity is quantified in terms of the percent maximum voluntary contraction level. Being simple to perform and effective in inducing neural changes in the trained muscle, it is important to incorporate isometric exercise into the therapy process of neuromuscular disorders [196].

It is further important to describe whether or not both limbs are involved in the training,

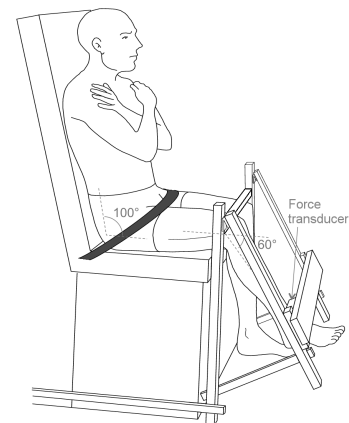


**Figure 2.13:** Experimental setup of unilateral isometric knee extension exercise. The subject is seated with a hip angle of  $^{\circ}100$  and a knee angle of  $^{\circ}60$  (from [275]).

which describes the laterality of the training. If both limbs are trained, the training is bi-lateral, whereas, the training is unilateral when one of the limbs is being trained and the other/contralateral limb remains in a resting state.

One type of unilateral isometric exercise is the unilateral isometric knee extension exercise (UIKKE). As the name suggests, the knee extensors (see Section 2.1.3) of the subject are trained unilaterally at a seated position (see Fig. 2.13).

## 2.3.4 Changes caused by isometric resistance training

### 2.3.4.1 Morphological changes

One common change observed in muscle properties due to exercise are the morphological changes. Morphological changes are related to the muscle size (cross-sectional area and volume), commonly referred to as hypertrophy. Hypertrophy is the increase in fibre diameter, which translate into increase muscle girth and volume. It is attributed to increased myofibril amount of the fibres of the trained muscle.

The exact mechanism behind hypertrophy is not well understood [228]. The overload due to exercise is thought to trigger the signalling pathway for the difference between protein synthesis and anabolism to be on the positive side, i.e., synthesis rate being higher than anabolism rate [228, 252]. Satellite cells, which are undifferentiated cells playing a key role in postnatal growth and repair of the muscle, are commonly referred as the trigger mechanism for hypertrophy [213, 252]. Although the matter is still under debate, the study by McCarthy et al. [213] compared the change in muscle mass of satellite cell depleted mice against a control group after hypertrophy was triggered by means of synergist ablation (removal of the gastrocnemius and soleus muscles causing functional overload of the remaining plantaris muscle [167]). They showed that in adult mice that satellite cells are not necessary for hypertrophy, but are needed for fibre formation and regeneration.

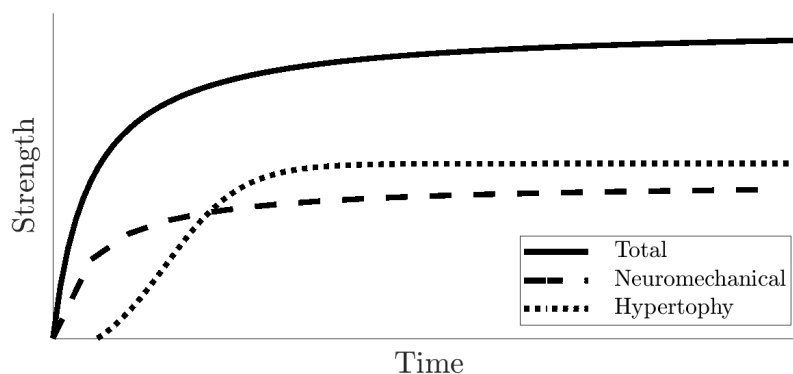


**Figure 2.14:** Qualitative description of the overall strength improvement due to resistance training caused by changes in neuromechanical system and hypertrophy over the course of time (adapted from [252]). Note that the contribution of hypertrophy becomes prominent later than the contribution of neuromechanical changes.

### 2.3.4.2 Changes related to the neuromechanical system

Muscle strength is known to increase without the presence hypertrophy (see Fig. 2.14). The cause of the strength increase without accompanying hypertrophy is attributed to neural adaptation mechanisms [326]. Neural adaptation includes decreased recruitment threshold, increase rate of firing and increased synchronised firing of the motor neurons of the trained muscle. It further includes increased activation of the agonists accompanied by a decrease in the activation of the antagonist muscles [177]. Nevertheless, a wholesome understanding of the adaptations of the neuromechanical system is still not present [117].

#### Voluntary activation

EMG measurements are widely used to study the adaptations of the neuromuscular system to resistance training. Time-course of the changes are also investigated by means of EMG [98]. However, limitations in the experimental methods combined with contradictory results on changes in the EMG, the exact physiological mechanisms behind neuromuscular adaptation in response to exercise is still unclear [78]. The data obtained from experimental studies on UIKEE is an example of such contradictory changes in EMG (see Fig. 2.15). When the change in EMG amplitude with respect to its baseline value is plotted over the course of trained week, a trend cannot be observed. Although most studies by Balshaw et al. [12], Kubo et al. [181], Weir et al. [320] show an increased EMG amplitude, studies by Rich & Cafarelli [263] and Garfinkel & Cafarelli [110] show a negative change. Furthermore, the study by Kubo et al. [181] has found a very high rate of increase in EMG amplitude compared to the rest of the studies.

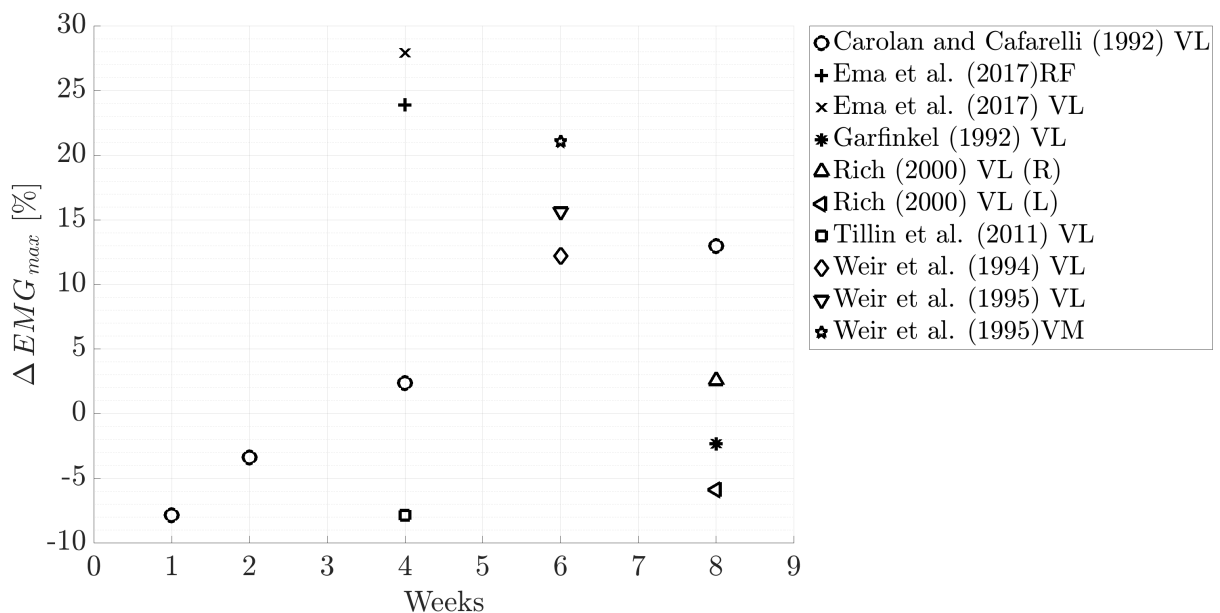


**Figure 2.15:** Change in EMG amplitude with respect to the baseline value over weeks for UIKEE studies. The abbreviations denote which muscle the data are obtained from, where RF: rectus femoris, VL: vastus lateralis, VM: vastus medialis and (R) and (L) denote right limb and left limb respectively.



### **Molecular changes in motor neurons**

Molecular mechanism that cause changes in the biophysical properties of motoneurons due to voluntary activity include changes in the dendrite structure, protein synthesis, axonal transport, neuromuscular propagation and some biophysical properties, which will influence how these cells behave during voluntary recruitment [89, 108]. These changes have been studied for rodents and rats by means of experiments as well as models for endurance exercise [107–109]. Such detailed investigations at the cellular level, however, are not available for isometric exercise.

Chronic activity is shown to cause changes in the intrinsic properties of the motor neurons, however, a casual relation between the cellular adaptations and increased performance has not been established yet [89]. This is attributed to limitations in the experimental methods combined with contradictory results on changes in the EMG [48, 65, 78, 159, 326].

### **Average motor unit firing rate**

Changes in the average firing rate are reflected on the total force output (see Section 2.2.6). It is suggested that the firing rate of motor units may increase either due to recruitment of previously inactive motor units or the readily recruited motor units firing faster [117]. Recruitment threshold is measured to decrease for motor units after dynamic exercise by Keen et al. [164], Van Cutsem et al. [310]) and isometric exercise by Del Vecchio et al. [66]. These data are still prone to the limitations of the EMG measurements.

## **2.4 Summary of the ‘end of a new beginning’**

Skeletal muscles alter their properties following long-term, consistent exercise via volumetric muscle growth preceded and accompanied by neural changes, i.e., neural adaptation. Neural adaptation has multiple components.

One of the common ways to investigate neural adaptation is to investigate EMG data. However, as presented in Fig. 2.15, this data does not follow a trend. Furthermore, although EMG measurements provide us with valuable insight into a limited portion of the motor neuron pool, it is still not possible to obtain detailed information on the contractile properties of the entire motor neuron pool, especially for large muscles.

Since isometric exercise is composed of isometric contractions, it is known as the simplest form of exercise. The force output and the change thereof is straightforward to measure and ample data on it is available in literature. Making use of a systematic review on a selected type of isometric exercise, we collect data available on the change in isometric strength in knee extensors following unilateral isometric knee extension exercise. We then model the time course of the change in isometric force output of vastus lateralis.

Our focus lies on the changes in the neural behaviour of the muscle in response to the selected exercise type and not merely the change in the isometric force output. As outlined previously in this and the preceding chapter, neural adaptation is a complex phenomenon. It is not possible to investigate all aspects of neural adaptation at once due to its inherent complexity.

In an attempt to further narrow the topic down, we focus on a single aspect of neural adaptation, namely the change in the discharge behaviour of the motor neuron pool. To investigate the change in the discharge behaviour, we make use of a computational model

of the motor neuron recruitment. Using the phenomenological motor neuron recruitment model, we set up the pre-exercise state of the muscle. The phenomenological model is brought closer to reality in light of experimental data. In Fig. 2.9 we present an overview of the data available on the time-to-peak force. A selection of this data is used to set up the pre-exercise state of the discharge behaviour of vastus lateralis.

Having discussed the limitations on the measurement of twitch properties of muscles in this chapter, it is clear that the force output of single motor neurons during a single twitch is strenuous to measure and data on a large number of motor neurons of the same muscle do not exist. In light of this, we determine the twitch force of individual motor neurons using the computational recruitment model along with the total muscle force output of vastus lateralis obtained from experimental data.

This has allowed us to create the pre-exercise state of the motor neuron pool (discharge behaviour and contractile properties). The total force output of the muscle can thus be computed based on the force output of individual motor neurons in the pool. By calibrating the total muscle force output obtained from simulations against the model of the time course of the change in the isometric force output, we determine the change in discharge behaviour of the motor neurons, which yields the expected change in the force.

To sum up, we make an effort to make use of the strengths of computational and experimental approaches in order to enhance the information available on the neural adaptation in skeletal muscles. We focus on a single and simple form of exercise and a single muscle in a muscle group. However, the methodology followed in this dissertation can be applied and extended to other muscle and exercise types. Details on the methodology have been provided in the following chapters.



## 3 Incorporating experimental data into the modelling framework

Statistical inference is a logical framework in which the beliefs about a given cause of a problem are tested against what is already known about the problem, e.g. frequently in terms of data. As the field of statistical inference has developed, two schools of thought have emerged. They differ mainly in their approach towards the definition of the probability of an event. The distinction between the two schools has first been made by Kendall [166] as “frequentists” and “non-frequentists”, the latter referring to the Bayesians. The Frequentist school were developed in the first half of the 20<sup>th</sup> century whereas the Bayesian school stems from the work of Reverend Thomas Bayes<sup>1</sup> dating back to 18<sup>th</sup> century [272].

Kendall [166] asserts that the frequentist treats the probability of an event to occur as an “unknown constant” whereas the non-frequentist does the opposite. They treat probability not as a constant, but it is rather allowed to vary according to the state of the knowledge about an event.

One other difference between the two schools lie in how they regard data. In the frequentist approach, the sample data are assumed to be the result of an infinite number of reruns of the same experiment. Data are assumed to be random and drawn from a sample of fixed population distribution. Conclusions drawn using this approach are based on the assumption that the event occurs with a given probability. The noise attributed to the data are thought to originate from sampling variation, which is caused by the fact that each sample is somewhat different from each other and is not an exact representation of the population [186].

The Bayesian approach, however, treats data as the known and fixed part of the system. They do not consider the reruns of an experiment to specify a probability of the occurrence of the event. Probability in Bayesian sense is rather a measure of certainty of a particular belief for an event to take place. It is not regarded as a measure of the underlying laws of the cause and effect. Therefore, the events do not need to be repeatable. Probability,

---

<sup>1</sup>Thomas Bayes is thought to live between 1701-1761. The exact year of his birth is not clear. Bayes entered the University of Edinburg in 1719 to study divinity. He is thought to have recieved mathematical training prior his university education. He became a Presbyterian minister Bellhouse [21].

Bayes’ first published work was a book entitled Divine Benevolence dating back to 1731. In this book, he tries to answer the motivating source of God’s actions in the world and attributes this to God’s goodness or benevolence Bellhouse [21].

Bayes himself wrote papers on various topics, however, he did not make these public due to his modesty. The paper on which his popularity rests regarding what is currently known as the Bayes’ theorem today, focuses on a solution to the following problem: ”Given the number of times in which an unknown event has happened and failed: Required the chance that the probability of its happening in a single trial lies somewhere between any two degrees of probability that can be named.” [223].

Richard Price started working on the paper after being approached by Bayes’ relatives to examine his unpublished works. The paper is prepared to be published by a friend of his, Richard Price, who is 22 years Bayes’ junior. It was published two years posthumously [21].

thus, describes how likely an event is to take place and can be “updated” in light of new data. This is due to the fact that probabilities are assumed to represent only the current state of belief for a given event [186].

Finally, the two schools of thought differ in their approach towards model parameters. Frequentists view model parameters as a fixed part of the system. However, in the Bayesian approach, the parameters of the system are thought to vary. This allows Bayesians to treat model parameters as tools to make inferences about a situation [186].

In this thesis, the Bayesian approach is followed as it is more suitable to tackle challenges related to skeletal muscle modelling. First of all, as experimental methods are developed and a high volume of studies continue to be conducted, new and more enhanced data will emerge in the future. Treating data as an updateable quantity is, therefore, one reason why Bayesian inference is a valid approach to follow regarding muscle modelling. Specifically for experiments performed on human subjects, a random sampling of the data are not feasible since number of subjects is usually limited (e.g., 10-20 subjects).

Secondly, exact input parameters of the motor neuron model (introduce in Chapter 4) that describe the vastus lateralis muscle is currently unknown. Force output of this muscle, however, can be estimated based on experimental data. Using Bayesian updating, the force output computed from simulations are calibrated against the experimental data on the force output. This then allows us to estimate the input parameters for the recruitment model. Hence, we make use of a quantity that can be retrieved from experimental data, i.e., force output, to estimate the unknown model input parameters.

The following sections provide further information on Bayesian inference (Section 5.2.1) including some of its application domains, the Bayes’ theorem (Section 3.2) and outline of the implementation of the method adopted in this thesis (Section 3.3). Note that as the Frequentist approach is not followed in this study, the reader is referred to e.g., Kolmogorov [171] for further information on this approach.

## 3.1 Bayesian inference

Calibration is defined as adjusting model input parameters in order to increase their accuracy with respect to experimental data. Bayesian inference is also known as Bayesian calibration, since it allows to calibrate input parameters against data. The method makes use of a basic law of probability, which is known as Bayes theorem (see Section 3.2). This probability rule combines what we already know about an event with new information to provide an updated belief about that event [73].

The procedure begins with formulating the uncertainty about the values of the model input parameter values. These values make up the “prior probability distribution” (see Section 3.2.3). First, the model is run using the model with the input parameters specified in the prior distribution, to obtain the corresponding model outputs. The prior parameter distribution is then updated by means of Bayes Theorem, which yields the posterior distribution of the parameters. The update can also be referred to as the calibration against experimental data (see Fig. 3.1 for a visual overview of the model) [312].

One advantage of Bayesian inference is that the method makes it possible to take what is already known about a topic, e.g., available data, and extrapolate backwards to make probabilistic statements regarding the model parameters [186]. The method allows to update the parameters as more/new data becomes available [20]. Furthermore, it applies

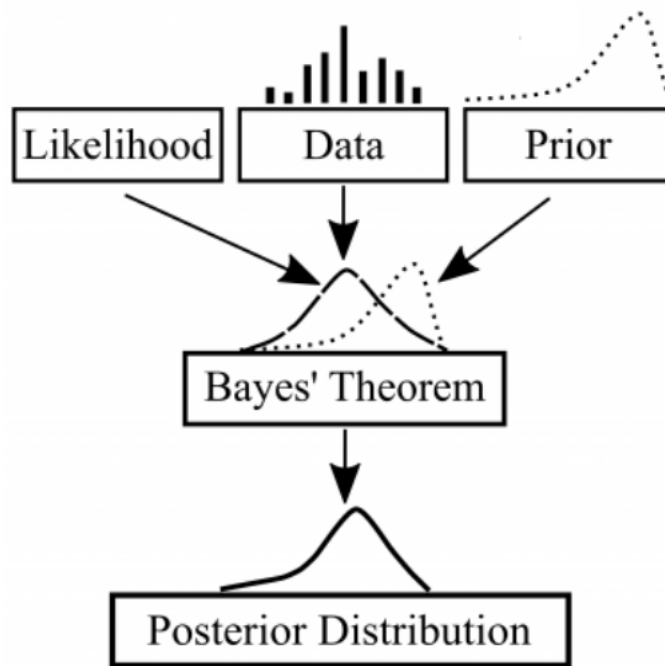


**Figure 3.1:** Scheme describing the Bayes' theorem, adapted from Doll & Jacquemin [73].

to models of any type or size as the method is indifferent to the inherent structure of the model [312]. Bayesian inference is applied to many areas of research including but not restricted to carbon dioxide storage (e.g., [234]), fisheries science ([73]) and psychology ([90]).

Besides being used as a method for model calibration, it is thought that humans also perform “near-optimal” Bayesian inference when they conduct a variety of tasks [200]. One example is the central nervous system, which is thought to make use of probabilistic models during sensorimotor learning<sup>2</sup>. In an experimental study by Körding & Wolpert [173], subjects were expected to point to a visual target in a virtual reality set-up. The visual feedback of their index finger is displaced laterally with shift of  $1 \pm 0.5$  cm. These trials made up the prior distribution. After training with 1000 trials, the subjects were able to point to  $0.97 \pm 0.06$  cm to the left of the target. This showed that they learned the shift imposed by the setup based on previous experience.

## 3.2 Bayes' theorem

Bayesian inference make use of a basic law of probability, known as Bayes theorem (see Section 3.2.1). This probability rule combines what we already know about an event with new information to provide an updated belief about that event [73].

Bayes' theorem is composed of four main parts, which are: the posterior (the updated belief, which is sought for), the prior (the current belief/knowledge about the event before

<sup>2</sup>Sensorimotor learning is the improvement in the performance of sensory-guided motor behaviour through repetitions of the task being practised [178].

taking evidence into consideration), the likelihood (how well the parameters describe the data) and a normalizing constant. The essence of the theorem is visualized as:

$$\text{posterior} \propto \text{prior} \times \text{likelihood}, \quad (3.1)$$

This description summarizes how the beliefs, expressed through the prior, are modified/updated by considering the available data by using the likelihood (also see Fig. 3.1 [189, 259]).

In the following sections of the present study, proof of Bayes' theorem using axioms of conditional probability, variables appearing in the theorem and the implementation of the framework as well as an overview of how the framework is applied to three modelling schemes are introduced.

### 3.2.1 Conditional probability

Some axioms of probability and their consequences leading to Bayes' theorem are included as follows:

Conditional probability describes the probability of the occurrence of one event,  $E_1$ , given the condition that another event,  $E_2$ , occurs, denoted by  $P(E_1 | E_2)$ . In simpler words,  $P(E_1 | E_2)$  is the measure of the degree of the modeller's belief in  $E_1$  knowing that  $E_2$  is true [189]. This can be expressed as:

$$P(E_1 | E_2) = \frac{P(E_1 \cap E_2)}{P(E_2)}. \quad (3.2)$$

Here,  $P(E_1 \cap E_2)$  refers to the probability of  $E_1$  and  $E_2$  occurring simultaneously,  $P(E_1)$  and  $P(E_2)$  are the probabilities of  $E_1$  and  $E_2$  occurring on their own. Rearranging Eqn. (3.2),  $P(E_1 \cap E_2)$  can be expressed as

$$P(E_1 \cap E_2) = P(E_1 | E_2) P(E_2). \quad (3.3)$$

Events  $E_1$  and  $E_2$  being independent from each other implies that

$$P(E_1 \cap E_2) = P(E_2 \cap E_1). \quad (3.4)$$

Furthermore, Eqn. (3.3) can be written as

$$P(E_2 \cap E_1) = P(E_2 | E_1) P(E_1). \quad (3.5)$$

Therefore using the equality in Eqn. (3.4), and the fact that  $E_1$  and  $E_2$  are independent, the following can be obtained

$$P(E_1 | E_2) P(E_2) = P(E_2 | E_1) P(E_1). \quad (3.6)$$

Rearranging Eqn. (3.6) for  $P(E_1 | E_2)$ , one obtains

$$P(E_1 | E_2) = \frac{P(E_2 | E_1) P(E_1)}{P(E_2)}, \quad (3.7)$$

which is the formal definition of the Bayes' theorem [292].

In this thesis, Bayesian inference is used to calibrate model input parameters against experimental data. Section 3.4 gives an overview of how Bayesian inference is applied to three parts of this work.

The parameters of Eqn. (3.7) is replaced as follows: Events,  $E_1$  and  $E_2$ , are replaced by the vector of input parameters,  $\Theta$ , and the available experimental data,  $D$ . The aim is to determine input parameters for a given model, so that the model output describes the experimental data at hand as accurate as possible. Therefore Eqn. (3.7) becomes

$$p(\Theta | D) = \frac{p(D | \Theta) p(\Theta)}{p(D)}, \quad (3.8)$$

where  $p(\Theta)$  the joint prior probability distribution function (PDF) of the model parameters  $\Theta$ ,  $p(D)$  the prior probability of the data,  $D$  used as the normalization constant and  $p(\Theta | D)$  is the conditional PDF of  $D$  for a given  $\Theta$ , i.e., the posterior distribution.

### 3.2.2 The coin tossing example

A typical example used to illustrate Bayesian inference is coin tossing<sup>3</sup>. By tossing a coin, a head ( $H$ ) or ( $T$ ) can be obtained, thus  $\Theta = \{H, T\}$ . Whether the coin is fair, i.e., equal probability of getting a head ( $H$ ) or a tail ( $T$ ) ( $p(H) = p(T) = 0.5$ ) or biased towards heads/tails ( $p(H) \neq p(T)$ ) is unknown<sup>4</sup>. A coin is flipped a number of times and the outcome is reported after each flip as  $H$  or  $T$ , which makes up the data on related to the bias. Using the coin tossing example, it is possible to illustrate the core of Bayesian inference, which lies in synthesizing prior knowledge on the problem and the new data to make a more informed decision [73]. The concepts in Section 3.2.2, are concretised using this example.

<sup>3</sup>Coin tossing is also known as "capita aut navia". The so-called game has been used since Ancient Romans to let luck/God decide on the outcome of an event, e.g., deciding on which team takes which half of the stadium in football games [309].

<sup>4</sup>Georges-Louis Leclerc in 1700, Karl Pearson in 1900 and John Kerrich during his imprisonment in World War II, did actually toss coins for 4040, 24000 and 10000 times and obtained 50,693 %, 50,05 %, 50,67 % heads respectively. On a long-run, the possibility of obtaining a head or a tail is equally possible [309]. Thus,  $B \approx 0.5$



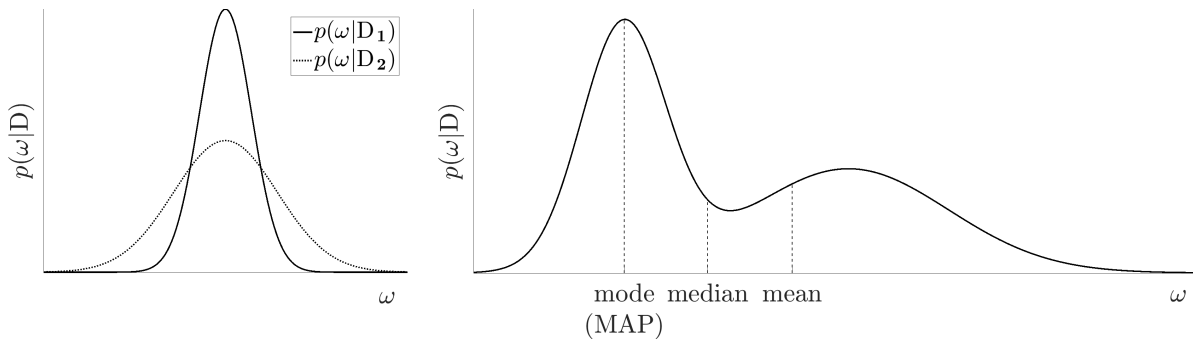


**Figure 3.2:** Posterior *left*: two posteriors distributions ( $p(\omega|D_1)$  and  $p(\omega|D_2)$ ) obtained using different data sets,  $D_1$  and  $D_2$ . Uncertainty in  $p(\omega|D_1)$  is less than  $p(\omega|D_2)$  (adapted from [186]), *right*: Posterior distribution of parameter  $\Theta$  and the point estimators, namely the mode, median and mean (adapted from [186]).

### 3.2.3 Prior

Prior sets are constructed by the modeller and are known to reflect the current knowledge of the modeller on the problem [186, 312]. The “current knowledge” is also referred to the subjective beliefs regarding the problem at hand. This an aspect of Bayesian inference that is highly criticized by the Frequentists as it introduces subjectivity to the problem [186]. However, the a-priori knowledge does not have to be comprised merely of beliefs about the problem at hand, but can be based on observations or literature [312].

Priors play an important role for determining the posterior, since the posterior distribution can only be obtained within the range of prior. Therefore, if the prior range is not defined correctly, then the posterior obtained as a result will also be faulty. Therefore, in this thesis, prior sets for the modelling schemes are set-up using samples of the input parameters instead of probability density functions. The sample space of input parameters are determined based on current knowledge on skeletal muscle physiology as well as experimental data available in literature. An overview of the selection of priors for each modelling scheme is outlined in Section 3.4.

### 3.2.4 Posterior

As mentioned earlier, the aim of Bayesian inference is to obtain the posterior probability distribution,  $p(\Theta|D)$ , or posterior in short. The posterior summarizes the uncertainty over the value of a parameter. When the width of the distribution is narrow, the estimate of the value of the parameter is more certain (see Fig. 3.2, left). To obtain narrower, thus more accurate posterior distributions, more data should be collected [186].

**Maximum a-posteriori** There are three point estimators in Bayesian statistics, which are namely the posterior mean, posterior median and the maximum a-posteriori. The posterior mean is the expected value of the posterior distribution, whereas, the posterior median is the mid-point of the posterior distribution, such that  $\sim 50\%$  of the probability of posterior values lie on either side of the posterior median. The maximum a-posteriori (MAP) denotes the parameter value that is referred to as the “posterior mode” (see Fig. 3.2, right) [186]. The MAP is expressed as:

$$\Theta^{\text{MAP}} = \underset{\Theta}{\operatorname{argmax}} p(\Theta | D) \quad (3.9)$$

Although it is possible to provide full posterior distribution of a parameter, it is often required to provide "point estimates" [186]. In this study, the MAP is used as a given model input that describes the current state of the VL muscle.

### 3.2.5 Likelihood

The probability of generating the data at hand ( $D$ ) for the parameters in  $\Theta$  is described by the likelihood function [186]. The function plays an important part in Bayesian statistics, as it encapsulates the information the data are able to convey related to the  $\Theta$  [292].

Likelihood function substitutes  $p(D | \Theta)$  and is commonly expressed as  $\mathcal{L}(\Theta | D)$ . It is not a probability, since in Bayesian inference, data are fixed and the parameters of the model is varied. The reason why this quantity is referred to as a likelihood rather than a probability is explained by using the coin tossing example (see Section 3.2.2) as in Lambert [186] as follows:

Suppose that the coin is tossed twice. The outcome of this specific case is thus  $D = \{HT, TH\}$ , which describes obtaining first a head or a tale in the tosses. To compute the posterior  $p(\Theta | D)$ , one needs to compute  $p(\Theta | D)$ . Knowing that tossing events are independent from each other,  $p(\Theta | D)$  can be expressed as:

$$\begin{aligned} p(\Theta | D) &= p(HT \cup TH | \Theta) \\ &= p(HT | \Theta) + p(TH | \Theta) \\ &= p(H | \Theta) p(T | \Theta) + p(T | \Theta) p(H | \Theta) \end{aligned} \quad (3.10)$$

Knowing that  $p(H | \Theta) + p(T | \Theta) \stackrel{!}{=} 1$  and assigning  $p(H | \Theta) = \theta$  and  $p(T | \Theta) = 1 - \theta$ , Eqn. (3.10) becomes:

$$\begin{aligned} p(\Theta | D) &= p(H | \Theta) p(T | \Theta) + p(T | \Theta) p(H | \Theta) \\ &= \theta(1 - \theta) + (1 - \theta)\theta \\ &= 2\theta(1 - \theta). \end{aligned} \quad (3.11)$$

Integrating Eqn. (3.11) yields

$$\int_0^1 2\theta(1 - \theta) d\theta = \frac{1}{3}, \quad (3.12)$$

which is not equal to 1, thus  $p(\Theta | D)$  cannot be denoted as a probability.

Therefore to emphasize the fact that likelihood expresses how likely a parameter (set)  $\Theta$  can be obtained when the data are held fixed, it is expressed as:

$$\mathcal{L}(\Theta | D) = p(\Theta | D), \quad (3.13)$$

which becomes  $\mathcal{L}(\Theta | D) = p(D | \Theta)$  using the notation in Section 3.8.

### 3.2.6 The denominator

The denominator in Eqn. (3.8) is referred to as the predictive distribution [189], normalising constant [315] or simply as 'the denominator' [186]. Note that  $p(D)$  does not depend on  $\Theta$ , which is why this quantity is disregarded in Eqn. (3.1). Even though it is disregarded in this thesis, the quantity will be briefly introduced.

The denominator has the following form:

$$p(D) = \int_{\Theta} p(D | \Theta) p(\Theta) d\Theta = \int_{\Theta} \mathcal{L}(\Theta | D) p(\Theta) d\Theta. \quad (3.14)$$

This integral may or may not have a closed-form solution.

Bayesian model selection and averaging are practices concerned with selecting the right statistical model to represent data. As the denominator represents the predictive distribution of the models being considered, it becomes significant when these methods are being used [315].

## 3.3 Implementation of Bayesian inference

After having introduced the components of the Bayes' theorem, the details related to the implementation of the theorem, cf. Bayesian inference, is covered in this section. In short, the implementation involves applying Monte-Carlo sampling to determine the properties of the posterior set of the model input parameters. After choosing the likelihood model, it is possible to obtain the posterior set of model parameters by using rejection sampling.

### 3.3.1 The likelihood model

A model to estimate the likelihood function  $\mathcal{L}(\Theta | D)$  should be selected. The selection is made based on how the error related to the experimental data are distributed. Owing to the "Central Limit Theorem"<sup>5</sup>, it is generally acceptable to assume an observation to be normally distributed [189]. Assuming that the measurement error of the experimental data are normally distributed, a Gaussian likelihood model is used. The derivation of the model is shown below.

Probability density function of a univariate Normal/Gaussian distribution for parameter  $x$  has the following form:

$$p(x; \mu, \sigma^2) = \frac{1}{\sqrt{2\pi}\sigma} \exp\left[-\frac{(x - \mu)^2}{2\sigma^2}\right], \quad (3.15)$$

where  $\mu$  and  $\sigma$  denote the mean and the standard deviation of  $x$ . Note that  $\sigma^2 = \text{var}$ , where  $\text{var}$  denotes the variance.

In Eqn. (3.15), the factor  $\sqrt{2\pi}\sigma$  does not depend on  $x$  and can be regarded as a

---

<sup>5</sup>The Central Limit Theorem briefly states that if a random variable can be expressed as a sum of a large number of approximately independent components, none of which being much bigger than the other, the sum would be normally distributed [189].

normalization constant that ensures

$$\int_{-\infty}^{\infty} p(x; \mu, \sigma^2) = \frac{1}{\sqrt{2\pi\sigma}} \int_{-\infty}^{\infty} \exp\left[-\frac{(x-\mu)^2}{2\sigma^2}\right] = 1. \quad (3.16)$$

The input parameters  $\Theta$  in this thesis, are multi-variate, i.e.,  $\Theta = \omega_1, \omega_2, \dots, \omega_n$ , where  $n$  denotes the number of input parameters. Therefore probability density function of a multi-variate Normal/Gaussian distribution needs to be introduced. For a parameter vector  $\mathbf{X}$  with  $n$  different components, i.e.,  $\mathbf{X} = \{X_1, X_2, \dots, X_n\}$ , the multi-variate Gaussian distribution has the following form:

$$p(\mathbf{X}; \boldsymbol{\mu}, \mathbf{R}) = \frac{1}{(2\pi)^{n/2} \sqrt{\det \mathbf{R}}} \exp[\mathbf{X} - \boldsymbol{\mu}]^T \mathbf{R}^{-1} (\mathbf{X} - \boldsymbol{\mu}), \quad (3.17)$$

where  $\boldsymbol{\mu}$  denotes the vector of the mean values and  $\mathbf{R}$  the covariance matrix.

Assuming that the measurement error,  $\epsilon$ , of the data,  $D$ , is normally distributed, i.e.,  $\epsilon \sim N(0, \epsilon)$ , based on Eqn. (3.17), the following likelihood model is used:

$$\mathcal{L}(\Theta | D) = \exp[-0.5 (D - \Omega(\Theta))^T \mathbf{R}^{-1} (D - \Omega(\Theta))], \quad (3.18)$$

where  $\Omega(\Theta)$  denotes the output of the model for given  $\Theta$  and  $\mathbf{R}$  is the (co)variance matrix of measurement errors of the data. In this work,  $\mathbf{R}$  is a diagonal matrix, i.e.,  $\mathbf{R} = \epsilon \mathbf{I}$ , since experimental data points are treated as independent from each other<sup>6</sup>. Also note that the size of the matrix depends on the number of data points available.

### 3.3.2 Setting up the prior set

Prior set for the model inputs are not composed of PDFs in this thesis, but are generated from samples. A pattern, which is applied throughout this thesis, is as follows:

- (1) Decide on how each parameter is distributed, i.e., whether it takes a single value or multiple values following a distribution.
- (2) For parameters taking a single value, create a uniform distribution within a selected range for the values each parameter is likely to take. For input parameters following a given distribution, select a range for the values of the shape factors needed to create the distribution.
- (3) Based on (2) and physiological knowledge, create sampling sets for each parameter, i.e., define the limits or the necessary constants to describe the distribution of the

---

<sup>6</sup>Proof of  $\mathbf{R} = \epsilon^2 \mathbf{I}$ : The covariance matrix of a bi-variate distribution of a random vector of variables  $\mathbf{X} = (X_1, X_2)$  has the form

$$\mathbf{R}(X_1, X_2) = \begin{bmatrix} \text{var}(X_1) & \text{cov}(X_1, X_2) \\ \text{cov}(X_2, X_1) & \text{var}(X_2) \end{bmatrix} \quad (3.19)$$

If  $X_1$  and  $X_2$  are independent from each other, then  $\text{cov}(X_1, X_2) = 0$ . Hence, the non-diagonal terms vanish and the covariance matrix becomes diagonal, i.e.,  $\mathbf{R}(X_1, X_2) = \text{var}(X_i) \delta_{i,j}$ . Also note that  $\text{var}(X_i) = X_1$  since  $X_1 \sim N(0, X_1)$

values the parameter can take.

- (4) Compute all possible combinations of the individual sampling sets created in (3). These combinations make up the prior sets.

How this pattern is applied to the model schemes is briefly introduced in the overview in Section 3.4 and also further in Chapter 5, Chapter 6 and Chapter 8.

After setting up the prior set, rejection sampling is performed to generate the posterior set.

### 3.3.3 Rejection Sampling

Monte-Carlo sampling is the practice of estimating the properties of a distribution from random samples taken from the distribution [259]. Analogously, in Bayesian inference, to obtain the posterior distribution of the problems at hand, samples from the prior distribution are taken.

For this, first weights need to be introduced. It is possible to assign weights to each sample by using  $\Theta^{\text{MAP}}$  (see Section 3.2.4 and Eqn. (3.20)). Normalizing  $p(\Theta | D)$  with  $\Theta^{\text{MAP}}$  yields the weight for each sample. Therefore, weight for an arbitrary sample  $m$  ( $w^m$ ) has the following form:

$$w^i = \frac{p(D | \Theta^i)}{\max(p(D | \Theta^i))}, \quad (3.20)$$

where  $\Theta^i$  is the model input parameter(s) for sample  $i$ . Note that the weights describe the importance of each realization [234].

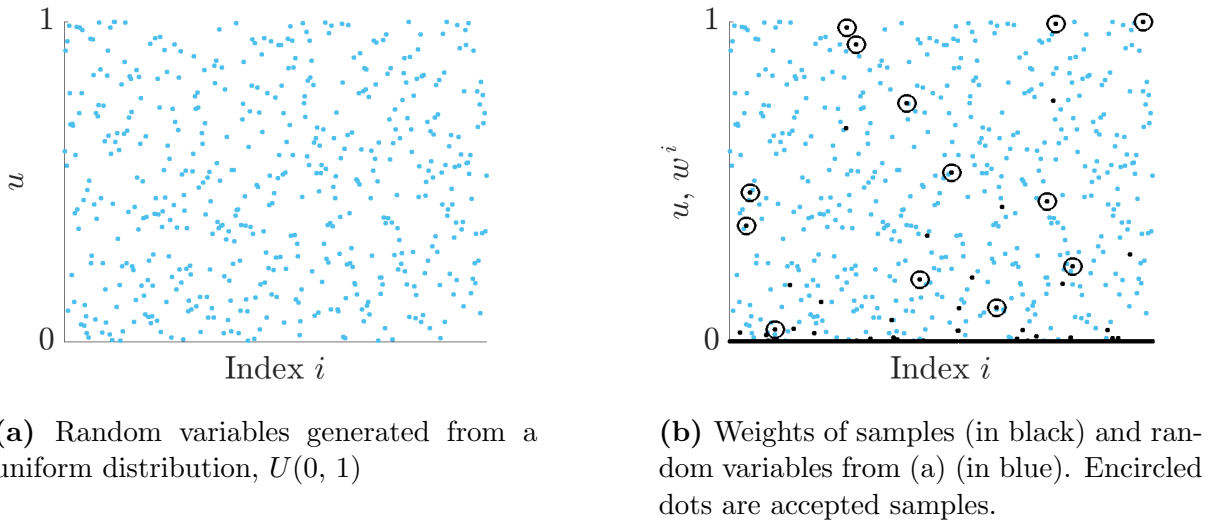
After assigning weights to each sample, the posterior distribution is estimated using a rejection sampling algorithm. In this algorithm, the weight of a sample is compared against a random value drawn from a uniform distribution. If the weight is less than the random value, the sample is taken into the posterior set. Using a uniform distribution allows to obtain a higher number of samples having the higher likelihood for representing the data at hand.

Following is a summary of the rejection-sampling algorithm:

1. Setup the priors for  $\Theta$
2. Compute the weight,  $w^i$  (see Eqn. (3.20)), for each  $\Theta^i$ , for  $i = 1, \dots, n$ , where  $n$  corresponds to the size of the prior
3. Generate  $u = \{u^1, u^2, \dots, u^n\}$  from uniform (0, 1)
4. If  $u^m \leq w^m$ , accept  $\Theta^m$  (see Fig. 3.3); otherwise, repeat Steps 1-4.

## 3.4 How the framework is used in this thesis

The aim of this present study is to investigate the changes in the discharge behaviour of the motor neuron pool of vastus lateralis muscle in response to isometric exercise.



(a) Random variables generated from a uniform distribution,  $U(0, 1)$

(b) Weights of samples (in black) and random variables from (a) (in blue). Encircled dots are accepted samples.

**Figure 3.3:** Rejection sampling of an arbitrary function  $f(x)$  for  $x^i$ , where  $i = 1, \dots, n$ , against a fictitious data set.

A similar pattern is applied in three parts of the modelling scheme presented in this study in order to determine the pre- and post-exercise state of the muscle. This pattern is composed of gathering experimental data from literature on a given property of the muscle and selecting the right set of parameters describing the property given the data using Bayesian inference techniques, i.e., rejection sampling as described in Section 3.3.3. This way, the limitations/“imperfections” of experimental methods are not completely disregarded, but used as a basis for the estimations. Experimental data are used to calibrate the models, as well as to determine prior sets for the parameters.

Note that, for the notation, the initial selection of the set of input parameters have been denoted by  $\Theta$ . For all schemes, parameters in  $\Theta$  has been filtered according to a physiological range. Thus, prior sets of model input parameters have been obtained. These sets are denoted by  $\tilde{\Theta}$  and they contain less number of elements than  $\Theta$ . Using  $\tilde{\Theta}$ , prior set of model outputs, simulations have been performed to obtain the prior set of model outputs, c.f.  $\Omega^{\text{sim}}(\tilde{\Theta})$ . By calibrating  $\Omega^{\text{sim}}(\tilde{\Theta})$  against experimental data yields the posterior set of model inputs,  $\tilde{\tilde{\Theta}}$ , as well as the posterior set of model outputs  $\Omega^{\text{sim}}(\tilde{\tilde{\Theta}})$ . The MAP set in  $\tilde{\tilde{\Theta}}$  has been used as the set of parameters that depict vastus lateralis.

### 3.4.1 Scheme I: Estimation of the input parameters for the recruitment model for vastus lateralis

The first part of the modelling scheme is related to the the input parameters of the motor neuron pool model (see Chapter 4) describing the pre-exercise of the pool. For this, data on the (mean) discharge rate of the motor neurons measured using various EMG methods during isometric contraction are collected from literature. Prior sets for the input parameters are created using discrete values.

The prior sets are first created within a wide range and then narrowed by using information on the force level upon which recruitment of motor neurons are known to end. This way, the priors are not purely random, but are informed by the available knowledge on

motor unit recruitment.

Using the discharge rate of vastus lateralis measured in a number of studies, the input parameters of the motor neuron pool model describing the pre-exercise state of the discharge behaviour of vastus lateralis are estimated via Bayesian updating. The MAP parameters make up the parameter set describing the discharge behavior of vastus lateralis muscle during an isometric contraction. These are then used in the modelling schemes II and III, which are described in the following.

### 3.4.2 Scheme II: Estimation of the contractile properties of vastus lateralis

Twitch properties (the time-to-peak-force,  $TTP$ , and peak twitch force,  $PTF$ ) of the motor neuron pool of a given muscle can only be obtained for a very small portion of the pool [94]. Furthermore, corresponding data for vastus lateralis muscle is lacking (see Table 6.2). In the second part of the modelling scheme, the twitch properties of the motor neuron pool of vastus lateralis are estimated.

It is known that  $TTP$  and  $PTF$  are coupled to each other (see Section 2.2.4). In setting up the prior set,  $PTF$  is first treated as an unknown. Experimental data gathered for multiple muscles from a number of experimental studies (see Table 6.2) are used to construct the prior set for the  $TTP$ . Using the isometric strength of vastus lateralis and the discharge instances at this force level, the prior set for  $PTF$  is constructed for each case of  $TTP$ .

The model output in this scheme is the isometric force output of the vastus lateralis. Force output of the motor unit pool at force levels 10 to 100 % MVC at each 10 % MVC is computed for the prior set of twitch properties. The model is then calibrated against the experimentally measured force output of vastus lateralis. The MAP of the twitch properties then define the corresponding values for the twitch properties of vastus lateralis (details in Chapter 6).

### 3.4.3 Scheme III: Estimation of the change in discharge rate of vastus lateralis due to UIKEE

The third part and final part of the modelling scheme suggested in this thesis is concerned with the order of magnitude of the change in the discharge rate of vastus lateralis to obtain strength gain triggered by unilateral isometric knee extension exercise. For this, first, the strength gain of the knee extensors over the course of weeks is modelled by using a Bayesian longitudinal model-based meta-analysis, BLMBMA (see Chapter 7). The strength gain computed using the model at each progressing week are used as calibration points.

Input parameters of the motor neuron pool model, which would describe the post-exercise state of the pool (i.e., parameters that would produce higher discharge rate), are selected. The change in the isometric force as well as the mean discharge rate for each parameter set are computed. Using the force output as the main model output, the model is calibrated against the time-course of strength gain obtained using BLMBMA. The discharge rate of the parameter sets in the posterior set describes the expected change in the discharge rate needed to attain the isometric strength increase due to UIKEE (details in Chapter 8).

## 4 Modelling total force output

Fuglevand et al. [104] have proposed a scheme to model the motor unit recruitment mechanism in skeletal motor units. The significance of the model in literature is already discussed in Chapter 1. For a given motor unit pool, the scheme models the discharge instances of motor units, computes the motor unit force, as well as the total muscle force output. The modelling scheme is composed of a “motor neuron pool model”, “isometric force model for motor units” and a final model for the “simulation of the surface EMG”.

“Motor neuron pool model” and the form of the twitch force as suggested in the “isometric force model for motor units” are used in this work. Details and capabilities of these models are explained in this chapter (in Section 4.1 and Section 4.2 respectively) by using mainly the set of input parameters suggested in Fuglevand et al. [104]. How the modelling scheme has been used in Chapter 5 and Chapter 6 in order to model the discharge instances and the contractile properties of the motor neurons of vastus lateralis muscle are explained in Section 4.3.

### 4.1 The motor neuron pool model

The motor neuron pool model captures the recruitment behaviour of a motor neuron pool during an isometric contraction. The model generates the discharge instances of each motor unit in the pool at various force levels.

The excitatory drive  $E(t)$  describes the effective synaptic current received by motor neurons. The target excitatory drive,  $E_{\text{target}}$ , is the drive, which is necessary to simulate an isometric contraction.

The profile of the excitatory drive needs to be defined by the user. Here, a ramped contraction is used. Excitatory drive increases linearly during a ramp phase, where  $t_{\text{ramp}}$  denotes the end of the ramp, and is kept constant from this point on until the contraction ends, which is denoted by  $t_{\text{end}}$  (see Fig. 4.1). Therefore, the excitatory drive has the following form:

$$E(t) = \begin{cases} E_{\text{target}} \cdot t & t \leq t_{\text{ramp}} \\ E_{\text{target}} & t_{\text{ramp}} < t \leq t_{\text{end}}. \end{cases} \quad (4.1)$$

In order to compute  $E_{\text{target}}$  for a given contraction, further parameters of the model need to be introduced.

Motor neuron  $i$  fires an action potential when  $E(t)$  exceeds its recruitment threshold,  $RTE_i$ , i.e.,  $E(t) \geq RTE_i$ . The recruitment threshold for motor unit  $i$  is defined by



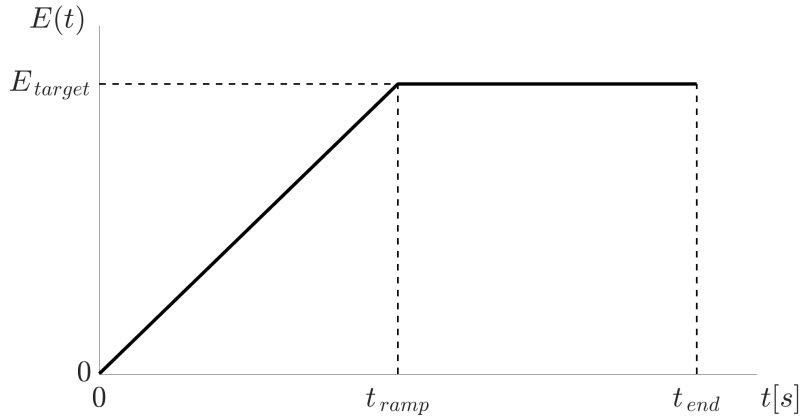


**Figure 4.1:** Excitatory drive function  $E(t)$  for a ramped isometric contraction. The drive increases linearly until  $t_{ramp}$  and is kept constant until  $t_{end}$ .

$$RTE_i = \exp \left[ \frac{\ln RR}{N} i \right], \quad (4.2)$$

where  $RR$  refers to the range of recruitment threshold of the motor unit pool in arbitrary units and  $N$  denotes to the size of the motor neuron pool, i.e., total number of motor units in the pool.

The instantaneous firing rate, which in return defines when a motor unit fires, is given for each motor unit  $i$  by

$$FR_i(t) = g_e (E(t) - RTE_i)_+ + MFR, \quad (4.3)$$

where  $(x)_+ := (x + |x|) / 2$  denotes the Macaulay brackets,  $g_e$  the gain of the excitatory drive,  $E(t)$  the excitatory drive,  $RTE_i$  the recruitment threshold of motor unit  $i$ , and  $MFR$  the mean value of the minimum firing rate of the motor units. Note that  $MFR$  is assigned the same value for all motor neurons.

Firing instances determine the inter-spike intervals, i.e., the inter-spike interval for a specific firing instance  $j$  and motor unit  $i$  is given by:

$$ISI_i^j = t_n^m - t_n^{m-1}. \quad (4.4)$$

Substituting the inverse of Eqn. (4.4), which is equivalent to the instantaneous firing rate of the  $j^{th}$  firing of motor unit  $i$ , into (4.3), one obtains

$$\frac{1}{t_n^m - t_n^{m-1}} = g_e (E(t_n^m) - RTE_i)_+ + MFR. \quad (4.5)$$

Rearranging Eqn. (4.5) yields the firing instance,

$$\begin{aligned}
t_n^m &= t_n^{m-1} + \frac{1}{g_e (E(t_n^m) - RTE_i)_+ + MFR} \\
&= t_n^{m-1} + \Delta t_n^{m-1},
\end{aligned} \tag{4.6}$$

which is solved by means of fixed-point iteration in Section 4.1.1.

To simulate a maximum voluntary contraction (MVC), the upper limit of  $E_{\text{target}}$  needs to be determined, c.f.  $E_{\text{max}}$ . During an MVC, all motor neurons discharge at their peak discharge rate. It is worth to note that the last recruited motor neuron, motor neuron  $N$  discharges at a slowest rate compared to the rest of the motor neurons. Therefore, the peak firing rate of motor neuron  $N$  ( $PFR_N$ ) becomes the limiting factor.

Thus, left-hand side of Eqn. (4.3) is replaced with  $PFR_N$  to obtain  $E_{\text{max}}$ :

$$PFR_N = g_e (E_{\text{max}} - RTE_N)_+ + MFR_N. \tag{4.7}$$

Rearranging Eqn. (4.7) for  $E_{\text{max}}$  yields:

$$E_{\text{max}} = RTE_N + \frac{PFR_N - MFR_N}{g_e}. \tag{4.8}$$

Rate coding and motor unit recruitment are both responsible for the increase in force during a voluntary contraction. Up to the force level at which all motor units in the motor unit pool are recruited, both rate coding and motor unit recruitment cause a force increase. Beyond this force level, increase in force is merely due to rate coding as there are no additional motor units that can be recruited within the pool [77].

The additive components of Eqn. (4.8) describes this phenomenon and are referred to as  $E^N$  and  $\Delta E_{\text{max}}^N$ . Thus Eqn. (4.8) can be written as

$$E_{\text{max}} = E^N + \Delta E_{\text{max}}^N. \tag{4.9}$$

From a physiological point of view,  $E^N$  denotes the upper limit of the excitation for recruiting additional motor units (see Fig. 4.2), while  $\Delta E_{\text{max}}^N$  contributes to the force increase due to a mere increase in firing frequency (see Fig. 4.3). Note that  $E_{\text{target}}$  is defined in proportion of  $E_{\text{max}}$  as

$$E_{\text{target}} = p/100 \cdot E_{\text{max}}, \tag{4.10}$$

where  $p$  denotes the level of force to be simulated.

The force level, at which the largest motor unit (motor unit  $N$ ) starts firing, is denoted by  $F_{\text{Full Recr}}$ . This is a muscle-specific quantity and based on the definitions in Eqn. (4.9) and Eqn. (4.10) can be quantified as:

$$F_{\text{Full Recr}} = \frac{E^N}{E_{\text{max}}} \cdot 100 = \frac{RTE_N}{E_{\text{max}}} \cdot 100. \tag{4.11}$$

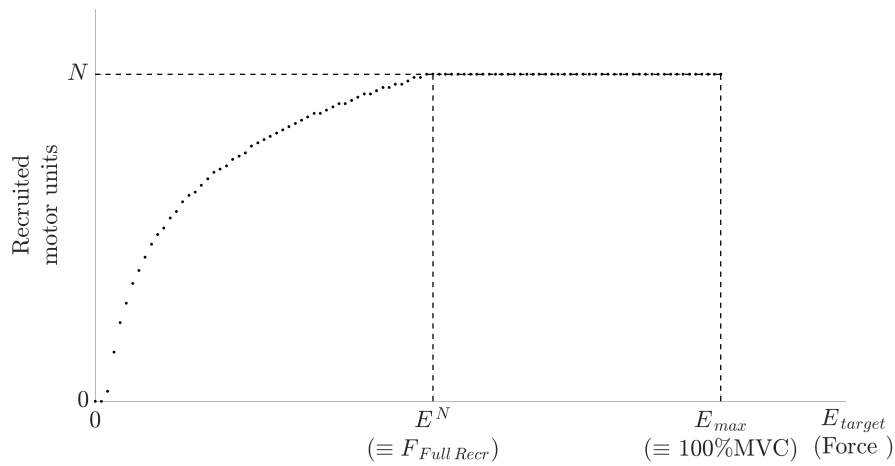


**Figure 4.2:** Number of recruited motor units for an increasing target excitatory drive  $E_{target}$  and the corresponding force level in brackets. Note that all motor units are recruited after  $E_{target} \geq E_N$  or  $Force \geq F_{Full Recr}$ . The plot is obtained by running the motor neuron pool model with parameters in Table 4.1.

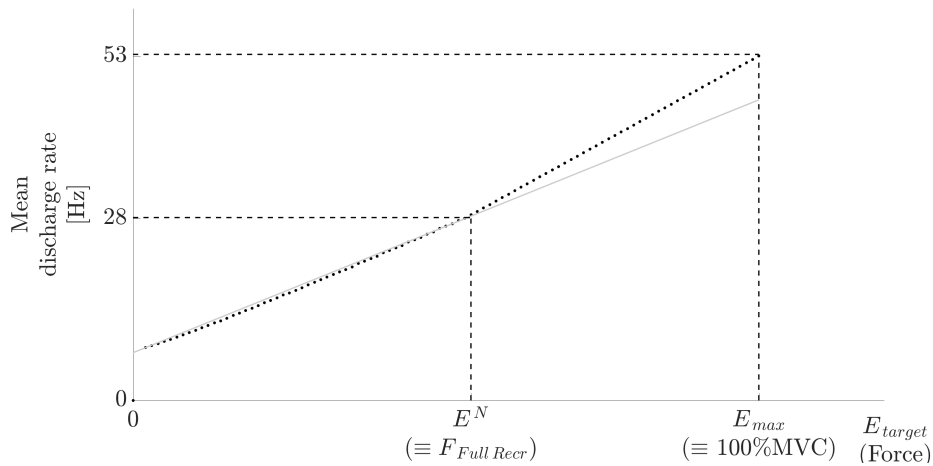


**Figure 4.3:** The mean discharge rate of the motor neuron pool for an increasing target excitatory drive  $E_{target}$  and the corresponding force level in brackets. Note the change in the slope of the curve after full recruitment is reached, i.e.,  $E_{target} \geq E_N$  or  $Force \geq F_{Full Recr}$ . The grey line emphasizes the change in the slope of the curve after this point. The plot is obtained by running the motor neuron pool model with parameters in Table 4.1.

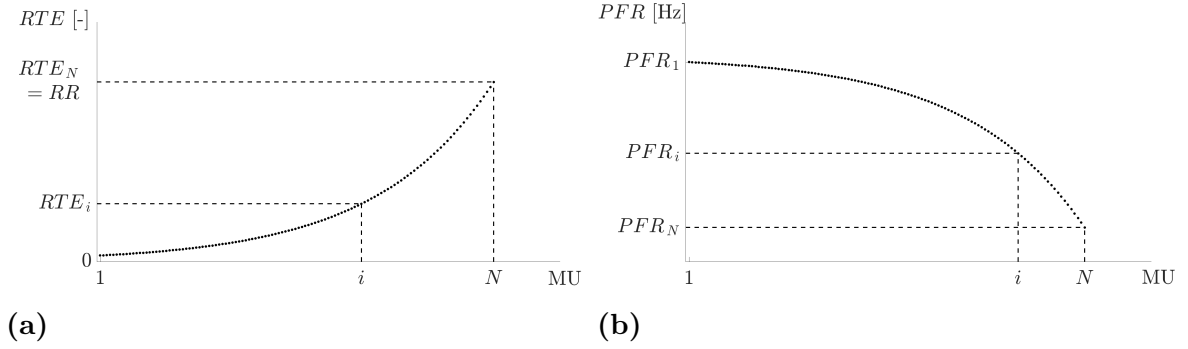


**Figure 4.4:** Profiles for (a) the recruitment threshold and (b) the peak firing rate of the motor unit pool.

The peak firing rate differs from motor neuron to motor neuron following

$$PFR_i = PFR_1 - PFRD \frac{RTE_i}{RTE_N} \quad (4.12)$$

with  $PFRD$  denoting the difference between the peak firing rate of the first and last motor unit.

### 4.1.1 Fixed-point iteration

The discharge instances for each motor unit at any force level is computed by solving Eqn. (4.6). To solve this equation, the fixed-point iteration scheme is used. First, the definition of a fixed point will be provided and the iterative scheme will explained. The application of the scheme to the problem at hand will then be described.

“A fixed point for a function is a number at which the value of the function does not change when the function is applied” [36]. Thus, a number  $m$  is a fixed point for a given function  $g$  if  $g(m) = m$ . Geometrically, fixed points of  $g$  correspond to the intersection(s) of the function with the curve/line  $y = x$  (see Fig. 4.5). Alternatively, if  $g$  has a fixed point at  $m$ , then the function defined by  $f(x) = x - g(x)$  is zero/has a root at  $m$ .

The root of the function  $f(x)$  can be determined by means of fixed-point iteration. This requires setting an initial guess for  $m$ , as  $m_0$ . The iteration continues until  $f(m_i) = m_i - g(m_{i-1})$  is less than or equal to a pre-defined tolerance. If the number of iterations exceeds the maximum number of pre-defined iterations, convergence could not be achieved.

Analogous to  $f(m_i) = m_i - g(m_{i-1})$ , Eqn. (4.6) can be written as  $f(t_n^m) = t_n^m - g(t_n^{m-1})$ . Here  $g(t_n^{m-1})$ , corresponds to the right-hand side of Eqn. (4.6), i.e.,  $t_n^{m-1} + \Delta t_n^{m-1}$ . Therefore, to obtain the discharge instances at a given excitation level, the root of the equation

$$f(t_n^m) = t_n^m - (t_n^{m-1} + \Delta t_n^{m-1}) \quad (4.13)$$

is sought for.

The process to obtain the root of Eqn. (4.13) is outlined in Algorithm 1. First, input parameters for the motor neuron pool model need are selected. Based on this, the max-

---

**Algorithm 1** Scheme to obtain discharge instances. Note that comments begin with #.

---

```

1: Set parameters for the motor neuron pool model:  $RR, PFR_1, PFRD, MFR, g_e,$ 
2: Compute  $PFR_n$  for all motor units(cf. Eqn. (4.12))
3: Compute  $RTE_n$  for all motor units (cf. Eqn. (4.2))
4: Compute  $E_{\max}$  (cf. Eqn. (4.8))
5: Set  $E_{\text{target}} = p \% E_{\max}$ 
6: Set the profile for excitatory drive  $E(t)$  (cf. Eqn. (4.1)) and total length of contraction
    $t_{\text{end}}$ 
7: Set time step for the contraction time,  $\Delta t^*$ 
8: Set parameters for the fixed-point iteration: tolerance,  $tol$ , maximum number of iter-
   ations,  $iter_{\max}$ 
9: for Each motor unit  $n, n = 1 \dots N$  do
10:   Set contraction time:  $t^* = 0$ 
11:   while  $t^* \leq t_{\text{end}}$  do
12:     # Check if the excitatory drive exceeds the recruitment threshold of motor
13:     if  $E(t^*) \geq RTE_n$  and then
14:       # Fixed-point iteration begins
15:       Initialize iteration counter:  $iter = 1$ 
16:       Initalize iterants:  $t_n^m = t^*,$ 
17:          $t_n^{m-1} = t_n^m$ 
18:       while  $|t_n^m - t_n^{m-1}| \leq tol$  and  $t^* \leq t_{\text{end}}$  and  $iter < iter_{\max}$  do
19:         Compute  $\Delta t_n^{m-1} = (g_e(E(t_n^{m-1}) - RTE_n) + MFR)^{-1}$ 
20:         Compute  $t_n^m = \Delta t_n^{m-1} + t^*$ 
21:         Compute error:  $t_n^m - t_n^{m-1}$ 
22:         Update iteration number  $iter \leftarrow iter + 1$ 
23:         Update iterant  $t_n^{m-1} \leftarrow t_n^m$ 
24:     else
25:       # Excitation is not high enough to trigger discharge
26:       # Change excitation by increasing time of contraction
27:       Increase contraction time  $t^* \leftarrow t^* + \Delta t^*$ 

```

---

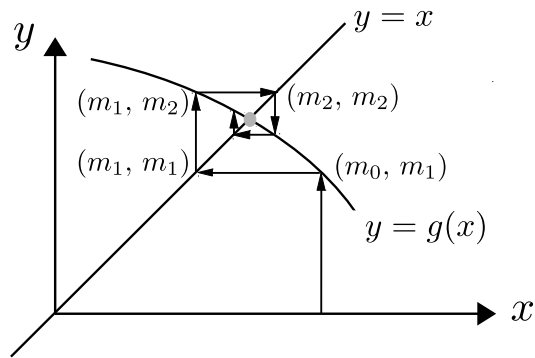


**Figure 4.5:** Schematic description of the fixed-point iteration to find the fixed-point of the function  $g(x)$ , which requires finding the intersection of the function with  $y = x$ . The grey point depicts the root, i.e.,  $g(m) = m$ ,  $m_0$  the initial guess,  $m_1$  and  $m_2$  updated solutions.

imum excitatory drive is computed, cf. Eqn. (4.8). The target level of excitation as a function of the maximum excitatory drive  $E_{\max}$  is also defined as  $E_{\text{target}} = p/100 \cdot E_{\max}$ . Then, the profile for the excitatory drive,  $E(t)$ , is set following Eqn. (4.1). Next, parameters required for the iterative scheme are defined, which include the tolerance,  $tol$ , for the error and the maximum number of iterations  $iter_{\max}$  are selected (see Table 4.1 for the summary of the parameters).

Iterants for the discharge instances are initialized  $t_n^m$  and  $t_n^{m-1}$ . The contraction instance,  $t^*$ , is set to zero. As described earlier in Section 4.1, if the excitatory drive at  $t^*$ , i.e.,  $E(t^*)$ , exceeds the recruitment threshold for motor unit  $i$ , the fixed-point iteration begins. If for a given  $t^*$ , convergence is not reached, then  $t^*$  is increased by  $\Delta t^*$  and the loop starts again. This continues until the total time set for contraction is completed, i.e.,  $t^* = t_{\text{end}}$ .

**Table 4.1:** Summary of the parameters used in this chapter to demonstrate the motor neuron model and the isometric force model as given in Fuglevand et al. [104]. The abbreviations denote the recruitment threshold range,  $RR$ , peak firing rate of motor neuron 1,  $PFR_1$ , slope of the distribution of the peak firing rate,  $PFRD$ , minimum firing rate  $MFR$ , the excitatory gain,  $g_e$ , range for the peak twitch force,  $RP$ , range for the time-to-peak,  $RT$  and size of the motor neuron pool,  $N$ .

$RR$	$PFR_1$	$PFRD$	$MFR$	$g_e$	$RP$	$RT$	$N$
[–]	[Hz]	[–]	[Hz]	[–]	[–]	[–]	[–]
30	45	10	8	1	100	3	100

## 4.2 Computing force output

A signal is defined as “any physical quantity that varies as a function of one or more independent variables” [71]. When there is one independent variable, the signal is a one-dimensional signal. These signals have a single independent variable, which is usually

time, and the signal amplitude varies with time. An example of one-dimensional signal is the variation of muscle force [71].

In order to demonstrate how time-dependent muscle force signal is computed in the present study, it is first necessary to break down the components making up the total force signal. These components are the discharge instances and the twitch response of motor units, as well as the resulting motor unit force. The following sections describe how these components have been obtained and treated.

### 4.2.1 Motor unit force

An impulse has a characteristic shape determined by the system. This shape is the same regardless of the amplitude of the impulse. This characteristic response is called the impulse response and essentially defines the system in the time domain.

A pulse signal having the smallest possible time slice is called the impulse function, or impulse signal. The systems response to this signal is called the impulse response. As the shape of the impulse response is unique to a given system, it can be used to represent the system over time [282].

An impulse function is an infinitesimally brief duration of a signal. Signals can be regarded as a continuum of scaled and shifted impulse functions. They can be stacked sequentially in time to represent the signal. If the response of a linear time-invariant system to a unit impulse is known, then the system response to any input signal may be calculated as the sum of the responses to the scaled and shifted impulses. This procedure is known as convolution [71].

To compute the one-dimensional, time-dependent signal describing the force output of a (synthetic) motor unit pool, the discharge instances obtained from Eqn. (4.6) and the twitch response of the motor units (see Eqn. (4.14)) are used. Thus, the twitch response is the impulse response and impulses are composed of the discharge instances.

It is common for motor units to discharge more than once during a given contraction. The force response of the motor unit to a number of discharges follows the principle of superposition. Superposition states that when multiple influences act on a system, the resultant response is the sum of the system's response to each influence acting alone. Therefore, when a system receives two or more signals, the response of the system can be obtained by solving for the response to each signal in isolation, and then algebraically summing these partial solutions [282].

If the inter-spike-interval of successive discharges are longer than the impulse response, i.e., twitch response, than the yielding force response does not superpose. When the opposite happens, individual responses fuse/superpose yielding a force output higher than a single twitch response (see Fig. 4.6).

#### 4.2.1.1 Twitch response

The motor unit twitch is considered as the impulse response of the motor unit system to a single action potential [104]. This response is modelled, c.f. [104], using the following function:

$$TF(t) = \frac{PTF}{TTP} \exp\left(1 - \frac{t}{TTP}\right) t, \quad (4.14)$$

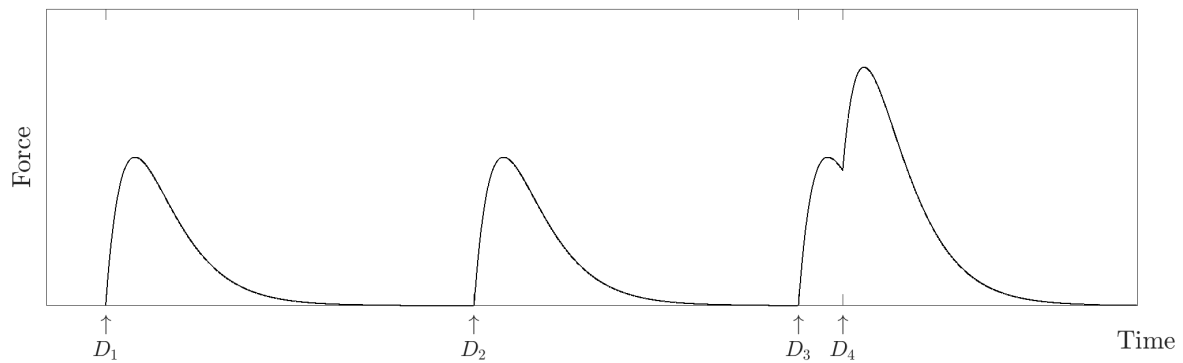


**Figure 4.6:** Four discharge instances indicated by the arrows ( $\uparrow$ ) and  $D_1$ ,  $D_2$ ,  $D_3$ ,  $D_4$ . Time interval between  $D_1$  and  $D_2$  is not short enough for the twitches to fuse. This is not the case for  $D_3$  and  $D_4$ . Twitches occurring after  $D_3$  and  $D_4$  superpose and the force output is higher than a single twitch.

where  $t$  denotes the time,  $PTF$  the peak twitch force and  $TTP$  the time-to-peak-twitch force, which would be referred to in short as the “time-to-peak”. Here,  $PTF$  and  $TTP$  describe the contractile properties of a motor neuron. The response to  $D_1$  in Fig. 4.6 shows the shape of the twitch response following Eqn. (4.14).

In order to convolute discharge instances with the twitch response, both quantities are converted to samples. This is done by simply multiplying each quantity with the sampling rate  $f_s$ . For the twitch response, this yields:

$$TF(\tau) = TF(t) \cdot f_s. \quad (4.15)$$

#### 4.2.1.2 Discharge instances

The set of discharges for motor unit  $i$  are computed from the motor neuron pool as described in Section 4.1. These discharges instances are converted to the impulse response by converting the discharge array into samples by multiplying a given discharge instance  $t_n^m$  with a sampling rate,  $f_s$ , i.e.,  $t_d^i = t_n^m f_s$ . They can be expressed using a Dirac  $\delta$  function as

$$D^n(\tau) = \delta(\tau - \tau_d) = \begin{cases} 1, & \text{for } t = t_d \\ 0, & \text{otherwise,} \end{cases} \quad (4.16)$$

where  $t$  denotes the time and  $t_d$  denotes the sampled time instance of a discharge.

#### 4.2.1.3 Obtaining the muscle force output

In order to compute the force output of a motor unit, the twitch response ( $TF^n$ ) and the discharge instances ( $\mathcal{F}^n(t)$ ) of the motor unit are convoluted. The formal definition (see e.g., Bronshtein & Semendyayev [34]) of the convolution of two functions  $f_1(x)$  and  $f_2(x)$  is the integral:

$$f_1 * f_2 = \int_0^t f_1(\tau) f_2(t - \tau) d\tau, \quad (4.17)$$



where  $*$  is the convolution operator

However, since in this case, discharge instances of each motor unit are not continuous functions, but vectors, convolution operation translates to (cf. [211]):

$$F_k^n = \sum_m TF_m^n D_{k-m}^n, \quad (4.18)$$

where  $m$  denotes all values that lead to legal indices for  $TF_m^n$  and  $D_{k-m}^n$ , cf.  $m = \max(1, k + 1 - r), \dots, \min(q, r)$ , where  $r$  and  $q$  correspond to the length of  $D^n$  and length of  $TF^n$ <sup>1</sup> respectively.

The total force output of the motor neuron pool is referred to as the muscle force output. In order to compute the muscle force,  $F^{sim}$ , individual motor unit forces are summed up linearly as:

$$F^{sim} = \sum_{i=1}^N F_i^n. \quad (4.20)$$

Here,  $N$  denotes the size of the motor neuron pool.

## 4.3 Notes on the use of the modelling scheme in this work

### 4.3.1 Inclusion of the variation in firing instances

It is evident that motor neuron discharges follow a stochastic process, i.e., the inter-spike interval varies for each contraction. Besides the motor unit force, variability in the discharge rate of motor units are known to influence the fluctuations in the total muscle force output [86]. The variation in the inter-spike interval is modelled in Fuglevand et al. [104] by introducing a variation to the discharge instances as:

$$t_n^m = \mu + \mu c.v. Z - t_n^{m-1}, \quad (4.21)$$

where  $\mu$  corresponds to  $\Delta t_n^{m-1}$  in Eqn. (4.6),  $c.v.$  to the coefficient of variation and  $Z$  is the Z-score describing how much  $\mu$  deviates following a normal distribution.

The variation in discharge instances has a profound effect on the number of iterations required for Eqn. (4.21) to converge. This effect is visualized in Fig. 4.7 by running 10 simulations with  $c.v. = 0.2$ . Using  $c.v. = 0.2$  required up to 3000 iterations to reach convergence, whereas, when the variation is excluded, i.e.,  $c.v. = 0$ , this number dropped

---

<sup>1</sup>For  $r = q$  Eqn. (4.18) yields

$$\begin{aligned} F_1^n &= TF_1^n D_1^n \\ F_2^n &= TF_1^n D_2^n + TF_2^n D_1^n \\ &\dots \\ F_q^n &= TF_1^n D_q^n + TF_2^n D_{q-1}^n + \dots + TF_q^n D_1^n \end{aligned} \quad (4.19)$$

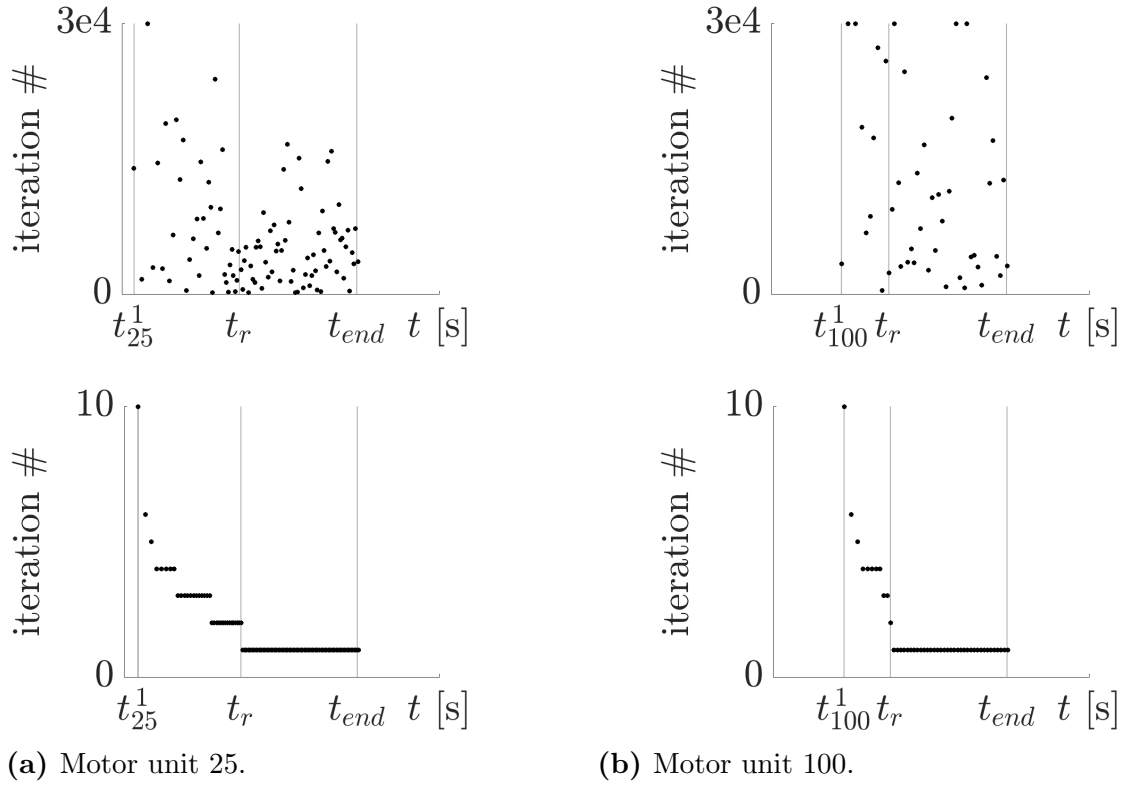


**Figure 4.7:** Influence of including coefficient of variation in the inter-spike intervals on the number of iterations required to find the fixed-point. The excitatory drive follows a ramped increase and a plateau as described in Eqn. (4.1). The ramped increase ends at  $t_r$  and the excitation ends at  $t_{end}$ . The first firing instance of the motor unit  $i$  is depicted with  $t_i^1$ . End of ramped Top figures depict the cases when a coefficient of variation of 0.2 is introduced, whereas the bottom ones show the number of iterations when no variation is present. Note the substantial decrease in the number of iterations when no variation is present.

to 10.

In order to set up the pre-exercise state of the motor neuron pool of vastus lateralis, Bayesian inference is used (see Chapter 3). This scheme requires a high number of model runs. The decrease in the number of iterations in turn decreases the total duration of the simulations. Therefore, number of model runs could be kept high.

To select the model input parameters for the motor neuron pool model, the model output is calibrated against the experimental data on the mean discharge rate of vastus lateralis. Ten model runs including  $c.v. = 0.2$  yielded  $53.87 \pm 0.094$  Hz. When the variation is excluded, i.e.,  $c.v. = 0$ , the mean discharge rate yielded 52.76 Hz. Thus,  $c.v. = 0.2$  produced a model output 0.18 % higher than that of  $c.v. = 0$ . We claim that, excluding the variation in discharges, therefore, poses no significance influence on the overall mean discharge rate (see Fig. 4.8).

Contractile properties of the vastus lateralis are determined by calibrating the total force output obtained from the model against the experimentally measured force output of the muscle. Ten model runs including  $c.v. = 0.2$  yielded a total force output of  $2.243 \times 10^4 \pm 79.36$  au. When the variation is excluded, i.e.,  $c.v. = 0$ , the total force output is  $2.242 \times 10^4$  au. Thus,  $c.v. = 0.2$  produced a model output 0.35 % higher than that of

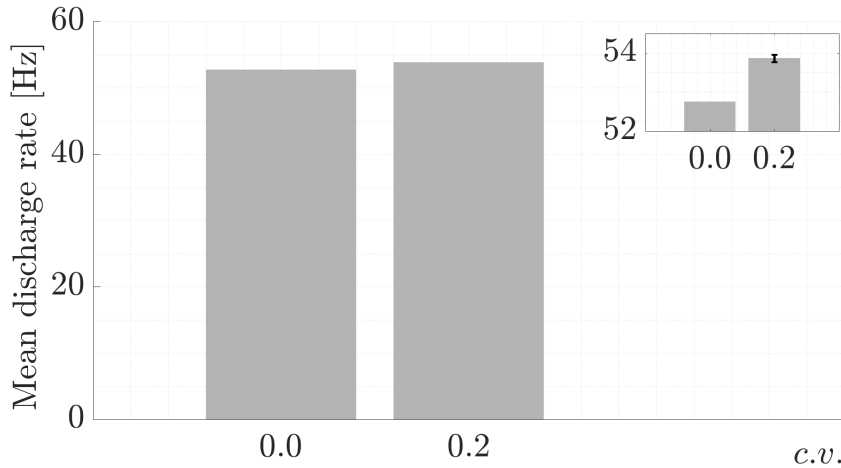


**Figure 4.8:** Effect of introducing coefficient of variation,  $c.v.$ , to the motor neuron model on the mean discharge rate. Labels of the bar plots denote whether or not  $c.v.$  was included, i.e.,  $c.v. = 0.0$  denote no variation and  $c.v. = 0.2$  denote a variation of 20 % in the discharge instances. The insets show a close-up view of the bar plots. The error bars on bars  $c.v. = 0.2$  depict the standard variation of the result of the simulation for 10 runs. Note that the standard deviation introduced by a non-zero  $c.v.$  is 0.18 % of the mean discharge rate case without  $c.v.$

$c.v. = 0$ . As a result, exclusion of the variation does not cause a significant difference in the total force output (see Fig. 4.9).

### 4.3.2 Distribution of the contractile properties

It is known that contractile properties,  $PTF$  and  $TTP$ , in a given motor neuron pool are negatively correlated [7]. This is due to the fact that motor neurons with more dendrites and larger axon diameters conduct the action potential faster. Thus, fibres innervated by these motor neurons also contract faster. Furthermore, such fibres are larger in diameter and hence are able to generate more force in comparison to fibres innervated by smaller motor neurons. As a result, fast motor units require shorter time to reach peak twitch force and can generate higher twitch force.

Adhering to this principle, in Fuglevand et al. [104], contractile properties of motor neurons are modelled following the relationship:

$$TTP_i = TTP_1 PTF_i^{-1/4.2}, \quad (4.22)$$

where  $(\cdot)_i$  denotes the contractile property  $(\cdot)$  of motor neuron  $i$ . Note that  $i = 1$  corresponds to the value of the slowest and thus first recruited motor neuron.

For a motor neuron pool composed of 100 motor neurons and  $TTP^1 = 90$  ms (value from [104]), the distribution of  $PTF$  follows an exponential distribution and  $TTP$  approximately a right-skewed beta distribution (see Fig. 4.10). The accuracy of the distributions of the contractile properties using the relationship in Eqn. (4.22) is debatable. To invest-

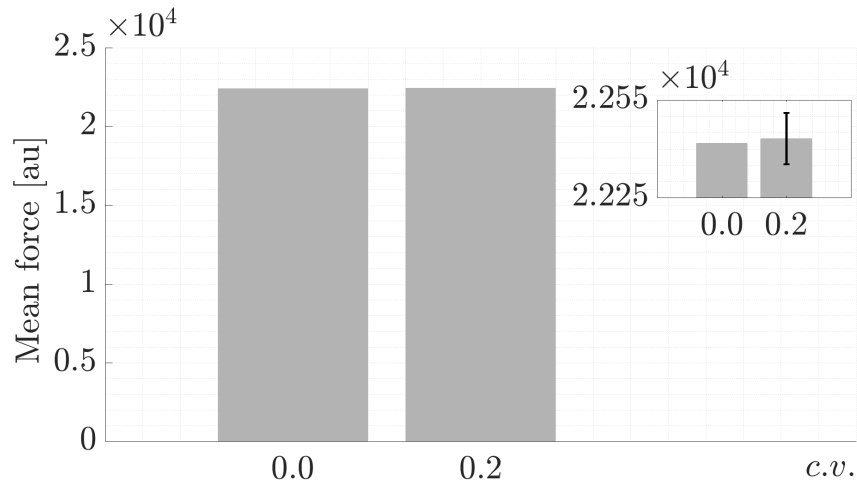


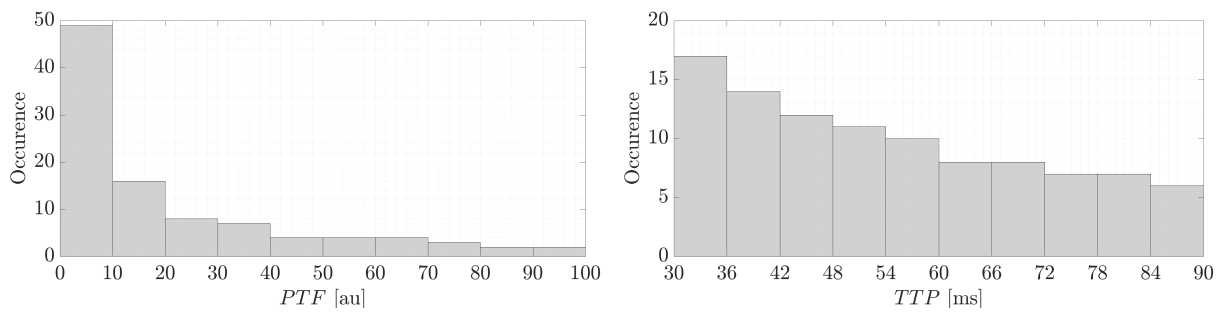
**Figure 4.9:** Effect of introducing coefficient of variation,  $c.v.$ , on the mean total force. Labels of the bar plots denote whether or not  $c.v.$  was present, i.e.,  $c.v. = 0, 2$  denote a variation of 20 % in the discharge instances. The insets show a close-up view of the bar plots. The error bars on bars  $c.v. = 0.2$  depict the standard variation of the result of the simulation for 10 runs. Note that the standard deviation introduced by a non-zero  $c.v.$  is 0.35 % of the mean force for the cases without  $c.v.$

igate this, the relationship between contractile properties, muscle fibre diameter, muscle fibre conduction velocity and motor unit conduction velocity in light of a recent study by Del Vecchio et al. [67] will be discussed.

Muscle fibre conduction velocity and diameter have been shown to be linearly related [26, 122]. This is due to motor neurons innervating muscle fibres with larger diameters possessing larger axons. They can thus transmit the action potential faster. Thus, the recruitment threshold of motor units and the motor unit conduction velocity are also correlated due to the principle of orderly recruitment. Thus, the recruitment threshold of motor units and the motor unit conduction velocity are also correlated due to the principle of orderly recruitment.

The study by Del Vecchio et al. [67] has investigated 406 motor units in the full recruitment range of the tibialis anterior muscle. They have shown that the muscle fibre diameters follow a continuous distribution, resembling a normal distribution. Furthermore, muscle fibre conduction velocity and contractile properties are also shown to be correlated [7, 227]. Thus, it can be inferred that the fibre diameter and contractile properties are also related.

In their study, Fuglevand et al. [104] made use of an exponential distribution for the contractile properties. However, in light of the recent finding by Del Vecchio et al. [67] regarding the distribution of the fibre diameters being normally distributed, it is likely that the distribution of the contractile properties of a motor neuron pool does not follow an exponential distribution. Therefore, in Chapter 6, a scheme is suggested to obtain the distribution of the contractile properties of vastus lateralis by using the isometric strength of the muscle and experimental data from literature.



(a) Distribution of the peak twitch force,  $PTF$  (b) Distribution of the time-to-peak  $TTP$ .

**Figure 4.10:** Distribution of the contractile properties using the relationships provided in Fuglevand et al. [104] for a motor unit pool size of 100 motor units.

# 5 Modelling isometric contraction

## 5.1 Introduction

Force output of a skeletal muscle is dependent on the number of motor neurons recruited and the rate these motor neurons generate motor unit action potential trains (MUAPTs) during the contraction [85, 87, 88, 131]. The discharge trains denote the time instance of the generation of the action potential. The discharge rate for a motor neuron can be computed from MUAPT, which is an important feature of the recruitment behaviour of motor neurons, as it contains information about the task that is being performed [131].

From an experimental point of view, the electrophysiological state of a skeletal muscle can be investigated using electromyographic (EMG) data (see Section 2.2.7). The MUAPTs can be extracted from the EMG data by means of decomposition algorithms [63, 96, 142, 144, 169]. Obtaining MUAPTs for larger muscles at higher force levels, however, produce less reliable insights. This is due to limitations in electrode technology and current algorithmic approaches to decompose the measured signal [248]. Therefore, using the current technology, an accurate description of the discharge behaviour of the entire motor neuron pool for large muscles merely from experimental data is not possible.

To overcome the limitations of the experimental data, the computational model of motor control by [104] is used. This model is already extensively described in Chapter 4 and hence details of the model will not be repeated in this chapter. The model also makes it possible to generate discharge instances at any force level. The prominence of this model and its use in other studies are discussed in Chapter 1 Section 1.2.2. This chapter focuses on the framework used to determine the set of input parameters for the “motor neuron pool model” suggested in [104].

Despite its widespread use, for the motor neuron pool model, there currently exists no study that defines muscle-specific model input parameters based on experimental evidence. The modelling framework described in this chapter makes use of Bayesian updating (see Chapter 3) to determine the input parameters for the vastus lateralis muscle based experimental data obtained from literature. Discharge instances of the entire motor neuron pool for the muscle at any level of force can then be modelled, which describes the pre-exercise state of the motor neuron pool. The model output is then used in Chapter 6 to model the contractile properties of the motor neuron pool. The post-exercise state of the motor neuron pool is later modelled in Chapter 8 by using the set of input parameters obtained in this chapter as the reference state.

## 5.2 Methods

To determine the muscle-specific input parameters for the motor neuron pool model, experimental data obtained from literature is used. First, admissible sets, for each input

parameter of the motor neuron pool model are created. These sets will be referred to as the initial selection of the admissible set of input parameters,  $\Theta$ . When possible, the ranges for the values each set spans are selected based on available experimental evidence. These sets are then narrowed down based on the parameter  $F_{Full Rec}$ , which corresponds to the force level at which all motor neurons contribute to the rate coding, to obtain the prior sets for the admissible input parameters,  $\tilde{\Theta}$ . This way, model runs for unrealistic cases are disregarded and the number of model runs are decreased. The motor neuron pool model is then run for each member of  $\tilde{\Theta}$  and discharge instances of the motor neurons at various levels of force are obtained. The mean discharge rate of the motor neurons at the force plateau is computed, which will be referred to as the model output,  $\Omega^{sim}(p, \tilde{\Theta})$ .

Literature data on the mean discharge rate of vastus lateralis during voluntary isometric knee extension at various force levels are gathered. The model output is then calibrated against the experimental data using a stochastic calibration method, i.e., a Bayesian updating scheme, instead of a deterministic one. This is necessary as the calibration data stems from multiple experimental studies [134]. The calibration yields the posterior sets for the input parameters of the motor neuron pool model, which describes the experimental data on a healthy vastus lateralis muscle. This scheme is visualized in Fig. 5.1. Using the parameter set, which leads to the most accurate mean discharge rate output, i.e., the maximum a-posteriori,  $\tilde{\tilde{\Theta}}$ , the synthetic discharge times for the entire motor neuron pool are generated.

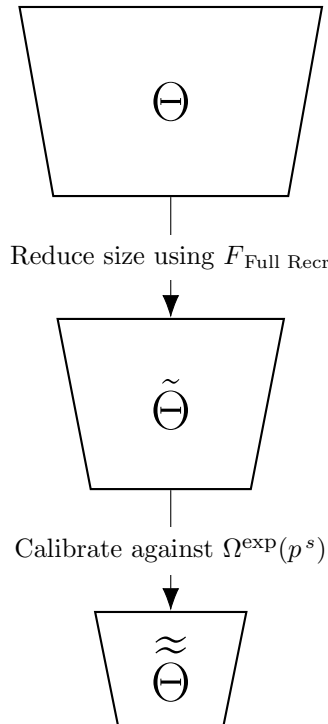


**Figure 5.1:** Visual depiction of the admissible sets for the input parameters. The initial selection for the set of admissible parameters,  $\Theta$ , are reduced to obtain the prior set of admissible parameters,  $\tilde{\Theta}$ , using the upper limit of the force level when all motor neurons are recruited,  $F_{Full Rec}$ , and further reduced down to the posterior set,  $\tilde{\tilde{\Theta}}$ , by calibration of the model output according to experimental data on mean discharge rate,  $\Omega^{exp}$ . Note that the areas of the trapezoids symbolize the size of the sets.

### 5.2.1 Selection of the set of input parameters

The five input parameters to the motor neuron pool model are the range of recruitment,  $RR$ , the minimum firing rate,  $MFR$ , the peak firing rate of the smallest motor neuron,  $PFR_1$ , difference between the first and last recruited motor neuron  $PFRD$ , and the gain in the excitatory drive,  $g_e$ . Based on existing knowledge on the five input parameters, admissible input parameters are determined (Section 5.2.1).

#### Admissible set of input parameters

The initially selected range for each parameter is given in Table 5.1. The range for  $PFR$  is informed from literature, which is known to go up to 100 Hz. Similarly,  $MFR$  is measured to be 5-8 Hz from EMG data [88], but an upper limit is not known. To span all possibilities regarding the discharge rate, the lower limit for parameters describing the discharge rate is taken as 1 Hz. Ranges for the remaining parameters are assumed.

**Table 5.1:** Ranges for the input parameters making up  $\Theta$ , where au denotes arbitrary units.

Variable	Range	Unit
$RR$	[1, 200]	au
$MFR$	[1,100]	Hz
$PFR_1$	[1, 100]	Hz
$PFRD$	[1, 50]	Hz
$g_e$	[1, 2]	au

Within this work, we only consider a finite subset  $\tilde{\Theta}$  of the infinite parameter space,  $\Theta$ . For this purpose, we reduce each of the sets to 10 parameters, so that the each parameter set contains 10 equally spaced values. All combinations of these parameters are computed, which are described using the input parameter vector,  $\Theta$ :

$$\Theta = RR \times MFR \times PFR_1 \times PFRD \times g_e. \quad (5.1)$$

Thus, the cardinality of the resulting parameter space,  $\Theta$  is  $10^5$ .

To determine the set of admissible input parameters,  $\tilde{\Theta}$ , we compute for each element in  $\Theta$  the resulting  $F_{\text{Full Recr}}$  according to Eqn. (4.11). The input parameters are considered to be admissible, if  $F_{\text{Full Recr}}$  is within its physiological range. For human skeletal muscles,  $F_{\text{Full Recr}}$  is typically obtained between 50% MVC and 100% MVC as suggested by Heckman & Enoka [131].

### 5.2.2 Selection of the calibration data

For deriving muscle-specific models, one needs to carry out a calibration step, i.e., derive from experimental data for the (missing) model parameters. Here, we chose to identify a muscle-specific model for the vastus lateralis muscle. Studies of De Luca & Hostage



[63], Jakobi & Cafarelli [152], Kamen & Knight [159], Martinez-Valdes et al. [208] and Martinez-Valdes et al. [207] focus on unilateral isometric knee extension experiments and report the mean discharge rates for various force levels using surface EMG. The relevant data for this study, i.e., the force levels and mean discharge rates, are depicted in Fig. 5.2.

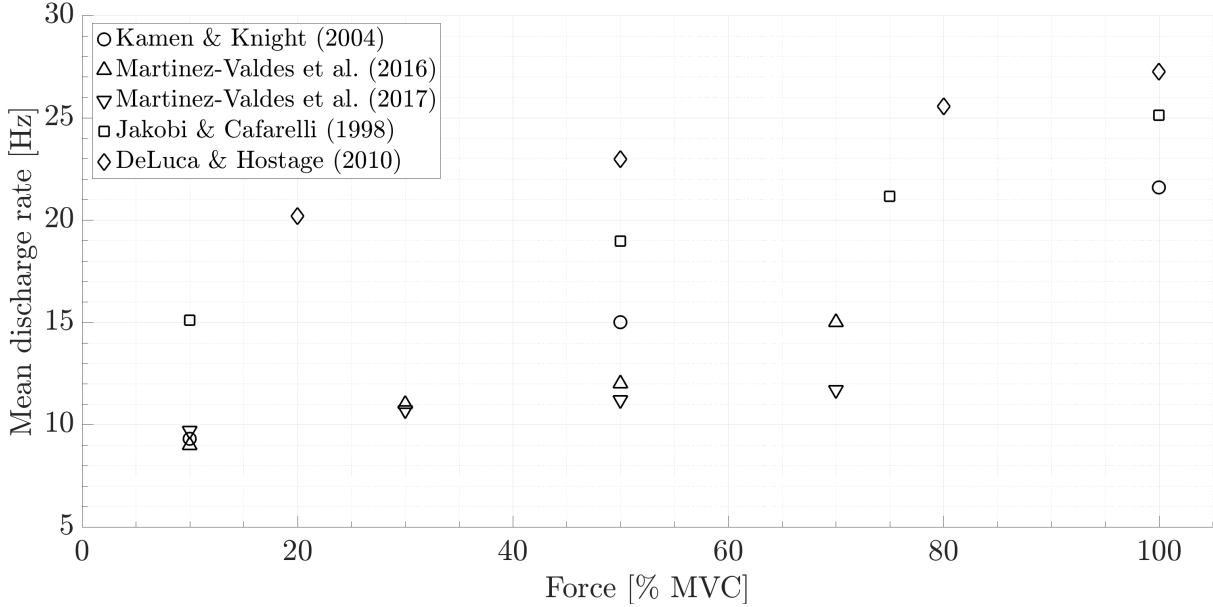


**Figure 5.2:** Mean discharge rate data vs %MVC from experimental studies on isometric voluntary knee extension. Note that at Force = 10 %MVC, three data points almost overlap.

Note that in De Luca & Hostage [63], EMG measurements are made at 20, 80, 100 % MVC. The data on the mean discharge rate at these contraction levels are, however, not reported. Instead, a function to describe the mean discharge rate is provided. The data points for the data set from De Luca & Hostage [63] in Figure 5.2 are computed using the provided function, but only at the levels of force in terms of %MVC at which experimental measurements were performed. The force level where data are reported in a study  $s$  is denoted by  $p^s$ . The set of all mean discharge rates extracted from the  $s = 5$  experimental studies is denoted by

$$\Omega^{\text{exp}} = \{D(p^s) \mid s = 1, \dots, 5\}.$$

### 5.2.3 Computing the mean discharge rate as model output

Given a specific force level, and a particular choice of input parameters, i.e.,  $\Theta \in \tilde{\Theta}$ , the motor neuron pool model can be used to compute the discharge instances for each motor neuron. From the individual motor neuron discharge instances, one can then compute as model output,  $\Omega^{\text{sim}}(p, \tilde{\Theta})$ , the overall mean discharge rate, which is also provided within the above-mentioned experimental studies.

To compute the mean discharge rate, we first define for each motor neuron  $n$ , two sets of discharge instance, i.e.,  $\mathcal{F}_n^1$  containing the discharge instances,  $t_n^m$ , during the force ramp and  $\mathcal{F}_n^2$  containing the ones while maintaining the force plateau. These two sets are

defined by

$$\mathcal{F}_n^1 := \{t_n^m \mid 0 \text{ s} \leq t_n^m \leq 1 \text{ s}\}$$

and

$$\mathcal{F}_n^2 := \{t_n^m \mid 1 \text{ s} < t_n^m \leq 2 \text{ s}\}$$

respectively.

Then the overall simulated mean discharge rate,  $\Omega^{\text{sim}}(p, \tilde{\Theta})$ , of the entire motor unit pool at the plateau region is computed by

$$\Omega^{\text{sim}}(p, \tilde{\Theta}) := \frac{1}{N} \sum_{n=1}^N \left( \frac{1}{|\mathcal{F}_n^2|} \sum_{m=|\mathcal{F}_n^1|}^{|\mathcal{F}_n^1|+|\mathcal{F}_n^2|-1} \left[ \frac{1}{t_n^{m+1} - t_n^m} \right] \right), \quad (5.2)$$

where  $N$  denotes the size of the motor neuron pool.

#### 5.2.4 Estimation of the total motor neuron number in vastus lateralis

Utilising the motor neuron pool model to predict the discharge instances of the vastus lateralis at a given force level requires an estimation of the size of the motor neuron pool,  $N$ . Following the method proposed by Rich et al. [264], the motor neuron pool size can be estimated based on the number of fibres and the innervation ratio of the respective muscle. According to [194], the number of fibres of a vastus lateralis of a healthy male aged between 18 and 30 ranges between 393 000 and 903 000 fibres (see Table 5.2). As far as the innervation ration is concerned, Rich et al. [264] estimated for the vastus lateralis an average innervation ratio of 1500 fibres per motor unit. Dividing the average number of fibres reported in Table 5.2 with the innovation ratio yields the motor neuron size, which is 424.

**Table 5.2:** The total number of fibres of vastus lateralis for subjects aged 18-30 (numbers taken from Lexell et al. [194]) and the corresponding average.

Subject	Age	Nr. of fibres
7	18	674 000
8	19	626 000
9	19	557 000
10	20	505 000
11	21	903 000
12	21	393 000
13	22	859 000
14	26	548 000
15	27	619 000
16	30	603 000
average:		629 000

### 5.2.5 Bayesian updating

The admissible set of input parameters ( $\tilde{\Theta}$ ) defined in Section 5.2.1 provide the first step for the application of Bayesian updating to the current problem. As described previously, these sets are based on existing skeletal muscles physiology knowledge. To select the parameter set describing vastus lateralis muscle within  $\tilde{\Theta}$ , the model output,  $\Omega^{\text{sim}}(p, \tilde{\Theta})$ , is calibrated against experimental data on the discharge rate of vastus lateralis collected from multiple studies. This selection is made based on the likelihood function, which yields for  $\tilde{\Theta}$  the likelihood describing how well the model output describes the experimental data. It is generated using a particular set in  $\tilde{\Theta}$  that represents the data at hand ( $\Omega^{\text{exp}}$ ).

Assuming that the measurement errors related to the data at hand are independent and normally distributed, the likelihood function  $f(D | \Theta)$  takes the following form:

$$f(\Omega^{\text{exp}} | \tilde{\Theta}^q) \propto \exp \left\{ -\frac{1}{2} \Xi^T \mathbf{R}^{-1} \Xi \right\} \quad (5.3)$$

with

$$\Xi := \begin{bmatrix} \Omega^{\text{exp}}(p^1) - \Omega^{\text{sim}}(p^1, \tilde{\Theta}^q) \\ \vdots \\ \Omega^{\text{exp}}(p^S) - \Omega^{\text{sim}}(p^S, \tilde{\Theta}^q) \end{bmatrix},$$

where  $\tilde{\Theta}^q \in \tilde{\Theta}$ , denotes the total number of available experimental data points, and  $\mathbf{R} \in \mathbb{R}^{S,S}$  is the (co)variance matrix of measurement errors. The covariance matrix is a diagonal matrix, as data points are considered to be independent from each other. Thus, the matrix can be expressed as  $\mathbf{R} = \epsilon^2 \mathbf{I}$ , where  $\epsilon$  denotes the measurement error.

Since the studies do not report the error associated with the data, the measurement error

is assumed. The smallest mean discharge rate is reported as 9 Hz at Force = 10 %MVC (see Fig. 5.2). To cover only non-negative values of the discharge rate,  $\epsilon$  is selected as 9 Hz, i.e.,  $\epsilon = 9$  Hz.

After the likelihoods have been computed, the values are normalised, i.e.,

$$w(\tilde{\Theta}^r) = \frac{f(D | \tilde{\Theta}^k)}{\max_q [f(D | \tilde{\Theta}^q)]} \quad \forall \tilde{\Theta}^r \in \tilde{\Theta}. \quad (5.4)$$

The normalised values are typically referred to as weights (e.g., [234]) and they describe the performance of each parameter set relative to the parameter set with the highest likelihood describing the data.

To select from  $\tilde{\Theta}$  the input parameters  $\tilde{\Theta}^r$  for which the likelihood that  $\Omega^{\text{sim}}(p, \tilde{\Theta}^r)$  is within the range of experimental data are large, a rejection sampling algorithm, cf. [291] and described in Section 3.3.3, is employed. The rejection sampling algorithm is defined as follows: first, a random number  $u^k$  is drawn from a uniform distribution  $U(0, 1)$ . Element  $\tilde{\Theta}^r \in \tilde{\Theta}$  is accepted as an element of  $\tilde{\Theta}$  if  $w(\tilde{\Theta}^r) \geq u^r$ . The parameter sets in  $\tilde{\Theta}$  make up the final set of input parameters, which specifically describe the calibration data. The elements of this set are called posteriors. The corresponding set of model outputs is then defined as  $\Omega^{\text{sim}}(p, \tilde{\Theta})$ .

Further, in this study, the input parameter set with the highest weight, known as “the maximum a-posteriori” (MAP) and expressed by

$$\tilde{\Theta}^{\text{MAP}} = \underset{\tilde{\Theta}^k \in \tilde{\Theta}}{\text{argmax}} [w(\tilde{\Theta}^k)]$$

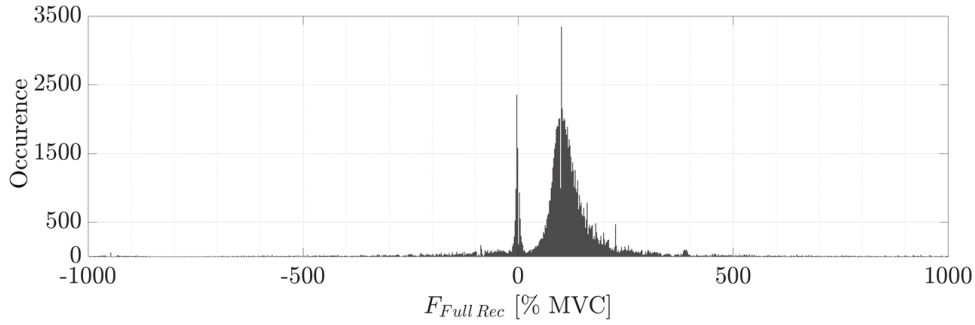
is the input parameter set for which the model generates with respect to the given experimental data the best-fitting output.

## 5.3 Results

### 5.3.1 Characteristics of the prior set of admissible input parameters

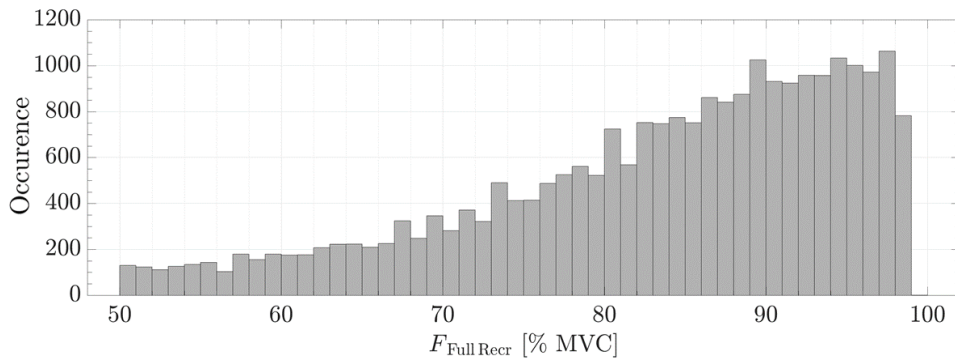
As mentioned before, not all sets of input variables lead to a physiological output. This is shown in Fig. 5.3. There,  $F_{\text{Full Recr}}$  is computed for all sets of input variables and visualised using a histogram (see Fig. 5.3). As  $F_{\text{Full Recr}}$  is expressed in terms of MVC, non-negative values, as well as values exceeding 100%MVC depict non-physiological values of force. Initial selection of the input parameters lead to  $F_{\text{Full Recr}}$  values ranging from  $-3.43 \times 10^5$  to  $\infty$ . The case when  $F_{\text{Full Recr}} \approx \infty$  occurs when the denominator of  $F_{\text{Full Recr}}$ , which is  $E_{\text{max}} = RTE_N + \frac{PFR_N - MFR_N}{g_e}$ , approaches zero. This occurs when  $\frac{PFR_N - MFR_N}{g_e} < 0$ , hence  $RTE_N = \frac{PFR_N - MFR_N}{g_e}$ . The minimum firing rate of motor neuron  $N$  cannot exceed its peak firing rate.

The physiological range for  $F_{\text{Full Recr}}$  for larger human muscles is reported to be between 50 and 100%MVC. When the parameter sets leading to value outside of the reported range



**Figure 5.3:** The force level at which motor unit recruitment is completed,  $F_{\text{Full Recr}}$ , computed from initial selection of the admissible set of input parameters,  $\Theta$ , using Eqn. (4.11).

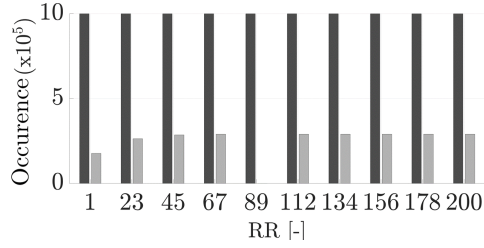
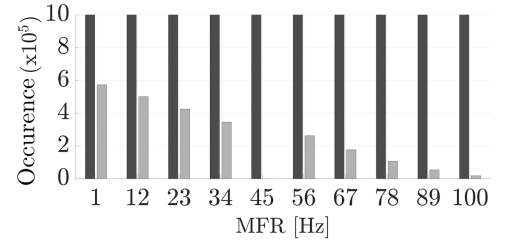
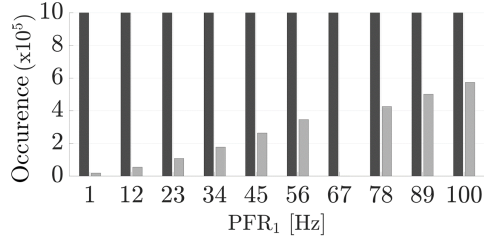
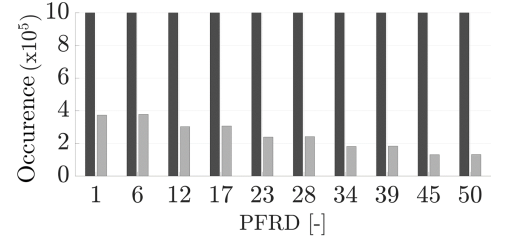
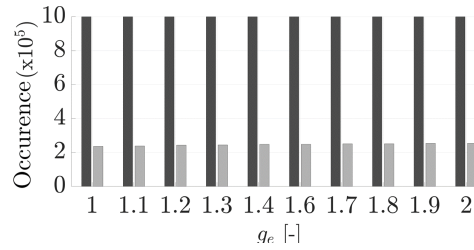
for  $F_{\text{Full Recr}}$  are excluded, the prior set of admissible input parameters,  $\tilde{\Theta}$ , are obtained. Qualitatively, the majority of the  $F_{\text{Full Recr}}$  values for  $\tilde{\Theta}$  seem to be higher than 75%MVC (see Fig. 5.4).



**Figure 5.4:** The force level at which motor unit recruitment is completed ( $F_{\text{Full Recr}}$ ) computed from the prior set of admissible input parameters,  $\tilde{\Theta}$ , using Eqn. (4.11).

The parameters are first selected from 10 equally spaced values within a given range (see Table 5.1). For example, for  $g_e$ , we can choose for each of the 10  $g_e$  values ( $g_e=1.0, 1.1, 1.2, 1.3, 1.4, 1.6, 1.7, 1.8, 1.9,$  and  $2.0$ ). This yields a total of  $10^5$  other variations for each member in  $g_e$ , i.e., different combinations of  $RR$ ,  $MFR$ ,  $PFR_1$ , and  $PFRD$  (see dark grey bars in Fig. 5.5 (e)). When parameter combinations that yield  $F_{\text{Full Recr}} \notin [50, 100]\%MVC$  are excluded, the size of the admissible set of parameters reduce to 24661. This is a reduction of 75.34% in the size of the parameter space. Light grey bars in Fig. 5.5 depict this.

The model output, cf. mean discharge rate of the recruited motor neurons at the force plateau, over force (for  $p = p^s$ ) is shown in Fig. 5.6). As the simulated force level increases, model outputs cover a wider range. This range increases from  $[2, 117]$  Hz at 10%MVC up to  $[21, 413]$  Hz at 100%MVC. Note that the  $\Omega^{\text{sim}}(p, \tilde{\Theta})$  does cover the range of the experimental data (cf. Fig. 5.6, rectangles).

(a) Range of recruitment threshold,  $RR$ .(b) Minimum firing rate,  $MFR$ .(c) Peak firing rate of the smallest motor neuron,  $PRF_1$ .(d) Difference between the peak firing rate of the smallest and largest motorneuron,  $PFRD$ .(e) Gain in excitatory drive,  $g_e$ .

**Figure 5.5:** Distribution of the number of elements for each discrete value. Dark grey bars denote contents of the initial selection of the admissible set of input parameters,  $\Theta$  and light gray ones that of the prior set,  $\tilde{\Theta}$ .

### 5.3.2 Characteristics of the posterior set of admissible input parameters

Bayesian updating lead to the posterior set of the admissible input parameters,  $\tilde{\tilde{\Theta}}$ , which contain 49 sets. Some of the input parameters in  $\tilde{\tilde{\Theta}}$ , depicted in Fig. 5.7, exhibit a trend given the values the parameteres and some do not. The posterior set for the variable  $RR$  is composed of a single value (Fig. 5.7 (a)), whereas, for  $MFR$ , two peaks at 1 Hz and 12 Hz are observed (see Fig. 5.7 (b)). Out of the 10 discrete values, the posterior set for  $PFR_1$  contain only 6 of the initial values (see Fig. 5.7 (c)). There are no gaps in the posterior set of  $PFRD$  (see Fig. 5.7 (d)), meaning that values in posterior set span the entire range selected for the priors. The posterior set for the last parameter  $g_e$  shows a tendency towards values smaller than 1.5, however the values span almost the entire range defined for the prior except for values 1.2 and 1.7 (see Fig. 5.7 (e)). The corresponding  $F_{Full Rec}$  span values within the range  $[50, 90]\%MVC$ , which is narrower than that of  $\tilde{\tilde{\Theta}}$  (see Fig. 5.8).

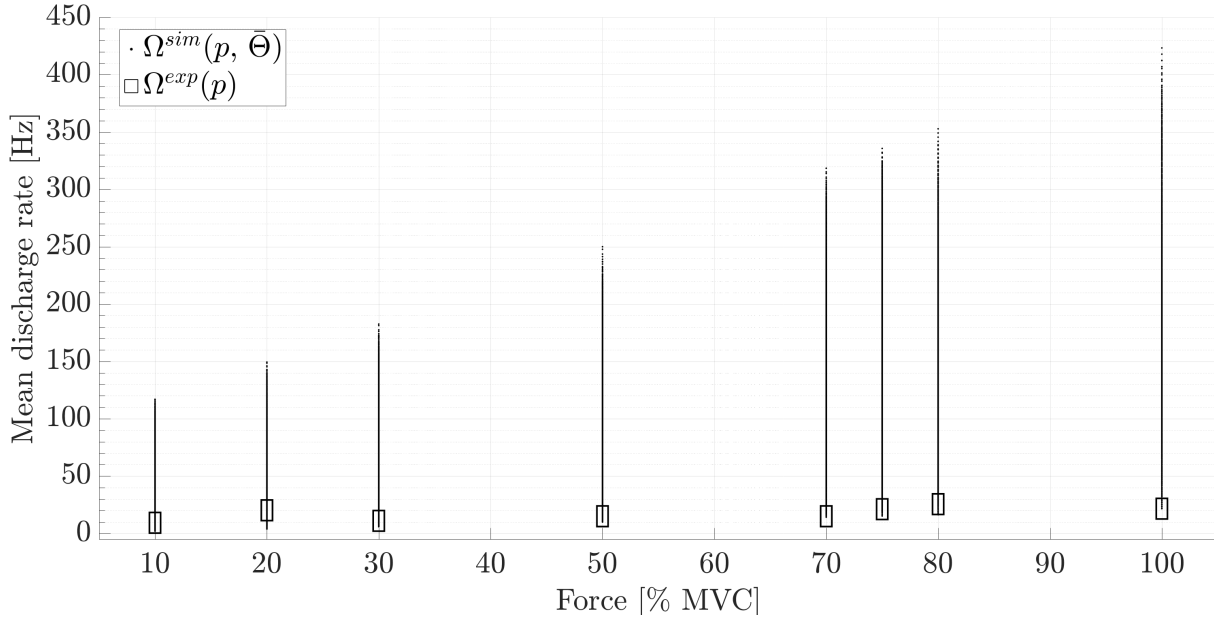


**Figure 5.6:** Mean and standard deviation of the model output (mean discharge rate), obtained from the prior set of admissible parameters,  $\Omega^{sim}(p, \tilde{\Theta})$ , over force,  $p$ . Rectangles denote the range of experimental data.

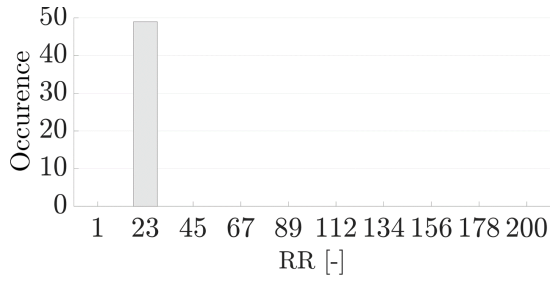
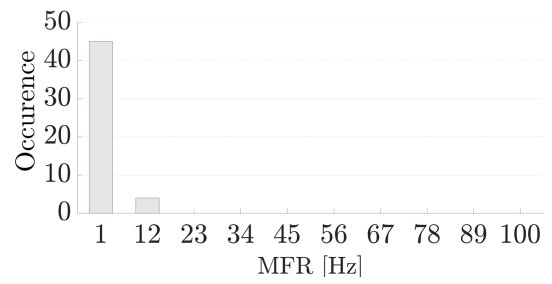
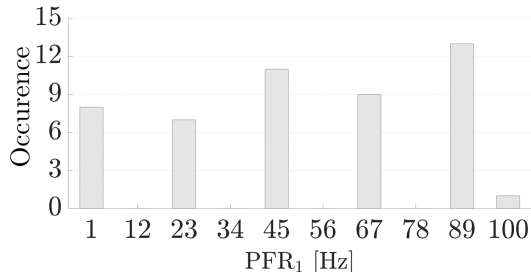
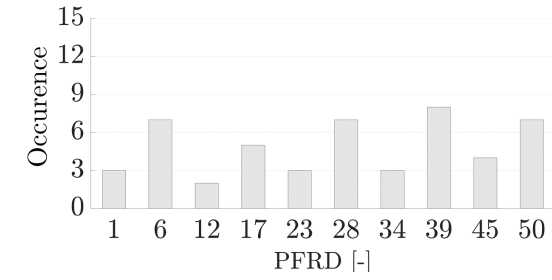
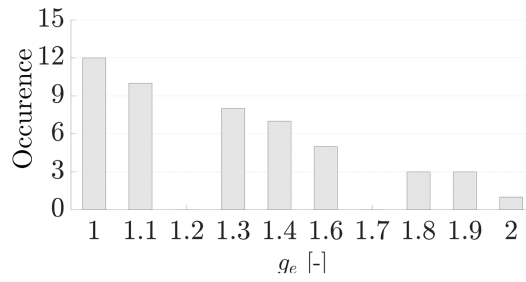
Similar to  $\Omega^{sim}(p, \tilde{\Theta})$ , the model output obtained from the posterior sets,  $\Omega^{sim}(p, \tilde{\tilde{\Theta}})$ , also increases as the simulated force level increases (see Fig. 5.9). Note that the order of magnitude of the model output in  $\Omega^{sim}(p, \tilde{\tilde{\Theta}})$  is much smaller in comparison to  $\Omega^{sim}(p, \tilde{\Theta})$ . Values in  $\Omega^{sim}(p, \tilde{\tilde{\Theta}})$  fall within the range of experimental data.

### 5.3.3 Recruitment behaviour of vastus lateralis

The parameter set yielding the best fit to the data is observed for  $\tilde{\Theta}^{\approx \text{MAP}} = \{23.1, 1.0, 12.0, 1.0, 1.1\}$ . The excitatory drive required to simulate an MVC for  $\tilde{\Theta}^{\approx \text{MAP}}$  is  $E_{\text{max}} = 32$ , with the components  $E^N = 23$  and  $E_{\text{max}}^{\text{II}} = 9$  (see Eqn. 4.8). When these are inserted into Eqn. (4.11),  $F_{\text{Full Recr}}$  is found to be 72% MVC.

The number of recruited motor units over the simulated force resembles the shape of a logarithmic function until  $F_{\text{Full Recr}} = 72\% \text{ MVC}$  (see Fig. 5.10). Up to this force level, total number of recruited motor neurons at the target force level increases with respect to the target force level. Beyond 72%MVC, number of recruited motor neurons stay constant, since the recruitment threshold for all motor neurons at the force plateau are exceeded.

Using  $\tilde{\Theta}^{\approx \text{MAP}}$ , ramped isometric contractions for 1-100% MVC at every 1% MVC is simulated. The mean discharge rate at the force plateau is found to be  $\Omega^{sim}(100, \tilde{\Theta}^{\approx \text{MAP}}) \in [1.16, 28.47]$  Hz. A slight increase in the slope of mean discharge rate with respect to force is observed when the force level exceeds  $F_{\text{Full Recr}}$  (see Fig. 5.11). Note that, the mean discharge rate is zero when target force is less than or equal to 4 %MVC. Motor neurons are found to discharge at a maximum rate of 36 Hz to a minimum of 1 Hz.

(a) Range of recruitment threshold,  $RR$ .(b) Minimum firing rate,  $MFR$ .(c) Peak firing rate of the smallest motor neuron,  $PRF_1$ .(d) Difference between the peak firing rate of the smallest and largest motor neuron,  $PFRD$ .(e) Gain in excitatory drive,  $g_e$ .

**Figure 5.7:** Distribution of the number of elements for each discrete value for the posterior set of admissible input parameters,  $\tilde{\Theta}$ .

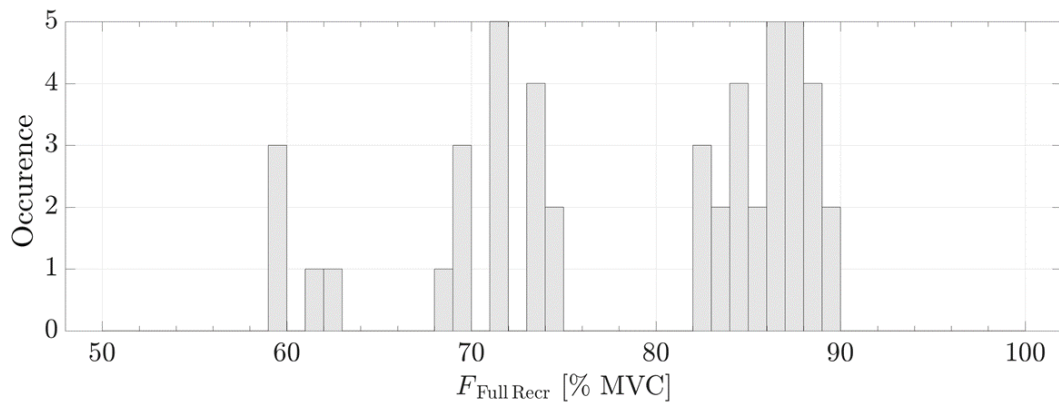


**Figure 5.8:** The force level at which motor unit recruitment is completed ( $F_{Full\ Recr}$ ) computed from the posterior set of admissible input parameters,  $\tilde{\Theta}$ , using Eqn. (4.11).



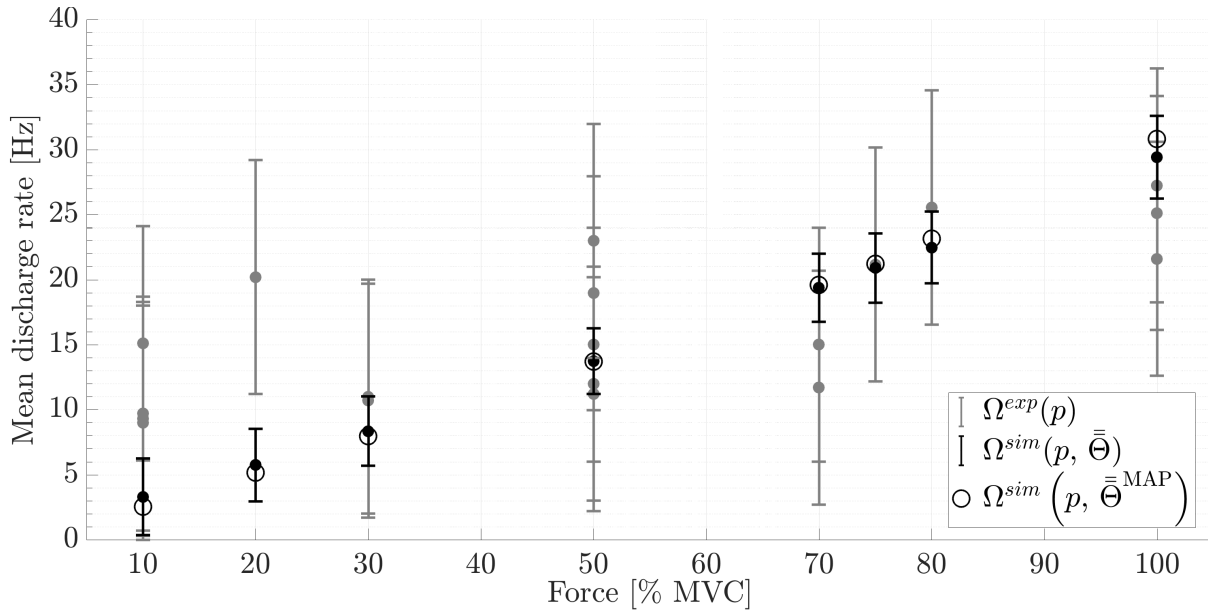


**Figure 5.9:** Mean discharge rate over force levels,  $p$ . Gray dots and error bars denote experimental data (mean and standard deviation) for each reported data point, black solid dots and the black error bars denote the mean and standard deviation of the model outputs obtained from the posterior set of admissible input parameters,  $\Omega^{\text{sim}}(p, \tilde{\Theta})$  and empty circles denote the model output computed from the maximum a-posteriori,  $\Omega^{\text{sim}}(p, \tilde{\Theta}^{\text{MAP}})$ .

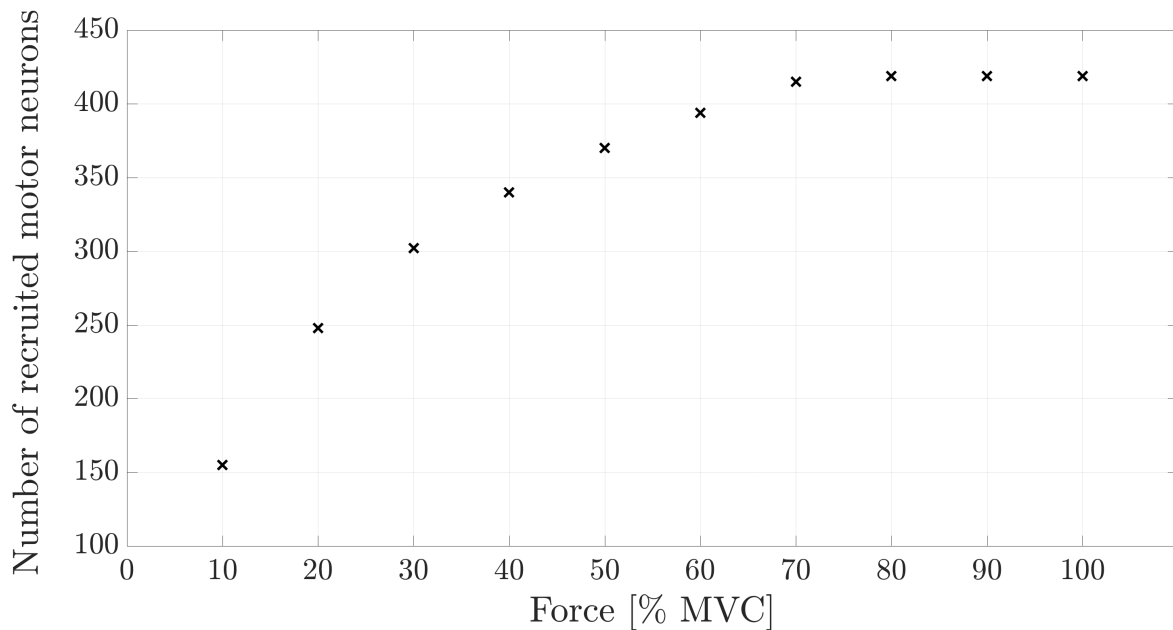


**Figure 5.10:** Number of recruited motor units for 10 to 100 % MVC at each 10 % MVC.

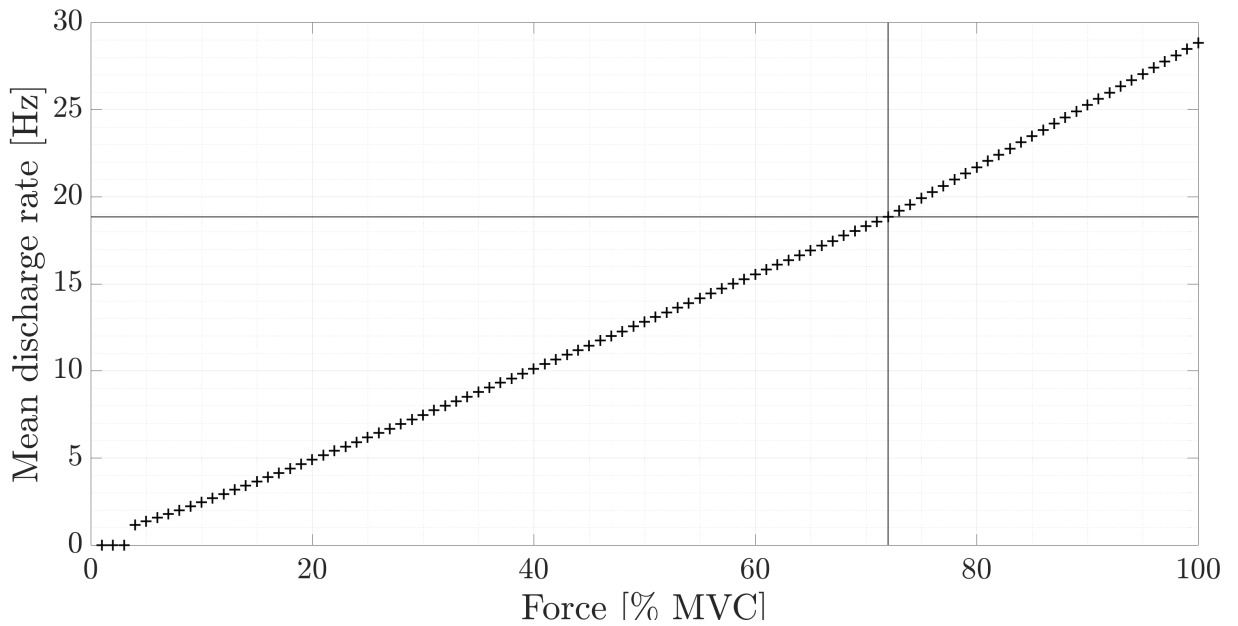


**Figure 5.11:** Mean firing rate of the MAP for 1-100 % MVC. The solid lines mark the force level at which MU recruitment is completed, i.e.,  $F_{Full\ Recr}$  and the corresponding mean firing rate.

The discharge times for the model output  $\Omega^{\text{sim}}(100, \bar{\Theta}^{\text{MAP}})$  are depicted in Fig. 5.12. The discharge rate of motor neurons increase during the force ramp ( $t \leq 1$  s). At the force plateau ( $1 < t \leq 2$  s), motor neurons discharge regularly with their peak discharge rate at the given force level.

## 5.4 Discussion

Even though the motor neuron pool model by Fuglevand et al. [104] is of phenomenological nature, we put the emphasis on the aspects of the model that are physiologically relevant. One such aspect is the force level when all motor neurons are recruited ( $F_{Full\ Recr}$ ), which is possible to compute using the model input parameters. Setting up the admissible set of input parameters according to this quantity helps to disregard non-physiological model runs and keeps the admissible parameter sets within a physiologically-relevant range. Excluding the parameter sets yielding non-physiological  $F_{Full\ Recr}$ , the size of the admissible set of input parameters could also be decreased from  $10^5$  to 26 661. This helped to reduce the number of model runs.

The real output of the motor neuron pool model is the discharge instances. However, by regarding the main model output as the mean discharge rate instead of discharge instances allows to calibrate the model against the experimental data on the mean discharge output. As a result, using the input parameters determined at the end of calibration, the discharge instances for each motor neuron within the motor neuron pool can be generated. Using experimental methods, discharge instances of only a small portion of the motor neuron pool can be obtained. It can therefore be said that the current data-driven scheme provides the means to make up for the limitations of experimental methods without completely disregarding the available experimental data.

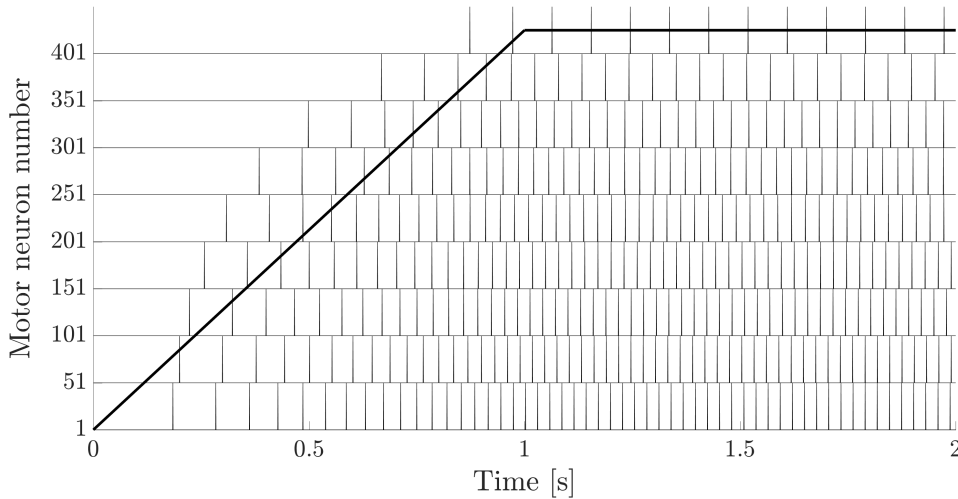


**Figure 5.12:** Discharge times at each 50<sup>th</sup> motor neuron (thin lines) for a simulation of 100% MVC using the maximum a-posteriori input parameters,  $\tilde{\Theta}^{\text{MAP}}$ . The thick line denotes the trace of the excitatory drive/force.

When the motor neuron pool model is implemented and the admissible input parameters are set up as described before, it is possible to obtain "muscle-specific input parameters" for the model by using data on the mean discharge rate of any muscle, since the admissible sets are constructed for any skeletal muscle. Up to now, studies that utilized this model mostly used values for the input parameters which were assumed, without using any scheme to estimate the parameters. The novelty of this work is thus applying Bayesian updating by using physiologically-relevant sets of the input parameters and obtaining muscle-specific parameters based on experimental data on a given muscle. Note that the de-recruitment behaviour of motor neurons upon the termination of excitation is not included in this modelling scheme.

The width of the standard deviation of  $\Omega^{\text{sim}}(p, \tilde{\Theta})$  falls within the range of experimental data and is much narrower than the range of  $\Omega^{\text{sim}}(p, \tilde{\Theta})$ . This points to the fact that the parameter sets in  $\tilde{\Theta}$  were in fact selected from a range of values, which are capable of describing the data at hand. It can therefore be said that the framework used to set up the admissible input parameter sets is feasible.

This model predicts for the vastus lateralis muscle,  $F_{\text{Full Recr}} = 72\% \text{MVC}$ . The recruitment range of vastus lateralis is investigated in the study by De Luca & Hostage [63]. They report that the motor neuron recruitment ends at 95 % MVC for vastus lateralis during a ramped isometric contraction. The corresponding force level found in the current work occurs at a lower contraction level. Once more experimental data is available on this, the result can be judged more accurately.

The results presented here can be revised as more data on the discharge rate of the motor unit pool of vastus lateralis becomes available, which would enhance the amount of calibration data. The revision would not require further model runs, as the model calibration method by using Bayesian update would only require updating the set of calibration data.

Data on the motor unit pool size of vastus lateralis computed using the Motor Unit Number Estimation (MUNE) method is available in literature. As the name suggests,

this is a method to estimate the size of the motor neuron pool of skeletal muscles. The study by Piasecki et al. [246] report the size of the motor neuron pool for measurements obtained from proximal and distal regions of vastus lateralis to be  $197 \pm 92$  and  $146 \pm 47$  respectively. An earlier study reports the motor neuron pool size as 195 [247]. These are based on compound muscle are techniques that utilize intramuscular EMG recordings for force levels not exceeding 25 % MVC. Therefore, it is highly unlikely that the number of motor neurons that detected at a recording at 25 % MVC corresponds to the size of the entire pool. The MUNE method is most commonly used to assess changes in the number of motor neurons in pathological cases or due to ageing (see e.g. Enoka [85], Gilmore et al. [112], Jacobsen et al. [151]). Moreover, as stated in Piasecki et al. [246], the results of the MUNE method represent the number of motor neurons only for a given muscle volume. Thus such results are not representative of the entire muscle volume. Therefore the motor neuron size of vastus lateralis estimated using MUNE is not utilized in this study. When more is known on the size of the motor neuron pool of vastus lateralis, the model can be updated accordingly.

The estimation of the size of the motor neuron pool employed in this study, is based on the assumption that vastus lateralis has the same innervation ratio as vastus medialis, as suggested in Rich et al. [264]. The average number of fibres measured in Lexell et al. [195] for healthy, young subjects are used. Note that data on fibre number are collected from cadavres and not living subjects. Data on the innervation ratio and the number of fibres employing more up-to-date experimental methods would provide a more accurate estimation of the motor unit size.

As seen in Fig. 5.11, all motor units are recruited after 4 % MVC. This means that target excitatory drive up to 4 % MVC ( $E_{target} < 0.04 E_{max}$ ) can not exceed the recruitment threshold of any motor neuron in the pool. Since the recruitment threshold of the motor unit with the lowest threshold can neither be set or nor is coupled to the maximum excitatory drive, the inability to simulate force levels less than or equal to 4% MVC is an inherent limitation of the motor neuron pool model.

The input parameter  $PFR_1$  in the  $\tilde{\Theta}^{\approx \text{MAP}}$  is found to be 12.0 Hz. This value supposedly describes the peak discharge rate of motor neuron 1, i.e., smallest motor neuron. The peak discharge rate should be observed at 100% MVC. When  $\Omega^{\text{sim}}(p, \tilde{\Theta}^{\approx \text{MAP}})$  is examined, the peak discharge rate of motor neuron 1 is found to be 35.6 Hz and occurs at 100 % MVC as expected. The discrepancy between the prescribed value of the input parameter  $PFR_1$  with its value obtained at the end of the simulation stems from the inherent structure of the motor neuron pool model. The reason for this is that  $PFR_1$  never enters the equation describing the discharge rate, i.e., Eqn. (4.3), for a given motor neuron  $i$ . This also applies to  $PFRD$  describing the difference between the peak discharge rate of motor unit 1 and motor unit  $N$ . The difference between the peak discharge rate of the smallest and largest motor neuron is prescribed as 1.0, however, the simulation results yield 24 for this parameter.

The variation in the  $ISIs$  to describe the stochastic nature of the motor unit discharge behavior is neglected in the current scheme. This is done to reduce model complexity and to enforce the reproducibility of the results. It is however known that the variation in  $ISI$  is a significant part of voluntary control. It is thought to be responsible for the force fluctuations in the force output of skeletal muscles [86]. The variation, however, does not

change the mean discharge rate only minimally (see Fig. 4.8). As the calibration is made according to the mean discharge rate, ignoring the variation in the discharges does not cause any significant disadvantage for the current modelling scheme.

As suggested in Revill & Fuglevand [260], high-density, multi-electrode surface arrays and advanced decomposition algorithms make tracking higher threshold motor units over a wider range of force levels more reliable as the methods are developed further. The current modelling framework can be used to model the discharge behaviour of larger muscles until such methods are proven to be dependable for the entire motor unit pool.

The experimental data used in this study is collected from various studies. Although each study employs experiments on isometric knee extension and report data on the vastus lateralis, other aspects in the studies show variations. One of the main aspects that might cause variation in the study outcome is related to the experimental method to collect EMG data and the corresponding signal processing method. Three different experimental methods have been employed to extract the action potential of motor units in the studies used as calibration points in this study. These methods are namely intramuscular EMG, surface EMG and high density surface EMG. Distinguishing between the strengths and weaknesses of each method could pave the way for a more detailed uncertainty quantification. One way to do this could be giving different weight to the measurement error assigned the data points obtained with different methods. A methodology could be developed to take into account the number of detected motor units, type of EMG measurement, gender/age/health of subjects the measurements are being performed on, the decomposition method and so on.

## 5.5 Conclusions

The input parameters  $RR$ ,  $MFR$ ,  $PFR_1$ ,  $PFRD$ ,  $g_e$  required by the motor neuron pool model by Fuglevand et al. [104] are estimated following a data-driven decision-making scheme. A wide range of values are assigned to the input parameter sets initially. Using the relationship between the recruitment range and the maximum excitatory drive, the level of force for the completion of recruitment is determined and the parameter sets that produce non-physiological values for this parameter are disregarded.

Experimental data on the discharge rate of vastus lateralis measured during isometric knee extension from 5 studies provided the calibration data for the Bayesian updating. The motor neuron model is run for the force levels at which experimental data was available. The parameter set that has the highest likelihood (maximum a-posteriori) is determined, which was found to be 23.1, 1.0, 12.0, 1.0, 1.1 for  $RR$ ,  $MFR$ ,  $PFR_1$ ,  $PFRD$  and  $g_e$  respectively. The recruitment is found to end at 72 %MVC for vastus lateralis. Mean discharge rate of the motor units is within the range [1, 36] Hz for 4-100% MVC.

## 6 Modelling contractile properties

Strength describes the state of the performance output of the motor system. The maximum voluntary isometric strength is a common and simple measure of muscle strength [82]. The ease of measurement stems from the absence of angular movement of a joint as the contraction is isometric. Thus, the complexity of the measurement is reduced.

Although isometric strength is simple to measure, measuring strength of an individual muscle is challenging. This is due to the fact that multiple muscles are involved in generating the force output during a given movement. Without precise knowledge of the level of activation as well as the line of action of each muscle, it is difficult to measure the strength of a muscle that belongs to a muscle group *in-vitro*. Computational models such as the model by Elias et al. [80] tackles this issue by estimating force output of individual muscles in quadriceps femoris by considering the cross-sectional area of each muscle.

With the advances in imaging techniques, muscle cross-sectional area can be estimated relatively easy and accurate. Although the strength of an individual muscle can be estimated using computational models, it is still necessary to consider the complicated interaction among neuromuscular elements of the muscle required to generate force. The neuromuscular elements can be divided into the neural and muscular elements. Neural elements are composed of the motor units, whereas the cross-sectional area and length of the muscle make up the muscular elements [82].

One aspect of motor unit activity having a direct influence on the force output of the muscle, is the force output of the motor unit pool, which is the summation of the force output of individual motor units. Motor unit force output is the result of the interaction of the rate modulation and the twitch response of the motor unit (see Section 2.2.6). The twitch response is commonly described by using time-to-peak-force and the peak force measured during a single twitch, which make up the contractile properties of a given motor unit.

Although the twitch response is required to estimate the motor unit force and eventually the total muscle force, data on the contractile properties of human motor units that describe a motor unit's twitch response, are sparse in comparison to other animal species [50]. One reason for the sparsity is the necessity to perform invasive experiments to measure contractile properties of motor units, which poses a challenge for experimental studies on human subjects due to ethical reasons. Furthermore, detailed information related to the motor unit activity is currently only possible to obtain for a small portion of a muscle at low levels of force (see Section 2.2.7).

A common method to measure contractile properties of individual motor units is the spike-triggered averaging of the force signal (see Section 2.2.7 for details regarding this method). Motor units that are detected using this method, are known to be biased towards low threshold motor units, since the measurements are made at low firing rates and contraction levels [216]. Therefore, contractile properties reported as a result of spike-triggered averaging are representative of the lower threshold motor units.

In this chapter a modelling scheme is suggested to quantify the contractile properties of the entire motor unit pool of vastus lateralis muscle. A number of sets for the distribution of each contractile property within the motor unit pool are generated based on existing experimental evidence. The peak twitch force is first treated as a dimensionless parameter. Using data on the isometric force output of vastus lateralis, a scaling factor for each case for the peak twitch force is computed. The distribution of the peak twitch force is then scaled by using this factor. Isometric force output of the muscle is computed using the updated sets of peak twitch force and sets for the time-to-peak force. Similar to the preceding chapter, Bayesian updating scheme is used to select the sets for the contractile properties of the motor unit pool, which describe the experimental data on the isometric force output. The maximum a-posteriori, MAP, (see Section 3.3) is selected as the set of contractile properties describing the vastus lateralis motor units. As the MAP of the contractile properties and the input parameters for the motor unit pool model from Chapter 5 are now known, the pre-exercise state of the motor unit pool of the muscle is now established.

## 6.1 Methods

The aim of this study is to estimate the contractile properties (peak twitch force,  $PTF$  and time-to-peak twitch force,  $TTP$ ) of the motor neuron pool of vastus lateralis. For this, admissible sets for each contractile property are generated. This is done based on experimental data on the contractile properties of other human muscles. Bayesian updating (see Chapter 3) has been used to calibrate the model.

The admissible sets for each contractile property are created using ranges reported in literature. As each motor neuron has different contractile properties, continuous distribution for the contractile properties are generated. These sets follow beta or gamma type of probability distribution.

Initial selection of the sets describing  $TTP$  and  $PTF$  fall within  $(0, 1]$ . Therefore these sets are referred to as normalized sets and are denoted by  $\Theta^{TTP}$  and  $\Theta^{PTF}$ . In order to determine the admissible sets for both properties, normalized sets are scaled by a scaling factor. The scaling factors for time-to-peak force,  $\alpha_r^{TTP}$ , and peak twitch force,  $\alpha_k^{PTF}$ , are determined using two different approaches.  $\alpha_r^{TTP}$  is selected merely based on the data on the slowest motor neuron, whereas  $\alpha_k^{PTF}$  is computed from a new modelling scheme. Using the scaling factors and the initial selection of the contractile properties, prior sets for admissible contractile properties,  $\tilde{\Theta}^{TTP}$  and  $\tilde{\Theta}^{PTF}$ , are obtained.

The input parameters for the motor neuron pool model, which describe the recruitment behaviour of vastus lateralis,  $\tilde{\Theta}^{\approx \text{MAP}}$ , have been determined in Chapter 5. Using the discharge instances obtained by running the motor neuron pool model with  $\tilde{\Theta}^{\approx \text{MAP}}$  and using  $\tilde{\Theta}^{PTF}$  and  $\tilde{\Theta}^{TTP}$ , to compute the twitch response, total force output of the muscle at various force levels are computed,  $F^{sim}$ .

The isometric strength of vastus lateralis is estimated using experimental data on the isometric strength of knee extensors and is indicated by  $F^{exp}$ . The total force output  $F^{sim}$  is calibrated against  $F^{exp}$  using Bayesian updating. Thus, posterior sets for each contractile property are obtained. This scheme is summarized in Fig. 6.1.

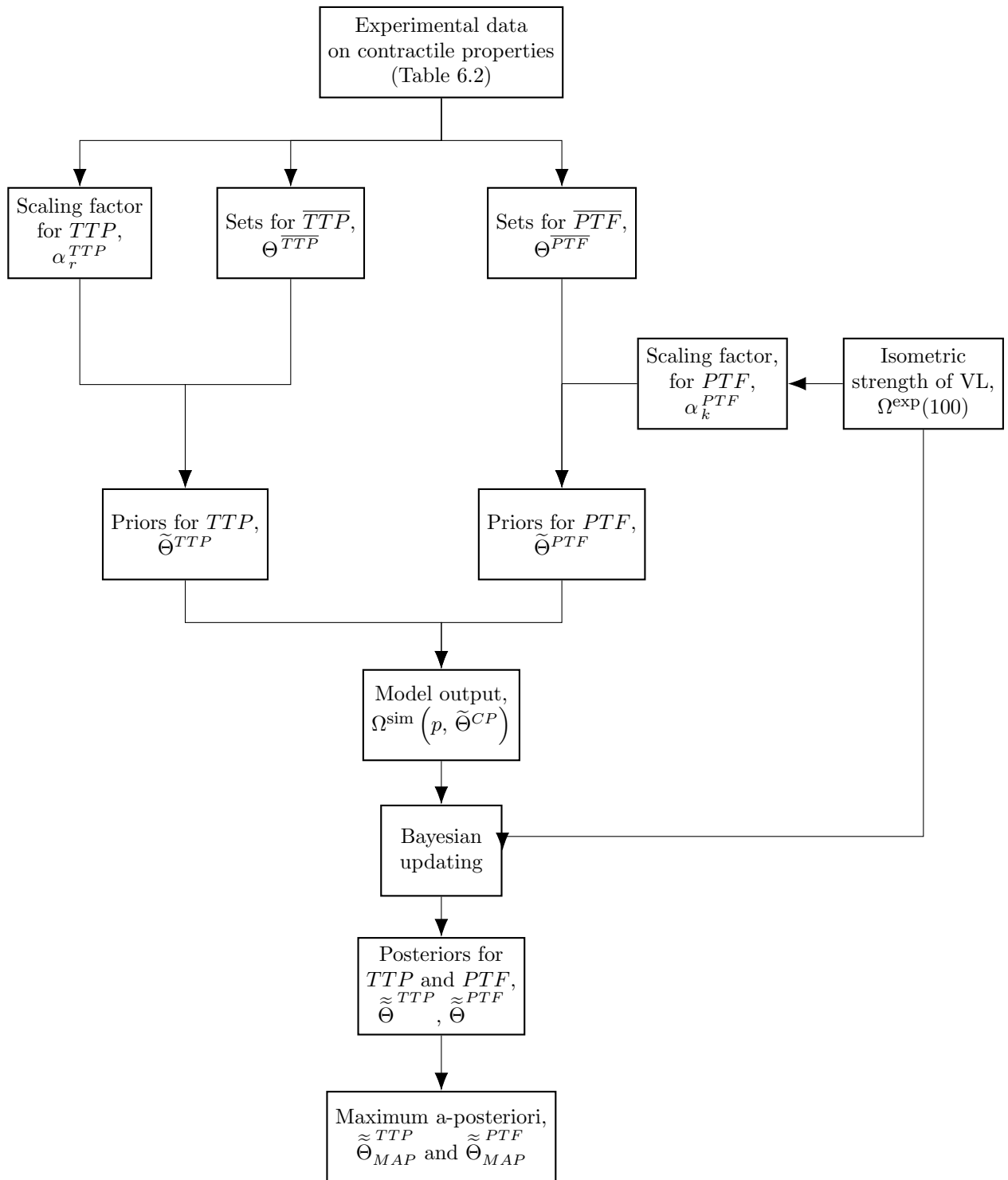


**Figure 6.1:** Overview of the modelling scheme.

### 6.1.1 Estimating the isometric strength of vastus lateralis

Experimental data from literature on the isometric voluntary strength of knee extensor muscles of healthy, young, male subjects, have been collected. The studies by Bigland-



Study	Mean [N]	Std [N]
<b>Kamen &amp; Knight [159]</b>	522	33
<b>Miller et al. [219]</b>	688	63
<b>Zhou et al. [329]</b>	583	36
<b>Bigland-Ritchie et al. [24]</b>	535	155
<i>Mean</i>	<i>582</i>	<i>71</i>

**Table 6.1:** Mean and standard deviation (Std) of isometric knee extensor strength reported in five different studies. All studies except for Miller et al. [219] report the value for maximum effort voluntary force output, corresponding to the maximum voluntary contraction (MVC). Miller et al. [219] reports the maximum voluntary torque (MVT). To convert this into MVC, MVT is divided by the mean femur length, which is reported as 0.4 m in the study.

Ritchie et al. [24], Kamen & Knight [159], Miller et al. [219], Nikolaidou et al. [233], Stock et al. [298], Zhou et al. [329] report the isometric voluntary strength of knee extensors of healthy, young, male subjects in terms of maximum voluntary contraction (MVC). The mean value of the data on the maximum voluntary force is then computed and regarded as the isometric strength of knee extensors (see Table 6.1).

In the study by Elias et al. [80], the distribution of the contribution of each knee extensor muscle on the total force output of the knee extensors was estimated. The estimation is based on the cross-sectional area proportion of each knee extensor muscle. Accordingly, vastus lateralis is said to take up 38% of the total force exerted by the knee extensors. The isometric voluntary strength of vastus lateralis, is computed by taking 38% of the mean isometric knee extensor strength. The isometric strength corresponds to a 100 %MVC, thus this parameter is expressed as  $F^{exp}(p = 100)$ , where  $p$  denotes the contraction level.

The force output of vastus lateralis over the entire range of force output, i.e., for  $[0, 100]$  %MVC, is computed simply as:

$$F^{exp}(p) = F^{exp}(100) \cdot p/100. \quad (6.1)$$

### 6.1.2 Experimental data on contractile properties

Data on the contractile properties of human skeletal muscles from experimental studies are extracted (see Table 6.2). This data set is used to set up the admissible sets for the contractile properties. Here, only the studies that report data obtained without or prior to any changes (training, pain induction, fatigue, temperature change) in the normal muscle condition are considered. Data from elderly subjects are also disregarded to exclude ageing effects.

A total of 18 studies have been found to report data on contractile properties after a single action potential. The data have been collected from various human skeletal muscles (see Table 6.2). Some studies report data on more than one muscle or measurement. Each individual measurement is taken as a separate data set, which yields 32 different data sets. Measurement methods used in the experimental studies include highly selective bipolar electrodes, intramuscular EMG, intraneural stimulation, needle in tendon, surface EMG and spike-triggered averaging. The muscles from which data have been collected are biceps

brachii, first dorsal interosseous, thenar, tibialis anterior, toe extensors, triceps brachii, gastrocnemius (medial and lateral), nasal distalators and platysma.

### 6.1.3 Constructing admissible sets of contractile properties

Sets following beta- and gamma-distributions are created for the contractile properties. These sets are customized for each property.

Implicit MATLAB functions `betarnd` and `gamrnd` were used to create the sets. These functions generate random numbers following beta and gamma distributions, respectively. These distributions have been selected since they allow us to create sets of values spanning a wide range. As input, they both require the size of the sets to be generated and two shape parameters ( $a$  and  $b$ ). The size of each set equals the size of the motor neuron pool since the aim is to determine the contractile property of each motor neuron in the pool. Each shape parameter is selected from a range of 1 to 100.

The beta distribution has the following probability distribution:

$$y = f(x; a, b) = \frac{1}{B(a, b)} x^{a-1} (1 - x)^{b-1} I_{[0,1]}(x), \quad (6.2)$$

where  $B(a, b)$  is the beta-function and  $I_{[0,1]}(x)$  is the indicator function ensuring that only values in  $x \in (0, 1]$  have non-zero probability [210].

The gamma distribution has the following probability distribution:

$$y = f(x; a, b) = \frac{1}{b^a \Gamma(a)} x^{a-1} e^{-x/b}, \quad (6.3)$$

where  $\Gamma(a)$  is the gamma function.

When  $a$  is large, the gamma distribution approximates a Gaussian distribution. The function has the advantage that the distribution has a probability density only for positive, real numbers [212].

The order of magnitude of the contractile properties are commonly described in literature in terms of X-folds, which is a rough description of the range of the values the contractile property of a motor neuron pool of a muscle spans. Therefore, the sets describing the contractile properties are generated such that a given combination of the shape parameters  $a$  and  $b$  span the range of values suggested in literature. The width of the range of values is described here by a parameter referred to as the “*range ratio*” and is computed from the ratio between the maximum and minimum values within a given data set.

Not all combinations of the shape parameters can generate sets following the beta or gamma distribution. This problem is more prominent for the sets for *PTF* as they span a wider range of values in comparison to *TTP*. To tackle this problem, a simple algorithm is used to generate the sets (see Algorithm 2). For a given set of shape parameters, this loop generates random numbers following beta and gamma distribution until *range* falls between the required range (e.g., a 4-5 for *TTP*). The number of attempts to generate a set for a given combination of shape parameters is counted. This is limited by a prescribed tolerance to prevent an infinite number of attempts. If the counter exceeds the tolerance for a combination, then the algorithm moves on to the the next set of shape parameters.

Study	Muscle	N <sub>MU</sub>	TTP [ms]					PTF						
			Mean	Std	Min.	Max.	%Std	Mean	Std	Min.	Max.	%Std	Unit	
[91]	TA	1 <sup>C1</sup>	70.9	5.9			8.32							
		1 <sup>C2</sup>	72.2	5.1										
		1 <sup>C3</sup>	74.6	5.0										
[92]	TA	32										98.21	mN m	
[114]	FDI	46	57.0	8.0	42	76	14.04	15	1	75	100.00		mN	
[294]	FDI	67							0.18	30			g	
[266]	TA <sup>C,2</sup>		61.8	2.8			4.53	2.7	2.8			103.70	mN m	
[311]	TA	528	45.6	13.8	20	86	30.26	25.5	21.5	0.7	171	84.31	mN m	
[310]	TA	256	71.0	10.1	20	90	14.23	32.2	1.9	0.7	170	5.9	mN m	
[35]	BCL	154	52.0	14.5	16	84	27.88							
		148	44.5	9.5	16	68	21.35							
		66	45.0	7.0	30	58	15.56							
		83	58.0	9.0	38	80	15.52							
		84	79.0	12.0	40	110	15.19							
		78	75.0	8.5	54	102	11.33							
[70]	FDI	54	74.0	11.0	52	100	14.86							
[174]	FDI	236	47.3	12.8	20	90	27.06	17.7	19.8	0.2	105	111.86	mN	
	BB	200	63.1	14.7	30	135	23.30	14.9	16.3	1	140	109.40	mN	
										0.01	2		kg	

**Table 6.2:** Literature data on time-to-peak-force and peak twitch force. Min. and max. columns refer to the limits of the data range. Abbreviations in muscles column denote the following: BB: biceps brachii, BCL: Biceps cap. long., FDI: first dorsal interosseous, TA: tibialis anterior. Here only the data measured before any further intervention (e.g. change in temperature, inducing pain, exercise) is taken. The abbreviations describing the data sets are  $C^x$ : contraction number  $x$ ,  $C^{x,2}$ : control, experiment 2.

**Table 6.3:** Parameters used to create random distributions for *PTF* and *TTP*. Range denotes the range of values reported in literature for each contractile property. Step denotes the step size used for generating the arrays for the shape parameter  $a$  and  $b$ .

	Range		a			b			Scale			tol
	min.	max.	min.	max.	step	min.	max.	step	min.	max.	step	
<i>PTF</i>	100	250	1	100	1	1	100	1	-	-	-	1000
<i>TTP</i>	4	5	2	100	2	2	100	2	80	160	20	3

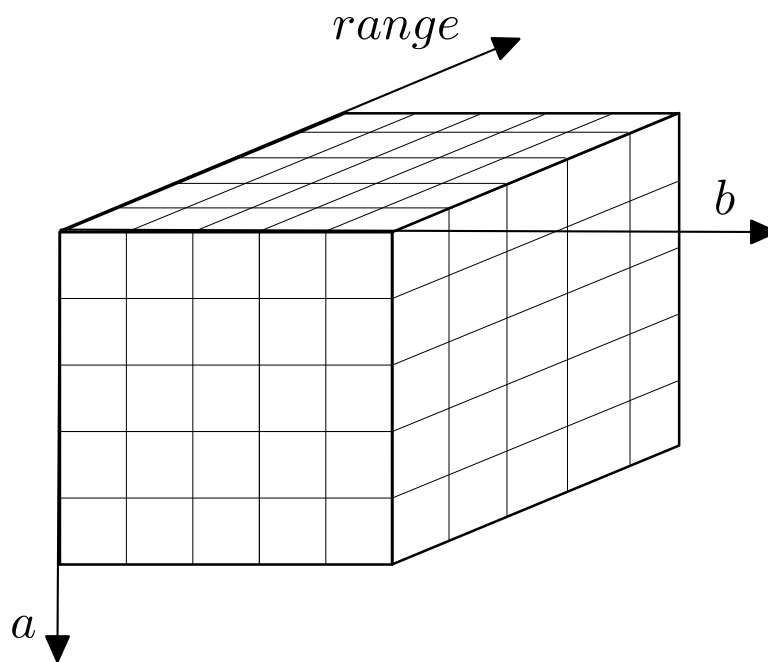


**Figure 6.2:** Symbolic description of combining shape parameters  $a$ ,  $b$  and the *range* to obtain normalized sets.

---

**Algorithm 2** Scheme to generate random numbers following beta and gamma distribution. The rightarrow  $\rightarrow$  denotes assigning parameters to the variable on the right side of the arrow. Values of the parameters are given in Table 6.3.

---

```

1: initialize shape parameters  $a$  and  $b$ 
2: generate all combinations of  $a, b \rightarrow$  shape_parameters
3: set size of the random number array (equals  $N_{MU}$ )
4: initialize the limits for the range  $\rightarrow$  min_range, max_range
5: set the tolerance for the counter  $\rightarrow$  tol

6: for each member in shape_parameters do
7:   get  $a$  from shape_parameters  $\rightarrow a_i$ 
8:   get  $b$  from shape_parameters  $\rightarrow b_i$ 
9:   initialize the counter to 1
10:  initialize range s.t. the while loop can be entered,
    e.g., range = min_range - 1

11:  while range < min_range
12:    or range > max_range
13:    and count < tol do
14:    generate random numbers following beta/gamma distribution
    using shape parameters  $a_i$  and  $b_i \rightarrow r$ 
15:    compute min. value in  $r \rightarrow$  min_r
16:    compute max. value in  $r \rightarrow$  max_r
17:    compute range for  $r \rightarrow$  max_r/min_r
18:    count  $\leftarrow$  count + 1

```

---

Note that these sets are normalized against its highest value (see Fig. A.1 and Fig. A.2 for a selection of the sets). This way, the highest value in each set is set to one and the distribution of the values in each set is preserved.

#### 6.1.4 Prior sets for time-to-peak-force

Experimental data shows that  $TTP$  values span 1.5-4 fold (see Table 6.2). However, most studies report data from only a small number of motor neurons. Out of the 32 data sets, only 4 data sets (i.e., the ones that reported in [174, 310, 311]) report contractile properties for 200 or more motor neurons (see Table 6.4).

**Table 6.4:** Literature data on time-to-peak-force and peak twitch force for studies which report data on more than 200 MUs. Min. and max. columns refer to the limits of the data range and mean and std refer to the mean and standard deviation of the data set respectively. Abbreviations in muscles column refer to BB: biceps brachii, FDI: first dorsal interosseous, TA: tibialis anterior.

Study	Muscle	$N_{\text{MU}}$	TTP [ms]			
			Mean	Std	Min.	Max.
Van Cutsem et al. [310]	TA	528	45.6	13.8	20	86
Van Cutsem et al. [311]	TA	256	71.0	10.1	20	90
Kossev et al. [174]	FDI	236	47.3	12.8	20	90
	BB	200	63.1	14.7	30	135

Since the aim is to model the entire motor neuron pool of vastus lateralis, which is estimated to have 424 motor neurons, only data sets that report data for a high number of motor neurons is used to construct the admissible sets for  $TTP$ . These data sets report  $TTP$  values that lie between 20-135 ms and the values for each data set vary by 4 to 5 fold. Based on this, sets for  $TTP$  that follow beta and gamma distributions with values spanning a 4-5 fold are created.

Sets for the time-to-peak values are expressed as:

$$\Theta_i^{TTP} = \{\overline{TTP}_i^n \mid n = 1, \dots, N; \overline{TTP}_i^1 = 1\} \quad (6.4)$$

where  $i$  denotes set number,  $\overline{TTP}_n^i$  the normalized and dimensionless time-to-peak value for a motor neuron  $n$  in set  $i = 1, \dots, I$ .

To mimic the size principle, time-to-peak-force values descend from  $TTP^1$  to  $TTP^N$  as the motor neuron 1 is smaller than motor neuron  $N$  and takes more time to reach the peak force. Thus in Eqn. (6.4),  $\overline{TTP}_i^1 = 1 > \overline{TTP}_i^2 > \overline{TTP}_i^N \forall i$ .

Values in  $\Theta_i^{TTP}$  are initially dimensionless/normalized, thus elements of these sets have values that lie within  $(0, 1]$ . To obtain the prior sets for  $TTP$  in milliseconds,  $\tilde{\Theta}_i^{TTP}$ ,  $\Theta_i^{TTP}$  is multiplied with a scaling factor. To determine the order of magnitude of the scaling factor, data sets given in Table 6.4 are used. These sets report for the smallest/slowest motor neurons, i.e., motor neuron 1,  $TTP$  values ranging from 80 to 135 ms.

Five different scaling factors are selected according to the data on the slowest motor neuron. The scaling factors are selected as  $\alpha_r^{TTP} = \{100, 120, 140, 160\}$  ms, i.e., 100 to 160 ms with a 20 ms interval. By selecting the minimum scaling factor as 100 ms, it is ensured that the  $TTP$  of the fastest motor neuron in any set is minimum 20 ms and the values cover a 5-fold range. Note that, the highest value for  $TTP$  is reported to be 20 ms within the 4 data sets (see Table 6.4). Using a number of scaling factors based on experimental evidence allowed to create a variety of different configurations for the distribution of  $TTP$  over a motor neuron pool.

Scaling  $\Theta^{\overline{TTP}}$  yields the prior set for  $TTP$ , denoted by  $\tilde{\Theta}^{TTP}$ . To illustrate, to obtain one set in  $\tilde{\Theta}^{TTP}$ :

$$\begin{aligned}\tilde{\Theta}_i^{TTP} &= \Theta_i^{\overline{TTP}} \cdot \alpha_r^{TTP}, \\ &= \{\overline{TTP}_i^n \cdot \alpha_r^{TTP}\},\end{aligned}\tag{6.5}$$

where  $r = 1, \dots, 4$ . Note that  $\overline{TTP}_i^1 = \alpha_r^{TTP} \forall i = 1, \dots, I$ , since  $\overline{TTP}_i^1 = 1$ .

### 6.1.5 Prior sets for the peak twitch force

Different motor neurons vary greatly in their force generating capacity. This difference is estimated to as 100-fold or more [216]. In Enoka [83], authors report a 150 folds-difference based on the earlier experiments by Burke et al. [38], Burke & Tsairis [39]. Whereas, Van Cutsem et al. [310, 311] found a 240 fold difference in  $PTF$  of the smallest and largest motor neuron (see (see Table 6.2)). Therefore, normalized sets for  $PTF$ , which cover a 100-250 fold range of  $PTF$  values are created using the scheme described in Section 6.1.3.

Once again, to mimic the size principle, elements of this set are arranged in ascending order as

$$\begin{aligned}\Theta_j^{\overline{PTF}} &= \{\overline{PTF}_j^n \mid n = 1, \dots, N\}, \\ &= \{\overline{PTF}_j^1, \overline{PTF}_j^2, \dots, \overline{PTF}_j^N\},\end{aligned}\tag{6.6}$$

where  $\overline{PTF}_j^1 < \overline{PTF}_j^2 < \overline{PTF}_j^N = 1 \forall j = 1, \dots, J$ .

To obtain the prior sets for  $PTF$ , similar to  $TTP$ , values in  $\Theta_j^{\overline{PTF}}$  is multiplied with the scaling factor,  $\alpha_k^{PTF}$ . To determine  $\alpha_k^{PTF}$ , instead of relying on experimental data, a new scheme has been introduced.

In an attempt to couple the  $TTP$  and  $PTF$ , all possible combinations of the contractile properties are generated. The admissible set of parameters describing the contractile properties can thus be expressed by

$$\Theta^{\overline{CP}} = \Theta^{\overline{PTF}} \times \tilde{\Theta}^{TTP},\tag{6.7}$$

where  $CP$  denotes contractile properties. The size of  $\Theta^{\overline{CP}}$  equals  $K = I \cdot J$ . Note that, at this point, values for  $\tilde{\Theta}^{TTP}$  have already been determined as described in Section 6.1.4.

To obtain the prior set for the contractile properties, i.e.,  $\tilde{\Theta}^{CP}$ , for each set in  $\Theta^{\overline{PTF}}$ , scaling factor  $\alpha_k^{PTF}$  needs to be determined. When  $\alpha_k^{PTF}$  is known,  $\tilde{\Theta}^{PTF}$  can then be

determined simply by:

$$\tilde{\Theta}_k^{PTF} = \Theta_k^{\overline{PTF}} \cdot \alpha_k^{PTF}, \quad (6.8)$$

where  $k = 1, \dots, K$ . Note that  $\alpha_k^{PTF}$  corresponds to the peak twitch force of motor neuron  $N$  in all sets in  $\Theta^{\overline{PTF}}$ .

To compute the  $\alpha_k^{PTF}$ , first, the motor unit force output at 100% MVC ( $\overline{F}_k^{sim}$ ) is computed. This is done for all sets in  $\Theta^{CP}$ . The steps to compute the motor unit force output is already described in Section 4.2.1. Discharge instances ( $\mathcal{D}$ ) generated using the MAP input parameters determined in Chapter 5 are used to compute the motor unit force output. Note that, as sets in  $\Theta^{CP}$  are used,  $PTF$  is replaced by  $\overline{PTF}$ . When any quantity is computed using  $\overline{PTF}$ , the corresponding output will be denoted by an overline, e.g., the twitch force  $TF$  becomes  $\overline{TF}$ .

Individual twitch responses superpose if the inter-spike-interval between successive discharges are narrow enough. The corresponding superposition yields the motor unit force output. This phenomenon was introduced in Section 2.2.6.

The scaling factor  $\alpha_k^{PTF}$  is computed based on the twitch superposition. The force output following the very first motor neuron discharge is equal to the peak twitch force of motor neuron  $n$ , i.e.,  $\overline{PTF}^n$ . Assigning the difference between the force output after successive motor unit discharges as  $\Delta_i$ , the superposed force output of a motor unit can be expressed as

$$\begin{aligned} \overline{F}^n &= (1 + \sum_m \Delta_m) \overline{PTF}^n \\ &= M^n \overline{PTF}^n \\ &= M^n \frac{PTF^n}{PTF^N}, \end{aligned} \quad (6.9)$$

where  $m$  denotes the discharge number (see Fig. 6.3).

To obtain the total muscle force output, individual motor unit force outputs are summed. As  $\overline{PTF}^n = \frac{PTF^n}{PTF^N}$ , and  $PTF^N$  is a constant, the total force output can be re-written as

$$\begin{aligned} \overline{F}^{sim} &= \sum_n^N \overline{F}^n \\ &= \frac{1}{PTF^N} \sum_n^N M^n PTF^n. \end{aligned} \quad (6.10)$$

Rearranging Eqn. (6.10) yields

$$\rightarrow \overline{F}^{sim} PTF^N = \sum_n^N M^n PTF^n. \quad (6.11)$$



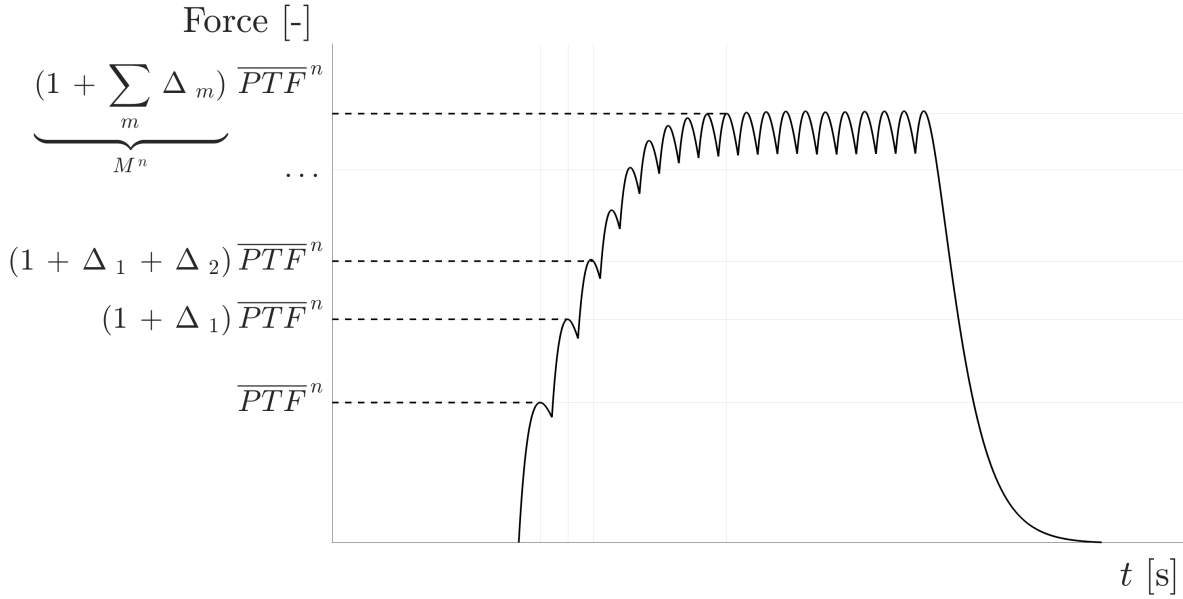


**Figure 6.3:** Superposition of the twitches and the resulting normalized motor unit force for motor neuron  $n$ , where  $\Delta_m$  denotes the vertical distance between two successive peaks,  $m$  denotes the peak number,  $\overline{PTF}^n$  denotes the normalized peak twitch force of motor neuron  $N$ . Note that this plot is for descriptive purposes only.

Had  $PTF$  been known, the total force output,  $\hat{F}$ , would be

$$\hat{F} = \sum_n^N M^n PTF^n. \quad (6.12)$$

Ideally, the simulated force would be equal to the experimentally measured force output, i.e.,  $\hat{F} = F^{exp}$ . Thus, replacing  $\hat{F} = F^{exp}$  in Eqn. (6.12) and plugging it into Eqn. (6.11), the following is obtained

$$F^{exp} = \overline{F}^{sim} PTF^N. \quad (6.13)$$

Rearranging Eqn. (6.14) to obtain  $PTF^N$  yields

$$PTF^N = \frac{F^{exp}}{\overline{F}^{sim}}. \quad (6.14)$$

Since  $\alpha_k^{PTF}$  equals  $PTF^N$ , to determine  $\alpha_k^{PTF}$ , cf. Eqn. (6.14), experimental force output is divided by the normalized total force output. This scheme is visualized in Fig. 6.4.

After  $\alpha_k^{PTF}$ , the real-valued (prior) sets for  $PTF$  are obtained as described in Eqn. (6.8). Thus, the prior sets for the contractile properties ( $\tilde{\Theta}^{CP}$ ) are now known.

Using  $\tilde{\Theta}^{CP}$ , the real-valued total force output is computed for 5-100% MVC at each 5% MVC. The mean value at the force plateau is used as the model output, i.e.,  $\Omega^{sim} = \text{mean}(F_k^{sim})$ .

Similar to Chapter 5, to determine the posterior set of contractile properties, Bayesian

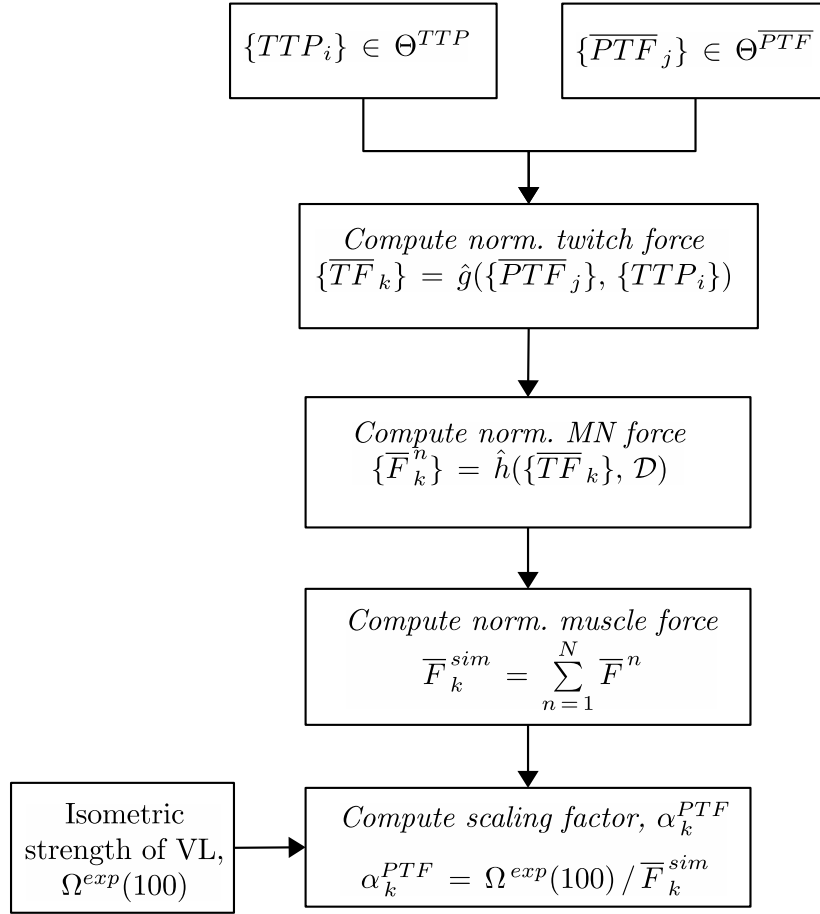


**Figure 6.4:** Overview of the scheme for computing the scaling factor for  $PTF$ ,  $\alpha_k^{PTF}$ . Here MN stands for motor neuron and VL denotes vastus lateralis.

updating scheme is employed. The calibration points are selected as the force output of the muscle estimated in Section 6.1.1 at each 5 %MVC. After the calibration, the posterior,  $\tilde{\Theta}^{\approx CP}$ , as well as MAP sets of contractile properties are obtained.

## 6.2 Results

The isometric voluntary strength of vastus lateralis is estimated as 221 N. The motor neuron pool size is found to be 424 .

### Sizes of the admissible sets

Total number of sets in  $\Theta^{\overline{TTP}}$  is 314, which is a consequence of Algorithm 2. Each set has a total of  $N = 424$  elements, as a  $\overline{TTP}$  value is assigned for all motor neurons.

When all possible combinations of the scaling factors with the sets in  $\Theta^{\overline{TTP}}$  are computed, size of  $\tilde{\Theta}^{\overline{TTP}}$  becomes  $I \times N = 314 \cdot 4 \times N = 1256 \times 424$ .

Size of  $\Theta^{\overline{PTF}}$  is  $J \times N$ , where  $J = 1314$  and is a consequence of Algorithm 2. Analogous to  $\Theta^{\overline{TTP}}$ , each set has a total of  $N = 424$  elements

The prior set of contractile properties,  $\tilde{\Theta}^{CP}$ , contains a total of  $1256 \cdot 1312 = 806352$  sets, i.e.,  $K = 806352$ .

After Bayesian updating, 17060 sets remain in the posterior set of contractile properties. This is a 98% reduction in the size of prior sets.

## Qualitative description of the admissible sets

The initial selection of  $TTP$  and  $PTF$  is done based on the random number generation algorithm. When the range of values for both properties are investigated, it is seen that, distribution of the range of values  $TTP$  takes is more uniform in comparison to the range of values for  $PTF$  (see Fig. 6.5). Distribution of the range of values for  $PTF$  resemble almost an exponential distribution, thus, majority of the values lie in the lower limit, which is 100.

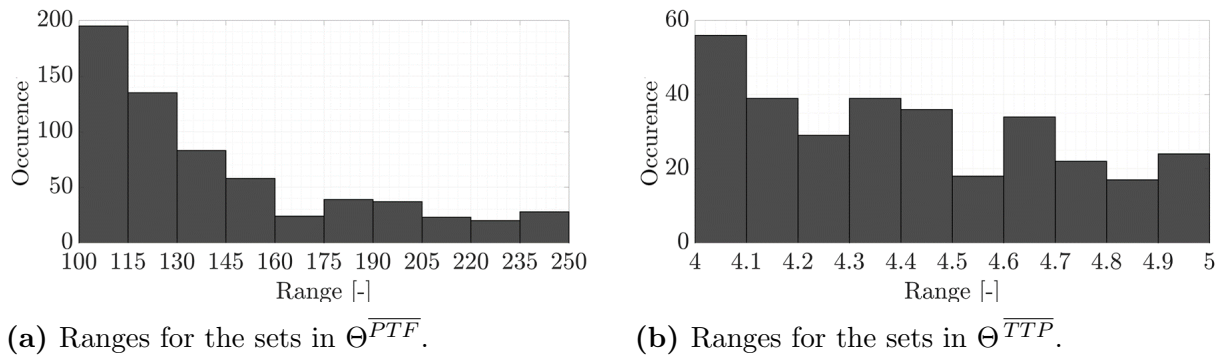


**Figure 6.5:** Ranges of normalized sets. Range for each set is computed through the ratio of the highest value over the lowest value.

As each set in prior and posterior sets for the contractile properties are composed of more than one element, their description is conducted based on the mean of each set. Mean  $PTF$  in the prior set ranges from 95-355 mN (see Fig. 6.6 (a)). The distribution resembles a right-skewed normal distribution. As for mean  $TTP$ , values range from 40-106 ms (see Fig. 6.6 (b)). The distribution is almost uniform.

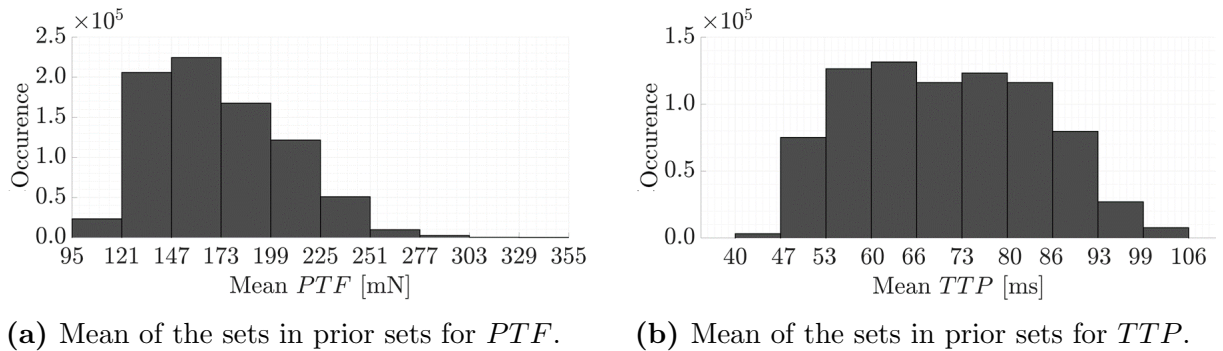


**Figure 6.6:** Mean of prior sets of the contractile properties.

The distribution of the mean values in the posterior sets of both parameters does not change. Range for  $PTF$  reduces to 95-251 mN, however, range for  $TTP$  remains the same (see Fig. 6.7 (a) and (b), respectively).

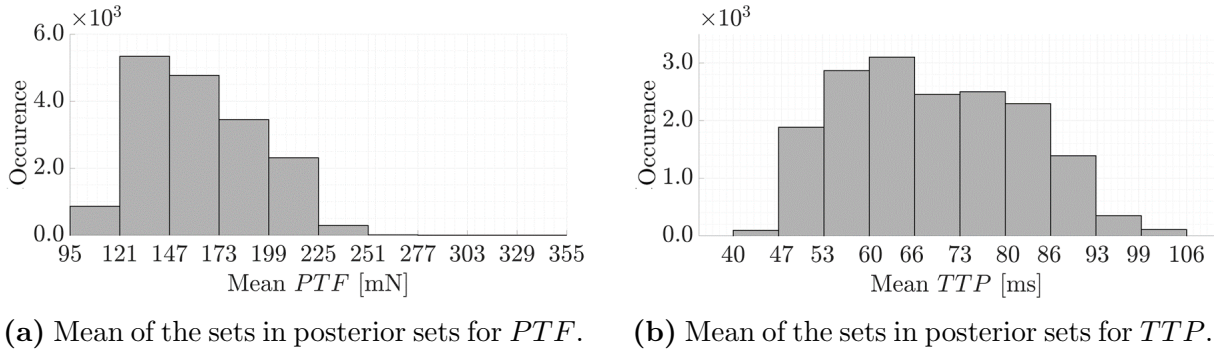


**Figure 6.7:** Mean of prior sets of the contractile properties.

Range of values in the posterior sets of  $PTF$ ,  $\Theta^{\approx PTF}$ , for the smaller motor units are narrower in comparison to that of larger motor neurons (see Fig. 6.8 (a)). Such a prominent difference in the range of values over motor neurons are not observed for the posterior sets of  $TTP$ ,  $\Theta^{\approx TTP}$  (see Fig. 6.8 (b)).

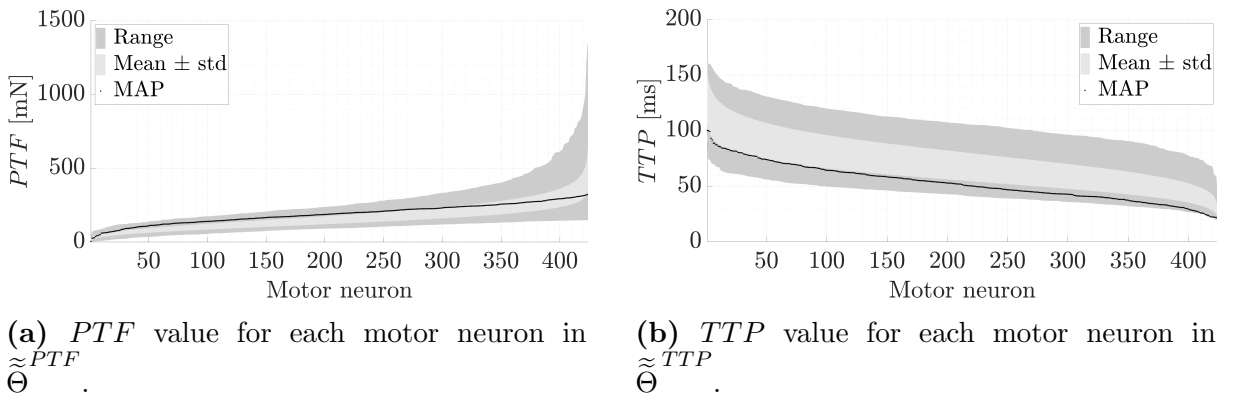


**Figure 6.8:** Value of the contractile properties of each motor neuron within the posterior sets,  $\Theta^{\approx CP}$ .

### Scaling factor for the peak twitch force

The scaling factor for the peak twitch force ( $\alpha_k^{PTF}$ ) computed using the prior set of contractile properties ranges from 149 to 2146 mN. Its distribution resembles a right-skewed normal distribution (see Fig. 6.9). After Bayesian updating,  $\alpha_k^{PTF}$  in the posterior set ranges from 146 mN to 1289 mN. Qualitatively, the distribution still resembles a right-skewed normal distribution (see Fig. 6.9, light gray histogram).

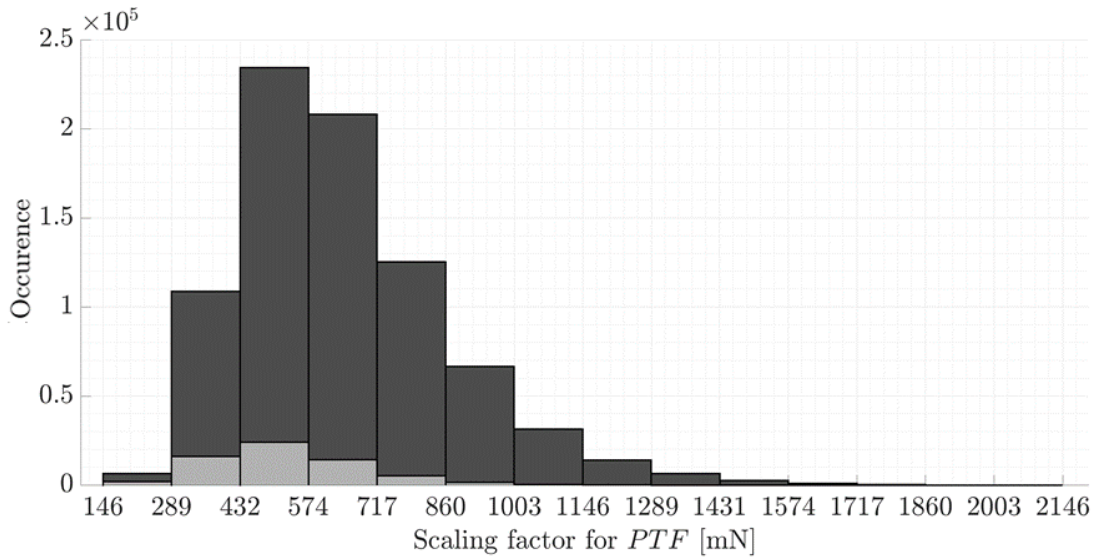
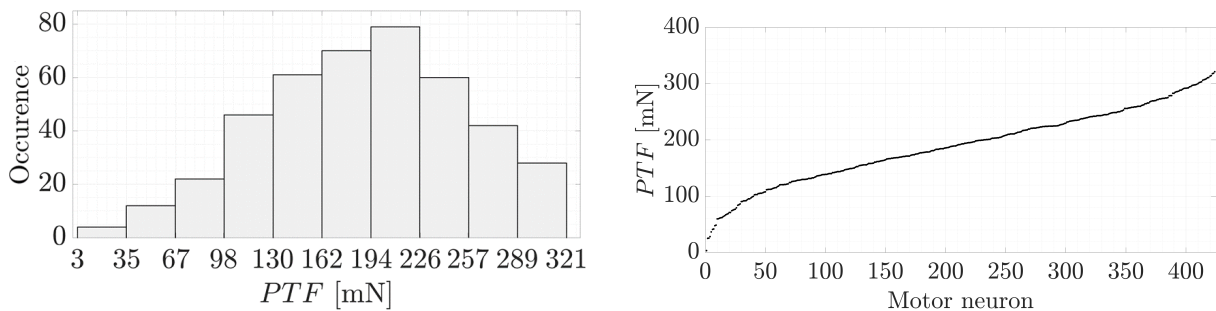


**Figure 6.9:** Scaling factor for  $PTF$ ,  $\alpha_k^{PTF}$  in prior (dark grey) and posterior (light grey) sets.

### Maximum a-posteriori for the contractile properties

The MAP for  $PTF$  is predicted to be  $189.3 \pm 65.6$  mN and ranges from 3-321 mN (see Fig. 6.10). Distribution of  $PTF$  in the motor neuron pool resembles a left-skewed normal distribution.



(a) Distribution of the peak twitch force,  $PTF$ , in the motor neuron pool.

(b) Peak twitch force,  $PTF$ , for each motor neuron.

**Figure 6.10:** The maximum a-posteriori (MAP) for the peak twitch force,  $\tilde{\Theta}_{MAP}^{PTF}$

The MAP for  $TTP$  is predicted to be  $52.8 \pm 16.3$  ms and ranges from 21-100 ms (see Fig. 6.11). Distribution of  $TTP$  in the motor neuron pool resembles a right-skewed normal distribution.

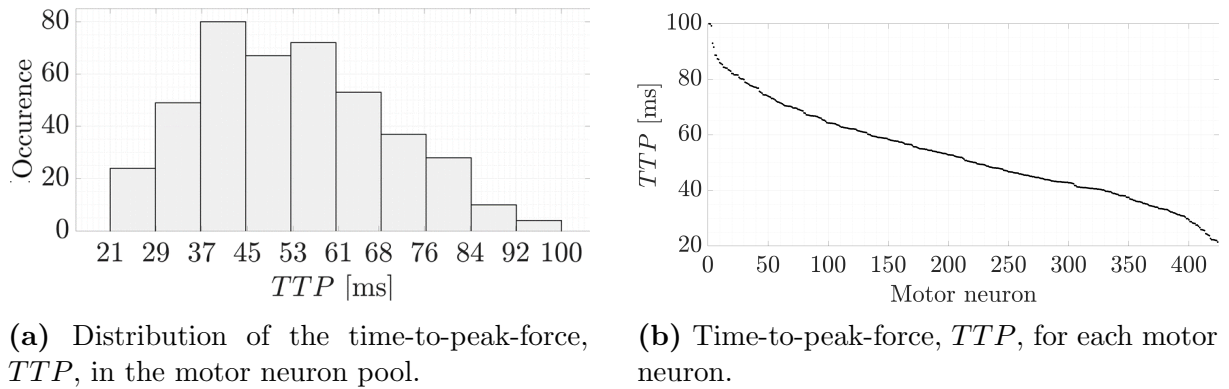


**Figure 6.11:** The maximum a-posteriori (MAP) for the peak twitch force,  $\tilde{\Theta}_{MAP}^{TTP}$

When the MAP of both properties are plotted against each other, the result can be fitted to a straight line (see Fig. 6.12). The line has the following form:

$$PTF_n = -4.03 \cdot TTP_n + 401.9. \quad (6.15)$$

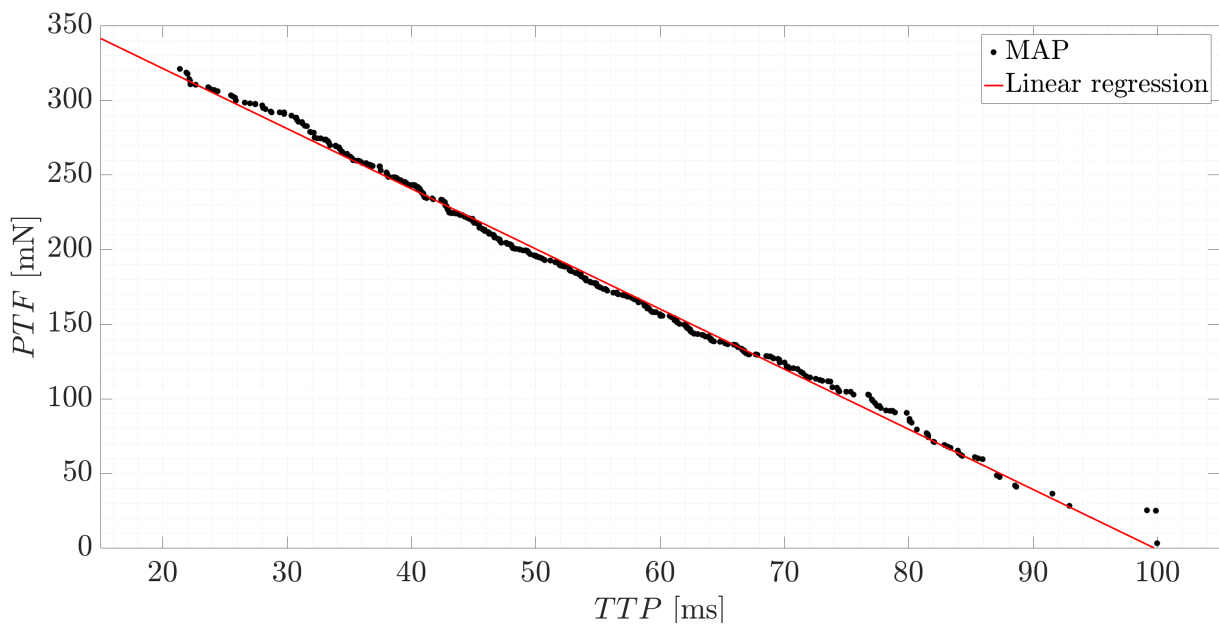


**Figure 6.12:**  $PTF$  with respect to  $TTP$  for the MAP. A linear relationship is observed.

## 6.3 Discussion

By first treating the  $PTF$  as an unknown, contractile properties of the motor neuron pool of vastus lateralis muscle are predicted. To do that, admissible sets for the distribution of both of the contractile properties using alpha and beta distributions with varying shape functions are created. These sets are referred to as the prior sets. The isometric force output of the muscle is estimated from the isometric strength of the quadriceps group

reported in experimental studies. The force output is then used as calibration points. Using the Bayesian updating scheme, the posterior sets of contractile properties could be selected. The calibration yielded 17 060 posterior sets for the contractile properties, which is around 98% reduction in the number of the prior sets. The MAP Among the posteriors, the MAP for  $PTF$  is predicted as  $189.3 \pm 65.6$  mN, with values ranging from 3-321 mN. The MAP for the  $TTP$  was found to be  $52.8 \pm 16.3$  ms, with values ranging from 21.4-100 mN. Distributions of  $PTF$  and  $TTP$  within the motor neuron pool have been found to be left-and right-skewed normal respectively.

In comparison to the experimental data on the time-to-peak of various muscles, the mean value of  $\tilde{\Theta}_{MAP}^{\approx TTP}$  is shorter (see Table 6.2). The predicted  $TTP$  being faster in comparison to other data could be due to muscle type, as well as, the limitations regarding the experimental data used to generate the initial ranges for this parameter to capture the entire motor neuron pool.

The study by Van Cutsem et al. [311] is one of the most comprehensive studies measuring both contractile properties of a human muscle, namely the tibialis anterior. They observed an exponential distribution for the  $PTF$  and a right-skewed distribution for the  $TTP$ . The distribution of the  $TTP$  obtained as a result of the simulation scheme introduced in this chapter is similar to the findings of this study.

When estimating the isometric strength, the contribution of passive structures, such as tendons and ligaments, are disregarded in this work. Therefore, estimated  $PTF$  of individual motor neurons could be higher than reality. However, it is known that the contribution of the passive force becomes more significant towards the end of the force-length curve of the muscle (e.g., [258]). Whether or not the passive force contribution is significant for vastus lateralis requires further experimental studies.

In this study, inter-spike variability of motor neuron discharges were disregarded. Although this phenomenon is an important property of voluntary contraction, disregarding this variability poses negligible influence on the total force output. This is shown in Chapter 4, Fig. 4.9. The motor neuron recruitment model is run 10 times with a 20% variability in the discharge instances. The total force output has then been computed using the contractile properties suggested in Fuglevand et al. [104] for each model run. The average total force output obtained with and without the inter-spike variability poses 0.35% difference in the total force output. It can thus be said that neglecting the inter-spike variability does not have a significant influence on the contractile properties estimated in this chapter. This was also shown in the study by Yao et al. [324].

Experimentally,  $PTF$  can be determined by means of spike-triggered averaging of the force signal. It is, however, known that this method has some limitations, such as detection of a small number of motor neurons. Further, Negro et al. [231] state that the technique performs with relative low estimation accuracy of the twitch force for the physiological inter-spike interval variability and discharge rate. Despite its limitations, the spike-triggered averaging is a very important tool to measure the time-to-peak-twitch-force. The scheme to estimate the twitch force outlined in this chapter, makes use of the time-to-peak data obtained b spike-triggered averaging. It can therefore be said that this scheme makes use of the strengths of this experimental method and tries to make up for its limitation by estimating the twitch force so that the entire motor neuron pool can be taken into consideration.

Burke [40] states that comprehensive models of motor control must take into account

the diversity within motor unit pools. Instead of considering the characteristics of motor units according to their types, the models should incorporate individual characteristics of the motor units. This statement is based on the fact that motor units can show multiple characteristics in form of MHC (see Section 2.2.3). Since this modelling scheme does not distinguish between fibre types, the complications arising due to motor units with multiple fibre types are overcome.

It is known that the histochemical and mechanical properties of fibres are identical [40]. Therefore, using the contractile properties detected in the maximum a-posteriori set could provide an idea about the order of magnitude of the contractile properties of type I and type II fibres. Using the innervation ratio of VL and dividing the motor neuron peak-twitch force with the innervation ratio of the muscle would provide an approximation of the peak twitch force of fibres. It would then be possible to comment on the order of magnitude of the contractile properties of different fibre types based on the distribution of fibre types within vastus lateralis.





# 7 Modelling the strength gain due to unilateral isometric knee extension exercise

## 7.1 Introduction

Training our muscular system in an effective and controlled way may lead to increased mobility [57], fosters faster recovery from injuries or surgical interventions through specialised and, thus, more efficient and subject-specific training/rehabilitation programs [251, 313], and potentially leads to performance enhancement in (professional) athletes [229]. Since muscle growth and adaptation is a very active field of (experimental) research, there exists a large body of literature, including several detailed systematic reviews on dynamic exercise modes, e.g., [179, 269, 280, 281]. Despite the large body of literature, the mechanisms of training-induced muscle adaptation are still not that well understood [307]. By restricting oneself to a particular and "simple" type of exercise such as, for example, isometric training and a specific muscle, there is hope that one can reveal by means of systematic investigations the complex mechanisms leading to muscle growth or adaptation.

Isometric training is a form of exercise that consists of muscle contractions performed without macroscopic changes to the position, i.e., without lengthening or shortening of the muscle belly [82] (see Section 2.3.3). If new insights can be gained from isometric training studies, specific training plans can be developed that can easily be employed in a home setting, since it requires little to no equipment to be performed, and is relatively easy to describe and to assess [237]. Further, it leads to an increase in muscle force with exerting minimal stress to the structures surrounding the involved muscles. This makes the experimental outcome less susceptible to inter-muscle force transmission and especially suitable for post-surgery rehabilitation [153].

Since training outcome is known to significantly depend on duration of the trained period [252], longitudinal studies are essential. Longitudinal studies quantifying the improvement in performance, however, require detailed data on the training outcome, ideally after each training session.

Systematic reviews allow to collect data from multiple studies that have a similar focus and fulfil a strict set of inclusion and exclusion criteria. Data can be extracted from the studies that fall into the selected criteria. This data can be analysed by means of meta-analysis (see Section B.1 for further information on systematic review and meta-analysis).

In this chapter, a longitudinal model of the change in isometric muscle strength has been proposed. This model is based on a systematic review on studies on unilateral isometric knee extension exercise. Data extracted from relevant studies have been analysed by means of the model-based meta-analysis method. This method combines longitudinal

models with meta-analytic methods to synthesize results from different primary trials [243]. Specifically, a Bayesian, longitudinal model-based meta-analysis (BLMBMA) as proposed in [33] has been used to analyse the collected data. Note that, in this chapter, emphasis has been placed on the outcome of the longitudinal model of the change in isometric strength. Plots and data relevant for the meta-analysis studies, such as the forest plots, spaghetti plots and data on demographics, have been provided in Appendix B. The full version of the study was accepted for publication on October 9, 2020 in *Frontiers in Sports and Active Living*, Section Biomechanics and Control of Human Movement (doi: 10.3389/fspor.2020.518148).

## 7.2 Methods

### 7.2.1 Study selection

The systematic review and data extraction was performed by Ekin Altan and Ismail Bayram. The last search took place in May 2019. The articles that appeared in the databases PubMed, Web of Science, SCOPUS, and Chochrane Library were included in the review. The search was performed on the title and abstract (see B.2 for the full search strategy). References of the relevant articles as well as reviews on the topic of resistance training were investigated manually. The PRISMA Statement [221] was followed.

### 7.2.2 Inclusion criteria

Only studies on voluntary UIKEE performed by young, healthy subjects were included within this review. Further, the search was restricted to articles in English and published after 1960.

As the neuromuscular system is thought to adapt itself to perform the (specific) training movement in an optimized manner [225, 252], the principle of exercise-specificity states that the highest effect of exercise is assumed. Adhering to the principle of exercise-specificity, i.e., , strength gain coincides with training (e.g. training angle, mode), a study was included only if it reported the isometric strength at pre- and post-training stages in terms of the maximum voluntary contraction/torque (MVC/MVT) of the trained limb.

In addition, if a study used different subject groups for different training modes, and one of these training modes was UIKEE, only data reported from the UIKEE group was taken into consideration.

### 7.2.3 Exclusion criteria

Studies following a training plan according to the principle of “training to exhaustion” were excluded as one cannot quantify in such studies the number of contractions per training session. Moreover, training with less than 50% MVC was deemed to be inadequate to impose strength improvement in the trained muscle [226]. Hence, studies reporting training intensity lower than 50% MVC were excluded. The same applies to studies accompanying training with electrical stimulation (during the warm-up and/or training). They were disregarded to minimize the training protocol heterogeneity.

It is known that training in one limb may cause strength improvement on the contralateral limb [see e. g., 46, 117, 319]), which is known as cross-education [82, 84] (see Section 2.3.2). If a study reports on training protocols that differed from side to side e.g. different angle, eccentric/concentric training, then the study was also excluded from the review. Furthermore, by focusing on unilateral exercise, studies reporting on some acute effects like the bilateral deficit phenomenon, which occurs in concurrent contraction of homologous muscles and yields reduced strength gain on both limbs, were disregarded [145]. Studies merely utilizing a bilateral training protocol or training the limbs in alternating manner were also excluded.

When progressive training programs are planned for elderly populations, the baseline fitness and potential pre-existing medical conditions need to be taken into consideration [116, 201]. Although it is known that elderly subjects also immensely benefit from resistance training, strength gains are dependent on the baseline fitness levels of the subject population [176]. The fact that the baseline fitness levels are typically lower for elderly subjects than for younger ones [197] leads to an increased data heterogeneity if such data are combined. Therefore, to keep the potential heterogeneity stemming from the demographics and health state of the subjects to a minimum, studies on elderly population, as well as, studies on young subject with pre-existing medical conditions or lower limb injuries were excluded.

#### 7.2.4 Data collection and extraction

One of the most prominent functional adaptation due to resistance training is improved muscle strength, which also indicates how well the trained muscle adapts to the training regimen [177]. Therefore, the isometric strength of the trained leg is chosen as the main summary measure. The secondary summary measures were chosen from quantities which are related to the causes of the strength improvement, namely the neuromechanical and morphological changes of the trained muscle.

EMG measurements, for example, are used to assess changes in the neuromuscular system [1, 87, 117]. They can be reported in terms of integrated EMG or normalized root mean square (RMS). Whereas, measurements on the muscle mass, cross-sectional area (CSA) or volume describe changes to the morphological properties. Positive changes in the morphological properties point to an increase in the amount of contractile proteins, known as hypertrophy [87]. EMG and morphological data were considered as secondary summary measures.

Demographical information related to the participants (age, weight, height, sex, history of physical activity) and information regarding the training variables employed in the studies were also extracted. The extracted training variables were: exercise intensity (in terms of % MVC), knee angle, number of contractions per set, rest between contractions, number of sets per training, rest between sets, contraction duration, number of training sessions per week and the weeks trained.

Unfortunately, the identified trials differed widely in design and not all of them were controlled trials. Furthermore, some of the studies with a controlled design relied on internal controls (the trained vs. the untrained leg), while others reported results from external control groups (trained vs. untrained participants). We were therefore unable

to obtain a sufficiently large data set for either of the types of controls. Thus, our main analysis relied on uncontrolled data, stemming from trained legs, and analyses using the two types of control were added as sensitivity analysis.

When multiple UIKEE exercise protocols (e.g. training at different knee angles, intensities) were used for different subject groups within one study, the data on different exercise protocols were treated as separate data sets [see, e.g., 14, 30, 299]. The reason for this is related to the principle of exercise-type specificity, which asserts that differences in the training protocols should be taken into account when the outcome of the training is evaluated [225].

The treatment effect of the summary measures were computed based on the change in the summary measure with respect to its baseline value, i.e., , value measured in the pre-exercise state. Muscle strength can be measured through MVT, MVC or weights, whereas, volumetric data can be reported through muscle mass, CSA or volume. Computing the relative change of these measures and using this as the treatment effect allows to evaluate the observed changes using a common unit.

The treatment effect at week  $T$  relative to its baseline was computed as:

$$TE_T = \left( \frac{\Delta_T}{Y_0} \right) 100 = \frac{Y_T - Y_0}{Y_0} * 100, \quad (7.1)$$

where TE denotes the treatment effect, T denotes the week number for which the data was reported, i.e.,  $T = 0$  refers to pre-exercise, and  $Y_{(\cdot)}$  stands for summary measure at week  $(\cdot)$ . The change in the summary measure is denoted by  $\Delta_T$ .

The variance of  $TE_T$  is needed for the meta-analysis. It is not possible to compute this quantity using conventional ways, since  $\Delta_T$  and  $Y_0$  in Eqn. (7.1) were both variables. The variance is thus approximated by means of a Taylor expansion. Following Munn et al. [226],

$$\text{var}(TE_T) = \text{var} \left( \frac{\Delta_T}{Y_0} \right) = \frac{\text{var}(\Delta_T)}{\overline{Y_0}^2} + \frac{\text{var}(Y_0) \overline{\Delta_T}^2}{\overline{Y_0}^4} - \frac{2 \overline{\Delta_T} \text{cov}(\Delta_T, Y_0)}{\overline{Y_0}^3}, \quad (7.2)$$

where  $\text{var}(\cdot)$ ,  $\text{cov}(\cdot)$  and  $\overline{(\cdot)}$  denote the variance, covariance and the mean of quantity  $(\cdot)$ , respectively.

The variance of  $\Delta_T$  is denoted by  $\text{var}(\Delta_T)$  and is calculated as

$$\text{var}(\Delta_T) = \text{var}(Y_T - Y_0) = \text{var}(Y_T) + \text{var}(Y_0) - 2 * \text{cov}(Y_T, Y_0). \quad (7.3)$$

Following [226], the correlation between  $(Y_T, Y_0)$  is taken as 0.5 and is used to for both  $\text{cov}(Y_T, Y_0)$  and  $\text{cov}(\Delta_T, Y_0)$ .

## 7.2.5 Synthesis of results

First, longitudinal information for the increase in strength and change in EMG within each study was evaluated descriptively to observe whether the data follow a trend. This was

done using spaghetti-graphs over the respective time period (see Fig. B.1 and Fig. B.2). The treatment effect at a given time point is expected to depend on weeks trained and exercise intensity.

BLMBMA makes it possible to model the time-course of the evolution of the treatment effect by using data reported at multiple end points. Furthermore, it is not constricted to a single time point like a landmark meta-analysis [32]. The time-dependent evolution of the treatment effects were modelled here using BLMBMA.

The Emax model is fitted to the data as proposed in [32]. This model captures the initial fast increase in performance improvement followed by a plateau, which is the case for subject with no prior strength training background [252]. The Emax model has the following form:

$$\text{Effect} = E_0 + \frac{E_{\max} C}{C_{50} + C} \quad , \quad (7.4)$$

where  $E_0$  and  $E_{\max}$  denote the baseline and the maximum effect of the drug, respectively,  $C$  is the drug concentration and  $C_{50}$  is the drug concentration at which 50% of the maximum effect is observed. The concentration-related parameters in Eqn. (7.4) were replaced with the weeks trained and the effect related parameters ( $E_{(\cdot)}$ ) that describe the treatment effect, i.e., the isometric strength, CSA or EMG.

To apply BLMBMA, first, admissible sets for the values of the model parameters  $E_{\max}$  and  $C_{50}$  were created. Such sets were known as prior sets in Bayesian statistics and they describe the the value a given parameter may take, without considering any quantitative evidence for both parameters. Prior sets from a normal distribution with a mean of 0 and standard deviation 10000, i.e.,  $\mathcal{N}(0, 10000)$ , were created. Such priors are known as weakly informative as they follow a normal distribution with a large variance, resulting in a flat distribution that reflects the lack of previous knowledge on that parameter.

The posterior density of the parameters describes the values, which the parameters can take after the data at hand is taken into consideration. To obtain the posterior density, Markov chain Monte Carlo method was used. Three Markov chains with 10000 repetitions each and a thinning factor of 10 were used to ensure convergence of the posteriors after a burn-in of 2000 observations. In addition to thinning, we discarded the burn-in samples and used multiple chains to account for an unlucky choice of initial values in this numerical process. In each trial, the baseline parameter,  $E_0$ , was set to 0. This is to account for the baseline adjustment in the individual studies.

Heterogeneity between studies was reflected on the  $E_{\max}$  parameter by including a normally distributed random-effect on this parameter. This allows the  $E_{\max}$  to vary between trials. Convergence of the estimation was assessed by means of Gelman-Rubin diagnostics, which gets close to 1 if convergence is reached [111]. This estimation was performed in R [253] and jags [249] using the extensions rjags [250], tidyverse [323], ggplot2 [322] and meta [11].

To illustrate the differences between individual studies, the increase in strength at the last available point in time per study was shown in a forest plot. Note that the forest plots were generated with meta [11] in the software R [253]. The plot was stratified by training duration and ordered by training intensity within similar training durations. This descriptive analysis was completed by a using the latest available time-point in each trial.

To evaluate the combined effect of this landmark analysis, a pairwise random-effects

meta-analysis was carried out based on the last available observation of each study. The  $I^2$  statistic was used to evaluate the amount of heterogeneity between the pooled studies in all cases. Potential study-level covariates were included in univariate and multiple meta-regression in a further step of the landmark analysis. This was done to explain the variation between studies.

### 7.2.6 Risk of bias in individual studies

The bias types outlined in the Cochrane Handbook for Systematic Reviews of Interventions version 5.2.0 were followed to assess the risk of bias (RoB) within this study [138]. The 'Cochrane risk-of-bias tool for randomized trials (RoB 2)' [295] was used for this purpose. How the risk of bias in each study has been provided in B.3. Since there is no tool to assess studies that do not employ a control group, we excluded studies that do not report data on an independent control group or the untrained leg.

### 7.2.7 Summary of evidence

The database search was conducted in May 2019. The search yielded 20 studies fulfilling the inclusion criteria (see Fig. 7.1).

These studies contained 65 data points. The main summary measure (isometric strength) was computed based on these data points. Except for Bonde Petersen [30], all studies reported a positive change with respect to the isometric strength of the trained leg. The change in isometric strength ranged from -4 to 46% (see Figure 7.2).

Out of the 20 studies that fulfilled the inclusion criteria, Carolan & Cafarelli [46], Ema et al. [81], Garfinkel & Cafarelli [110], Rich & Cafarelli [263], Weir et al. [319, 320] reported at 11 data points the EMG values for the vastus lateralis muscle (see Figure B.2). Weir et al. [320] and Ema et al. [81] additionally reported data on the vastus medialis and rectus femoris. Note that data on the vastus medialis and rectus femoris were excluded from the analysis in order to keep the heterogeneity to a minimum. The relative change in EMG ranges from -5.9 to 27.9% with an average of  $9 \pm 12.6\%$  (see Fig. B.8 (a)).

As far as the increase in CSA is concerned, Garfinkel & Cafarelli [110], Jones & Rutherford [155] and Lewis et al. [193] reported an increase of the CSA between 5 to 14.6%, while Kubo et al. [182] reported an increase of  $7.6 \pm 4.6\%$  in muscle volume (see Fig. B.8 (b)).

The number of subjects in the trained group across all studies was 307. A total of 163 subjects (54%) were female. Although this study looks like gender balanced (163 female and 144 male subjects have been included), the majority of the the female subjects stem from the study of Bandy & Hanten [14]. They report on the outcome of 107 female subjects. If the number of female subjects used in this study is subtracted from the total number of females, only 56 female subjects are left. The age, weight and height of the trained subjects were  $22.6 \pm 3.1$  years,  $60.6 \pm 9.8$  kg,  $166.3 \pm 8.1$  m for the female subjects, and  $23.9 \pm 3.0$  years,  $65.3 \pm 8.3$  kg,  $176.0 \pm 5.2$  m for male subjects respectively (see Table S1 in Supplementary Material). The shortest [222] and longest [273] training periods lasted 3 and 19 weeks respectively. Qualitatively, the highest rate of change of strength over weeks was reported by Szeto et al. [299].

For studies included in this systematic review, the training regimen was composed of 6

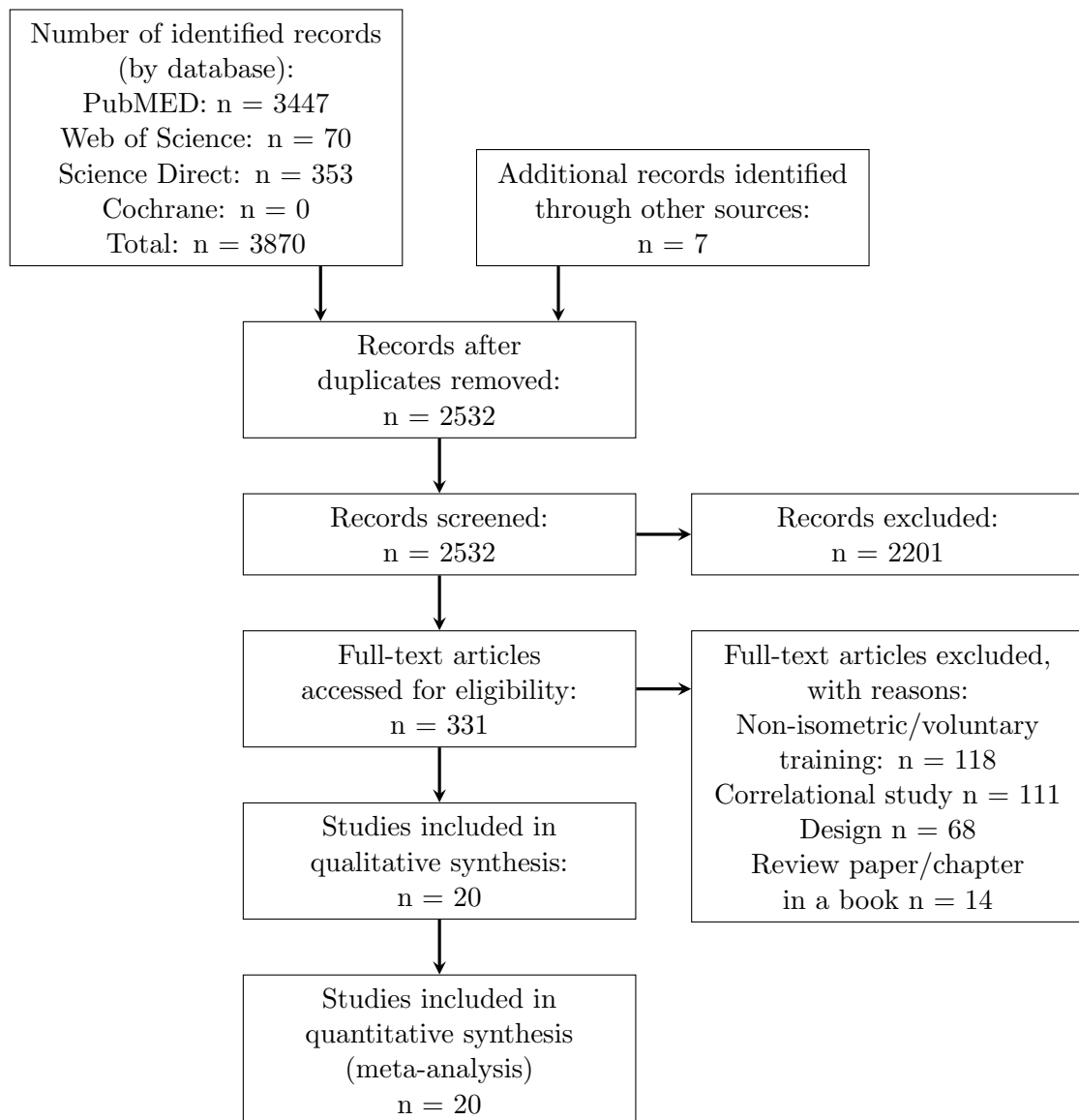


**Figure 7.1:** PRISMA 2009 Flow Diagram.



$\pm 4$  s long contractions,  $11 \pm 13$  repetitions per set,  $6 \pm 6$  sets and rest periods between contractions of  $12 \pm 13$  s and between sets of  $1 \pm 1$  min. The frequency employed in the studies were  $4 \pm 1$  training sessions per week and the total duration of the training sessions went for  $7 \pm 4$  weeks. The intensity was on the average  $84 \pm 29\%$  MVC with the angle of knee positioned at  $78 \pm 17$  degrees, with 0 degrees corresponding to a fully extended leg. In Szeto et al. [299], three subject groups were trained with same training volume, but at different levels of intensity (25, 50, 100% MVC). Within the meta-analysis, the groups that trained with 50% MVC ([299]) and 100% MVC ([299]) were regarded as two separate groups. The group that trained with 25% MVC was disregarded (see Section 7.2.3).

From the included studies, only Parker [239] report that the daily activity levels of the subjects were higher than those of recreationally active individual. Jones & Rutherford [155] provided no information on the activity level of the subjects. Since nothing was explicitly stated in this study, we considered the subjects as recreationally active individuals. Therefore, only 4 subjects, the ones in Parker [239], were considered as recreationally highly active individuals. Total number of trained subjects in the studies included in this review is 307. Subjects in Parker [239] corresponds to 1.3% of the total trained subjects.

As far as control group data are concerned, Bonde Petersen [30], Carolan & Cafarelli [46], Garfinkel & Cafarelli [110], Lucca & Recchiuti [199], Rich & Cafarelli [263], Weir et al. [319, 320] report data on a control group and the untrained contralateral leg. Bandy & Hanten [14], Grimby et al. [118], Kubo et al. [182] do not report any form of control data (see Table B.4). Spaghetti plots for the control group and untrained leg data are provided in Fig. B.3 and Fig. B.4. Fig. B.5 and Fig. B.6 depicts the difference between the change in strength and EMG of the trained leg versus the control group/untrained leg.

The trend of an increase in strength plateauing after week 4 is still prominent for the change in strength when the data on the untrained leg were considered.

The change in isometric strength of the control groups ranges from -8% to 10%, whereas the corresponding change with respect to the untrained leg ranges from -12 to 18%. When the available control group data on the change in strength is taken into consideration (change in strength in the control group subtracted from the change in strength in the trained leg), the change in strength in the trained leg ranges from 1.28% to 35.88%. When data on the untrained leg is considered analogously, the change in strength in the trained leg ranges from 3.96% to 31.38%.

As for the control group data obtained for the vastus lateralis is concerned, the EMG data shows a change between -9.15% to 6.70%, whereas, EMG data for the untrained leg ranges from -15.30% to 15.51%. The difference between the change in EMG for trained leg and the untrained leg is between -9.03% to 19.56%. If the control group is considered, then the difference is -9.03% to 32.75%. Note, however, that only 4 data points for EMG data exist for the control group.

## 7.2.8 Assessment of the risk of bias across studies

Carolan & Cafarelli [46], Garfinkel & Cafarelli [110], Parker [239], Rich & Cafarelli [263], Szeto et al. [299] stated that the subjects were assigned to training or control groups in a randomized manner. Bandy & Hanten [14], Grimby et al. [118], Jones & Rutherford [155], Lewis et al. [193], Parker [239], Szeto et al. [299], Tillin et al. [306] do not employ

an untrained control group (see Table B.4) and hence do not report on randomization. However, the contralateral leg was considered to be untrained for all those studies since the training mode was unilateral in all studies. Therefore, the fact if a study included a randomized control or not is less significant for the analysis in this study and would not introduce extra heterogeneity to the data.

Food intake and daily activities during the exercising period and previous training experience might effect the strength outcome [4, 58]. Bandy & Hanten [14], Parker [239], Rutherford & Jones [273] and Weir et al. [320] explicitly state that the participants were instructed to keep these unchanged. Others did not provide explicit information with respect to this concern. Although the study by Garfinkel & Cafarelli [110] provides no explicit information regarding food intake or daily activity, measuring the mean weight of the subjects before and after the training period revealed that the weight remained unchanged.

In all studies, training took place in laboratory setting, supervised by one or more researcher. Withdrawal of some subjects due to health reasons or not complying with the exercise protocol occurred in the studies by Bandy & Hanten [14] and Parker [239]. In these studies, it was stated that the withdrawals did not effect the statistical sensitivity negatively, so the effect of the attrition bias can be regarded as insignificant.

Negative change in strength was only reported in the study of Bonde Petersen [30]. Since the aim of resistance training is to increase muscle strength, negative changes in strength point to over-training or problems with the experimental set-up or the outcome measurement [103] (see Table B.1 for a summary).

### 7.2.9 Longitudinal model-based meta-analysis

BLMBMA allowed us to fit the increase in strength with respect to the baseline strength over time to an  $E_{max}$  model. Since the percent change in strength is modelled,  $E_0$  is taken as 0. The combined maximal increase, which is described by  $E_{max}$  in Eqn. (7.4), was found to be 41.83% (36.60% - 47.73%) (see Fig. 7.2). Half of the maximal strength increase is reached after 4.39 (3.31 - 5.84) weeks of training. This time instance described parameter  $C_{50}$  in Eqn. (7.4).

The initial increase in the isometric strength was slightly steeper and becomes flatter over the number of weeks training is performed. This indicates a faster rate of adaptation at the early phases of the exercise period. As some of the individual trials identified by the systematic review were small in size, the shape of the combined curve was heavily influenced by the largest identified study, which estimated the affect most precisely and therefore had a large weight in the meta-analysis. This was also illustrated by the size of the points in Fig. 7.2.

BLMBMA was not feasible for the secondary summary measures (EMG and CSA), since the number of trials was inadequate (7 and 4 studies with 13 and 4 data points, respectively). Therefore, one can only include these data in the analysis according to the last available time point (see Fig. B.8).

The landmark analysis of all three outcomes indicate considerable variation between the different trials and time points, e.g. with point estimates that varied in the 65 time points using different follow-up lengths between -4.43 and 43.47 (see Fig. B.7). Three additional explanatory covariates, namely the proportion of males, mean age and

intensity were included. These variables did not explain the observed heterogeneity.

## 7.3 Discussion

### Summary of the major findings

This study aims to provide an overview of the UIKEE training effect in healthy, sedentary subjects. The systematic review yielded 20 studies, which fulfilled the inclusion and exclusion criteria. The time-course of the main treatment effect, i.e., the change in isometric strength, could be modelled using a BLMBMA and Emax model. This model showed that isometric strength can increase up to 46%. Half of the increase occurs after the fourth ( $4.39 \pm 1.45$  weeks) week of training. The treatment effect of the secondary summary measures, namely the change in cross-sectional area and EMG, could not be modelled longitudinally using BLMBMA, since the number of data points was insufficient due to lack of data.

Pooling data gathered from different studies in form of a systematic review yields a data set with a sample size larger than the subject space of a single experimental study. Further, a longitudinal model-based meta-analysis allows to investigate the time-dependent effects of a given intervention from multiple studies, with different duration and data at different time points. The longitudinal model-based meta-analysis demonstrated its suitability for training data obtained from a quantitative description of the time-dependent training effects of the respective muscles.

### Parameters that influence the primary summary measure

Gender [74, 261, 262] and the overall general physical condition of the subjects play a (significant) role [22, 146, 230, 262, 265, 317]. The overall number of subjects (see Section 7.2.7) are such that one would not expect much impact. Since there is only one study that reported on subjects with daily activity levels higher than those of recreationally active individuals [239] and one study that does not provide any information about this [155], we believe that the activity of the subjects might be comparable. Hence, we believe that the physical condition, i.e., if non-active or athletes perform the same isometric training program [240], did not influence the outcome of this meta analysis.

A further key parameter is the training protocol and the time period for which the training was maintained, i.e., the number of trained weeks. The meta-analysis studies investigating the effects of exercise on strength consider the number of weeks trained as an independent variable, e.g., [226]. Lesinski et al. [191] investigated the effect of various resistance training protocols on the observed changes based on a dose-response relationship, such as training frequency and training intensity. Apart from investigating the effects of individual training variables on the response, a more generic measure describing the “amount” of exercise a muscle was exposed over the course of training, could be established. Such an “amount” could be then associated with the training volume that could be regarded as a specialized time measure depicting the cumulative training volume.

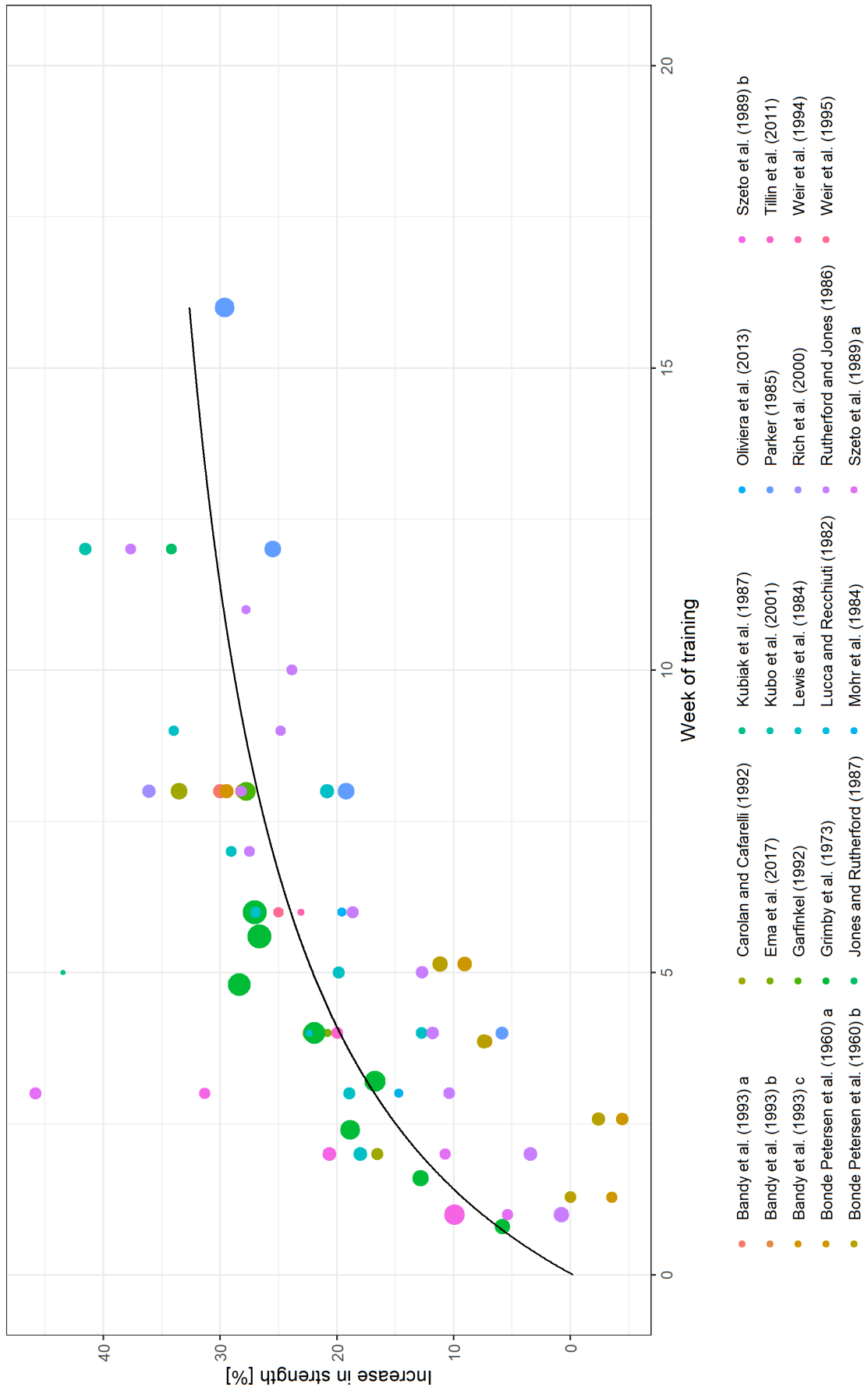


**Figure 7.2:** Fitted Emax model (black line) for the relative change in isometric strength over weeks trained together with data points obtained from multiple studies (coloured dots). Note that the size of the coloured dots are proportional to the subject size of a given study.

## Secondary summary measures

Resistance training is one type of training that leads to muscle hypertrophy (see, e.g., [321]). Hence, the amount and type of training should have a direct impact on muscle hypertrophy. Although isometric knee extension training is one type of resistance training, only 4 out of 20 studies quantified hypertrophy. In these studies, all data showed an increase in either the CSA or the volume of the knee extensors. This is, for example, consistent with [237]. The low number of reported data on hypertrophy is unfortunate, since additional experimental data on hypertrophy would provide a much better insight into the influences of UIKEE induced volumetric muscle growth. However, the available data in [110, 155, 182, 193] are insufficient for a quantitative analysis.

Besides pure anatomical measures, i.e., muscle hypertrophy, training has an effect on the functional (physiological) aspects of skeletal muscles, e.g., on neural adaptation [117, 155, 321]. One way of identifying neural adaptation is by recording EMG [99]. For example, the change in integrated EMG or the root mean square of the recorded signal are common ways of investigating the extent of neural adaptation due to exercise [117].

Only studies of Carolan & Cafarelli [46], Ema et al. [81], Garfinkel & Cafarelli [110], Rich & Cafarelli [263], Tillin et al. [306], Weir et al. [319, 320] reported on EMG data. All of these studies obtained the EMG data from the vastus lateralis. Weir et al. [320] and Ema et al. [81] report additionally data from vastus medialis and rectus femoris respectively, however, since there is only one data point available for these muscles, they were not considered in the analyses. As a result, only 11 data points remained for the EMG data.

Among studies that report EMG data, only Carolan & Cafarelli [46] measured EMG data for multiple time instances, i.e., , at 1, 2, 4, and 8 weeks. The rest of the studies report data only for the end of the training period. Given the fact that the duration of training differed between the studies, the time instances at which the data was recorded and reported do scatter. As a consequence, BLMBMA could not be performed on the EMG data. Despite being informative, EMG data also might be a less reliable source of data for identifying the functional adaptations of training [8]. For example, estimating motor units from EMG is a biased process favouring motor units closer to the surface [94].

To significantly improve the information content of the collected UIKEE data would require further measurements, such as, for example, voluntary activation, antagonist co-activation and the rate of force development. Without such data, it is difficult to judge neural adaptation in response to isometric exercise. Among studies that report data on EMG, only some made additional measurements to investigate neural adaptation. [46] and [306] reported that hamstring co-activation during UIKEE decreased significantly, which is attributed to neural adaptation mechanisms. [81] and [306] report a significant increase in voluntary activation of the knee extensors (from  $89.4\% \pm 7.0\%$  to  $92.5\% \pm 6.4\%$ ) correlated with the relative change in knee extensor isometric strength, whereas, [306] did not find any changes in the voluntary activation. [46], [110] and [263] reported no change in the EMG amplitude. [319, 320] detected changes in the EMG amplitude, which were, however, not significant. [263] investigated changes in the motor unit firing rate of vastus lateralis, but they did not detect any changes. Note that EMG data was selected as a secondary summary measure. Note that studies, which do investigate neural adaptation, might have discarded as they do not report on muscle strength, which was the inclusion criteria.

### Availability of control data and its use in this study

The BLMBMA could only be performed for data originating from the trained leg. There existed only five studies that reported data on a control group and the untrained leg. Furthermore, only Carolan & Cafarelli [46] reports on intermediate data points. Considering the control group and untrained leg data would increase the accuracy of the analysis, however, this would decrease the size of the already sparse data set even further. Moreover, the difference between the treatment effect of the untrained leg and the control group would make it possible to comment on the contralateral training effect, however, data is too sparse to reach a conclusion on this matter. Further, data on the untrained leg is subject-dependent, whereas control group data is a result of an independent observation. The subject dependency cannot be taken into consideration as the mean difference between the data sets is not reported. Therefore, data on the untrained and trained legs cannot be combined.

### Comparison of the findings with similar studies

In Oranchuk et al. [237], they focused on the longitudinal adaptation due to isometric training and investigated changes in the morphological, neurological and performance-related properties. They did not distinguish between unilateral and bilateral training and pooled data from studies on large muscles. Furthermore, they included studies training programs that use exercises other than isometric exercise, such as counter-movement jumps. Bohm et al. [27] investigated the effects of dynamic and isometric exercise on the stiffness, Young's modulus and cross-sectional area of tendons. They found that all exercise modes (eccentric, concentric and isometric) significantly increased these properties when performed with high intensity (for isometric exercise, more than 70 % MVC) and became more significant with increased training duration (more than 8 weeks, up to 3 months). In this study, we disregarded the effect of UIKEE on tendon tissue, however, the fact that Bohm et al. [27] showed that high intensity training triggers adaptation in tendon tissue, in a way, supports the fact that moderate to high training intensity is required to observe improvements to the musculoskeletal systems.

Maffiuletti & Martin [205] studies bilateral isometric knee extension training. They trained two subject groups with ballistic and progressive contractions over 7 weeks and observed 15.7 % and 27.4 % improvement in isometric strength at the trained angle, respectively. At 7 weeks, our model predicts 26 % increase in the isometric strength. In Kubo et al. [181], subjects were trained with isometric and dynamic knee extensions on either side of the limb. Despite the fact that different training modes were used for each limb, this study can also be regarded as a bilateral training study as both limbs were trained simultaneously. After 14 weeks of training, isometric training yielded 49 %, whereas, dynamic training yielded 32 % increase in the isometric strength, i.e., MVC. Neural and morphological adaptation were found to be equal for both sides, where isometric training caused 4.5 % increase in the cross-sectional area of the leg that was trained isometrically. At 14 weeks of training, our model predicts 32 % increase in the isometric strength. Similar to their previous studies [182–185], they further found that isometric training is more effective than dynamic training in improving the tendon stiffness and cross-sectional area. It is known that dynamic training also increases isometric strength, e.g., [160], thus the greater improvement in isometric strength in Kubo et al. [181] com-

pared to our findings, may be attributed to the cross-training effect that yields from dynamic training of the contralateral side.

## Limitations

Limitations of this study includes lack of a sufficient amount of control data. Studies that fulfilled the selected criteria are mainly cohort trials without a control group. If a control group is considered at all, an internal control, i.e., the untrained leg, has been used e.g., citeJones1987. However, it is known that cohort studies are more prone to bias than randomized control trials [138]. For example, if one computes the treatment effect of the trained leg based on the isometric strength of the untrained leg, the computed change in strength would include the cross-training effect. Taking the control as the baseline strength of the trained leg, one would obtain an unbiased way to compute the treatment effect.

Some limitations associated with the current systematic review also include possible publication bias. If there exist studies, which remained unpublished since they found statistically insignificant findings or data was reported in an unpublished dissertation, i.e., grey literature, e.g., [31], it is difficult to spot them by means of electronic search engines. Furthermore, we only included studies published in English and did not investigate studies published in other languages. However, to evaluate the quality and findings of a study which is not written in a language known to the authors, who performed the review, would be difficult. One other limitation regarding the current study is the lack of prospective registration. The systematic review was, nevertheless, conducted according to the remaining items of the PRISMA guideline.

Training intensity is important for initiating improvements in muscle performance [176]. In this study, we only considered reported data with a minimum of 50 % MVC isometric training intensity, cf., [226]. One could argue that this poses a potential loss of data and effects our interpretation of the change in isometric strength. However, it is known that training protocols with moderate to high intensity trigger hormonal changes that would induce improved muscle performance [176], while training protocols with low intensity isometric exercise mostly effect blood pressure levels [45, 149, 238, 301]. Among the studies included in this review, only Szeto et al. [299] reported also on the outcome of a low intensity training group, i.e., a group that trained at 25 % MVC. Despite reporting on an increase in isometric strength, the increase was not statistically significant. Therefore one can conclude that the selected level of training intensity matches the intensity required to trigger an improvement in muscle performance.

## 7.4 Conclusions

This study aims to provide an overview of the training effect of UIKEE performed by healthy, sedentary subjects. The systematic review yielded 20 fulfilling the inclusion and exclusion criteria. The time-course of the main treatment effect, i.e., the change in isometric strength, could be modelled using BLMBMA by using the Emax model. The model predicts that the isometric strength can increase up to 46 %, where half of the increase occurred at the fourth week of training. It was not possible to model the treatment effect of the secondary summary measures (change in CSA and EMG) longitudinally

---

using BLMBMA due to insufficient data. If the number of controlled trials consistently reporting data on both a separate control group and the untrained leg would have been available, which also take the subject-dependency into consideration, a significant improvement for the analysis of the training effect would have been achieved. In the case of our study, to keep size of the data set at a maximum, all available data on the trained leg was used even if a control group was not reported. The interpretation of the training effect was only possible based on the change from the baseline values, which also allowed to disregard differences in measurement methods e.g., measurement of strength through force or torque output.





# 8 Changes in discharge behaviour due to unilateral isometric knee extension exercise

## 8.1 Introduction

Training mode is known to be highly influential in changes observed in the muscle. It is also known that adaptations in the neuromuscular system optimizes primarily the practiced movement [18]. Not only is isometric training the simplest training mode, but the training effect is commonly quantified through the increase in isometric muscle strength. Therefore, the training mode and the training outcome overlap. Furthermore, the most significant mode of adaptation following isometric exercise is known to be of neuromechanical nature. Such neuromechanical changes include increased motor neuron discharge rate, decreased coactivation of the agonist and antagonist muscles and increased use of active muscle volume.

It is difficult to distinguish the individual contribution of each of these neuromechanical changes. This is partially due to the complexity of muscle and exercise physiology as well as the limitations in experimental technology. Changes in the neuromechanical activity of skeletal muscles are commonly quantified through surface EMG [117] (see Section 2.2.7). However, the amplitude of the EMG measured after strength training is known to show contradictory results [65, 78] (see Fig. 2.15). This discrepancy in the EMG data is said to occur due to shifts in the location of electrodes, altered extracellular volume and/or osmolarity, changes in subcutaneous fat and skin temperature, as well as differences in phase cancellation following weeks of training [1, 117]. Furthermore, EMG data is known to be biased towards faster motor neurons as they are closer to the muscle surface [93].

Computational models can be useful to make up for the limitations of the experimental equipment. Therefore, in this chapter, one neuromechanical adaptation mechanism, namely the increased discharge rate, following isometric training is investigated. To do that, findings from previous chapters is used.

## 8.2 Methods

In Chapter 5, the input parameter set for the motor neuron recruitment model (see Chapter 4), which allows to model the pre-exercise state, were determined. Using this parameter set, the discharge behaviour of vastus lateralis during an isometric contraction at various force levels was modelled. In order to compute the force output of the muscle during an isometric contraction, contractile properties of the motor neuron pool are required. Therefore, in Chapter 6, contractile properties (time-to-peak-force and peak

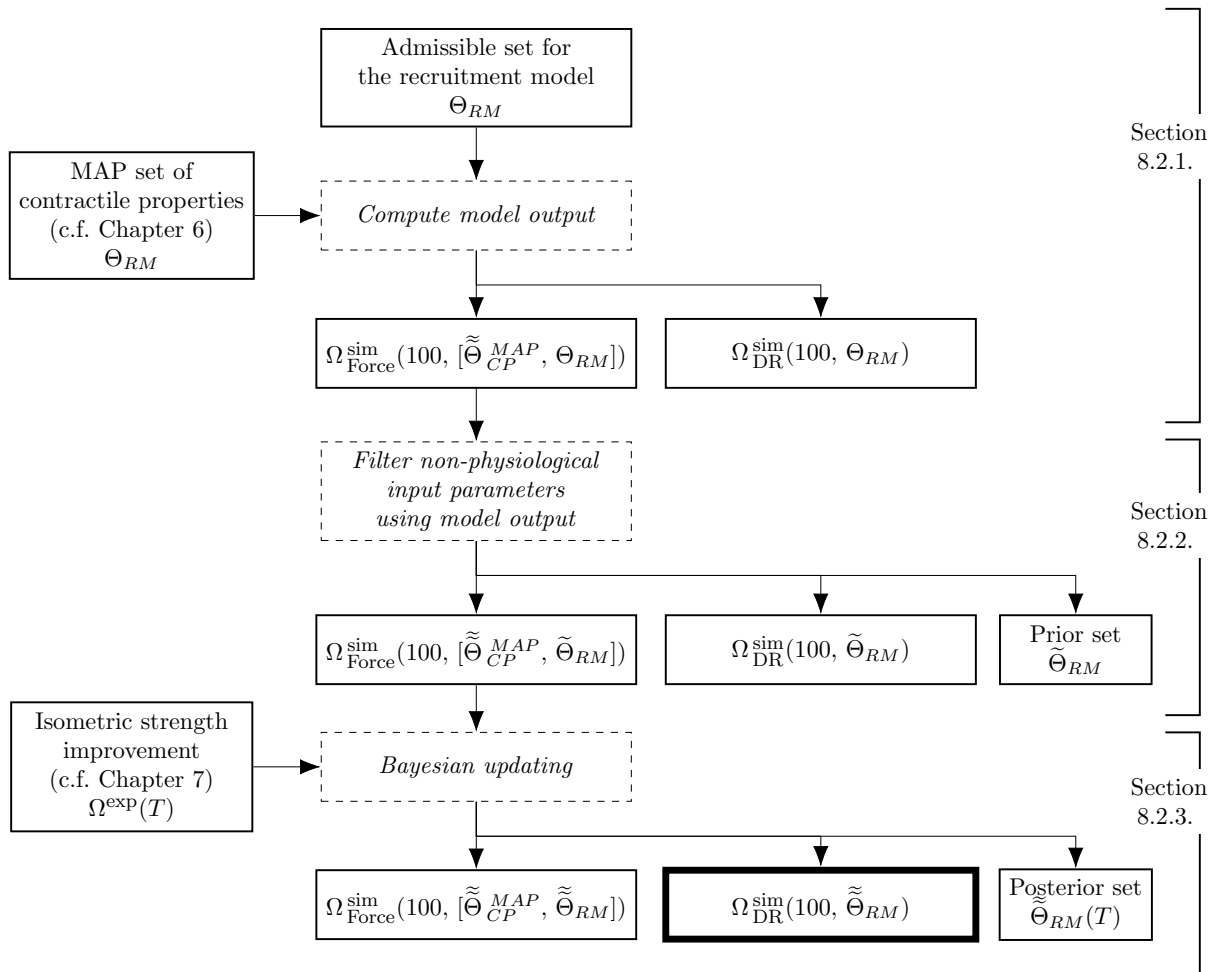


**Figure 8.1:** Overview of the scheme.

twitch force) were estimated. Furthermore, in Chapter 7, change in isometric strength of the quadriceps group is modelled based on data a systematic review study. Data collected during the systematic review is modelled longitudinally by means of a longitudinal model-based meta-analysis.

In this chapter, building up on the findings of the aforementioned chapters are used to investigate the change in discharge rate in the vastus lateralis muscle. Using the input parameters for the pre-exercise state and the contractile properties as the baseline, new parameter sets for the motor neuron recruitment model that yield an increase force output of the muscle, which match the longitudinal change in the isometric strength, are determined in this chapter. Similar to Chapter 6 and Chapter 5, Bayesian updating framework (see Chapter 3) is employed. In Fig. 8.1, an overview of the modelling scheme used in this chapter is provided.

### 8.2.1 Admissible set of model input parameters

In Chapter 5, it became evident that the slope of the peak discharge rate ( $PFRD$ ) and the peak firing rate of the first motor neuron ( $PFR_1$ ) do not contribute to the model output (see Section 5.4). Therefore, in this chapter, these two parameters are disregarded.

Only three parameters, namely the range of recruitment,  $RR$ , the peak firing rate of the last motor neuron,  $PFR_N$ , and the minimum firing rate,  $MFR$ , are calibrated using the Bayesian updating framework (see Chapter 3).

Analogous to previous chapters, admissible sets for the input parameters are selected (see Table 8.1). For each input parameter, a range that covers up to 20% change from the baseline value is assumed. The baseline value of each parameter corresponds to the MAP set of the model input parameters determined in Chapter 5, which are  $RR = 23.11$  [-],  $PFR_1 = 11$  Hz and  $MFR = 1$  Hz. For  $PFR_N$  and  $MFR$ , the admissible sets include values with an increasing order compared to the baseline, i.e., pre-training, value. Analogously, the admissible set for  $RR$  includes values of decreasing order.

**Table 8.1:** Ranges for the admissible sets of input parameters,  $\Theta$ .

	$RR$	$PFR_1$	$MFR$
Range	0 23.5	11 55	1 5
Unit	[-]	Hz	Hz

Range of each parameter is divided into 100 elements, such that each parameter has 100 different distinct values. All possible combination of each admissible set,  $\Theta_{RM}$ , is computed ( $RM$  in  $\Theta_{RM}$  stands for the motor neuron *recruitment model*). The cardinality of the set is hence  $10^6$ .

The maximum isometric force output is required for the model calibration. Therefore, for all elements in  $\Theta_{RM}$ , the maximum isometric force output,  $\Omega_{\text{Force}}^{\text{sim}}(100, [\tilde{\Theta}_{CP}^{MAP}, \Theta_{RM}])$ , is computed. Since the aim is to find the change in the mean discharge rate of the motor neurons caused by UIKEE, the corresponding mean discharge rate is also saved. This is denoted by  $\Omega_{\text{DR}}^{\text{sim}}(100, \Theta_{RM})$ .

To compute the isometric force output and the discharge rate, analogous to previous chapters, the motor neuron recruitment model is used. The model input parameters for the recruitment model are  $\Theta_{RM}$ . To compute the force output, contractile properties are also needed (see Chapter 4). The contractile properties obtained in the MAP set in Chapter 6 are used in this chapter, which is denoted by  $\tilde{\Theta}_{CP}^{MAP}$ .

## 8.2.2 Prior set of model input parameters

The aim of this chapter is to determine the extent of the increase in discharge rate that yields the increase in force output, which was modelled in Chapter 7. Using two criteria based on muscle adaptation due to isometric exercise, the size of the model input parameter set and the corresponding model output are filtered. This way, non-physiological model runs could be eliminated, such that the calibration can yield a more accurate outcome.

First criterion is related to the force at which all motor neurons are recruited ( $F_{Full Rec}$ ). It is suggested that the baseline/pre-exercise state of  $F_{Full Rec}$ , denoted by  $F_{Full Rec}^{Pre}$ , decreases due to isometric training (see [66]). Therefore, parameters that yield  $F_{Full Rec} > F_{Full Rec}^{Pre}$  are disregarded.

The second criterion is the increase in isometric strength of the muscle. As the aim is to determine the discharge rate that causes an increase in the isometric strength of the

muscle, parameters that yield decreased force output in comparison to the baseline/pre-exercise isometric strength are eliminated.

This way, the size of the parameter space in  $\Theta$  and the corresponding model output  $\Omega_{\text{Force}}^{\text{sim}}(100, [\tilde{\Theta}_{CP}^{MAP}, \Theta_{RM}])$  were filtered and non-physiological cases were disregarded. Thus, the size of  $\Theta$  and  $\Omega_{\text{Force}}^{\text{sim}}(100, [\tilde{\Theta}_{CP}^{MAP}, \Theta_{RM}])$  are reduced. The reduced set of model input parameters,  $\tilde{\Theta}$ , serves as the prior set of input parameters, whereas,  $\Omega_{\text{Force}}^{\text{sim}}(100, [\tilde{\Theta}_{CP}^{MAP}, \tilde{\Theta}_{RM}])$  is used as the model output in Bayesian updating.

### 8.2.3 Calibration points

The longitudinal model of the change in isometric strength over the weeks trained in Chapter 7 (see Fig. 7.2) is used to determine the calibration points. The change in isometric strength over 16 trained weeks,  $T$ , is divided into 100 intervals to obtain the calibration data,  $\Omega^{\text{exp}}(T)$ .

For each  $T \in (0, 16]$ , input parameters are calibrated against  $\Omega^{\text{exp}}(T)$  to obtain the posterior set of input parameters,  $\tilde{\Theta}$ , and the posterior set of model output using Bayesian updating. To set up the covariance matrix ( $\mathbf{R}$ ) required for the Bayesian updating, the confidence intervals of the parameters of the longitudinal model, which are  $E_{\text{max}}^{\text{BLMBA}}$ ,  $E_0$  and  $C_{50}$ . For this, the upper limit and the lower limit of the confidence intervals for these parameters are used and two curves are generated (see Fig. 8.2). Thus, the measurement error at each time point has a different magnitude, which increases over the weeks trained.

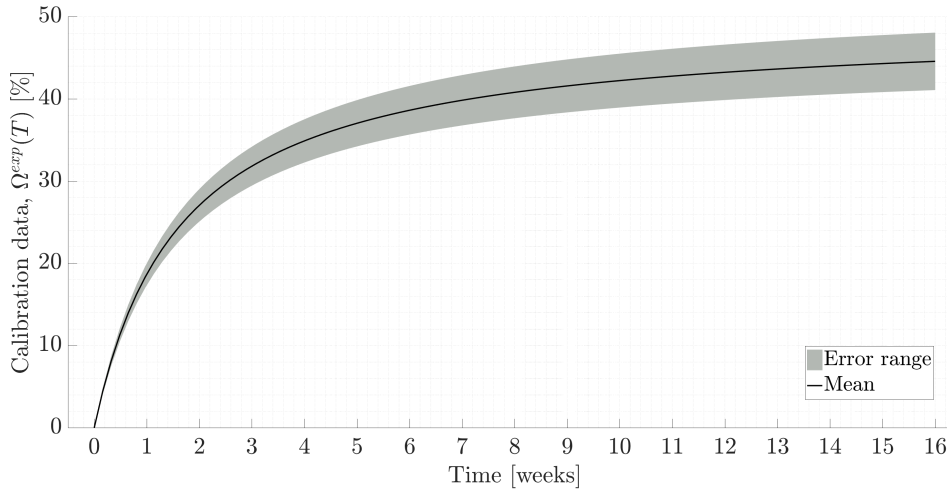


**Figure 8.2:** Calibration data obtained from the longitudinal model of the change in isometric strength in Chapter 7. The solid line corresponds to the curve generated using the point estimates of the model parameters and the gray area spans the upper and lower limits of the measurement error. This range is set up using the confidence intervals of the model parameters.

The posterior set of model output includes both  $\Omega_{\text{Force}}^{\text{sim}}(100, [\tilde{\Theta}_{CP}^{MAP}, \tilde{\Theta}_{RM}])$  and  $\Omega_{\text{DR}}^{\text{sim}}(100, \tilde{\Theta}_{RM})$ , since the two are coupled to each other. The change in mean discharge rate over the weeks trained can thus be computed by subtracting the baseline/pre-exercise value of the discharge rate from  $\Omega_{\text{DR}}^{\text{sim}}(100, \tilde{\Theta}_{RM})$ .

## 8.3 Results

### 8.3.1 Size of parameter sets

The admissible set of input parameters has a total of  $10^6$  elements. When parameters that yield non-physiological model outputs are disregarded, the size of set is reduced to 74 690 elements and the prior set of input parameters are obtained. The reduction in size corresponds to a 92.5% reduction of the parameter space of the admissible set.

Posterior sets are obtained by means of Bayesian updating over the trained weeks. Since the measurement error increases over weeks trained, the size of the posterior sets increase over time. The smallest posterior set has 1558, which is at week 0.16 (see Fig. 8.3). Size of the posteriors increase up to 7062 at the third week of training and shows a slight decrease after this time point. At the week 16, i.e., at the last data point, the size of the posterior set is 5637.

When the size of the posterior sets are compared to that of the prior set, it is seen that the size of the largest posterior (at week 3), corresponds to 9.63% of the size of the prior set. Thus, the calibration yielded a maximum of 90.36% and a minimum of 77.9% reduction compared to the prior set (see Fig. 8.3). Note that the sizes of the posterior set conforms to the size of each input parameter for the recruitment model.

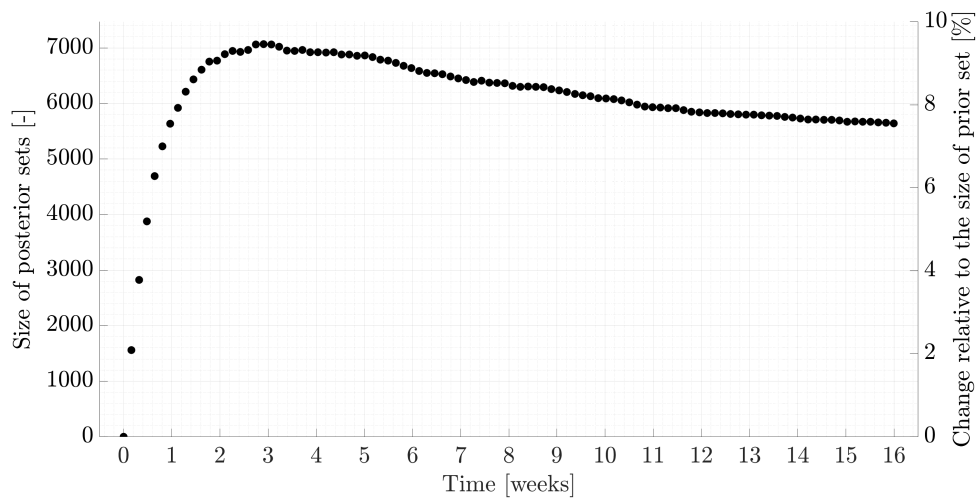


**Figure 8.3:** Size of the posterior sets over weeks trained. Right axis shows the size of posteriors compared to the size of the prior set.

### 8.3.2 Posterior sets over trained weeks

The evolution of the three parameters of the recruitment model ( $RR^{post}$ ,  $PFR_N^{post}$ ,  $MFR^{post}$ ) over the weeks trained is investigated. For this, the range of values each parameter takes in the posterior sets as well as the mean and standard deviation of the corresponding ranges at each time point is computed. The behaviour of the posterior set of each parameter is discussed in the following.

### Recruitment range

The upper limit of the range of values the recruitment range parameter,  $RR^{post}$ , stays constant over the trained weeks and is equal to the parameter's baseline value,  $RR^{pre} = 23.5$  (see Fig. 8.4(a)). On the other hand, the lower limit of the range increases longitudinally accompanied by a decreased width of the range of values. Since the range is wider at the beginning, the corresponding standard deviation is also wider, which also decreases over trained weeks. After week 8, the width of the range and the standard deviation becomes constant, with only a minor decrease in the width after week 15.

Mean value of the posterior set starts from 18.8 at week 0.16 (first available time point). At the last time point at week 16,  $RR^{post}$  increases to 22, which is almost equal to  $RR^{pre}$ . Similar to the evolution of the change in strength, mean the posterior value increases rapidly until week 3. The rate of increase slows after this time point.

### Peak firing of the last motor neuron

Unlike  $RR^{post}$ , the upper limit of the range of values of the peak firing rate of the last motor neuron,  $PFR_N^{post}$ , increases over the trained weeks (see Fig. 8.4(b)). The lower limit of the range follows an identical trend.

Similar to  $RR^{post}$ , the mean value of the posterior set increases rapidly until 3 weeks, where it reaches 22 Hz. The increase continues at a slower rate after this time point. Peak value of the mean occurs at 25 Hz at week 16.

### Minimum firing rate

Change in  $MFR$  is not as prominent as the other two parameters (see Fig. 8.4(c)). At the end of the first trained week, mean  $MFR$  reaches 3 Hz. There is only a slight increase in the mean after the first week, which goes up to 3.2 Hz. The range of the posterior set does not differ from the prior set.

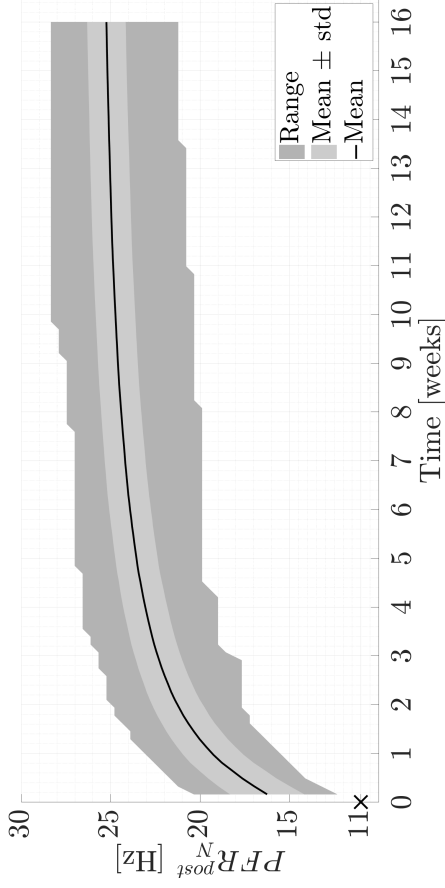
### 8.3.3 Change in mean discharge rate over trained weeks

The trend in the change in mean discharge rate of the motor neuron pool,  $\Omega_{DR}^{sim}(100, \tilde{\Theta}_{RM})$ , follows that of the calibration data. The rapid increase up to week five is followed by a plateau, which also shows a slight increase (see Fig. 8.4(d)).

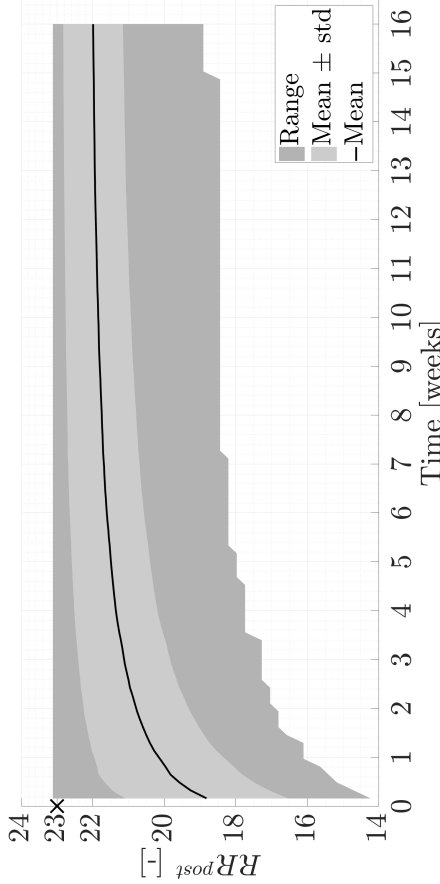
At the end of the first trained week, the mean discharge rate is 30.5 Hz and goes up to 42.1 Hz at week 16. At week 16, the posterior set covers values between 38.2 Hz to 45.7 Hz. This corresponds to 34.4-60.5% increase from the baseline value. The mean increase at the last data point corresponds to 47.9%.

## 8.4 Summart and discussion

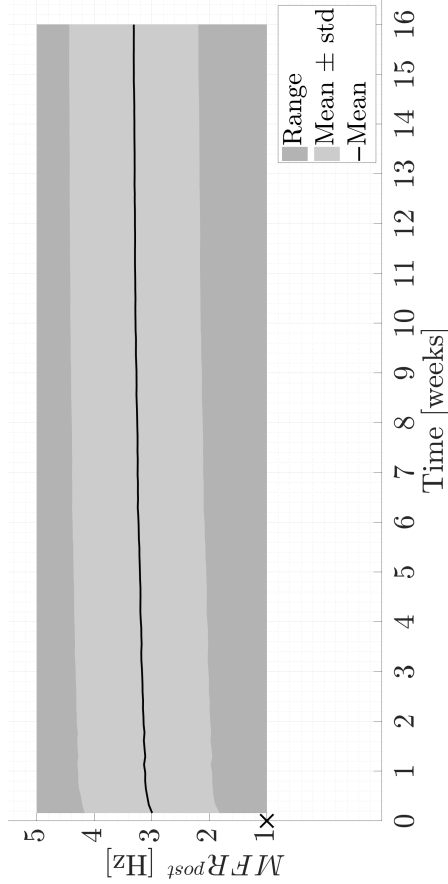
Using the longitudinal model of the change in isometric strength (see Chapter 7), the change in the mean discharge rate of the motor neuron pool of vastus lateralis muscle in response to UIKEE is estimated. When physiological constraints are applied, the size of the initial set of admissible parameters ( $\Theta_{RM}$ ) was reduced from  $10^6$  to 74 690, which is a significant reduction. Posterior sets over weeks trained, which are obtained after the



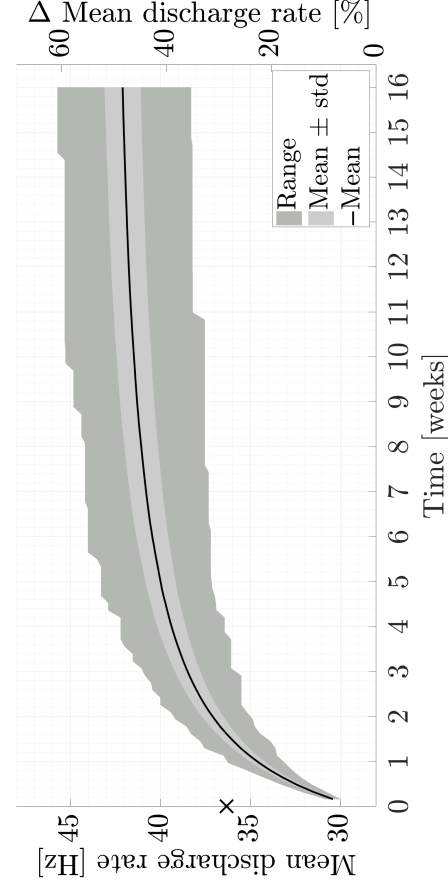
(a) Range of recruitment threshold,  $RR^{post}$ .



(b) Peak firing rate of the smallest motor neuron,  $PFR_N^{post}$ .



(c) Minimum firing rate,  $MFR^{post}$ .



(d) Change in the mean discharge rate,  $\Omega_{DR}^{sim}(100, \tilde{\Theta}_{RM})$ .

**Figure 8.4:** (a)-(c): The posterior set of input parameters,  $\tilde{\Theta}_{RM}$ , (d) the posterior set of model output for the mean discharge rate,  $\Omega_{DR}^{sim}(100, \tilde{\Theta}_{RM})$ . In all figures, the range is denoted by the area in dark gray, whereas mean and standard deviation (std) are covered by the area in lighter gray and the mean value is depicted by the black curves. The crosses denote the baseline value of each parameter.



calibration, contain 1553 to 7062 elements, the largest one occurring at the third week of training. The mean discharge rate is found to increase up to 42.1 Hz (38.2 – 45.7 Hz). In comparison to its pre-exercise/baseline value, this corresponds to a 47.9% (34.4-60.5%) increase. The posterior sets of the model input parameters of the recruitment model that yield this model output

The 92.5% reduction in the size of the admissible input parameters to obtain the prior set points to the fact that many elements in the initial set were irrelevant for the current problem. It can, however, be argued that applying the physiological constraints were necessary and beneficial to obtain a narrower set of posteriors, which would in turn increase the accuracy of the calibration.

The range of the calibration data varies over the weeks trained, since two curves with the upper and lower limit of the point estimates of the longitudinal model were used. Therefore, the range of data is narrower at the beginning and gets wider as training proceeds. This had a direct influence on the size of the posteriors over trained weeks as the calibration data also covered a wider range.

When setting up the range for the admissible set of input parameters for the recruitment model, the baseline values of the parameters, cf. pre-exercise state, determined in Chapter 5 were used. When the  $RR^{post}$  was set up initially, as the recruitment range is expected to decrease, all positive values smaller than the baseline value up to 0 were used. Therefore, the range of this parameter was restricted and nothing was assumed. The baseline value of  $RR^{post}$  occurs in each set of posterior parameters over the weeks trained, whereas the lower limit of the range of the posterior starts from 14.2. This shows that values lower than 14.2 were disregarded when the physiological constraints were applied or during the calibration.

Recruitment range is a parameter that is related to, as the name suggests, the recruitment behaviour of the motor neuron pool. It defines the recruitment threshold of a motor neuron. When  $RR$  decreases, the recruitment threshold of each motor neuron decreases, thus a given motor neuron is recruited at an earlier phase of the contraction. Motor neurons with lower thresholds also discharge at a higher rate, cf. the onion skin principle [62]. Although a higher discharge rate is expected as a part of neuromechanical adaptation in response to exercise, change in the discharge rate does not occur suddenly. Despite the fact that the model output regarding the discharge rate increases over time and no sudden change is observed (see Fig. 8.4(d)), a similar change distributed over the trained weeks is not observed for the mean value of  $RR$ , considering the baseline value of the parameter is considered. This parameter in the post-training phase decreases from 23.1 at week 0 to 14.2 at week 0.16, followed by an increase as the training proceeds. This is also due to the curvature of the calibration data.

The data on the change in isometric strength shows a consistent positive change over the weeks trained and this behaviour is directly transformed to the model input parameters. In order to obtain a slower decrease in the recruitment threshold distributed over the entire training period, this parameter could be calibrated against a different model. To do that, ideally, experimental data on the recruitment threshold is required, which is currently not available.

As mentioned before, the discharge rate is expected to increase over weeks. The evolution of  $PFR_N^{post}$  is more physiologically relevant, since the posterior set and the mean value of the posterior set shows a consistent increase, compared to the baseline

value of the parameter.

Similarly for  $MFR^{post}$ , an increase is expected and the calibration partially adheres to this expectation. Although the mean value of the posterior set increases, this increase over the trained week is very subtle. However, when the baseline value of the parameter is compared, which is 1 Hz, there is also a sudden increase at the first data point, which is available at week 0.16. If the calibration had been made by taking a finer resolution of the longitudinal model, i.e., by taking more than 100 data points, this sharp increase could have been partially avoided. Even if this was the case, since the order of magnitude of the calibration data stays the same, the mean  $MFR^{post}$  at week 0.16 would still be the same. Furthermore, the change of this parameter over the weeks trained is also quite small (from 3 Hz at week 0 to 3.2 Hz at week 16). This could be a result of the selection of the range for the admissible parameter set. The range for the admissible set covers values from 1 - 5 Hz and this range is divided into 100 elements. Therefore, the discrete values of the parameter set are very close to each other. Would one have considered a wider range was selected, the discrete values would have had more variation, which could increase the accuracy of the calibration.

## Limitations

The increase in strength is assumed to be equally transformed to each muscle of the quadriceps. The longitudinal UIKEE study by Kubo et al. [182] found no significant differences in the relative increase in muscle volume among knee extensors. Therefore it is a valid assumption to use the strength increase collected from knee extensors as the expected strength increase for vastus lateralis with the current knowledge.

Passive structures, i.e., connective tissues, are known to influence force output of individual motor units, since they contribute to the transmission of force to the tendon [82]. The concentration for the endomysial collagen is found to differ between fibre types, the concentration being higher for slow fibres when compared to fast fibres in rats (in [82], [175]). Properties of connective tissues were shown to alter in response to training, which is manifested by increased tensile strength (in [82], [175];[182]). However, since passive structures are not included in the current modelling framework and their contribution to the total force output is disregarded, it is assumed that the entire increase in strength is caused by the active force.

Isometric exercise is thought to alter the rate of force development [66]. Changes in rate of force development cannot be tested due to the limitations of the motor neuron recruitment model. As discussed earlier in Chapter 4, the rate of excitation cannot be altered, thus rate of force development remains the same for any choice of input parameters. The recruitment model used in this work could be improved by introducing an equation that is capable of capturing force development at different rates. This would make it possible to investigate the corresponding changes caused by UIKEE.

The range for the admissible set of input parameters  $PFR_N$  and  $MFR$  is assumed to cover 20% change in the input parameters. Since data on the input parameters for the change triggered by isometric training is lacking, this range is assumed. A wider range and more elements might make the estimation more accurate.



# 9 Discussion and Outlook

## 9.1 Discussion

The present study aims to provide a modelling framework to investigate the changes in the motor neuron discharge rate in vastus lateralis muscle due to UIKEE. Since the most prominent change observed due to UIKEE is the change in muscle strength, the force output of the muscle needs to be modelled in detail. To model the force output, the discharge instances and the contractile properties of the muscle is required. The motor neuron recruitment model by Fuglevand et al. [104] has been used, both for the pre- and post-exercise states of the muscle, to model the discharge instances. For the contractile properties, a novel scheme has been suggested. A similar pattern has been applied for each part of the modelling framework. Model input parameters for the motor neuron recruitment model and the scheme for the contractile properties have all been determined based on available experimental data retrieved from multiple studies. Final selection of the input parameters has been made using Bayesian updating. However, the change in isometric force output, i.e., isometric strength, has been modelled using BLMBMA. The discharge rate of the motor neuron pool has been found to increase from 28 Hz up to 42 Hz following 16 weeks of UIKEE. The isometric strength increased up to 33% following the same training period.

Each part of the modelling framework has been formerly discussed in detail within the corresponding chapters. Therefore, in this chapter, an overall discussion regarding the use of Bayesian updating in this present study as well as how well each part of the framework has been connected to each other will be provided.

Experimental data on the neuromechanical system is tedious to obtain and that provides information for only some portion of the entire muscle, thus, despite a vast amount of past and on-going research on the topic, many aspects of the voluntary motor control is to date still not understood completely. Besides advances in the technological equipment and the data analysis methodology, complexity of the voluntary motor control play an important role in this knowledge gap. Computational models of the neuromechanical system aim to close this gap by providing insight into aspects that cannot be investigated experimentally. However, computational models require experimental data as an input in order to simulate the reality as accurately as possible.

One way to incorporate existing experimental data into such models is using the Bayesian updating framework. Strength of the Bayesian updating framework lies in its ability to be applicable to any problem, where the exact magnitude of model input parameters are unknown. What is required by the framework is an estimate of the range of values that the model input parameters may take. This range can either be completely assumed, which decreases the accuracy of the final estimate of the input parameters, or can be constructed based on empirical evidence. Furthermore, when available, the empirical evidence, e.g., in the form of experimental data, does not need to stem from a single

study, but evidence from multiple studies can be pooled together to calibrate the model input parameters.

Since a vast amount of research on the motor control behaviour of muscles do exist, in this study, experimental data on the recruitment behaviour of skeletal muscles have been used to set up the ranges for the parameters. Not only multiple sources of experimental studies were used, but ranges for each parameter obtained from data has been narrowed down using the physiological knowledge on motor neuron recruitment. The calibration has also been performed based on the available experimental evidence. Therefore, it can be said that, in the present study, Bayesian updating has been used in such a manner that admissible ranges for the input parameters have been selected using the available evidence to a maximum, i.e., in terms of quantitative data and physiological knowledge.

There are three parts in the modelling framework suggested in this study. The first one is for determining the model input parameters for the motor neuron recruitment model that allows us to obtain the discharge instances at multiple force levels. From this, it is also possible to compute the mean discharge rate of the motor neuron pool. The second part deals with finding the contractile properties of the vastus lateralis muscle. This part receives the input from part one. The third part uses the results of part one and two. The outcome of part one is used as the baseline values for the input parameters of the motor neuron recruitment model and the outcome of part two is used to compute the isometric strength.

The input parameters received from each part corresponds to the MAP set of input parameters. Although some argue that the advantage of using MAP is its simplicity, MAP is a point parameter estimates (see Section 3.2.4). Being the mode of the posterior distribution, it is possible that the MAP lies further away from the posterior median, thus not representing the bulk of the posterior distribution [186].

One way to overcome this limitation could be by setting up the entire modelling framework so that it allows to test the effect of a wider range of input parameters when these parameters are used in another part of the framework. To illustrate, instead of using a single set parameters of the motor neuron recruitment model in part two, where we determine the contractile properties, entire posterior set found in part one could be used. Again, all combinations of the admissible sets for the motor neuron recruitment model and the contractile properties could be created, thus the recruitment model and the contractile properties would hence be coupled to each other. Calibration of the contractile properties would again yield the desired result. This would, however, increase the amount of model runs.

Despite the limitations of the framework proposed in this study, such a comprehensive study on a specific exercise type, i.e., UIKKEE, and on one muscle, i.e., vastus lateralis, does not exist to this date. The principles suggested in the present study can be applied to other modes of exercise, such as dynamic modes, as the change in the discharge rate have been obtained merely using experimental data on the change in isometric strength. If longitudinal data for the change in strength for other forms of exercise can be obtained, changes in the recruitment behaviour can easily be investigated using the present framework.

## 9.2 Outlook

The musculoskeletal system has the capability to adapt and alter its properties if conditions they are normally subject to change. Such a change of conditions include, but is not limited to, exercise. Exercise causes a number of properties of the trained muscle(s) to change. Despite a vast amount of research on the adaptive mechanisms of skeletal muscles, the phenomenon is still not understood completely [117].

Computational models of the adaptive mechanisms of muscles have been and are still being used up to this date to investigate multiple aspects of this complex phenomenon. These models are constructed based on the current state of empirical knowledge on the physiology of the system and the corresponding changes. Thus, it is common to incorporate experimental data or principles of physiology into computational models. In the present study, we have proposed a modelling framework to examine the neuromechanical adaptation of a muscle, cf. vastus lateralis, in response to a specific exercise type, namely UIKEE.

It is our hope that the novelties as well as the limitations of the framework will inspire other researchers to construct more comprehensive models to investigate the neuromechanical adaptation phenomenon in muscles. Here, some suggestions that could improve the proposed framework have been provided. Ideas for further research topics based on the framework have also been suggested.

### **Improving the construct of the motor neuron pool for vastus lateralis**

The modelling scheme suggested in this study has been constructed by making extensive use of experimental data from literature. Data on the vastus lateralis muscle has been used to select relevant model input parameters, which has allowed us to set up a muscle-specific framework. As more data on the discharge and contractile properties of the vastus lateralis available, these can be introduced to the current framework following the steps outlined in the previous chapters. This would improve the calibration accuracy.

To illustrate, the model input parameters of the motor neuron recruitment model describing the pre-exercise state of the muscle have been selected based on data on the mean discharge rate of vastus lateralis. There were 19 data points available at 8 different contraction levels. At 75 % MVC, only one data point is available. As more data on the discharge rate of vastus lateralis becomes available, calibration data for the motor neuron recruitment model can be enhanced. Selecting new sets of input parameters would not require further model runs. A re-run of the rejection sampling would be sufficient.

The scheme to determine the contractile properties of the muscle made use of experimental data to select the range of admissible input parameters and the prior sets have been constructed. The data set used for this purpose, however, is composed of data on muscles other than vastus lateralis. The set includes data from larger, e.g., tibialis anterior, as well as smaller muscles, e.g., first dorsal interosseous. Therefore, an enhanced data set would also improve the framework to select contractile properties, once more data ideally on vastus lateralis or larger muscles become available.

## **Model of the longitudinal change in muscle strength**

One novelty of the present study is the use of BLMBMA to model the longitudinal change in muscle strength over trained weeks. BLMBMA has been used for the data on UIKEE. Such an approach has never been used in the field of sports science. This method can be applied to data on other training modes and the changes in the muscle performance can be modelled. In this study, only the change in isometric muscle strength could be modelled, but the same framework can be used for data on the EMG, cross-sectional area or even molecular changes in the trained muscle(s) if sufficient data is available.

For the longitudinal model of muscle strength increase, only data on the trained limb has been used. However, it is known that unilateral training triggers changes in the performance of the untrained/contralateral limb due to the cross-education phenomenon [82]. Although the performance changes in the contralateral limb is not as prominent as the trained limb, these changes are more often statistically significant and, e.g., for the improvement in strength, can go up to 21% [226]. In our case, data on the untrained limb was insufficient and a longitudinal model could not be fitted, however, the trend of the change in muscle strength is similar to that of the trained limb. In light of this, instead of using BLMBMA, a simple evolution equation can be fitted to the available data on the change in strength in the untrained limb. The approach for the trained limb could be then be used for the untrained limb and changes in the discharge rate of the untrained limb can be investigated.

## **Extending the modelling framework to include other muscles of the knee extensors**

The proposed modelling framework is muscle-specific. Although all knee extensors are used in UIKEE, only changes in vastus lateralis have been investigated and the remaining three muscles, namely the rectus femoris, vastus intermedius and vastus medialis, have been neglected. For a wholesome investigation of the adaptation of the knee extensors, ideally, all knee extensors should be included in the framework. To do that, the pre-exercise state of all four muscles needs to be constructed. For this, data on the discharge rate of the muscles should be gathered from literature. To set up the contractile properties, only data on the isometric strength is required, which is, in comparison to data on the discharge rate, more straightforward to obtain. Elias et al. [80] provides an estimate of the contribution for the muscles of the knee extensors. Using this piece of information, the contractile properties for the motor neurons of the remaining muscles can be constructed. Changes in the EMG activity of each knee extensor muscle for bilateral isometric training has been provided in Rabita et al. [254]. Results of this study could be used to validate and compare the results for the changes in the discharge rate.

## **Including other aspects of muscle adaptation**

### **Neural adaptation due to exercise**

In an effort to keep the complexity to a minimum, we focused on a single adaptation mechanism, which is the change in the discharge rate of the motor neuron pool. However, in reality, different adaptation mechanisms are known to work together to yield an

increase in the muscle performance following exercise. Such mechanisms include changes in voluntary activation, conversion of fibre types from IIa to IIx and changes in the rate of force development.

To illustrate, healthy subjects are thought to activate 80-95% of the quadriceps muscle during knee extension. Despite conflicting evidence, see e.g., [42], exercise is said to improve the volume of active muscle during a given contraction [55, 288]. One way to include the changes in the voluntary activation could be by using only a portion of the motor neuron pool, i.e., 80-95% of the estimated size of the pool, to construct the pre-exercise state of the muscle. The remaining, inactive motor neurons can be recruited at a certain rate over the trained weeks. The change in the number of active motor neurons can be modelled using different evolution equations, e.g., sigmoidal or exponential, and the effect on the overall force output can be investigated.

### **Volumetric adaptation due to exercise**

Although it becomes more prominent in later stages of training, volumetric muscle growth, i.e., hypertrophy, also contributes to improvement in muscle performance [279]. Despite a three-dimensional model is lacking in the present framework, the contribution of hypertrophy to the strength improvement could be potentially included in the framework. To do that, the model of the overall strength improvement could be split into two distinct curves, one for the neuromechanical adaptation and another one for the hypertrophy. This is already shown qualitatively in Fig. 2.14. Assumptions on the weight of each curve for the overall strength increase could be made. Instead of using the model of the overall strength improvement, the model for the neuromechanical adaptation can be used as calibration data to investigate the change in discharge rate.

### **Molecular adaptation mechanisms due to exercise**

Molecular mechanism that cause changes in the biophysical properties of motoneurons due to voluntary activity include changes in the dendrite structure, protein synthesis, axonal transport, neuromuscular propagation and some biophysical properties, which will influence how these cells behave during voluntary recruitment [89, 108]. Such changes have been studied for rodents and rats by means of experiments as well as models for endurance exercise [107–109]. Such detailed investigations at the cellular level, however, are lacking for isometric exercise. When a computational model of the molecular changes become available, such a model could easily be incorporated into this present framework.

### **Adaptation due to diseases**

Based on the model including data on healthy subjects, a diseased configuration of the motor neuron pool could be created. Depending on the disease being modelled, discharge rate and contractile properties of the motor neurons could be altered as needed. Furthermore, calibration data on the isometric strength can also be adjusted to mimic the strength output of the diseased configuration.



### **Adaptation due to ageing**

Muscle performance is known to change with age. Age-related changes in muscle properties are being investigated extensively, e.g., [42, 123], as the understanding of age-related changes in skeletal muscle activity can aid in finding solutions to common problems that the elderly population experience. Analogous to the example on the model of a diseased muscle, state of the muscle-of-interest, e.g., vastus lateralis, can be constructed for an elderly population using available data, e.g., [147, 270].

### **Closing remarks**

Due to the complexity of biological tissues, any research topic on tissues requires extensive knowledge on the biology, physiology and anatomy of the tissue of interest as well as the tissue's contribution to the organ systems. As a result, to increase the accuracy and detail on studies constructed around biological tissues requires knowledge and expertise from multiple disciplines. Therefore, interdisciplinary team work is of utmost importance in the field of biomechanics. A proper fusion of theoretical knowledge, experimental evidence as well as the capability of modellers' to de-construct and simplify complex systems to set up a concise model of the system-of-interest will definitely improve our understanding of the human body.

# A Admissible sets for the contractile properties

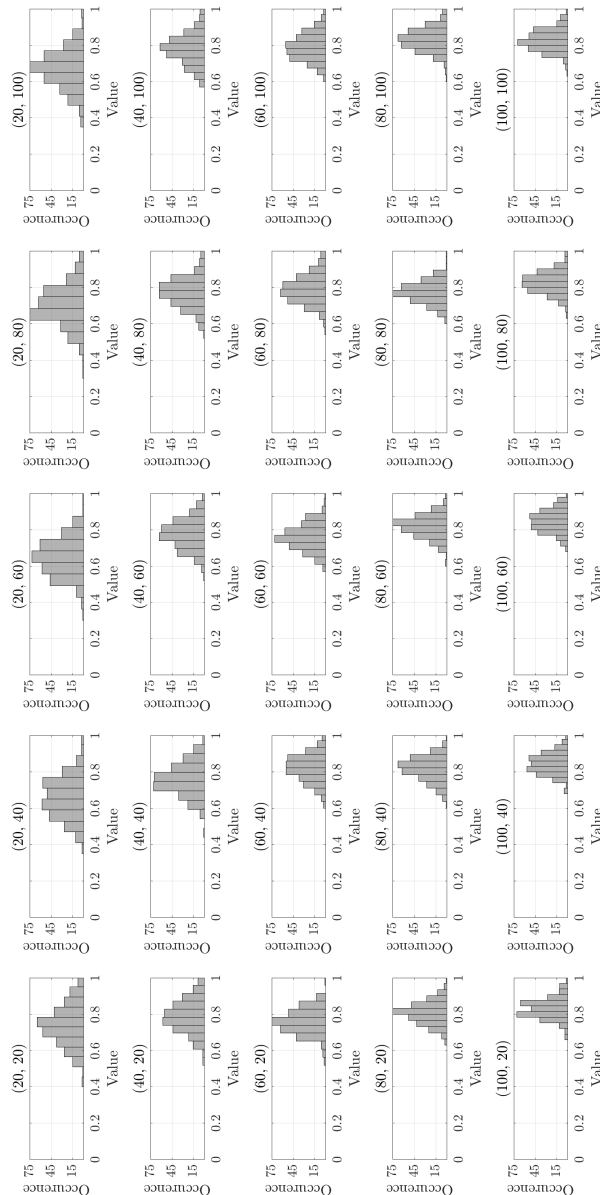


Figure A.1: One set of the combinations of shape parameters  $a$  and  $b$  used in Chapter 6 and their influence on the output of the random numbers following beta distribution. Values of the shape parameters are shown in brackets.

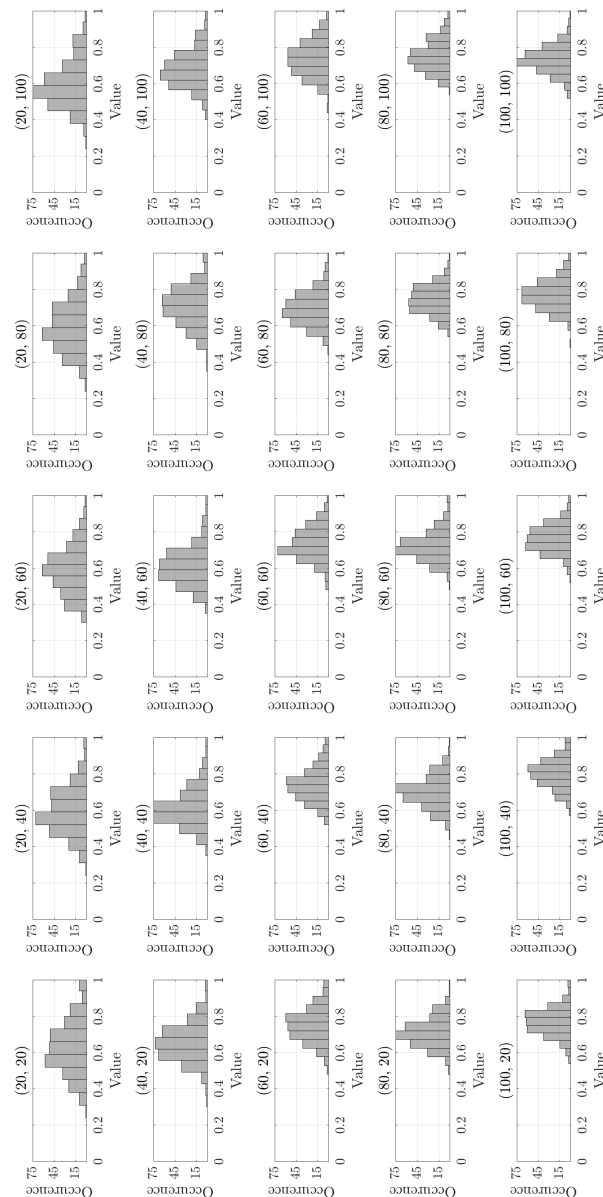


Figure A.2: One set of the combinations of shape parameters  $a$  and  $b$  used in Chapter 6 and their influence on the output of the random numbers following gamma distribution. Values of the shape parameters are shown in brackets.

# B Systematic review and meta-analysis

## B.1 Background information and significance

### Narrative vs systematic reviews

Literature review studies are methodological studies, which discuss a specific topic by using database searches to retrieve research results. There exist two main types of review studies, namely the narrative and systematic reviews. Narrative reviews critically analyse and discuss the current state of science for a given topic from a theoretical and contextual perspective. Although they are significant for providing up-to-date information to researchers, these reviews, however, do not specify what types of databases and methodological approaches are used to conduct the study. It is also not possible to answer specific quantitative research questions using these reviews[271]. They are also difficult to reproduce, thus the findings and conclusions presented in the study rely heavily on the insight of its author(s) [10].

Contrary to narrative reviews, systematic reviews aim to gather all empirical evidence, which fits within pre-specified eligibility criteria in order to answer a specific research question [138, 221]. These reviews rely on on explicit, systematic methods that are selected in order to minimize bias. Thus, in comparison to narrative reviews, they provide more reliable findings from which conclusions can be drawn and decisions made [138]. This review type is commonly used in health-related areas [138] (e.g., medicine, pharmaceuticals, physiotherapy, exercise science) as well as social sciences [198]. They are an important component of evidence-based medicine as they summarize existing knowledge and data on a particular topic.

### The PRISMA statement

Systematic reviews are performed according to structured guidelines in order to maintain their scientific integrity and minimize bias [120]. Such guidelines include, but not limited to, the "PRISMA Statement" (Preferred Reporting Items for Systematic Reviews and Meta-Analyses, see [221])<sup>1</sup>. The PRISMA Statement consists of a 27-item checklist listing the pieces of content that the manuscript must contain and a four-phase flow diagram that outlines the layers/phases of the systematic review [221].

---

<sup>1</sup>Since only the PRISMA Statement is followed in the later part of the thesis (Chapter 7), other guidelines are not mentioned here.

## Analysing the extracted data - meta-analysis

When there are several small studies on a specific question, combining/pooling data may improve statistical power [300]. Meta-analysis<sup>2</sup> is the use of statistical methods to estimate an average/common effect from the results of independent studies on a common subject [120, 244]. This analysis can provide a precise and robust summary estimate after a systematic and rigorous integration of the available evidence [300]. It is common to pool the quantitative data obtained from a systematic review by means meta-analysis. It is worth to note that every meta-analysis study must include a systematic review of the literature, but not every systematic review provides enough data for pooling by means of a meta-analysis [120].

Results of the meta-analysis are reported in graphical form using “forest plots”. Such plots present the findings for each study, as well as the combined results [244].

There exist two main models for combining studies, namely the fixed-effect model and the random-effects model. The fixed-effect model treats the variability between studies as merely due to random variation. This describes the when the studies were infinitely large and would all produce the same result. Whereas, the random-effects model considers a different underlying reason for each study and takes regards this as an additional source of variation. This model is formulated by Hedges and Olkin Therefore, in the hypothetical case that the studies were infinitely large, they would still report different results for the effect of the intervention. The outcomes of the studies are assumed in this model to be distributed randomly. The central point of this distribution denotes the focus of the combined, i.e., pooled effect estimate [244].

## Summary measures and forest plots

Results of a given study may be summarised in multiple ways. For continuous outcomes, which applies to the focus of this thesis, the options are the difference in means or standardised means between the reported outcome of the interventions [244]. Defining/selecting the outcome of interest is the starting point of all meta-analyses. This particular outcome is known as the summary (outcome) measure. It describes the observed effect in each trial, from which the overall meta-analytical summary can be calculated [64].

There are mainly two types of summary measures, namely the primary and secondary summary measures. A primary summary measure is selected among the outcome that would be expected to be analysed from the relevant studies. Conclusions drawn about the effects of the interventions are based largely on these outcomes. Whereas, secondary summary measures may include a limited number of additional outcomes the review intends to address. They may be specific to only some comparisons in the review [138].

---

<sup>2</sup>The roots of meta-analysis are attributed to the study by the biometrician Karl Pearson ([242]) conducted in 1904 [49]. Pearson reviewed the effects of a vaccine against typhoid, in which he gathered data from a total of eleven relevant studies of immunity and mortality among soldiers of the British Empire. He computed correlation coefficients for each study and synthesized these coefficients within two subgroups according to immunity and mortality. Pearson also noted that these correlations are highly variable and discussed how this variation could be interpreted [49].

## Longitudinal meta-analysis

Hierarchical data formed by the serial measurement of a quantity on an individual is known as longitudinal data [9]. This data type is common in clinical and epidemiological research to and is used to assess the effect of a treatment or exposure over time measured at pre-determined intervals [150]. It is also possible to perform meta-analyses of longitudinal studies using standard approaches. However, when effect estimates are reported at different times, these approaches are insufficient [150].

## B.2 Search strategy

Keywords, which are used in the review process are categorized as describing

- C I the nature of the exercise: “isometric”, “static”
- C II training: “training”, “exercise”
- C III which the body part is being trained: “knee extensor”, “lower limb”, “quadriceps”
- C IV the undesired subject group: “medicated”, “ill”, “illness”, “sickness”, “elder”, “elderly”, “old”, “osteoarthritis”

All permutations of each keyword in categories **C I** – **C III** are created and the keywords are combined with an AND. This yields 12 different cases. How each category was combined is illustrated in the following:

1. isometric AND training AND knee extensor
2. static AND training AND knee extensor
3. isometric AND exercise AND knee extensor
4. static AND exercise AND knee extensor
5. isometric AND training AND upper limb
6. static AND training AND upper limb
7. isometric AND exercise AND upper limb
8. static AND exercise AND upper limb
9. isometric AND training AND quadriceps
10. static AND training AND quadriceps
11. isometric AND exercise AND quadriceps
12. static AND exercise AND quadriceps

Keywords in **C IV** were added to each combination with NOT, since papers with these keywords are to be excluded. Note that for the search in Science Direct, only 8 Boolean operators are allowed. Therefore, only “ill”, “elder”, “old”, “osteoarthritis”, “handgrip” are added among the keywords in **C IV**.

Below are the search strategies for each database for search case number 1 (see above) in terms of the database’s own syntax:

PubMed:

```
isometric[Title/Abstract] AND training[Title/Abstract] AND knee extensor[Title/Abstract] NOT medicated[Title/Abstract] NOT ill[Title/Abstract] NOT illness[Title/Abstract] NOT sickness[Title/Abstract] NOT elder[Title/Abstract] NOT elderly[Title/Abstract] NOT old[Title/Abstract] NOT osteoarthritis[Title/Abstract] NOT handgrip
```

Web of Science:

```
TI=(isometric) AND TI=(training) AND TI=(knee* AND extensor) NOT TI=(medicated) NOT TI=(ill) NOT TI=(illness) NOT TI=(sickness) NOT TI=(elder) NOT TI=(elderly) NOT TI=(old) NOT TI=(osteoarthritis) NOT TI=(handgrip)
```

Science Direct (under the section “Title, abstract or author-specified keywords” in the advanced search):

```
isometric AND training AND knee extensor NOT ill NOT elder NOT old NOT osteoarthritis NOT handgrip
```

Chochrane Library:

```
(isometric):ti,ab,kw AND (training)ti,ab,kw AND ("knee extensor")ti,ab,kw NOT (medicated)ti,ab,kw NOT (ill)ti,ab,kw NOT (illness)ti,ab,kw NOT (sickness)ti,ab,kw NOT (elder)ti,ab,kw NOT (elderly)ti,ab,kw NOT (old)ti,ab,kw NOT (osteoarthritis)ti,ab,kw NOT (handgrip)
```

### B.3 Risk of bias assessment

The risk of bias (RoB) of individual studies were assessed using the Risk of Bias Tool, version 2 (Sterne et al., 2019). The study design is selected as “individually randomized parallel-group trial”. The outcome of the being assessed is specified as ‘strength’. The reviewer team’s aim for this result is selected as “to assess the effect of adhering to training intervention”. Deviations from intended interventions are selected according to “failures in implementing the intervention that could have affected the outcome”. The crib sheet for the tool is used as a guideline when assessing the RoB of each study (see <https://drive.google.com/file/d/1Q4Fk3HCuBRwIDWTGZa5oH110dR4Gbhd0/view>). Answers to the questions provided in the tool were given according to the following criteria:

- Bias due to the randomization process (RoB 1): The trained side of the limb (right/left) was assessed by checking if the choice was made based on the dominance of the limb or b random assignment. If the trained side was assigned according to limb dominance, the bias type is selected to raise “some concerns”, since dominant

limbs are known to have a higher baseline strength. Baseline characteristics of the subject groups were assessed according to group size, variation in the demographical information and baseline muscle strength.

- Bias due to deviations from intended interventions (RoB 2): This RoB was assessed based on whether it was reported that participants were instructed to keep the food intake and daily activity unaltered. Furthermore, any manipulations to the trained muscle, such as taking a biopsy from the muscle during the training period, was also assessed. Studies were further investigated, if verbal encouragement or biofeedback was provided during maximal force exertion.
- Bias due to missing outcome data (RoB 3): This bias type was assessed whether the number of subjects that withdrew from the study was statistically significant.
- Bias due to presentation of the measured results (RoB 4): This bias was assessed if results of the intermediary as well as pre-and post-training tests were reported in a tabular form or within a figure.
- Bias due to the selection of the reported result (RoB 5): Studies included in the review were assessed whether they report outcomes of the training effect they investigate and which were described in the methodology.



## B.4 Additional data

**Table B.1:** The results of risk of bias assessment for each study. Here, RoB denotes risk of bias, SC denotes some concerns, LR denotes low risk and HR denotes high risk.

Study	RoB 1	RoB 2	RoB 3	RoB 4	RoB 4	RoB 5
[30]	SC	HR	LR	LR	LR	SC
[46]	LR	SC	LR	LR	LR	LR
[81]	LR	LR	LR	LR	LR	LR
[110]	LR	LR	LR	LR	LR	LR
[155]	LR	LR	LR	LR	LR	LR
[180]	LR	SC	LR	LR	LR	LR
[193]	LR	LR	LR	LR	LR	HR
[199]	LR	SC	LR	LR	LR	LR
[222]	LR	SC	LR	LR	LR	LR
[235]	LR	SC	LR	LR	LR	LR
[239]	SC	SC	LR	LR	LR	SC
[263]	LR	SC	LR	LR	LR	LR
[273]	LR	LR	LR	LR	LR	LR
[299]	LR	SC	LR	LR	LR	LR
[306]	LR	SC	LR	LR	LR	LR
[319]	LR	LR	LR	LR	LR	LR
[320]	LR	LR	LR	LR	LR	LR



**Table B.3:** Training variables given in the studies. CD: contraction duration [s], R1: rest between each contraction [s], R2: rest between each set [min], TD: duration of the whole training period [weeks], Freq: frequency of training [sessions/week], Rep: repetitions, Int.: training intensity [%MVC], Angle: angle in degrees that the knee was trained, 0 degrees corresponds to the fully extended leg.

Study	CD	R1	R2	TD	Freq	Sets	Rep/set	Int	Angle
[14] a	6	0	0	8	3	20	1	100	30
[14] b	6	0	0	8	3	20	1	100	60
[14] c	6	0	0	8	3	20	1	100	90
[30]	6	20	2	4	3	5	5	80	90
[46]	4	3	0	8	3	1	30	100	90
[81]	3	17	2	4	3	4	10	100	90
[110]	4	25	-	8	3	3	10	100	90
[118]	5	3	0	6	5	1	30	100	90
[155]	4	2	1	12	3	4	6	100	90
[180]	10	50	0	5	3	10	1	100	60
[182]	20	0	1	12	4	4	1	70	90
[193]	5	10	NI	9	5	2	60	100	90
[199]	6	25	0	4	5	5	1	100	60
[222]	10	10	0	3	5	1	10	100	60
[235]	5	15	2	6	3	3	8	100	75
[239]	2	10	0	19	3	1	10	100	90
[263]	4	NI	NI	8	3	5	10	100	90
[273]	4	2	1	12	3	4	6	80	90
[299] a	5	5	1	3	5	3	10	50	90
[299] b	5	5	1	3	5	3	10	100	90
[306]	3	2	2	4	4	4	10	100	85
[319]	6	30	2	6	3	2	10	80	135
[320]	6	30	2	6	3	2	10	80	135
Mean	6	12	1	7	4	6	11	84	78
St.D.	4	13	1	4	1	6	13	29	17

**Table B.4:** Breakdown of studies included in the review and if they report data on a control group or the untrained leg (internal control). Apart from [14], [118] and [182] all studies report data for a control group, an internal control or both.

Study	Control group	Internal control
[14]	No	No
[30]	Yes	Yes
[46]	Yes	Yes
[81]	Yes	No
[110]	Yes	Yes
[118]	No	No
[155]	No	Yes
[180]	Yes	No
[182]	No	No
[193]	No	Yes
[199]	Yes	Yes
[222]	Yes	No
[235]	Yes	No
[239]	No	Yes
[263]	Yes	Yes
[273]	No	Yes
[299]	No	Yes
[306]	No	Yes
[319]	Yes	Yes
[320]	Yes	Yes

## B.5 Descriptive visualization of collected data

### B.5.1 Spaghetti Plots

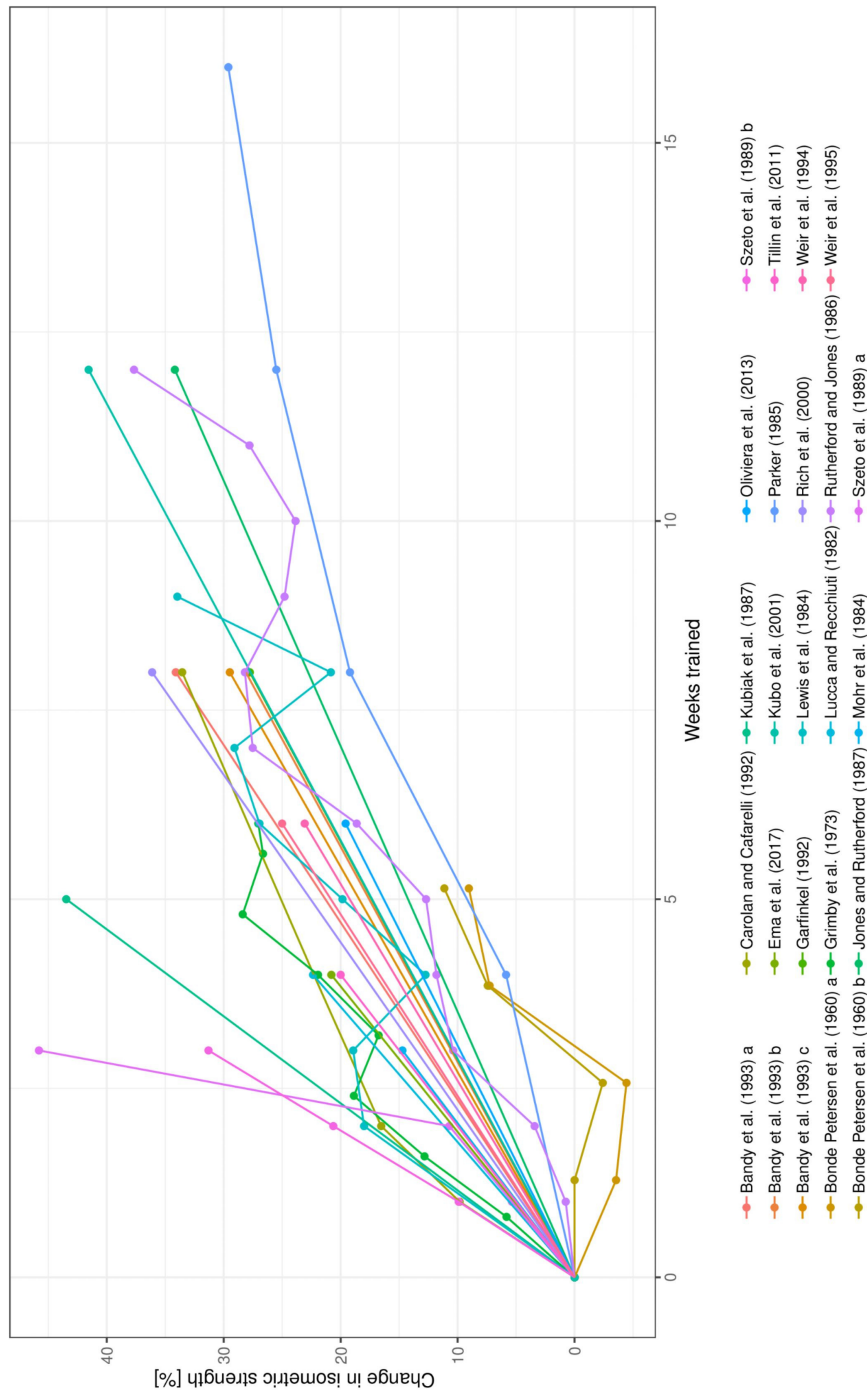


**Figure B.1:** Spaghetti plot of the data on change in isometric strength over time in weeks for all studies included in the systematic review.

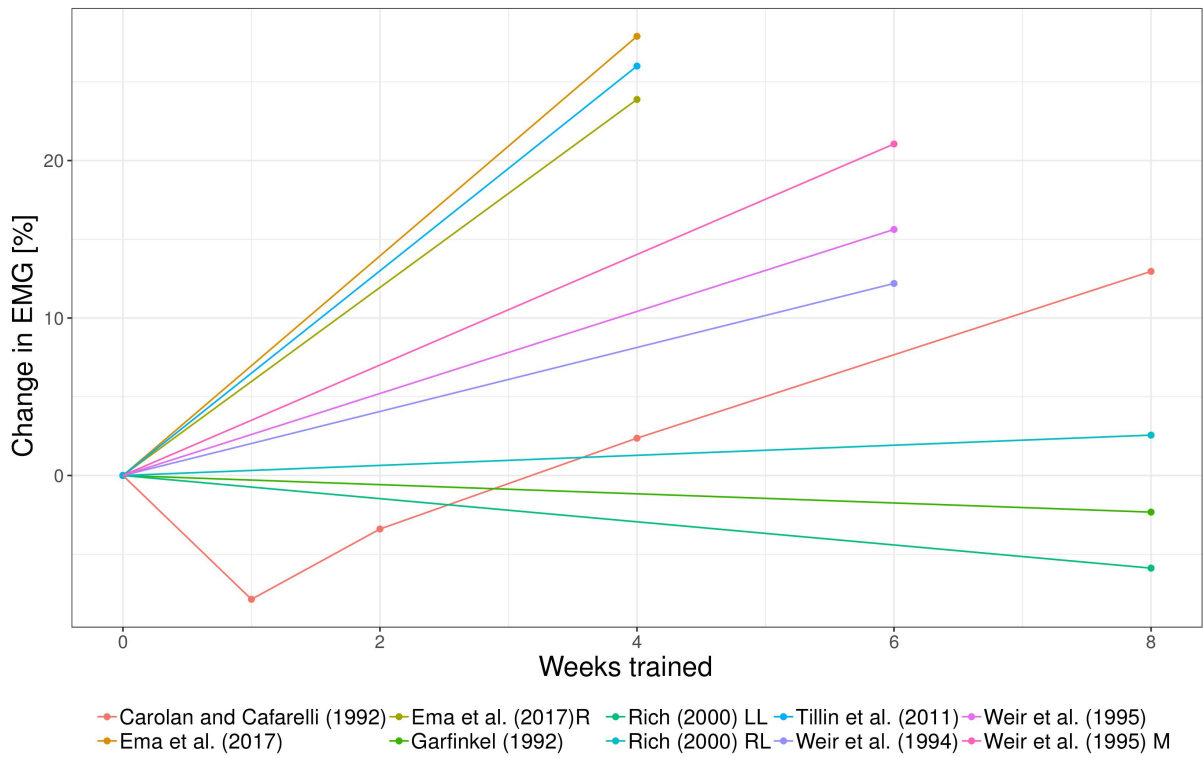
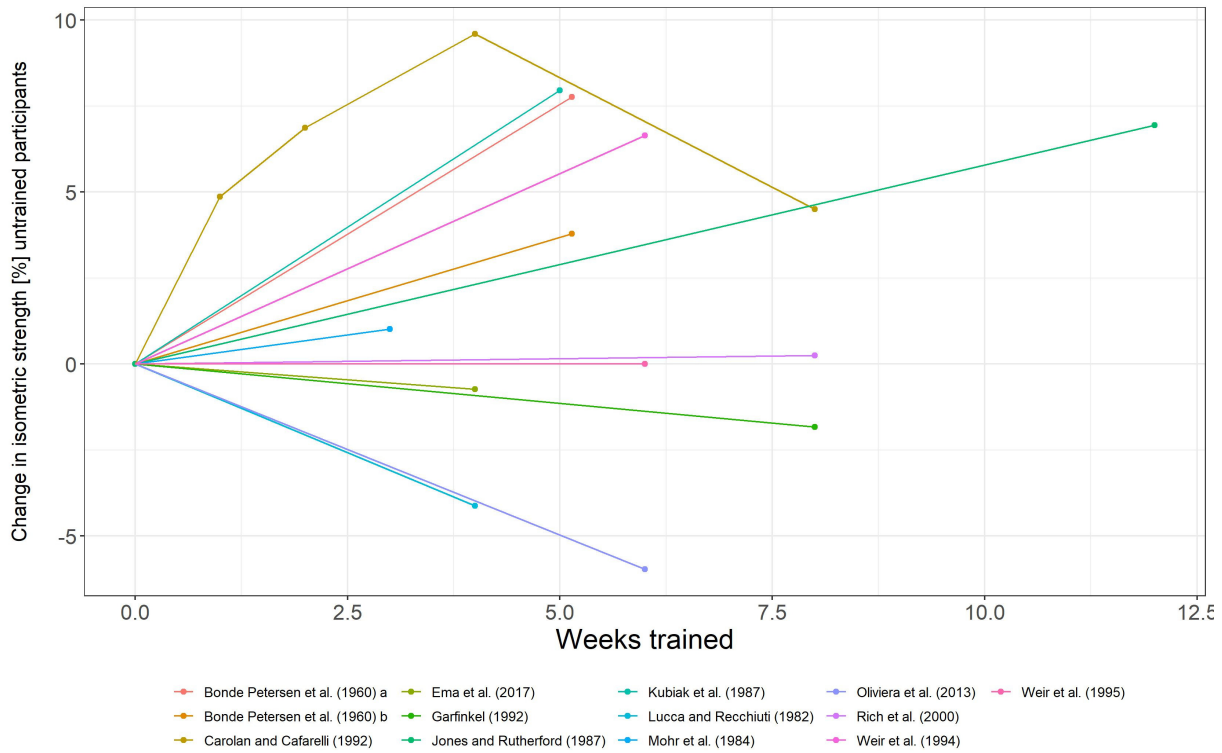
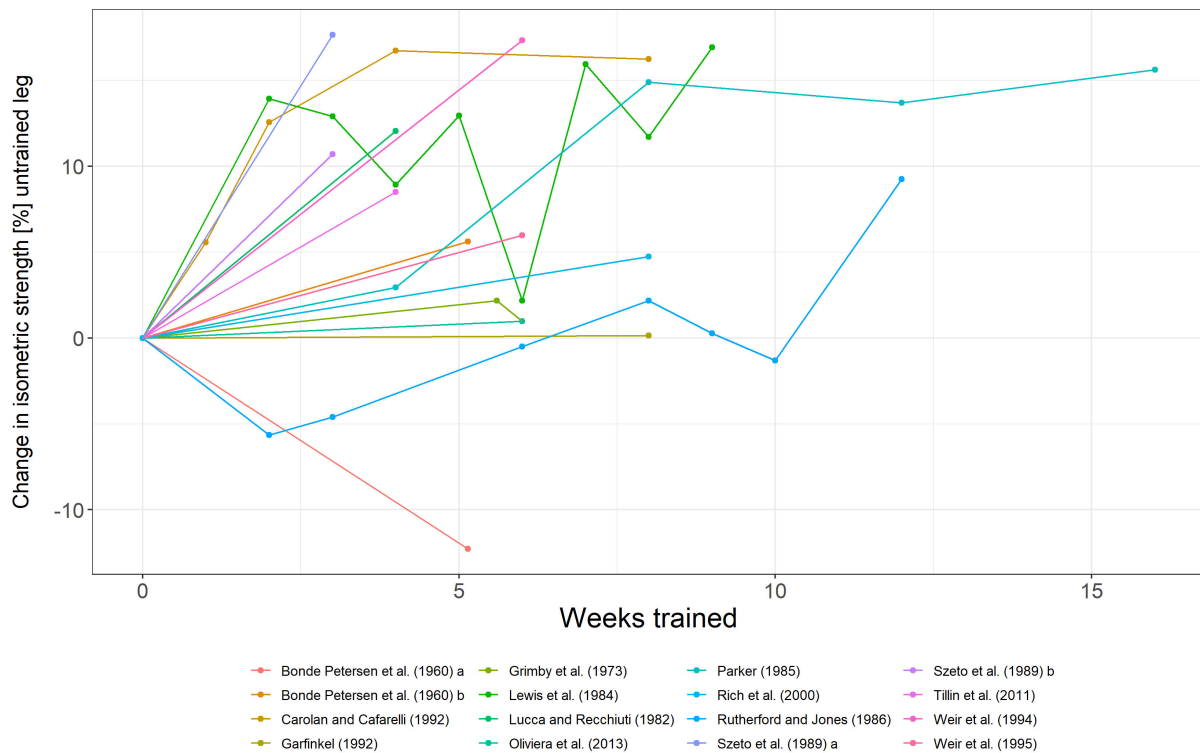


**Figure B.2:** Spaghetti plot of the data on EMG over time in weeks obtained from [46, 81, 110, 263, 306, 319, 320]. Here R: rectus femoris, LL: left limb, RL: right limb and M: vastus medialis. Where not specified, data were obtained from vastus lateralis muscle.

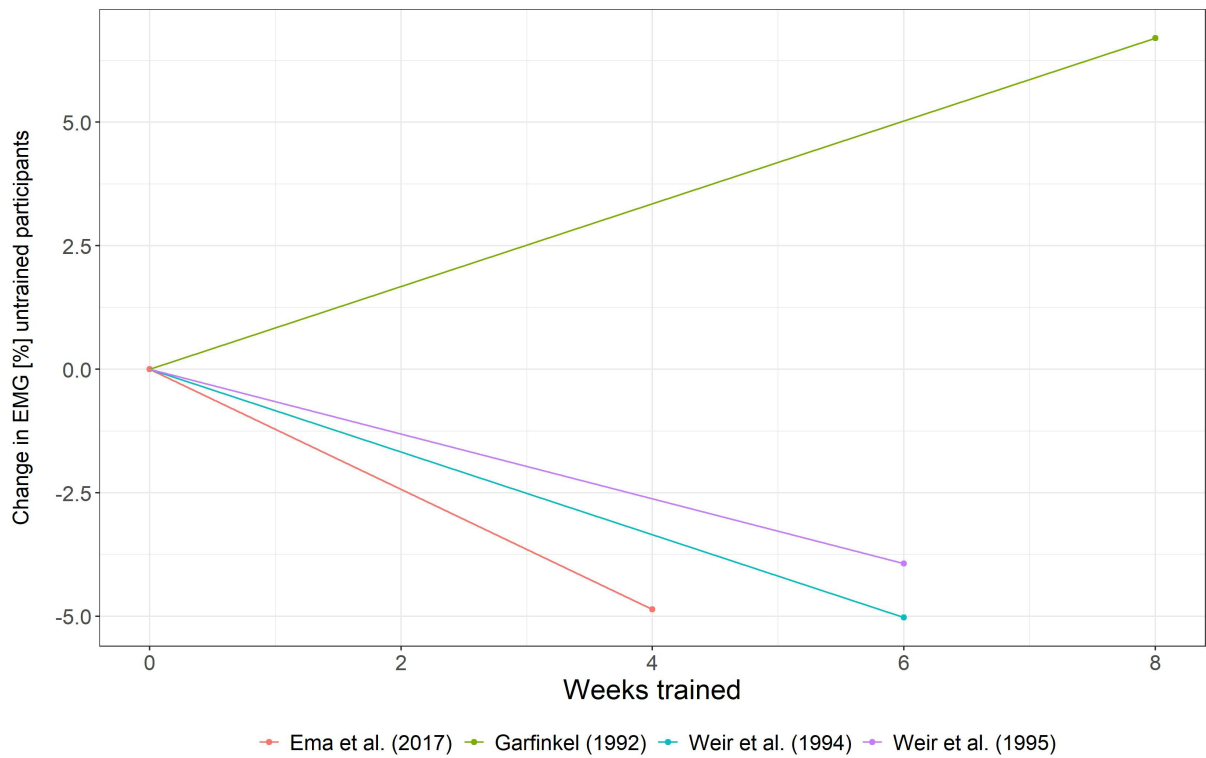


(a) Control group data for change in isometric strength.

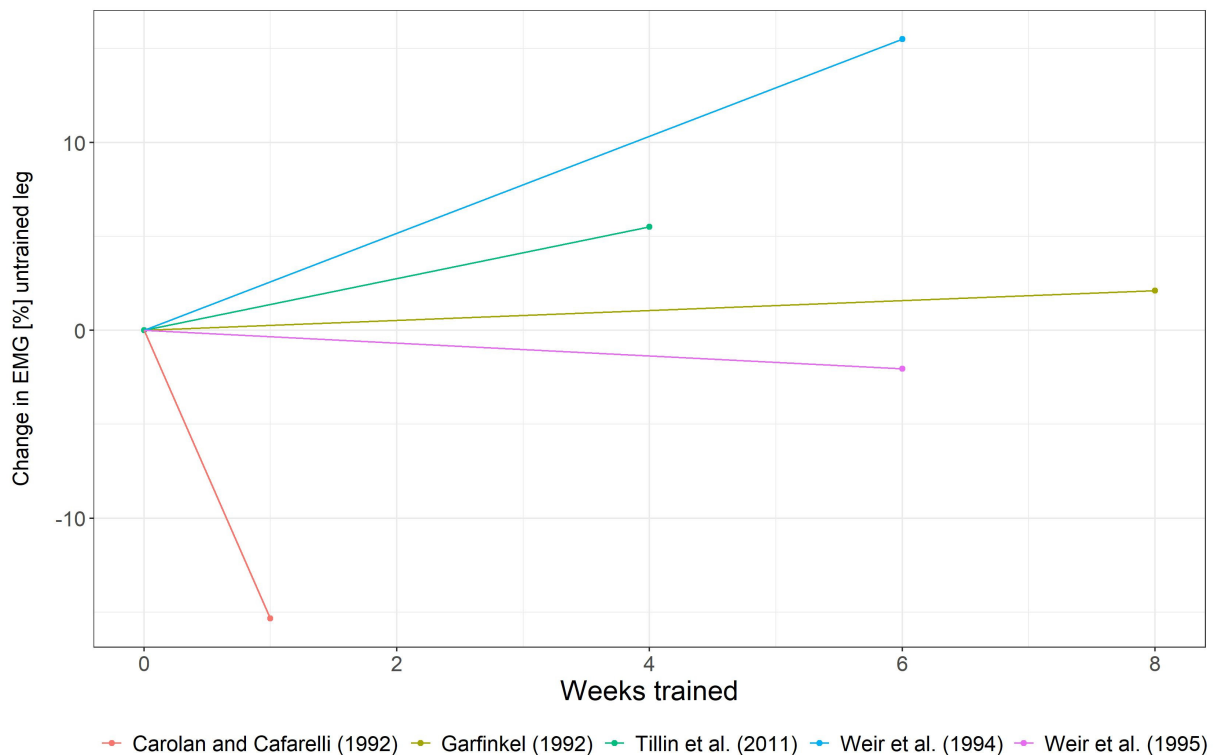


(b) Untrained leg data for change in isometric strength.

Figure B.3: Change in isometric strength for the control group and untrained leg data.



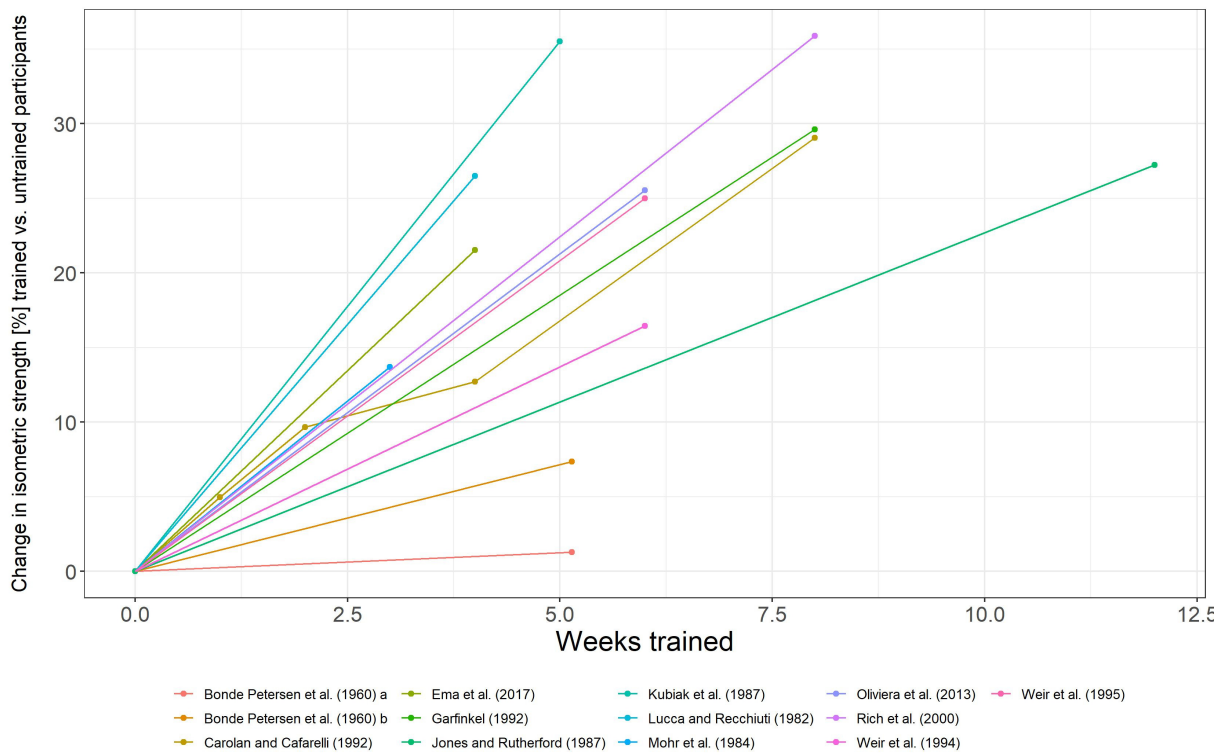
(a) Control group data for change in EMG.



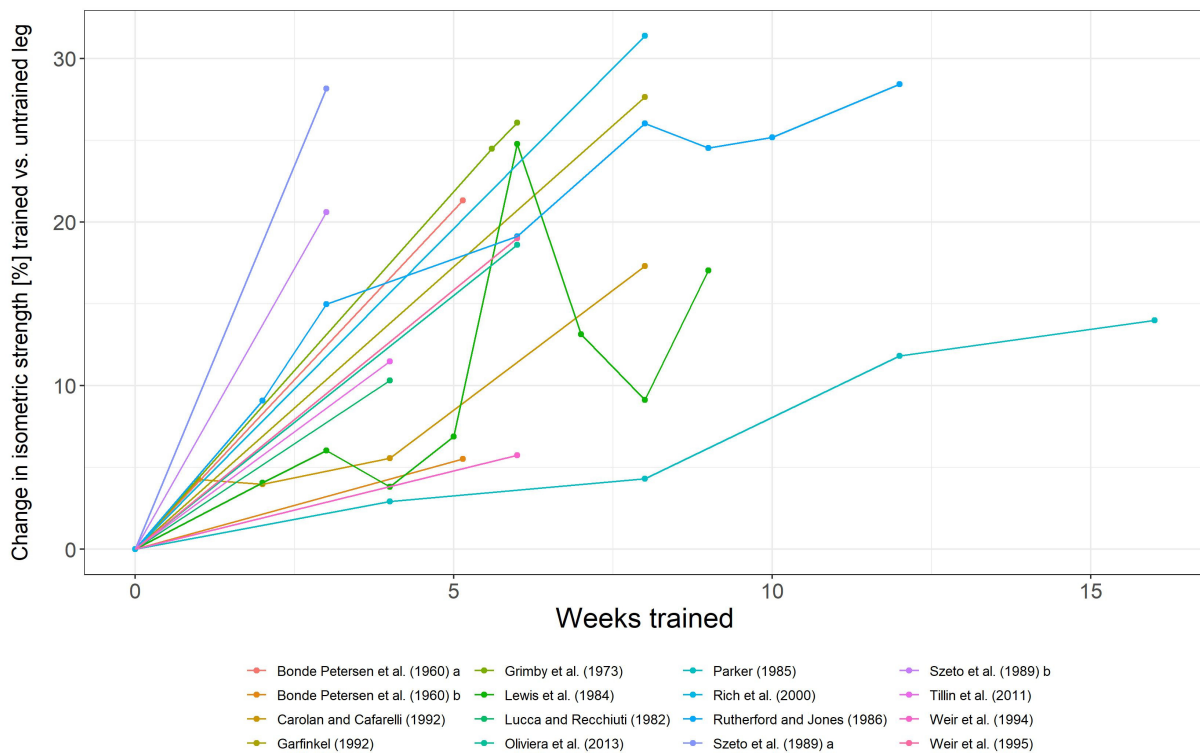
(b) Untrained leg data for change in EMG.

**Figure B.4:** Change in EMG for the control group and untrained leg data.



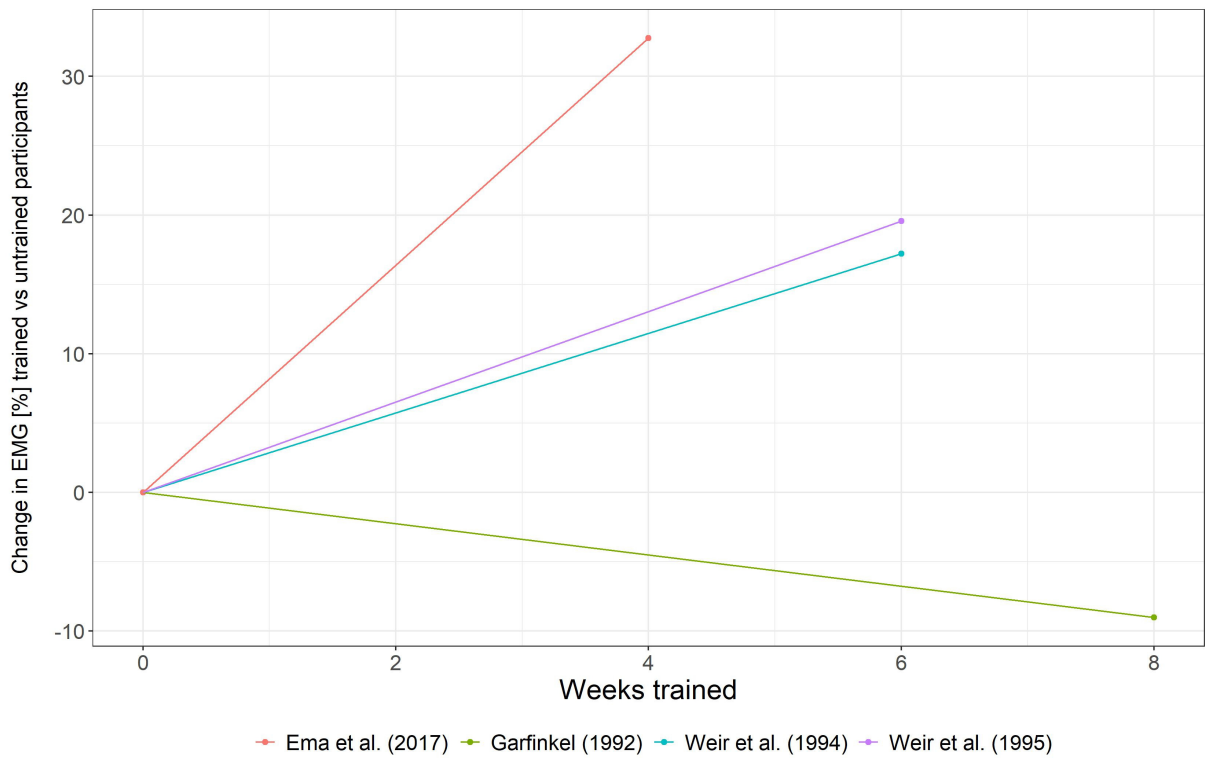


(a) Difference between the change in isometric strength for the trained leg and the control group.

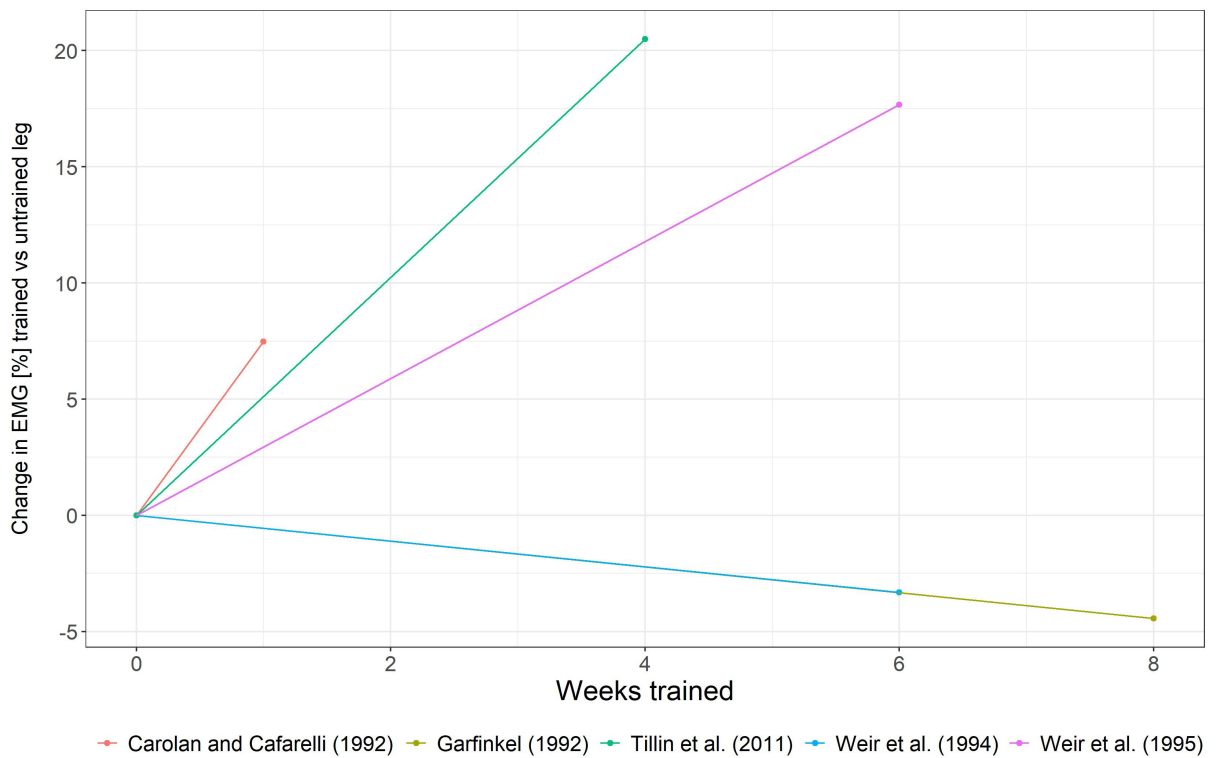


(b) Difference between the change in isometric strength for the trained leg and the untrained leg.

**Figure B.5:** Difference between the change in isometric strength for the control group and untrained leg data.



(a) Difference between the change in EMG for the trained leg and the control group.



(b) Difference between the change in EMG for the trained leg and the untrained leg.

**Figure B.6:** Difference between the change in EMG for the control group and untrained leg data.

### B.5.2 Forest plots

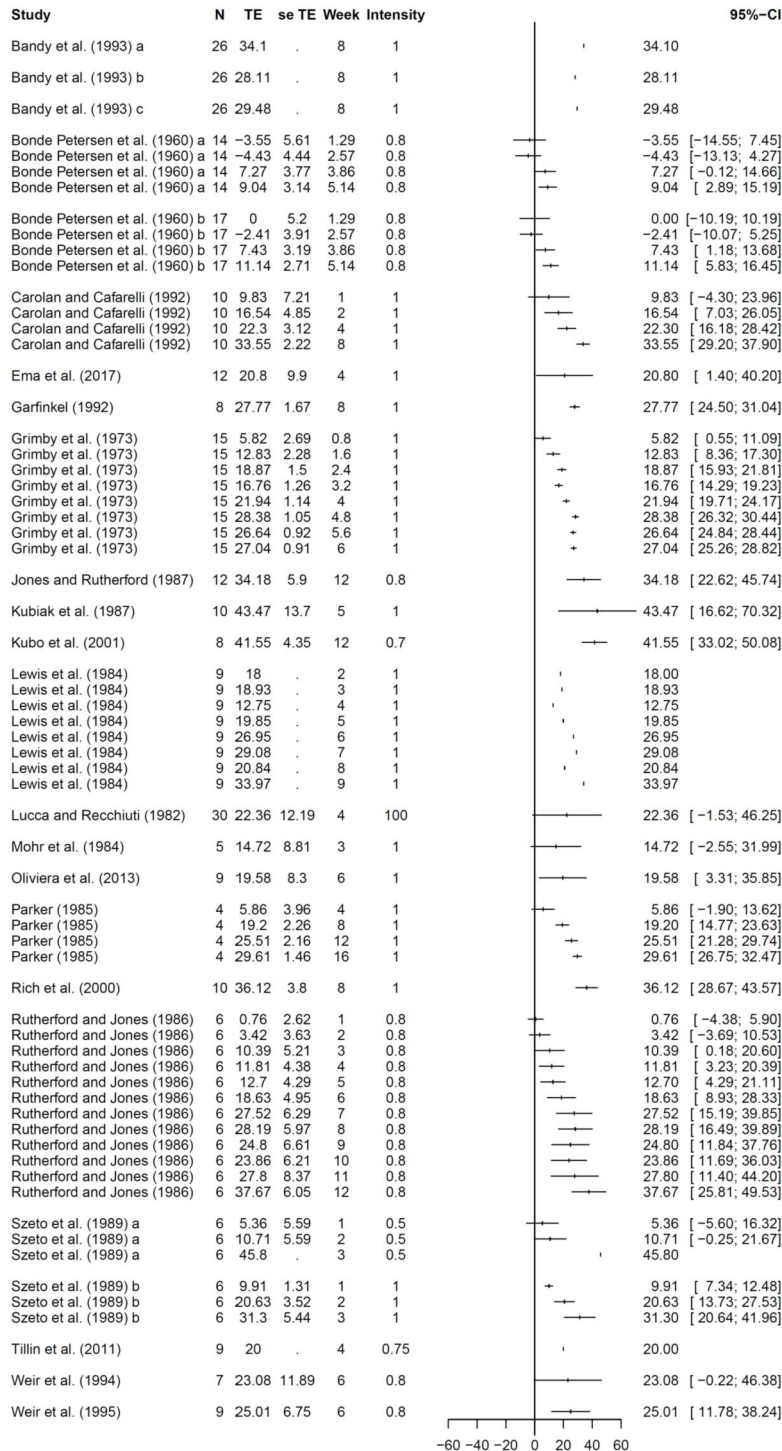
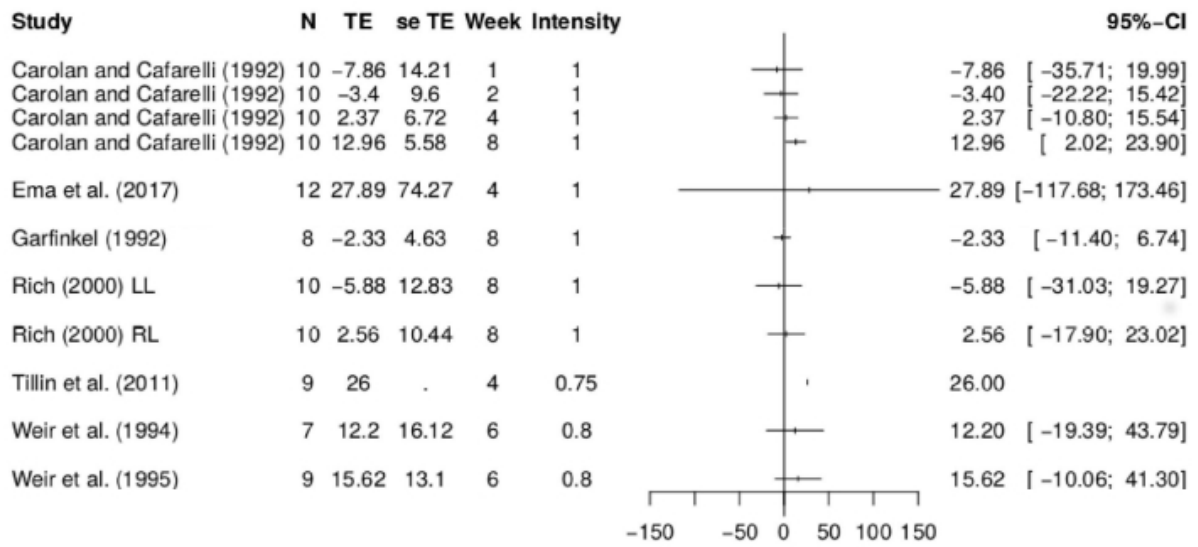
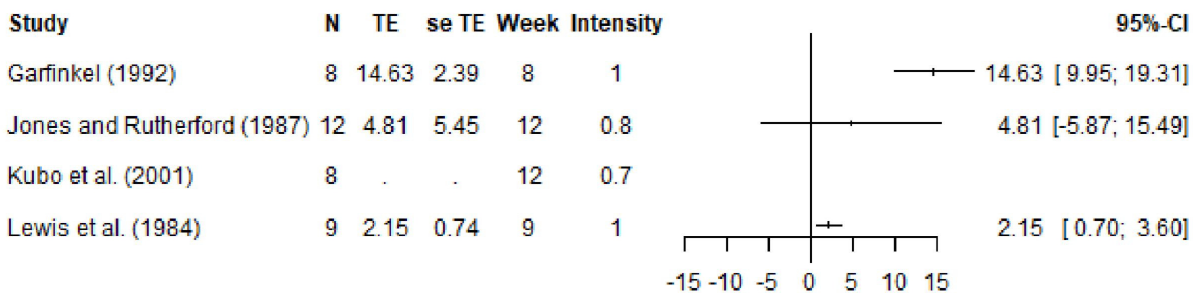


**Figure B.7:** Forest plot of the data on change in isometric strength. Here N denotes the number of subjects, TE and se TE denote the mean and standard deviation of the treatment effect, week denotes the time point and intensity denotes the training intensity. A training intensity of 1 corresponds to 100% MVC.



(a) Forest plot for the data on EMG.



(b) Forest plot for the data on volumetric changes.

**Figure B.8:** Forest plots for the data on EMG and volumetric changes. Here N denotes the number of subjects, TE and se TE denote the mean and standard deviation of the treatment effect, week denotes the time point and intensity denotes the training intensity. A training intensity of 1 corresponds to 100% MVC.



# Bibliography

- [1] Aagaard, P.: Training-induced changes in neural function. *Exercise and sport sciences reviews* **31** (2003), 61–67.
- [2] Aagaard, P.; Andersen, J. L.; Dyhre-Poulsen, P.; Leffers, A.-M.; Wagner, A.; Magnusson, S. P.; Halkjor-Kristensen, J. & Simonsen, E. B.: A mechanism for increased contractile strength of human pennate muscle in response to strength training: changes in muscle architecture. *The Journal of Physiology* **534** (2001), 613–623, URL <https://physoc.onlinelibrary.wiley.com/doi/abs/10.1111/j.1469-7793.2001.t01-1-00613.x>.
- [3] Abraham, R. J.; See, L. M. & Solomatine, D. P. (eds.): *Data-Driven Modelling: Concepts, Approaches and Experiences*, Springer Berlin Heidelberg, Berlin, Heidelberg 2008. pp. 17–30.
- [4] Ahtiainen, J. P.; Walker, S.; Peltonen, H.; Holviala, J.; Sillanpää, E.; Karavirta, L.; Sallinen, J.; Mikkola, J.; Valkeinen, H.; Mero, A.; Hulmi, J. J. & Häkkinen, K.: Heterogeneity in resistance training-induced muscle strength and mass responses in men and women of different ages. *Age* **38** (2016), 10.
- [5] Allen, T. J.; Jones, T.; Tsay, A.; Morgan, D. L. & Proske, U.: Muscle damage produced by isometric contractions in human elbow flexors. *Journal of Applied Physiology* (2017).
- [6] Alway, S. E.; MacDougall, J. D. & Sale, D. G.: Contractile adaptations in the human triceps surae after isometric exercise. *Journal of Applied Physiology* **66** (1989), 2725–2732, ISSN 8750-7587, URL <http://jap.physiology.org/content/66/6/2725>.
- [7] Andreassen, S. & Arendt-Nielsen, L.: Muscle fibre conduction velocity in motor units of the human anterior tibial muscle: a new size principle parameter. *The Journal of Physiology* **391** (1987), 561–571.
- [8] Arabadzhev, T. I.; Dimitrov, V. G. & Dimitrov, G. V.: The increase in surface emg could be a misleading measure of neural adaptation during the early gains in strength. *European Journal of Applied Physiology* **114** (2014), 1645–1655.
- [9] Armitage, P.; Berry, G. & Matthews, J. N. S.: *Statistical methods in medical research*. John Wiley & Sons 2002.
- [10] Aromataris, E. & Pearson, A.: The systematic review: an overview. *The American Journal of Nursing* **114** (2014), 53–58.
- [11] Balduzzi, S.; Rcker, G. & Schwarzer, G.: How to perform a meta-analysis with R: a practical tutorial. *Evidence-Based Mental Health* (2019).

- [12] Balshaw, T. G.; Massey, G. J.; Maden-Wilkinson, T. M.; Morales-Artacho, A. J.; McKeown, A.; Appleby, C. L. & Folland, J. P.: Changes in agonist neural drive, hypertrophy and pre-training strength all contribute to the individual strength gains after resistance training. *European Journal of Applied Physiology* (2017), 1–10.
- [13] Balshaw, T. G.; Massey, G. J.; Maden-Wilkinson, T. M.; Tillin, N. A. & Folland, J. P.: Training-specific functional, neural, and hypertrophic adaptations to explosive-vs. sustained-contraction strength training. *Journal of Applied Physiology* **120** (2016), 1364–1373.
- [14] Bandy, W. D. & Hanten, W. P.: Changes in torque and electromyographic activity of the quadriceps femoris muscles following isometric training. *Physical Therapy* **73** (1993), 455–465.
- [15] Barnouin, Y.; Butler-Browne, G.; Voit, T.; Reversat, D.; Azzabou, N.; Leroux, G.; Behin, A.; McPhee, J. S.; Carlier, P. G. & Hogrel, J.-Y.: Manual segmentation of individual muscles of the quadriceps femoris using mri: A reappraisal. *Journal of Magnetic Resonance Imaging* **40** (2014), 239–247.
- [16] Baskan, E.; Cavlak, U. & Yildiz, H. H.: Comparison of electrical stimulation and isometric training on isokinetic strength of knee extensors a randomized clinical trial. *Pakistan Journal of Medical Sciences* (2011).
- [17] Baudry, S.; Klass, M. & Duchateau, J.: Postactivation potentiation influences differently the nonlinear summation of contractions in young and elderly adults. *Journal of Applied Physiology* **98** (2005), 1243–1250.
- [18] Bawa, P.: Neural control of motor output: can training change it? *Exercise and sport sciences reviews* **30** (2002), 59–63.
- [19] Behm, D. G. & Sale, D. G.: Intended rather than actual movement velocity determines velocity-specific training response. *Journal of Applied Physiology* **74** (1993), 359–368.
- [20] Beisbart, C. & Saam, N. J.: *Computer Simulation Validation: Fundamental Concepts, Methodological Frameworks, and Philosophical Perspectives*. Springer 2018.
- [21] Bellhouse, D. R.: The reverend thomas bayes, frs: A biography to celebrate the tercentenary of his birth. *Statistical Science* **19** (2004), 3–43.
- [22] Benton, M. J.; Raab, S. & Waggener, G. T.: Effect of training status on reliability of one repetition maximum testing in women. *The Journal of Strength & Conditioning Research* **27** (2013), 1885–1890.
- [23] Bertorini, T. E.: *Neuromuscular Case Studies E-Book*. Elsevier Health Sciences 2008.
- [24] Bigland-Ritchie, B.; Furbush, F. & Woods, J. J.: Fatigue of intermittent sub-maximal voluntary contractions: central and peripheral factors. *Journal of Applied Physiology* **61** (1986), 421–429.

- [25] Blemker, S. S.; Pinsky, P. M. & Delp, S. L.: A 3d model of muscle reveals the causes of nonuniform strains in the biceps brachii. *Journal of Biomechanics* **38** (2005), 657–665.
- [26] Blijham, P. J.; Ter Laak, H. J.; Schelhaas, H. J.; Van Engelen, B.; Stegeman, D. F. & Zwarts, M. J.: Relation between muscle fiber conduction velocity and fiber size in neuromuscular disorders. *Journal of Applied Physiology* **100** (2006), 1837–1841.
- [27] Bohm, S.; Mersmann, F. & Arampatzis, A.: Human tendon adaptation in response to mechanical loading: a systematic review and meta-analysis of exercise intervention studies on healthy adults. *Sports Medicine - Open* **1** (2015), 7.
- [28] Böl, M.; Iyer, R.; Dittmann, J.; Garcés-Schröder, M. & Dietzel, A.: Investigating the passive mechanical behaviour of skeletal muscle fibres: Micromechanical experiments and bayesian hierarchical modelling. *Acta Biomaterialia* (2019).
- [29] Böl, M.; Weikert, R. & Weichert, C.: A coupled electromechanical model for the excitation-dependent contraction of skeletal muscle. *Journal of the mechanical behavior of biomedical materials* **4** (2011), 1299–1310.
- [30] Bonde Petersen, F.: Muscle training by static, concentric and eccentric contractions. *Acta Physiologica Scandinavica* **48** (1960), 406–416.
- [31] Borenstein, M.; Hedges, L. V.; Higgins, J. P. & Rothstein, H. R.: *Introduction to meta-analysis*. John Wiley & Sons 2011.
- [32] Boucher, M. & Bennetts, M.: The many flavors of model-based meta-analysis: Part i introduction and landmark data. *CPT: Pharmacometrics & Systems Pharmacology* **5** (2016), 54–64.
- [33] Boucher, M. & Bennetts, M.: Many flavors of model-based meta-analysis: Part ii—modeling summary level longitudinal responses. *CPT: pharmacometrics & systems pharmacology* **7** (2018), 288–297.
- [34] Bronshtein, I. N. & Semendyayev, K. A.: *Handbook of Mathematics*. Springer Science & Business Media 2007.
- [35] Buchthal, F. & Schmalbruch, H.: Contraction times and fibre types in intact human muscle. *Acta Physiologica Scandinavica* **79** (1970), 435–452.
- [36] Burden, R. L. & Faires, J. D.: *Numerical analysis*. Brooks/Cole 2011, 9 edn.
- [37] Burgess, K. E.; Connick, M. J.; Graham-Smith, P. & Pearson, S. J.: Plyometric vs. isometric training influences on tendon properties and muscle output. *The Journal of Strength & Conditioning Research* **21** (2007), 986–989.
- [38] Burke, R.; Levine, D.; Tsairis, P. & Zajac, F.: Physiological types and histochemical profiles in motor units of the cat gastrocnemius. *The Journal of physiology* **234** (1973), 723–748.



- [39] Burke, R. & Tsairis, P.: The correlation of physiological properties with histochemical characteristics in single muscle units. *Annals of the New York Academy of Sciences* **228** (1974), 145–158.
- [40] Burke, R. E.: *Motor Units: Anatomy, Physiology, and Functional Organization*, American Cancer Society 2011. pp. 345–422.
- [41] Burke, R. E.; Rudomin, P. & Zajac, F. E.: The effect of activation history on tension production by individual muscle units. *Brain research* **109** (1976), 515–529.
- [42] Cannon, J.; Kay, D.; Tarpinning, K. M. & Marino, F. E.: Comparative effects of resistance training on peak isometric torque, muscle hypertrophy, voluntary activation and surface emg between young and elderly women. *Clinical physiology and functional imaging* **27** (2007), 91–100.
- [43] Cannon, R. J. & Cafarelli, E.: Neuromuscular adaptations to training. *Journal of Applied Physiology* **63** (1987), 2396–2402.
- [44] Carlson, B. M.: Chapter 5 - the muscular system. In Carlson, B. M. (ed.): *The Human Body*. Academic Press 2019, ISBN 978-0-12-804254-0, pp. 111 – 136, URL <http://www.sciencedirect.com/science/article/pii/B9780128042540000053>.
- [45] Carlson, D. J.; Dieberg, G.; Hess, N. C.; Millar, P. J. & Smart, N. A.: Isometric exercise training for blood pressure management: A systematic review and meta-analysis. *Mayo Clinic Proceedings* **89** (2014), 327 – 334, ISSN 0025-6196.
- [46] Carolan, B. & Cafarelli, E.: Adaptations in coactivation after isometric resistance training. *Journal of Applied Physiology* **73** (1992), 911–917.
- [47] Carroll, T. J.; Riek, S. & Carson, R. G.: The sites of neural adaptation induced by resistance training in humans. *The Journal of Physiology* **544** (2002), 641–652, ISSN 1469-7793, URL <http://dx.doi.org/10.1113/jphysiol.2002.024463>.
- [48] Carroll, T. J.; Selvanayagam, V. S.; Riek, S. & Semmler, J. G.: Neural adaptations to strength training: Moving beyond transcranial magnetic stimulation and reflex studies. *Acta Physiologica* **202** (2011), 119–140.
- [49] Chalmers, I.; Hedges, L. V. & Cooper, H.: A brief history of research synthesis. *Evaluation & the Health Professions* **25** (2002), 12–37.
- [50] Chan, K. M.; Doherty, T. J. & Brown, W. F.: Contractile properties of human motor units in health, aging, and disease. *Muscle & Nerve* **24** (2001), 1113–1133.
- [51] Christakos, C. N.: A study of the muscle force waveform using a population stochastic model of skeletal muscle. *Biological Cybernetics* **44** (1982), 91–106, ISSN 1432-0770, URL <https://doi.org/10.1007/BF00317969>.
- [52] Cisi, R. R. L. & Kohn, A. F.: Simulation system of spinal cord motor nuclei and associated nerves and muscles, in a web-based architecture. *Journal of Computational Neuroscience* **25** (2008), 520–542.

- [53] Clark, D.: Muscle counts of motor units: a study in innervation ratios. *American Journal of Physiology-Legacy Content* **96** (1931), 296–304.
- [54] Coleman, A. E.: Effect of unilateral isometric and isotonic contractions on the strength of the contralateral limb. *Research Quarterly. American Association for Health, Physical Education and Recreation* **40** (1969), 490–495.
- [55] Colson, S. S.; Martin, A. & Hoecke, J. V.: Effects of electromyostimulation versus voluntary isometric training on elbow flexor muscle strength. *Journal of Electromyography and Kinesiology* **19** (2009), e311 – e319, ISSN 1050-6411.
- [56] Contessa, P.; Nawab, S. H. & Luca, C. J. D.: A model of motoneuron behavior and muscle-force generation for sustained isometric contractions. In *2011 Annual International Conference of the IEEE Engineering in Medicine and Biology Society*, 2011, ISSN 1094-687X, pp. 4072–4075.
- [57] Daley, M. J. & Spinks, W. L.: Exercise, mobility and aging. *Sports medicine* **29** (2000), 1–12.
- [58] Damas, F.; Libardi, C. A. & Ugrinowitsch, C.: The development of skeletal muscle hypertrophy through resistance training: the role of muscle damage and muscle protein synthesis. *European Journal of Applied Physiology* (2017).
- [59] Darcus, H. D. & Salter, N.: The effect of repeated muscular exertion on muscle strength. *The Journal of Physiology* **129** (1955), 325.
- [60] Davies, J.; Parker, D. F.; Rutherford, O. M. & Jones, D. A.: Changes in strength and cross sectional area of the elbow flexors as a result of isometric strength training. *European Journal of Applied Physiology and Occupational Physiology* **57** (1988), 667–670.
- [61] De Luca, C. J.; Adam, A.; Wotiz, R.; Gilmore, L. D. & Nawab, S. H.: Decomposition of surface emg signals. *Journal of Neurophysiology* **96** (2006), 1646–1657.
- [62] De Luca, C. J. & Erim, Z.: Common drive of motor units in regulation of muscle force. *Trends in neurosciences* **17** (1994), 299–305.
- [63] De Luca, C. J. & Hostage, E. C.: Relationship between firing rate and recruitment threshold of motoneurons in voluntary isometric contractions. *Journal of Neurophysiology* **104** (2010), 1034–1046.
- [64] Deeks, J. J. & Altman, D. G.: *Effect Measures for MetaAnalysis of Trials with Binary Outcomes*, John Wiley & Sons, Ltd 2008, chap. 16. ISBN 9780470693926, pp. 313–335, URL <https://onlinelibrary.wiley.com/doi/abs/10.1002/9780470693926.ch16>.
- [65] Del Balso, C. & Cafarelli, E.: Adaptations in the activation of human skeletal muscle induced by short-term isometric resistance training. *Journal of Applied Physiology* **103** (2007), 402–411.

- [66] Del Vecchio, A.; Casolo, A.; Negro, F.; Scorcelletti, M.; Bazzucchi, I.; Enoka, R.; Felici, F. & Farina, D.: The increase in muscle force after 4 weeks of strength training is mediated by adaptations in motor unit recruitment and rate coding. *The Journal of Physiology* (2019).
- [67] Del Vecchio, A.; Negro, F.; Felici, F. & Farina, D.: Distribution of muscle fibre conduction velocity for representative samples of motor units in the full recruitment range of the tibialis anterior muscle. *Acta Physiologica* **222** (2018), e12930, URL <https://onlinelibrary.wiley.com/doi/abs/10.1111/apha.12930>.
- [68] Denny-Brown, D.: Interpretation of the electromyogram. *Archives of Neurology & Psychiatry* **61** (1949), 99–128.
- [69] Denny-Brown, D. & Pennybacker, J.: Fibrillation and fasciculation in voluntary muscle. *Brain* **61** (1938), 311–312.
- [70] Desmedt, J. & Godaux, E.: Fast motor units are not preferentially activated in rapid voluntary contractions in man. *Nature* **267** (1977), 717.
- [71] Devasahayam, S. R.: *Signals and systems in biomedical engineering: signal processing and physiological systems modeling*. Springer Science & Business Media 2012.
- [72] Dideriksen, J. L. & Negro, F.: Spike-triggered averaging provides inaccurate estimates of motor unit twitch properties under optimal conditions. *Journal of Electromyography and Kinesiology* **43** (2018), 104–110.
- [73] Doll, J. C. & Jacquemin, S. J.: Introduction to bayesian modeling and inference for fisheries scientists. *Fisheries* **43** (2018), 152–161.
- [74] Donnelly, J. E. & Smith, B. K.: Is exercise effective for weight loss with ad libitum diet? energy balance, compensation, and gender differences. *Exercise and sport sciences reviews* **33** (2005), 169–174.
- [75] Driss, T.; Serrau, V.; Behm, D. G.; Lesne-Chabran, E.; Le Pellec-Muller, A. & Vandewalle, H.: Isometric training with maximal co-contraction instruction does not increase co-activation during exercises against external resistances. *Journal of sports sciences* **32** (2014), 60–69.
- [76] Duchateau, J. & Hainaut, K.: Isometric or dynamic training: differential effects on mechanical properties of a human muscle. *Journal of Applied Physiology* **56** (1984), 296–301.
- [77] Duchateau, J.; Semmler, J. G. & Enoka, R. M.: Training adaptations in the behavior of human motor units. *Journal of Applied Physiology* **101** (2006), 1766–1775.
- [78] Ebersole, K. T.; Housh, T. J.; Johnson, G. Q.; Perry, S. R.; Bull, A. J. & Cramer, J. T.: Mechanomyographic and electromyographic responses to unilateral isometric training. *The Journal of Strength & Conditioning Research* **16** (2002), 192–201.

- [79] Ehret, A. E.; Bl, M. & Itskov, M.: A continuum constitutive model for the active behaviour of skeletal muscle. *Journal of the Mechanics and Physics of Solids* **59** (2011), 625 – 636, ISSN 0022-5096, URL <http://www.sciencedirect.com/science/article/pii/S0022509610002486>.
- [80] Elias, J. J.; Bratton, D. R.; Weinstein, D. M. & Cosgarea, A. J.: Comparing two estimations of the quadriceps force distribution for use during patellofemoral simulation. *Journal of biomechanics* **39** (2006), 865–872.
- [81] Ema, R.; Saito, I. & Akagi, R.: Neuromuscular adaptations induced by adjacent joint training. *Scandinavian Journal of Medicine & Science in Sports* **28** (2017), 947–960.
- [82] Enoka, R. M.: Muscle strength and its development. *Sports Medicine* **6** (1988), 146–168.
- [83] Enoka, R. M.: Morphological features and activation patterns of motor units. *Journal of Clinical Neurophysiology* **12** (1995), 538–559.
- [84] Enoka, R. M.: Neural adaptations with chronic physical activity. *Journal of Biomechanics* **30** (1997), 447 – 455.
- [85] Enoka, R. M.: *Neuromechanics of human movement*. Human kinetics 2015.
- [86] Enoka, R. M.; Christou, E. A.; Hunter, S. K.; Kornatz, K. W.; Semmler, J. G.; Taylor, A. M. & Tracy, B. L.: Mechanisms that contribute to differences in motor performance between young and old adults. *Journal of Electromyography and Kinesiology* **13** (2003), 1 – 12.
- [87] Enoka, R. M. & Duchateau, J.: Inappropriate interpretation of surface emg signals and muscle fiber characteristics impedes understanding of the control of neuromuscular function. *Journal of Applied Physiology* **119** (2015), 1516–1518.
- [88] Enoka, R. M. & Fuglevand, A. J.: Motor unit physiology: some unresolved issues. *Muscle & nerve* **24** (2001), 4–17.
- [89] Enoka, R. M. & Gandevia, S. C.: Editorial. *Journal of Applied Physiology* **101** (2006), 1009–1010.
- [90] Etz, A. & Vandekerckhove, J.: Introduction to bayesian inference for psychology. *Psychonomic Bulletin & Review* **25** (2018), 5–34.
- [91] Farina, D.; Arendt-Nielsen, L. & Graven-Nielsen, T.: Effect of temperature on spike-triggered average torque and electrophysiological properties of low-threshold motor units. *Journal of Applied Physiology* **99** (2005), 197–203.
- [92] Farina, D.; Arendt-Nielsen, L.; Roatta, S. & Graven-Nielsen, T.: The pain-induced decrease in low-threshold motor unit discharge rate is not associated with the amount of increase in spike-triggered average torque. *Clinical Neurophysiology* **119** (2008), 43 – 51.

- [93] Farina, D.; Fosci, M. & Merletti, R.: Motor unit recruitment strategies investigated by surface emg variables. *Journal of applied physiology* **92** (2002), 235–247.
- [94] Farina, D.; Holobar, A.; Merletti, R. & Enoka, R. M.: Decoding the neural drive to muscles from the surface electromyogram. *Clinical Neurophysiology* **121** (2010), 1616 – 1623.
- [95] Farina, D.; Merletti, R. & Enoka, R. M.: The extraction of neural strategies from the surface emg. *Journal of applied physiology* **96** (2004), 1486–1495.
- [96] Farina, D.; Negro, F.; Gazzoni, M. & Enoka, R. M.: Detecting the unique representation of motor-unit action potentials in the surface electromyogram. *Journal of Neurophysiology* **100** (2008), 1223–1233.
- [97] Farina, D.; Negro, F.; Muceli, S. & Enoka, R. M.: Principles of motor unit physiology evolve with advances in technology. *Physiology* **31** (2016), 83–94.
- [98] Felici, F.: Chapter 14: Applications in exercise physiology. In *Electromyography: Physiology, Engineering and Non-Invasive Applications*. 2004.
- [99] Felici, F.: Neuromuscular responses to exercise investigated through surface emg. *Journal of Electromyography and Kinesiology* **16** (2006), 578 – 585, ISSN 1050-6411, URL <http://www.sciencedirect.com/science/article/pii/S1050641106001039>, special Section (pp. 541610): 2006 ISEK Congress.
- [100] Fisher, T.: *Compensatory acceleration training and size principle* (2014 (retrieved on: July 3, 2019)), <https://tdfathletics.wordpress.com/2014/09/20/compensatory-acceleration-training-and-the-size-principle/>.
- [101] Folland, J.; Leach, B.; Little, T.; Hawker, K.; Myerson, S.; Montgomery, H. & Jones, D.: Angiotensin-converting enzyme genotype affects the response of human skeletal muscle to functional overload. *Experimental Physiology* **85** (2000), 575–579.
- [102] Folland, J. P.; Hawker, K.; Leach, B.; Little, T. & Jones, D. A.: Strength training: Isometric training at a range of joint angles versus dynamic training. *Journal of Sports Sciences* **23** (2005), 817–824.
- [103] Fry, A.; Kraemer, W.; van Borselen, F.; Lynch, J.; Marsit, J.; Roy, E.; Triplett, N. & Knuttgen, H.: Performance decrements with high-intensity resistance exercise overtraining. *Medicine and Science in Sports and Exercise* **26** (1994), 1165–1173.
- [104] Fuglevand, A. J.; Winter, D. A. & Patla, A. E.: Models of recruitment and rate coding organization in motor-unit pools. *Journal of Neurophysiology* **70** (1993), 2470–2488.
- [105] Gagn, F.: Chapter 2 - tissue preparation and subcellular fractionation techniques. In Gagn, F. (ed.): *Biochemical Ecotoxicology*. Academic Press, Oxford 2014, ISBN 978-0-12-411604-7, pp. 21 – 31, URL <http://www.sciencedirect.com/science/article/pii/B9780124116047000027>.

- [106] Gandevia, S.; Allen, G. & McKenzie, D.: Central fatigue. In *Fatigue*, Springer 1995, pp. 281–294.
- [107] Gardiner, P.; Beaumont, E. & Cormery, B.: Motoneurons” learn” and” forget” physical activity. *Canadian journal of applied physiology* **30** (2005), 352–370.
- [108] Gardiner, P.; Dai, Y. & Heckman, C. J.: Effects of exercise training on *alpha*-motoneurons. *Journal of Applied Physiology* **101** (2006), 1228–1236.
- [109] Gardiner, P. F.: Changes in *alpha*-motoneuron properties with altered physical activity levels. *Exercise and sport sciences reviews* **34** (2006), 54–58.
- [110] Garfinkel, S. & Cafarelli, E.: Relative changes in maximal force, emg, and muscle cross-sectional area after isometric training. *Medicine and science in sports and exercise* **24** (1992), 1220–1227.
- [111] Gelman, A. & Rubin, D. B.: Inference from iterative simulation using multiple sequences. *Statist. Sci.* **7** (1992), 457–472.
- [112] Gilmore, K. J.; Kirk, E. A.; Doherty, T. J. & Rice, C. L.: Effect of very old age on anconeus motor unit loss and compensatory remodelling. *Muscle & Nerve* **57** (2018), 659–663.
- [113] Göktepe, S.; Menzel, A. & Kuhl, E.: The generalized hill model: A kinematic approach towards active muscle contraction. *Journal of the Mechanics and Physics of Solids* **72** (2014), 20–39.
- [114] Gossen, E. R.; Ivanova, T. D. & Garland, S. J.: The time course of the motoneurone afterhyperpolarization is related to motor unit twitch speed in human skeletal muscle. *The Journal of physiology* **552** (2003), 657–664.
- [115] Gray, H.: *Anatomy of the human body*. Philadelphia: Lea & Febiger 1918, 20 edn., retrieved from [www.bartleby.com/107/](http://www.bartleby.com/107/), on 10/07/2019.
- [116] Greig, C.; Young, A.; Skelton, D.; Pippet, E.; Butler, F. & Mahmud, S.: Exercise studies with elderly volunteers. *Age and ageing* **23** (1994), 185–189.
- [117] Griffin, L. & Cafarelli, E.: Resistance training: cortical, spinal, and motor unit adaptations. *Canadian Journal of Applied Physiology* **30** (2005), 328–340.
- [118] Grimby, G.; Bjorntorp, P.; Fahlen, M.; Hoskins, T. A.; Hook, O.; Oxhoj, H. & Saltin, H.: Metabolic effects of isometric training. *Scandinavian Journal of Clinical and Laboratory Investigation* **31** (1973), 301–305.
- [119] Günther, M.; Schmitt, S. & Wank, V.: High-frequency oscillations as a consequence of neglected serial damping in hill-type muscle models. *Biological Cybernetics* **97** (2007), 63–79, ISSN 1432-0770, URL <https://doi.org/10.1007/s00422-007-0160-6>.
- [120] Haase, S. C.: Systematic reviews and meta-analysis. *Plastic and reconstructive surgery* **127** (2011), 955–966.

- [121] Haffajee, D.; Moritz, U. & Svantesson, G.: Isometric knee extension strength as a function of joint angle, muscle length and motor unit activity. *Acta Orthopaedica Scandinavica* **43** (1972), 138–147.
- [122] Hakansson, C. H.: Conduction velocity and amplitude of the action potential as related to circumference in the isolated fibre of frog muscle. *Acta Physiologica Scandinavica* **37** (1956), 14–34.
- [123] Häkkinen, K.; Alen, M.; Kallinen, M.; Newton, U. R. & Kraemer, J. W.: Neuromuscular adaptation during prolonged strength training, detraining and re-strength-training in middle-aged and elderly people. *European Journal of Applied Physiology* **83** (2000), 51–62.
- [124] Hamilton, A. F. d. C.; Jones, K. E. & Wolpert, D. M.: The scaling of motor noise with muscle strength and motor unit number in humans. *Experimental Brain Research* **157** (2004), 417–430.
- [125] Handsfield, G. G.; Meyer, C. H.; Hart, J. M.; Abel, M. F. & Blemker, S. S.: Relationships of 35 lower limb muscles to height and body mass quantified using mri. *Journal of Biomechanics* **47** (2014), 631–638.
- [126] Hartsell, H. D.: Electrical muscle stimulation and isometric exercise effects on selected quadriceps parameters. *Journal of Orthopaedic & Sports Physical Therapy* **8** (1986), 203–209.
- [127] Hatze, H.: A myocybernetic control model of skeletal muscle. *Biological cybernetics* **25** (1977), 103–119.
- [128] Hatze, H.: A general myocybernetic control model of skeletal muscle. *Biological Cybernetics* **28** (1978), 143–157, ISSN 1432-0770, URL <https://doi.org/10.1007/BF00337136>.
- [129] Hatze, H.: The charge transfer model of myofilamentary interaction: prediction for force enhancement and related myodynamic phenomena. In Winters, J. M. & Woo, S. L. (eds.): *Multiple muscle systems: Biomechanics and movement organization*. Springer Science & Business Media 1990, chap. 2.
- [130] Heckman, C. J. & Binder, M. D.: Computer simulation of the steady-state input-output function of the cat medial gastrocnemius motoneuron pool. *Journal of Neurophysiology* **65** (1991), 952–967.
- [131] Heckman, C. J. & Enoka, R. M.: Motor unit. *Comprehensive Physiology* (2012).
- [132] Heidlauf, T. & Röhrle, O.: Modeling the chemoelectromechanical behavior of skeletal muscle using the parallel open-source software library opencmss. *Computational and Mathematical Methods in Medicine* **2013** (2013).
- [133] Heidlauf, T. & Röhrle, O.: A multiscale chemo-electro-mechanical skeletal muscle model to analyze muscle contraction and force generation for different muscle fiber arrangements. *Name: Frontiers in Physiology* **5** (2014), 498.

- [134] Henderson, D. A.; Boys, R. J. & Wilkinson, D. J.: Bayesian calibration of a stochastic kinetic computer model using multiple data sources. *Biometrics* **66** (2010), 249–256.
- [135] Henneman, E.: Relation between size of neurons and their susceptibility to discharge. *Science* **126** (1957), 1345–1347.
- [136] Herbert, R.; Dean, C. & Gandevia, S.: Effects of real and imagined training on voluntary muscle activation during maximal isometric contractions. *Acta Physiologica Scandinavica* **163** (1998), 361–368, ISSN 1365-201X, URL <http://dx.doi.org/10.1046/j.1365-201X.1998.t01-1-00358.x>.
- [137] Herbert, R. D. & Gandevia, S. C.: Twitch interpolation in human muscles: mechanisms and implications for measurement of voluntary activation. *Journal of Neurophysiology* **82** (1999), 2271–2283.
- [138] Higgins, J. P. T.; Green, S. et al.: Cochrane handbook for systematic reviews of interventions (2008).
- [139] Hill, A. V.: The heat of shortening and the dynamic constants of muscle. *Proceedings of the Royal Society of London. Series B - Biological Sciences* **126** (1938), 136–195, URL <https://royalsocietypublishing.org/doi/abs/10.1098/rspb.1938.0050>.
- [140] Hodgkin, A. L. & Huxley, A. F.: A quantitative description of membrane current and its application to conduction and excitation in nerve. *The Journal of Physiology* **117** (1952), 500–544.
- [141] Hodgson, M.; Docherty, D. & Robbins, D.: Post-activation potentiation. *Sports Medicine* **35** (2005), 585–595.
- [142] Hogrel, J.-Y.: Use of surface emg for studying motor unit recruitment during isometric linear force ramp. *Journal of Electromyography and Kinesiology* **13** (2003), 417–423.
- [143] Holloszy, J. O. & Booth, F. W.: Biochemical adaptations to endurance exercise in muscle. *Annual review of physiology* **38** (1976), 273–291.
- [144] Holobar, A. & Zazula, D.: Multichannel blind source separation using convolution kernel compensation. *IEEE Transactions on Signal Processing* **55** (2007), 4487–4496.
- [145] Howard, J. D. & Enoka, R. M.: Maximum bilateral contractions are modified by neurally mediated interlimb effects. *Journal of Applied Physiology* **70** (1991), 306–316.
- [146] Hrysomallis, C. & Buttifant, D.: Influence of training years on upper-body strength and power changes during the competitive season for professional australian rules football players. *Journal of science and medicine in sport* **15** (2012), 374–378.



- [147] Hurley, M. V.; Rees, J. & Newham, D. J.: Quadriceps function, proprioceptive acuity and functional performance in healthy young, middle-aged and elderly subjects. *Age and ageing* **27** (1998), 55–62.
- [148] Ikai, M. & Fukunaga, T.: A study on training effect on strength per unit cross-sectional area of muscle by means of ultrasonic measurement. *Internationale Zeitschrift für angewandte Physiologie einschließlich Arbeitsphysiologie* **28** (1970), 173–180, ISSN 1439-6327, URL <http://dx.doi.org/10.1007/BF00696025>.
- [149] Inder, J. D.; Carlson, D. J.; Dieberg, G.; McFarlane, J. R.; Hess, N. C. & Smart, N. A.: Isometric exercise training for blood pressure management: a systematic review and meta-analysis to optimize benefit. *Hypertension Research* **39** (2016), 88.
- [150] Ishak, K. J.; Platt, R. W.; Joseph, L.; Hanley, J. A. & Caro, J. J.: Meta-analysis of longitudinal studies. *Clinical Trials* **4** (2007), 525–539.
- [151] Jacobsen, A. B.; Bostock, H. & Tankisi, H.: Following disease progression in motor neuron disorders with 3 motor unit number estimation methods. *Muscle & Nerve* **59** (2019), 82–87.
- [152] Jakobi, J. M. & Cafarelli, E.: Neuromuscular drive and force production are not altered during bilateral contractions. *Journal of Applied Physiology* **84** (1998), 200–206.
- [153] Jaramillo, J.; Worrell, T. W. & Ingersoll, C. D.: Hip isometric strength following knee surgery. *Journal of Orthopaedic & Sports Physical Therapy* **20** (1994), 160–165, URL <https://doi.org/10.2519/jospt.1994.20.3.160>, PMID: 7951293.
- [154] Jiang, N.; Englehart, K. B. & Parker, P. A.: Extracting simultaneous and proportional neural control information for multiple-dof prostheses from the surface electromyographic signal. *IEEE transactions on Biomedical Engineering* **56** (2009), 1070–1080.
- [155] Jones, D. & Rutherford, O.: Human muscle strength training: the effects of three different regimens and the nature of the resultant changes. *The Journal of physiology* **391** (1987), 1.
- [156] Jones, K. E.; Hamilton, A. F. d. C. & Wolpert, D. M.: Sources of signal-dependent noise during isometric force production. *Journal of neurophysiology* **88** (2002), 1533–1544.
- [157] Joyner, M. J. & Coyle, E. F.: Endurance exercise performance: the physiology of champions. *The Journal of Physiology* **586** (2008), 35–44.
- [158] Kamavuako, E. N. & Farina, D.: Time-dependent effects of pre-conditioning activation on muscle fiber conduction velocity and twitch torque. *Muscle & Nerve* **42** (2010), 547–555.
- [159] Kamen, G. & Knight, C. A.: Training-related adaptations in motor unit discharge rate in young and older adults. *The Journals of Gerontology Series A: Biological Sciences and Medical Sciences* **59** (2004), 1334–1338.

- [160] Kanehisa, H. & Miyashita, M.: Effect of isometric and isokinetic muscle training on static strength and dynamic power. *European journal of applied physiology and occupational physiology* **50** (1983), 365–371.
- [161] Kanehisa, H.; Nagareda, H.; Kawakami, Y.; Akima, H.; Masani, K.; Kouzaki, M. & Fukunaga, T.: Effects of equivolume isometric training programs comprising medium or high resistance on muscle size and strength. *European Journal of Applied Physiology* **87** (2002), 112–119, ISSN 1439-6327, URL <http://dx.doi.org/10.1007/s00421-002-0604-6>.
- [162] Karathanasopoulos, N.; Angelikopoulos, P.; Papadimitriou, C. & Koumoutsakos, P.: Bayesian identification of the tendon fascicles structural composition using finite element models for helical geometries. *Computer Methods in Applied Mechanics and Engineering* **313** (2017), 744–758.
- [163] Katirji, B.: Chapter 2 - routine clinical electromyography. In Katirji, B. (ed.): *Electromyography in Clinical Practice (Second Edition)*. Mosby, Philadelphia 2007, second edition edn., ISBN 978-0-323-02899-8, pp. 13 – 36, URL <http://www.sciencedirect.com/science/article/pii/B9780323028998500070>.
- [164] Keen, D. A.; Yue, G. H. & Enoka, R. M.: Training-related enhancement in the control of motor output in elderly humans. *Journal of Applied Physiology* **77** (1994), 2648–2658.
- [165] Keenan, K. G.; Farina, D.; Maluf, K. S.; Merletti, R. & Enoka, R. M.: Influence of amplitude cancellation on the simulated surface electromyogram. *Journal of Applied Physiology* **98** (2005), 120–131.
- [166] Kendall, M. G.: On the reconciliation of theories of probability. *Biometrika* **36** (1949), 101–116.
- [167] Kirby, T. J.; McCarthy, J. J.; Peterson, C. A. & Fry, C. S.: *Synergist Ablation as a Rodent Model to Study Satellite Cell Dynamics in Adult Skeletal Muscle*, Springer New York, New York, NY 2016. pp. 43–52.
- [168] Kitai, T. A. & Sale, D. G.: Specificity of joint angle in isometric training. *European Journal of Applied Physiology and Occupational Physiology* **58** (1989), 744–748, ISSN 1439-6327, URL <http://dx.doi.org/10.1007/BF00637386>.
- [169] Kleine, B. U.; van Dijk, J. P.; Zwarts, M. J. & Stegeman, D. F.: Inter-operator agreement in decomposition of motor unit firings from high-density surface emg. *Journal of Electromyography and Kinesiology* **18** (2008), 652–661.
- [170] Knapik, J. J.; Mawdsley, R. H. & Ramos, M. U.: Angular specificity and test mode specificity of isometric and isokinetic strength training. *Journal of Orthopaedic & Sports Physical Therapy* **5** (1983), 58–65.
- [171] Kolmogorov, A. N.: *Foundations of the theory of probability: Second English Edition*. Chelsea Publishing Company: New York 1950.

- [172] Komi, P. V.; Viitasalo, J. T.; Rauramaa, R. & Vihko, V.: Effect of isometric strength training on mechanical, electrical, and metabolic aspects of muscle function. *European Journal of Applied Physiology and Occupational Physiology* **40** (1978), 45–55, ISSN 1439-6327, URL <http://dx.doi.org/10.1007/BF00420988>.
- [173] Körding, K. P. & Wolpert, D. M.: Bayesian integration in sensorimotor learning. *Nature* **427** (2004), 244.
- [174] Kossev, A.; Elek, J.; Wohlfarth, K.; Schubert, M.; Dengler, R. & Wolf, W.: Assessment of human motor unit twitches—a comparison of spike-triggered averaging and intramuscular microstimulation. *Clinical Neurophysiology* **93** (1994), 100–105.
- [175] Kovanen, V.; Suominen, H. & Heikkinen, E.: Collagen of slow twitch and fast twitch muscle fibres in different types of rat skeletal muscle. *European journal of applied physiology and occupational physiology* **52** (1984), 235–242.
- [176] Kraemer, W. J. & Ratamess, N. A.: Fundamentals of resistance training: progression and exercise prescription. *Medicine and science in sports and exercise* **36** (2004), 674–688.
- [177] Kraemer, W. J. & Spiering, B. A.: Skeletal muscle physiology: Plasticity and responses to exercise. *Hormone Research in Pediatrics* **66** (2006), 2–16.
- [178] Krakauer, J. W. & Mazzoni, P.: Human sensorimotor learning: adaptation, skill, and beyond. *Current Opinion in Neurobiology* **21** (2011), 636 – 644, sensory and motor systems.
- [179] Krieger, J. W.: Single vs. multiple sets of resistance exercise for muscle hypertrophy: a meta-analysis. *The Journal of Strength & Conditioning Research* **24** (2010), 1150–1159.
- [180] Kubiak, R. J.; Whitman, K. M. & Jonhston, R. M.: Changes in quadriceps femoris muscle strength using isometric exercise versus electrical stimulation. *Journal of Orthopaedic & Sports Physical Therapy* **8** (1987), 537–541.
- [181] Kubo, K.; Ikebukuro, T.; Yaeshima, K.; Yata, H.; Tsunoda, N. & Kanehisa, H.: Effects of static and dynamic training on the stiffness and blood volume of tendon in vivo. *Journal of Applied Physiology* **106** (2009), 412–417.
- [182] Kubo, K.; Kanehisa, H.; Ito, M. & Fukunaga, T.: Effects of isometric training on the elasticity of human tendon structures in vivo. *Journal of Applied Physiology* **91** (2001), 26–32.
- [183] Kubo, K.; Komuro, T.; Ishiguro, N.; Tsunoda, N.; Sato, Y.; Ishii, N.; Kanehisa, H. & Fukunaga, T.: Effects of low-load resistance training with vascular occlusion on the mechanical properties of muscle and tendon. *Journal of applied biomechanics* **22** (2006), 112–119.
- [184] Kubo, K.; Morimoto, M.; Komuro, T.; Yata, H.; Tsunoda, N.; Kanehisa, H. & Fukunaga, T.: Effects of plyometric and weight training on muscle-tendon complex

- and jump performance. *Medicine & Science in Sports & Exercise* **39** (2007), 1801–1810.
- [185] Kubo, K.; Ohgo, K.; Takeishi, R.; Yoshinaga, K.; Tsunoda, N.; Kanehisa, H. & Fukunaga, T.: Effects of isometric training at different knee angles on the muscle–tendon complex in vivo. *Scandinavian journal of medicine & science in sports* **16** (2006), 159–167.
- [186] Lambert, B.: *A students guide to Bayesian statistics*. Sage 2018.
- [187] Latash, M. L.: *Neurophysiological basis of movement*. Human Kinetics 2008.
- [188] Lee, M.; Gandevia, S. C. & Carroll, T. J.: Unilateral strength training increases voluntary activation of the opposite untrained limb. *Clinical Neurophysiology* **120** (2009), 802 – 808, ISSN 1388-2457.
- [189] Lee, P. M.: *Bayesian statistics: an introduction*. (1997).
- [190] Lee, S. E. K.; de Lira, C. A. B.; Nouailhetas, V. L. A.; Vancini, R. L. & Andrade, M. S.: Do isometric, isotonic and/or isokinetic strength trainings produce different strength outcomes? *Journal of bodywork and movement therapies* **22** (2018), 430–437.
- [191] Lesinski, M.; Prieske, O. & Granacher, U.: Effects and dose–response relationships of resistance training on physical performance in youth athletes: a systematic review and meta-analysis. *British Journal of Sports Medicine* **50** (2016), 781–795.
- [192] Levangie, P. K. & Norkin, C. C.: *Joint structure and function: a comprehensive analysis*. 3rd. Philadelphia: FA. Davis Company (2000).
- [193] Lewis, S.; Nygaard, E.; Sanchez, J.; Egebald, H. & Saltin, B.: Static contraction of the quadriceps muscle in man: Cardiovascular control and responses to one-legged strength training. *Acta Physiologica Scandinavica* **122** (1984), 341–353.
- [194] Lexell, J.; Sjöström, M.; Nordlund, A.-S. & Taylor, C. C.: Growth and development of human muscle: a quantitative morphological study of whole vastus lateralis from childhood to adult age. *Muscle & nerve* **15** (1992), 404–409.
- [195] Lexell, J.; Taylor, C. C. & Sjstrm, M.: What is the cause of the ageing atrophy? *Journal of the Neurological Sciences* **84** (1988), 275 – 294.
- [196] Lieber, R. L.: *Skeletal muscle structure, function, and plasticity*. Lippincott Williams & Wilkins 2010.
- [197] Lindle, R.; Metter, E.; Lynch, N.; Fleg, J.; Fozard, J.; Tobin, J.; Roy, T. & Hurley, B.: Age and gender comparisons of muscle strength in 654 women and men aged 20–93 yr. *Journal of Applied Physiology* **83** (1997), 1581–1587.
- [198] Littell, J. H.: Systematic reviews in the social sciences: a review. *Evidence & Policy A Journal of Research Debate and Practice* (2006).

- [199] Lucca, J. A. & Recchiuti, S. J.: Effect of electromyographic biofeedback on an isometric strengthening program. *Physical Therapy* **63** (1983), 200–203.
- [200] Ma, W. J.; Beck, J. M.; Latham, P. E. & Pouget, A.: Bayesian inference with probabilistic population codes. *Nature Neuroscience* **9** (2006), 1432.
- [201] Macaluso, A. & De Vito, G.: Muscle strength, power and adaptations to resistance training in older people. *European journal of applied physiology* **91** (2004), 450–472.
- [202] Macaluso, A.; De Vito, G.; Felici, F. & Nimmo, M. A.: Electromyogram changes during sustained contraction after resistance training in women in their 3rd and 8th decades. *European Journal of Applied Physiology* **82** (2000), 418–424, ISSN 1439-6327, URL <http://dx.doi.org/10.1007/s004210000212>.
- [203] Macefield, V. G.; Fuglevand, A. J. & Bigland-Ritchie, B.: Contractile properties of single motor units in human toe extensors assessed by intraneural motor axon stimulation. *Journal of Neurophysiology* **75** (1996), 2509–2519.
- [204] MacIntosh, B. R.; Gardiner, P. F. & McComas, A. J.: *Skeletal muscle: form and function*. Human Kinetics 2006.
- [205] Maffiuletti, N. A. & Martin, A.: Progressive versus rapid rate of contraction during 7 wk of isometric resistance training. *Medicine and science in sports and exercise* **33** (2001), 1220–1227.
- [206] Manca, A.; Ginatempo, F.; Cabboi, M. P.; Mercante, B.; Ortu, E.; Dragone, D.; De Natale, E. R.; Dvir, Z.; Rothwell, J. C. & Deriu, F.: No evidence of neural adaptations following chronic unilateral isometric training of the intrinsic muscles of the hand: a randomized controlled study. *European Journal of Applied Physiology* **116** (2016), 1993–2005.
- [207] Martinez-Valdes, E.; Falla, D.; Negro, F.; Mayer, F. & Farina, D.: Differential motor unit changes after endurance or high-intensity interval training. *American College of Sports Medicine* (2017).
- [208] Martinez-Valdes, E.; Laine, C. M.; Falla, D.; Mayer, F. & Farina, D.: High-density surface electromyography provides reliable estimates of motor unit behavior. *Clinical Neurophysiology* **127** (2016), 2534–2541.
- [209] Martinsen, E. W.: Benefits of exercise for the treatment of depression. *Sports Medicine* **9** (1990), 380–389.
- [210] MathWorks: Beta distribution. <https://www.mathworks.com/help/stats/beta-distribution.html> (2019), retrieved on: 2019-09-16.
- [211] MathWorks: Convolution and polynomial multiplication. <https://www.mathworks.com/help/matlab/ref/conv.html> (2019), retrieved on: 12/11/2019.
- [212] MathWorks: Gamma distribution. <https://www.mathworks.com/help/stats/gamma-distribution.html> (2019), retrieved on: 2019-09-16.

- [213] McCarthy, J. J.; Mula, J.; Miyazaki, M.; Erfani, R.; Garrison, K.; Farooqui, A. B.; Srikuea, R.; Lawson, B. A.; Grimes, B.; Keller, C.; Van Zant, G.; Campbell, K. S.; Esser, K. A.; Dupont-Versteegden, E. E. & Peterson, C. A.: Effective fiber hypertrophy in satellite cell-depleted skeletal muscle. *Development* **138** (2011), 3657–3666.
- [214] McDonagh, M.; Hayward, C. & Davies, C.: Isometric training in human elbow flexor muscles. the effects on voluntary and electrically evoked forces. *Bone & Joint Journal* **65-B** (1983), 355–358.
- [215] Merletti, R. & Farina, D.: Analysis of intramuscular electromyogram signals. *Philosophical Transactions of the Royal Society A: Mathematical, Physical and Engineering Sciences* **367** (2009), 357–368, URL <https://royalsocietypublishing.org/doi/abs/10.1098/rsta.2008.0235>.
- [216] Merletti, R.; Parker, P. A. & Parker, P. J.: *Electromyography: physiology, engineering, and non-invasive applications*, vol. 11. John Wiley & Sons 2004.
- [217] Merriam-Webster: "isoform" (2011), URL <https://www.merriam-webster.com/dictionary/isoform>.
- [218] Meyers, C. R.: Effects of two isometric routines on strength, size, and endurance in exercised and nonexercised arms. *Research Quarterly. American Association for Health, Physical Education and Recreation* **38** (1967), 430–440.
- [219] Miller, A. E. J.; MacDougall, J.; Tarnopolsky, M. & Sale, D.: Gender differences in strength and muscle fiber characteristics. *European journal of applied physiology and occupational physiology* **66** (1993), 254–262.
- [220] Milner-Brown, H.; Stein, R. & Yemm, R.: The orderly recruitment of human motor units during voluntary isometric contractions. *The Journal of physiology* **230** (1973), 359–370.
- [221] Moher, D.; Liberati, A.; Tetzlaff, J.; Altman, D. G. & Group, T. P.: Preferred reporting items for systematic reviews and meta-analyses: The prisma statement. *PLOS Medicine* **6** (2009), 1–6.
- [222] Mohr, T.; Carlson, B.; Sulentic, C. & Landry, R.: Comparison of isometric exercise and high volt galvanic stimulation on quadriceps femoris muscle strength. *Physical therapy* **65** (1985), 606–609.
- [223] Morgan, W.: *Memoirs of the Life of the Rev. Richard Price*. R. Hunter 1815.
- [224] Moritz, C. T.; Barry, B. K.; Pascoe, M. A. & Enoka, R. M.: Discharge rate variability influences the variation in force fluctuations across the working range of a hand muscle. *Journal of Neurophysiology* **93** (2005), 2449–2459.
- [225] Morrissey, M. C.; Harman, E. A. & Johnson, M. J.: Resistance training modes: specificity and effectiveness. *Medicine and Science in Sports and Exercise* **27** (1995), 648–660.

- [226] Munn, J.; Herbert, R. D. & Gandevia, S. C.: Contralateral effects of unilateral resistance training: a meta-analysis. *Journal of Applied Physiology* **96** (2004), 1861–1866.
- [227] Murakami, K.; Fujisawa, H.; Onobe, J. & Sato, Y.: Relationship between muscle fiber conduction velocity and the force-time curve during muscle twitches. *Journal of Physical Therapy Science* **26** (2014), 621–624.
- [228] Murton, A. & Greenhaff, P.: Resistance exercise and the mechanisms of muscle mass regulation in humans: Acute effects on muscle protein turnover and the gaps in our understanding of chronic resistance exercise training adaptation. *The International Journal of Biochemistry & Cell Biology* **45** (2013), 2209 – 2214, ISSN 1357-2725, URL <http://www.sciencedirect.com/science/article/pii/S1357272513002288>, molecular Basis of Muscle Wasting Dedicated to Alfred L. Goldberg.
- [229] Myer, G. D.; Ford, K. R.; PALUMBO, O. P. & Hewett, T. E.: Neuromuscular training improves performance and lower-extremity biomechanics in female athletes. *The Journal of Strength & Conditioning Research* **19** (2005), 51–60.
- [230] do Nascimento, M. A.; Ribeiro, A. S.; de Souza Padilha, C.; da Silva, D. R. P.; Mayhew, J. L.; do Amaral Campos Filho, M. G. & Cyrino, E. S.: Reliability and smallest worthwhile difference in 1rm tests according to previous resistance training experience in young women. *Biology of Sport* **34** (2017), 279–285.
- [231] Negro, F.; Yavuz, U. Ş. & Farina, D.: Limitations of the spike-triggered averaging for estimating motor unit twitch force: a theoretical analysis. *PloS one* **9** (2014).
- [232] Nicholl, J. P.; Coleman, P. & Brazier, J. E.: Health and health care costs and benefits of exercise. *Pharmacoeconomics* **5** (1994), 109–122.
- [233] Nikolaidou, M. E.; Marzilger, R.; Bohm, S.; Mersmann, F. & Arampatzis, A.: Operating length and velocity of human m. vastus lateralis fascicles during vertical jumping. *Royal Society of Open Science* **4** (2017), 170185.
- [234] Oladyshkin, S.; Class, H. & Nowak, W.: Bayesian updating via bootstrap filtering combined with data-driven polynomial chaos expansions: methodology and application to history matching for carbon dioxide storage in geological formations. *Computational Geosciences* **17** (2013), 671–687.
- [235] Oliveira, F. B. D.; Oliveira, A. S. C.; Rizzato, G. F. & Denadai, B. S.: Resistance training for explosive and maximal strength: effects on early and late rate of force development. *Journal of Sports Science & Medicine* **12** (2013), 402.
- [236] OpenStax: Anatomy and physiology. <https://openstax.org/details/books/anatomy-and-physiology> (2013), retrieved on: 02/07/2019.
- [237] Oranchuk, D. J.; Storey, A. G.; Nelson, A. R. & Cronin, J. B.: Isometric training and long-term adaptations: Effects of muscle length, intensity, and intent: A systematic review. *Scandinavian Journal of Medicine & Science in Sports* **29** (2019), 484–503, URL <https://onlinelibrary.wiley.com/doi/abs/10.1111/sms.13375>.

- [238] Owen, A.; Wiles, J. & Swaine, I.: Effect of isometric exercise on resting blood pressure: a meta analysis. *Journal of Human Hypertension* **24** (2010), 796.
- [239] Parker, R. H.: The effects of mild one-legged isometric or dynamic training. *European Journal of Applied Physiology and Occupational Physiology* **54** (1985), 262–268.
- [240] Patrick, B. & Caterisano, A.: Influence of weight training status on hemodynamic adjustments to isometric actions. *Journal of Sports Medicine and Physical Fitness* **42** (2002), 451–457.
- [241] Patten, C.; Kamen, G. & Rowland, D. M.: Adaptations in maximal motor unit discharge rate to strength training in young and older adults. *Muscle & Nerve* **24** (2001), 542–550, ISSN 1097-4598.
- [242] Pearson, K.: Report on certain enteric fever inoculation statistics. *The British Medical Journal* (1904), 1243–1246.
- [243] Pedder, H.; Dias, S.; Bennetts, M.; Boucher, M. & Welton, N. J.: Modelling time-course relationships with multiple treatments: Model-based network meta-analysis for continuous summary outcomes. *Research synthesis methods* **10** (2019), 267–286.
- [244] Perera, R. & Heneghan, C.: Interpreting meta-analysis in systematic reviews. *BMJ Evidence-Based Medicine* **13** (2008), 67–69.
- [245] Petersen, E. & Rostalski, P.: A comprehensive mathematical model of motor unit pool organization, surface electromyography, and force generation. *Frontiers in Physiology* **10** (2019), 176, ISSN 1664-042X, URL <https://www.frontiersin.org/article/10.3389/fphys.2019.00176>.
- [246] Piasecki, M.; Ireland, A.; Piasecki, J.; Stashuk, D. W.; McPhee, J. S. & Jones, D. A.: The reliability of methods to estimate the number and size of human motor units and their use with large limb muscles. *European Journal of Applied Physiology* **118** (2018), 767–775.
- [247] Piasecki, M.; Ireland, A.; Stashuk, D.; Hamilton-Wright, A.; Jones, D. A. & McPhee, J. S.: Age-related neuromuscular changes affecting human vastus lateralis. *The Journal of Physiology* **594** (2016), 4525–4536.
- [248] Piotrkiewicz, M. & Türker, K. S.: Onion skin or common drive? *Frontiers in Cellular Neuroscience* **11** (2017), 2.
- [249] Plummer, M.: Jags: A program for analysis of bayesian graphical models using gibbs sampling. 2003.
- [250] Plummer, M.: rjags: Bayesian graphical models using mcmc (2018), URL <https://CRAN.R-project.org/package=rjags>, r package version 4-8.
- [251] Plüss, M.; Schellenberg, F.; Taylor, W. R. & Lorenzetti, S.: Towards subject-specific strength training design through predictive use of musculoskeletal models. *Applied bionics and biomechanics* **2018** (2018).



- [252] Powers, S. K. & Howley, E. T.: *Exercise physiology: Theory and application to fitness and performance*. McGraw-Hill Boston, MA 2007.
- [253] R Core Team: R: A language and environment for statistical computing (2018), URL <https://www.R-project.org/>.
- [254] Rabita, G.; Pérot, C. & Lensele-Corbeil, G.: Differential effect of knee extension isometric training on the different muscles of the quadriceps femoris in humans. *European Journal of Applied Physiology* **83** (2000), 531–538, ISSN 1439-6327, URL <http://dx.doi.org/10.1007/s004210000325>.
- [255] Ramírez, A.; Grasa, J.; Alonso, A.; Soteras, F.; Osta, R.; Muñoz, M. & Calvo, B.: Active response of skeletal muscle: in vivo experimental results and model formulation. *Journal of theoretical biology* **267** (2010), 546–553.
- [256] Rasband, M. & Trimmer, J.: Ion channel localization in axons. In Squire, L. R. (ed.): *Encyclopedia of Neuroscience*. Academic Press, Oxford 2009, ISBN 978-0-08-045046-9, pp. 229 – 235, URL <http://www.sciencedirect.com/science/article/pii/B9780080450469016417>.
- [257] Rasch, P. J. & Morehouse, L. E.: Effect of static and dynamic exercises on muscular strength and hypertrophy. *Journal of Applied Physiology* **11** (1957), 29–34.
- [258] Rassier, D. E.; Lee, E.-J. & Herzog, W.: Modulation of passive force in single skeletal muscle fibres. *Biology letters* **1** (2005), 342–345.
- [259] van Ravenzwaaij, D.; Cassey, P. & Brown, S. D.: A simple introduction to markov chain monte-carlo sampling. *Psychonomic Bulletin & Review* **25** (2018), 143–154.
- [260] Revill, A. L. & Fuglevand, A. J.: Inhibition linearizes firing rate responses in human motor units: implications for the role of persistent inward currents. *The Journal of physiology* **595** (2017), 179–191.
- [261] Ribeiro, A. S.; Avelar, A.; Schoenfeld, B. J.; Trindade, M. C.; Ritti-Dias, R. M.; Altimari, L. R. & Cyrino, E. S.: Effect of 16 weeks of resistance training on fatigue resistance in men and women. *Journal of Human Kinetics* **42** (2014), 165–174.
- [262] Ribeiro, A. S.; do Nascimento, M. A.; Mayhew, J. L.; Ritti-Dias, R. M.; Avelar, A.; Okano, A. H. & Cyrino, E. S.: Reliability of 1rm test in detrained men with previous resistance training experience. *Isokinetics and Exercise Science* **22** (2014), 137–143.
- [263] Rich, C. & Cafarelli, E.: Submaximal motor unit firing rates after 8 wk of isometric resistance training. *Medicine and science in sports and exercise* **32** (2000), 190–196.
- [264] Rich, C.; O’ Brien, G. L. & Cafarelli, E.: Probabilities associated with counting average motor unit firing rates in active human muscle. *Canadian Journal of Applied Physiology* **23** (1998), 87–94.

- [265] Ritti-Dias, R. M.; Avelar, A.; Salvador, E. P. & Cyrino, E. S.: Influence of previous experience on resistance training on reliability of one-repetition maximum test. *The Journal of Strength & Conditioning Research* **25** (2011), 1418–1422.
- [266] Roatta, S.; ArendtNielsen, L. & Farina, D.: Sympathetic-induced changes in discharge rate and spiketriggred average twitch torque of lowthreshold motor units in humans. *The Journal of Physiology* **586** (2008), 5561–5574.
- [267] Röhrle, O.; Davidson, J. B. & Pullan, A. J.: A physiologically based, multi-scale model of skeletal muscle structure and function. *Frontiers in physiology* **3** (2012), 358.
- [268] Röhrle, O. & Pullan, A. J.: Three-dimensional finite element modelling of muscle forces during mastication. *Journal of biomechanics* **40** (2007), 3363–3372.
- [269] Roig, M.; O'Brien, K.; Kirk, G.; Murray, R.; McKinnon, P.; Shadgan, B. & Reid, D. W.: The effects of eccentric versus concentric resistance training on muscle strength and mass in healthy adults: a systematic review with meta-analyses. *British Journal of Sports Medicine* (2008).
- [270] Roos, M. R.; Rice, C. L.; Connelly, D. M. & Vandervoort, A. A.: Quadriceps muscle strength, contractile properties, and motor unit firing rates in young and old men. *Muscle & nerve* **22** (1999), 1094–1103.
- [271] Rother, E. T.: Systematic literature review x narrative review. *Acta Paul Enferm* **20** (2007), 2.
- [272] Rudas, T.: *Handbook of probability: theory and applications*. Sage Publications 2008.
- [273] Rutherford, O. M. & Jones, D. A.: The role of learning and coordination in strength training. *European Journal of Applied Physiology and Occupational Physiology* **55** (1986), 100–105.
- [274] Rhrle, O.; Davidson, J. B. & Pullan, A. J.: Bridging scales: A three-dimensional electromechanical finite element model of skeletal muscle. *SIAM Journal on Scientific Computing* **30** (2008), 2882–2904.
- [275] Salomoni, S.; Tucker, K.; Hug, F.; McPhee, M. & Hodges, P.: Reduced maximal force during acute anterior knee pain is associated with deficits in voluntary muscle activation. *PLOS ONE* **11** (2016), 1–14.
- [276] Saltin, B. & Gollnick, P. D.: *Skeletal Muscle Adaptability: Significance for Metabolism and Performance*, American Cancer Society 1977. ISBN 9780470650714, pp. 555–631.
- [277] Saltin, B. & Gollnick, P. D.: Skeletal muscle adaptability: significance for metabolism and performance. *Comprehensive Physiology* (2011), 555–631.
- [278] Schiaffino, S. & Reggiani, C.: Myosin isoforms in mammalian skeletal muscle. *Journal of Applied Physiology* **77** (1994), 493–501.

- [279] Schoenfeld, B. J.: The mechanisms of muscle hypertrophy and their application to resistance training. *The Journal of Strength & Conditioning Research* **24** (2010), 2857–2872.
- [280] Schoenfeld, B. J.; Grgic, J.; Ogborn, D. & Krieger, J. W.: Strength and hypertrophy adaptations between low-vs. high-load resistance training: a systematic review and meta-analysis. *The Journal of Strength & Conditioning Research* **31** (2017), 3508–3523.
- [281] Schoenfeld, B. J.; Wilson, J. M.; Lowery, R. P. & Krieger, J. W.: Muscular adaptations in low-versus high-load resistance training: A meta-analysis. *European Journal of Sport Science* **16** (2016), 1–10.
- [282] Semmlow, J.: Chapter 5 - linear systems analysis in the time domain convolution. In Semmlow, J. (ed.): *Circuits, Signals and Systems for Bioengineers (Third Edition)*. Academic Press 2018, Biomedical Engineering, third edition edn., ISBN 978-0-12-809395-5, pp. 209 – 243, URL <http://www.sciencedirect.com/science/article/pii/B9780128093955000059>.
- [283] Seyedsalehi, S.; Zhang, L.; Choi, J. & Baek, S.: Prior distributions of material parameters for bayesian calibration of growth and remodeling computational model of abdominal aortic wall. *Journal of biomechanical engineering* **137** (2015), 101001.
- [284] Shadmehr, R. & Arbib, M. A.: A mathematical analysis of the force-stiffness characteristics of muscles in control of a single joint system. *Biological cybernetics* **66** (1992), 463–477.
- [285] Shadmehr, R.; Wise, S. P.; Wise, S. P. et al.: *The computational neurobiology of reaching and pointing: a foundation for motor learning*. MIT press 2005.
- [286] Sharifimajd, B. & Stålhand, J.: A continuum model for skeletal muscle contraction at homogeneous finite deformations. *Biomechanics and modeling in mechanobiology* **12** (2013), 965–973.
- [287] Sherrington, C. S.: Remarks on some aspects of reflex inhibition. *Proceedings of the Royal Society of London. Series B, Containing Papers of a Biological Character* **97** (1925), 519–545.
- [288] Shima, N.; Ishida, K.; Katayama, K.; Morotome, Y.; Sato, Y. & Miyamura, M.: Cross education of muscular strength during unilateral resistance training and de-training. *European Journal of Applied Physiology* **86** (2002), 287–294.
- [289] Shorten, P. R.; O Callaghan, P.; Davidson, J. B. & Soboleva, T. K.: A mathematical model of fatigue in skeletal muscle force contraction. *Journal of Muscle Research and Cell Motility* **28** (2007), 293–313.
- [290] Sica, R. E. P. & McComas, A. J.: Fast and slow twitch units in a human muscle. *Journal of Neurology, Neurosurgery & Psychiatry* **34** (1971), 113–120.
- [291] Smith, A. F. M. & Gelfand, A. E.: Bayesian statistics without tears: a sampling-resampling perspective. *The American Statistician* **46** (1992), 84–88.

- [292] Spiegelhalter, D. J.; Abrams, K. R. & Myles, J. P.: *Bayesian approaches to clinical trials and health-care evaluation*, vol. 13. John Wiley & Sons 2004.
- [293] Staudenmann, D.; Roeleveld, K.; Stegeman, D. F. & Van Dieën, J. H.: Methodological aspects of semg recordings for force estimation—a tutorial and review. *Journal of electromyography and kinesiology* **20** (2010), 375–387.
- [294] Stephens, J. & Usherwood, T.: The mechanical properties of human motor units with special reference to their fatiguability and recruitment threshold. *Brain Research* **125** (1977), 91 – 97.
- [295] Sterne, J.; Savovi, J.; Page, M.; Elbers, R.; Blencowe, N.; Boutron, I.; Cates, C.; Cheng, H.-Y.; Corbett, M.; Eldridge, S.; Hernn, M.; Hopewell, S.; Hrbjartsson, A.; Junqueira, D.; Jni, P.; Kirkham, J.; Lasserson, T.; Li, T.; McAleenan, A.; Reeves, B.; Shepperd, S.; Shrier, I.; Stewart, L.; Tilling, K.; White, I.; Whiting, P. & Higgins, J.: Rob 2: a revised tool for assessing risk of bias in randomised trials. *British Medical Journal* **366** (2019).
- [296] Stifani, N.: Motor neurons and the generation of spinal motor neurons diversity. *Frontiers in Cellular Neuroscience* **8** (2014), 293, ISSN 1662-5102, URL <https://www.frontiersin.org/article/10.3389/fncel.2014.00293>.
- [297] Stocchi, V.; De Feo, P. & Hood, D. A.: *Role of Physical Exercise in Preventing Disease and Improving the Quality of Life*. Springer 2007.
- [298] Stock, M. S.; Beck, T. W. & De Freitas, J. M.: Effects of fatigue on motor unit firing rate versus recruitment threshold relationships. *Muscle & nerve* **45** (2012), 100–109.
- [299] Szeto, G.; Strauss, G. R.; de Domenico, G. & Lai, H. S.: The effect of training intensity on voluntary isometric strength improvement. *Australian Journal of Physiotherapy* **35** (1989), 210 – 217.
- [300] Tatsioni, A. & Ioannidis, J.: Meta-analysis. In Heggenhougen, H. K. K. (ed.): *International Encyclopedia of Public Health*. Academic Press, Oxford 2008, pp. 442 – 450.
- [301] Taylor, A. M.; Christou, E. A. & Enoka, R. M.: Multiple features of motor-unit activity influence force fluctuations during isometric contractions. *Journal of Neurophysiology* **90** (2003), 1350–1361.
- [302] Thepaut-Mathieu, C.; Van Hoecke, J. & Maton, B.: Myoelectrical and mechanical changes linked to length specificity during isometric training. *Journal of Applied Physiology* **64** (1988), 1500–1505, ISSN 8750-7587.
- [303] Thewlis, J.: *Concise dictionary of physics and related subjects*. New York, Pergamon Press 1973.
- [304] Thomas, C. K.; Bigland-Richie, B. & Johansson, R. S.: Force-frequency relationships of human thenar motor units. *Journal of Neurophysiology* **65** (1991), 1509–1516.

- [305] Thomas, C. K.; Johansson, R. S. & Bigland-Ritchie, B.: Attempts to physiologically classify human thenar motor units. *Journal of Neurophysiology* **65** (1991), 1501–1508.
- [306] Tillin, N. A.; Pain, M. T. G. & Folland, J. P.: Short-term unilateral resistance training affects the agonist–antagonist but not the force–agonist activation relationship. *Muscle & nerve* **43** (2011), 375–384.
- [307] Timmons, J. A.: Variability in training-induced skeletal muscle adaptation. *Journal of applied physiology* **110** (2011), 846–853.
- [308] Valero-Cuevas, F. J.; Hoffmann, H.; Kurse, M. U.; Kutch, J. J. & Theodorou, E. A.: Computational models for neuromuscular function. *IEEE Reviews in Biomedical Engineering* **2** (2009), 110–135.
- [309] Vallverdú, J.: *Bayesians versus frequentists: A philosophical debate on statistical reasoning*. Springer 2016.
- [310] Van Cutsem, M.; Duchateau, J. & Hainaut, K.: Changes in single motor unit behaviour contribute to the increase in contraction speed after dynamic training in humans. *The Journal of Physiology* **513** (1998), 295–305.
- [311] Van Cutsem, M.; Feiereisen, P.; Duchateau, J. & Hainaut, K.: Mechanical properties and behaviour of motor units in the tibialis anterior during voluntary contractions. *Canadian Journal of Applied Physiology* **22** (1997), 585–597.
- [312] Van Oijen, M.; Rougier, J. & Smith, R.: Bayesian calibration of process-based forest models: bridging the gap between models and data. *Tree Physiology* **25** (2005), 915–927.
- [313] Warburton, D. E.; McKenzie, D. C.; Haykowsky, M. J.; Taylor, A.; Shoemaker, P.; Ignaszewski, A. P. & Chan, S. Y.: Effectiveness of high-intensity interval training for the rehabilitation of patients with coronary artery disease. *The American Journal of Cardiology* **95** (2005), 1080–1084.
- [314] Ward, S. R.; Eng, C. M.; Smallwood, L. H. & Lieber, R. L.: Are current measurements of lower extremity muscle architecture accurate? *Clinical orthopaedics and related research* **467** (2009), 1074–1082.
- [315] Wasserman, L.: Bayesian model selection and model averaging. *Journal of Mathematical Psychology* **44** (2000), 92 – 107, ISSN 0022-2496.
- [316] Watkins, J. V. (ed.): *Structure and function of the musculoskeletal system*. Human Kinetics, Leeds 2010, 2. ed. edn., ISBN 978-0-7360-7890-0.
- [317] Weakley, J. J.; Till, K.; Darrall-Jones, J.; Roe, G. A.; Phibbs, P. J.; Read, D. B. & Jones, B. L.: The influence of resistance training experience on the between-day reliability of commonly used strength measures in male youth athletes. *The Journal of Strength & Conditioning Research* **31** (2017), 2005–2010.

- [318] Webber, S. C.; Porter, M. M. & Gardiner, P. F.: Modeling age-related neuromuscular changes in humans. *Applied Physiology, Nutrition, and Metabolism* **34** (2009), 732–744, URL <https://doi.org/10.1139/H09-052>.
- [319] Weir, J. P.; Housh, T. J. & Weir, L. L.: Electromyographic evaluation of joint angle specificity and cross-training after isometric training. *Journal of Applied Physiology* **77** (1994), 197–201.
- [320] Weir, J. P.; Housh, T. J.; Weir, L. L. & Johnson, G. O.: Effects of unilateral isometric strength training on joint angle specificity and cross-training. *European Journal of Applied Physiology and Occupational Physiology* **70** (1995), 337–343.
- [321] Wernbom, M.; Augustsson, J. & Thomeé, R.: The influence of frequency, intensity, volume and mode of strength training on whole muscle cross-sectional area in humans. *Sports Medicine* **37** (2007), 225–264.
- [322] Wickham, H.: *ggplot2: Elegant Graphics for Data Analysis*. Springer-Verlag New York 2016, ISBN 978-3-319-24277-4, URL <http://ggplot2.org>.
- [323] Wickham, H.: tidyverse: Easily install and load the 'tidyverse' (2017), URL <https://CRAN.R-project.org/package=tidyverse>, r package version 1.2.1.
- [324] Yao, W.; Fuglevand, R. J. & Enoka, R. M.: Motor-unit synchronization increases emg amplitude and decreases force steadiness of simulated contractions. *Journal of Neurophysiology* **83** (2000), 441–452.
- [325] Young, K.; McDonagh, M. & Davies, C.: The effects of two forms of isometric training on the mechanical properties of the triceps surae in man. *Pflügers Archiv European Journal of Physiology* **405** (1985), 384–388.
- [326] Yue, G. & Cole, K. J.: Strength increases from the motor program: comparison of training with maximal voluntary and imagined muscle contractions. *Journal of neurophysiology* **67** (1992), 1114–1123.
- [327] Zahalak, G. I.: Modeling muscle mechanics (and energetics). In Winters, J. M. & Woo, S. L. (eds.): *Multiple muscle systems: Biomechanics and movement organization*. Springer Science & Business Media 1990, chap. 1.
- [328] Zajac, F. E. & Faden, J. S.: Relationship among recruitment order, axonal conduction velocity, and muscle-unit properties of type-identified motor units in cat plantaris muscle. *Journal of Neurophysiology* **53** (1985), 1303–1322.
- [329] Zhou, S.; Lawson, D. L.; Morrison, W. E. & Fairweather, I.: Electromechanical delay in isometric muscle contractions evoked by voluntary, reflex and electrical stimulation. *European Journal of Applied Physiology and Occupational Physiology* **70** (1995), 138–145.
- [330] Zierath, J. R. & Hawley, J. A.: Skeletal muscle fiber type: Influence on contractile and metabolic properties. *PLOS Biology* **2** (2004).



# Curriculum Vitae

## Personal Data:

Name: Neriman Ekin Altan  
Date of birth: October 9, 1990  
Place of birth: Ankara, Turkey  
Nationality: Turkish

## Education:

2011 – 2013 Master of Science  
Computational Mechanics of Materials and Structures  
University of Stuttgart  
2007 – 2011 Bachelor of Science  
Department of Civil Engineering  
Middle East Technical University  
2004 – 2007 High school diploma  
TED Ankara College Foundation High School

## Work experience:

2013 – 2019 Research and teaching assistant at the Continuum Biomechanics and Mechanobiology Research Group at the Institute for Modeling und Simulation of Biomechanical Systems at the University of Stuttgart  
2020 – present Consultant, CENIT AG



